Informatics Control Measurement
in Economy and Environment Protection

1/2023

# Informatyka Automatyka Pomiary

## w gospodarce i ochronie środowiska

www.e-IAPGOS.pl

ISSN 2083-0157

Kwartalnik Naukowo-Techniczny

fot. arch. KPI

National Technical University of Ukraine
"Igor Sikorsky Kyiv Polytechnic Institute"
(Kyiv, Ukraine)

1/2023

styczeń – marzec

Wydanie pod redakcją naukową
prof. dr hab. inż. Waldemara Wójcika

INFORMATYKA AUTOMATYKA POMIARY
W GOSPODARCE i OCHRONIE ŚRODOWISKA
Informatics Control Measurement in Economy and Environment Protection

p-ISSN 2083-0157, e-ISSN 2391-6761, www.e-iapgos.pl



## EDITORIAL OFFICE
## REDAKCJA

**Redakcja czasopisma**
**Informatyka, Automatyka, Pomiary w Gospodarce i Ochronie Środowiska**
Katedra Elektroniki i Technik Informacyjnych
Politechnika Lubelska
ul. Nadbystrzycka 38A, 20-618 Lublin
tel. +48 81 53 84 309,
fax: +48 81 53 84 312
iapgos@pollub.pl
www.e-iapgos.pl
iapgos.pollub.pl
ph.pollub.pl/index.php/iapgos

## PUBLISHER
## WYDAWCA

**Politechnika Lubelska**
ul. Nadbystrzycka 38D
20-618 Lublin
tel. +48 81 53 84 100
www.pollub.pl
ph.pollub.pl

## PRINTING HOUSE – DRUKARNIA

**PPH Remigraf Sp. z o.o.**
ul. Dźwigowa 61, 01-376 Warszawa
https://remigraf.pl/

nakład: 100 egzemplarzy

## OTHER INFORMATION – INNE INFORMACJE

**Czasopismo jest indeksowane w bazach:**

| | |
|---|---|
| DOAJ | doaj.org |
| BazTech | baztech.icm.edu.pl |
| IC Journals Master List | www.journals.indexcopernicus.com |
| Google Scholar | scholar.google.pl |
| POL-index | pbn.nauka.gov.pl |
| Sherpa RoMEO | www.sherpa.ac.uk |
| OAJI | oaji.net |
| SCOPUS | www.scopus.com |
| EBSCO | www.ebsco.com |

Czasopismo *Informatyka, Automatyka, Pomiary w Gospodarce i Ochronie Środowiska* zostało objęte finansowaniem przez Ministerstwo Nauki i Szkolnictwa Wyższego w ramach programu *Wsparcie dla czasopism naukowych* w latach 2019-2020.

Czasopismo znajduje się w wykazie czasopism naukowych opublikowanym w Komunikacie Ministra Edukacji i Nauki z dnia 1 grudnia 2021 r., Unikatowy Identyfikator Czasopisma: 200167 – z przypisaną liczbą punktów przyznawanych za publikację artykułu równą 20.

Zasady publikowania artykułów, przygotowania tekstów, zasady etyczne, procedura recenzowania, wykazy recenzentów oraz pełne teksty artykułów dostępne są na stronie internetowej czasopisma:

www.e-iapgos.pl

W celu zwiększenia oddziaływania czasopisma w środowisku naukowym redakcja zaleca:

- w artykułach publikowanych w IAPGOS cytować artykuły z renomowanych czasopism międzynarodowych (szczególnie indeksowanych w bazach Web of Science oraz Scopus) używając oficjalnych skrótów nazw czasopism,
- w artykułach publikowanych w innych czasopismach (zwłaszcza indeksowanych w bazach Web of Science oraz Scopus) cytować prace publikowane w IAPGOS – zwłaszcza posługując się numerami DOI, np.:
  Kluszczyński K. *Modelowanie – umiejętność czy sztuka?* Informatyka, Automatyka, Pomiary w Gospodarce i Ochronie Środowiska – IAPGOS, 1/2016, 4–15, https://doi.org/10.5604/20830157.1193833.

## CONTENTS – SPIS TREŚCI

http://doi.org/10.35784/iapgos.3366

*received: 12.12.2022 | revised: 5.03.2023 | accepted: 13.03.2023 | available online: 31.03.2023*

# AN ENHANCED DIFFERENTIAL EVOLUTION ALGORITHM WITH ADAPTIVE WEIGHT BOUNDS FOR EFFICIENT TRAINING OF NEURAL NETWORKS

**Saithip Limtrakul, Jeerayut Wetweerapong**
Khon Kaen University, Faculty of Science, Department of Mathematics, Khon Kaen, Thailand

***Abstract.*** *Artificial neural networks are essential intelligent tools for various learning tasks. Training them is challenging due to the nature of the data set, many training weights, and their dependency, which gives rise to a complicated high-dimensional error function for minimization. Thus, global optimization methods have become an alternative approach. Many variants of differential evolution (DE) have been applied as training methods to approximate the weights of a neural network. However, empirical studies show that they suffer from generally fixed weight bounds. In this research, we propose an enhanced differential evolution algorithm with adaptive weight bound adjustment (DEAW) for the efficient training of neural networks. The DEAW algorithm uses small initial weight bounds and adaptive adjustment in the mutation process. It gradually extends the bounds when a component of a mutant vector reaches its limits. We also experiment with using several scales of an activation function with the DEAW algorithm. Then, we apply the proposed method with its suitable setting to solve function approximation problems. DEAW can achieve satisfactory results compared to exact solutions.*

**Keywords**: neural network, differential evolution, training neural network, function approximation

## ULEPSZONY ALGORYTM EWOLUCJI RÓŻNICOWEJ Z ADAPTACYJNYMI GRANICAMI WAG DLA EFEKTYWNEGO SZKOLENIA SIECI NEURONOWYCH

***Streszczenie.*** *Sztuczne sieci neuronowe są niezbędnymi inteligentnymi narzędziami do realizacji różnych zadań uczenia się. Ich szkolenie stanowi wyzwanie ze względu na charakter zbioru danych, wiele wag treningowych i ich zależności, co powoduje powstanie skomplikowanej, wielowymiarowej funkcji błędu do minimalizacji. Dlatego alternatywnym podejściem stały się metody optymalizacji globalnej. Wiele wariantów ewolucji różnicowej (DE) zostało zastosowanych jako metody treningowe do aproksymacji wag sieci neuronowej. Jednak badania empiryczne pokazują, że cierpią one z powodu ogólnie ustalonych granic wag. W tym badaniu proponujemy ulepszony algorytm ewolucji różnicowej z adaptacyjnym dopasowaniem granic wag (DEAW) dla efektywnego szkolenia sieci neuronowych. Algorytm DEAW wykorzystuje małe początkowe granice wag i adaptacyjne dostosowanie w procesie mutacji. Stopniowo rozszerza on granice, gdy składowa wektora mutacji osiąga swoje granice. Eksperymentujemy również z wykorzystaniem kilku skal funkcji aktywacji z algorytmem DEAW. Następnie, stosujemy proponowaną metodę z jej odpowiednim ustawieniem do rozwiązywania problemów aproksymacji funkcji. DEAW może osiągnąć zadowalające rezultaty w porównaniu z rozwiązaniami dokładnymi.*

**Słowa kluczowe**: sieć neuronowa, ewolucja różnicowa, trening sieci neuronowej, aproksymacja funkcji

## Introduction

The artificial neural network (ANN) is one of the most popular machine learning techniques and has continuously gained attention in many research fields. The ANN learning procedure imitates the behavior of the nervous system and has multiple characteristics, such as the number of connecting nodes and layers, the initial values of weights, and the types of a transfer function (or activation function). The procedure forwardly transforms input data to output as a mapping function using weights and the transfer function. The network training finds the optimal weights that minimize the error between the actual target and network output on the sample input data. Therefore, the training algorithm which applies an optimization method for minimization strongly affects the performance of ANN.

In the beginning, Back-propagation (BP) [24] was the training method for the multilayer perceptron algorithm. The BP algorithm is a gradient descent optimizer technique that minimizes functions by iteratively moving in the direction of the steepest descent as defined by the negative of the gradient. The BP algorithm has powerful local search capability but has a few drawbacks. Since the objective function of ANN is a multi-modal function [9] that has several local minima, the algorithm can get stuck into a local minimum. Moreover, it possibly has a slow convergence speed depending on the learning parameter values [4, 22–23, 28].

Global search methods are an alternative approach widely studied and applied as training methods for neural networks to overcome the limitation of the traditional gradient-based algorithm. Over the last decade, many researchers have developed global techniques based on natural inspiration that are population-based and capable of parallel calculations. They do not require the derivative computation and can provide the global minimum for the multi-modal objective functions of ANN.

The Differential Evolution (DE) algorithm is one of those popular global approaches. The method is an efficient population-based technique developed by Rainer Storn and Kenneth Price [26] for optimization problems over continuous domains. Many DE variants were proposed based on various modifications of initialization, mutation, crossover, selection, and hybridization schemes [20]. Mezura et al. [16] empirically compared some DE variants to solve global optimization problems. The results showed that the rand/1/bin mutation scheme performs well for multimodal functions. The DE is an attractive optimization tool compared with other evolutionary algorithms due to ease of implementation, robustness, and a few control parameters. The beneficial usages of the DE algorithm for training networks are its ability to reach a global minimum of the objective function, quick convergence, and a small number of parameters of the network settings. Moreover, it is possible to adjust some essential parameters during the process execution. Also, the DE can train the network with non-differentiable transfer functions where the gradient information is unavailable.

In this study, we concern with the learning algorithm of the feed-forward neural network using the DE. We study the capabilities of the network parameters, i.e., weight bounds and scaling of activation function, which affects the performances of DE for finding the solution in terms of search space and output space. The automatic adjustment of the weight bounds in the mutation processing stepand various scale parameters in the activation function are studied.

We organize the rest of this paper into the following sections. Section 1 provides the literature reviews concerning training ANN using the DE algorithm and the influences of weight bounds. The DEAW algorithm, an implementation of DE with the weight bound adjustment as a training approach, is described in section 2. Then, we use the DEAW algorithm to solve the function approximation problems. The preliminary and comparison experiments, results, and discussion are presented in Section 3. Finally, section 4 is a conclusion and future work.

# 1. Literature reviews

## 1.1. Training neural networks using differential evolution

In 2008, Gao and Liu [10] proposed a modified DE by introducing the mutation operator coupled with Back-propagation (BP) training algorithm to solve the exclusive-OR (XOR) problem and function approximation. The method can reduce the training time, improve the training accuracy, and perform more steadily than the classical BP. Subudhi and Jena [27] solved a non-linear system identification problem using an improved DE with Lavenberg Marquardt (LM) algorithm to train the ANN. The method gives better results in terms of convergence speed and identification errors. Garro et. al. [11] applied the classical DE to ANN for solving the non-linear pattern classification problems. The algorithm can search for optimal synaptic weights by employing a few parameters to tune and perform better than the PSO algorithm on the UCI machine learning benchmark repository [31]. Morse and Stanley [19] also applied the self-adaptive DE algorithm (SDE) to train the ANN. The parameters $F$ and $CR$ of the DE are adaptively adjusted. The SDE gives better results when compared to training ANN by GA algorithm and standard DE on four sets of the UCI dataset. Si et al. [25] presented a DEGL approach to combine global and local mutation steps to create a candidate population vector using the mutation probability adaptation to balance the searchability. They tested the method on four benchmark functions and seven classification problems. The proposed method shows superior performance in less complex networks with a small number of generations compared to the classical DE algorithm. Comparative performances of a neural network trained with variant DE also have been studied. Baioletti et al. [1] tested various combinations of self-adaptive methods (i.e., JDE, JADE, ShaDE, L-ShaDE, MAB-ShaDE, SAMDE), mutation, and crossover operators on some well-known classification problems. The experiments showed that the results from the neural network obtained with DE training are better and more robust than those from back-propagation.

Nevertheless, Piotrowski [21] studied the performance of variant DE such as DEGL, DE-SG, DEGL-Epitr, JADE, SADE, SspDE, Trig-DEGL, Trig-DEGL-Epitr, and the empirical experiments showed that various DE algorithms fell into stagnation during the training of ANN. Moreover, the methods performed poorer than the classical Levenberg-Marquardt algorithm. The stagnation of DE occurs because of the undesired effect of the lack of difference vectors of small magnitude; in other words, the population stops proceeding toward the optimum even though the population diversity remains high. The paper showed that the appropriate range initialization and bound limitation strongly influence speed and efficiency for exploring the solution and are critical to convergence. In that research, they demonstrated that the smaller range and the broader bound gave the best results. By using the set-up, initial the weights with [-1,1] and limit the bound to [-1000,1000], during the beginning stage, the individual disperses rapidly in the decision space, and the magnitude of the difference vector increase, irrespective of DE variant used; however, the improvement slows down during the later stage of the run and leads the algorithm to fall into stagnation. However, several works on training ANN using the DE method did not investigate how to calibrate the weight bound that significantly affects the process of finding the solutions.

## 1.2. The influence of weight bound

Since the solutions of network training are the synaptic weights in various ranges, DE suffers from the problem of the bound and size of search space [21]. The population-based method needs to search the solution space. It is not only the bounds of the solution that should limit during the initialization but also the diversity of initial weights should vary to cover all over the solution space. Bartlett [2-3] proposed that, by computation theory, the number of training data growing linearly with the number of adjustable parameters leads to good generalization performance. The performance also depends on the bound of the weights rather than the number of the weight connections. The proof also supports heuristics that attempt to keep the weight vectors small during training. Ismailov [13] referred to many previous works that the weights are not necessary a large magnitude. Then the author proposed the sets of weights consisting of a finite number of directions. The result shows that the weights vectors can do well approximation but not always possible. Hahm and Hong [12] mentioned that the weights in the neural networks vary; hence it is too difficult to be applied in applications. In their work, they showed that a network with suitable fixed weights and a sufficient number of neurons can approximate any continuous function over a compact interval.

In 2014, H. Migdady [17] proved the delta rule for hidden and input weights to help understand and explain the behavior of the weight vectors in the feed-forward neural networks with BP. The proof shows that the weight vectors in the neural network are upper bounded, i.e., do not approach infinity. Jesus et al. [14] studied the effects of the initial configuration of weights on the training and activation function of neural networks. They found that the efficiency of the learning process depends on fine-tuning the weight vectors of the networks. In the appropriate case, the networks always converge to the neighborhood of their initial configuration. Cong et al. [6] also analyzed the effect of the initial weights vector in the learning process by BP. The result shows that the process tends to get stuck into the local minima if the weights start from the area which does not contain a global minimum.

Therefore, the weight vectors of the neural networks should be initialized in a small magnitude and near the global minimum. They should be limited by a suitable fixed bound; otherwise, fine-tuned within a small range.

Another essential factor that involves the weights of ANN is the activation function. Many functions have been proposed for different tasks, for example, binary function, radial basis function, and ReLu function, but the most widely used function is the sigmoid function. The sigmoid function consists of 3 parameters that affect the range of the outputs as illustrated in the figure 1.

As shown in figure 1, if input $x_1$ and $x_2$ are slightly different values, a small parameter $c_1$ gives a smoother different output than a large one which provides rapid change. Increasing the parameter $c_1$ in the ANN training by DE application for approximation and classification, the magnitude of the difference of output vectors will be increased, thus, leading the individual population to explore the search space rapidly. Therefore, we investigate the various values of parameter $c_1$, called the activation scale.

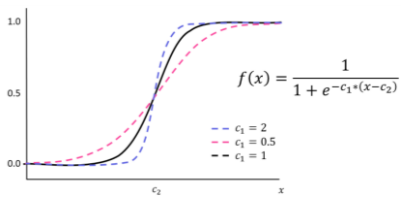


*Fig. 1. Basic sigmoid function. The 3 parameters are $x, c_1$ and $c_2$. $x$ is an input of the function, $c_1$ affects the slope of the function and $c_2$ is a translation of axes*

## 2. Background and methodology

### 2.1. Feed-forward neural network

In this work, the Multilayer perceptron (MLP) is a general structure of our study. MLP is a feed-forward neural network consisting of multiple layers: an input layer, one or more hidden layers, and an output layer. Each layer has nodes where each node is fully weight interconnected to all nodes in the subsequent layer as shown in figure 2.

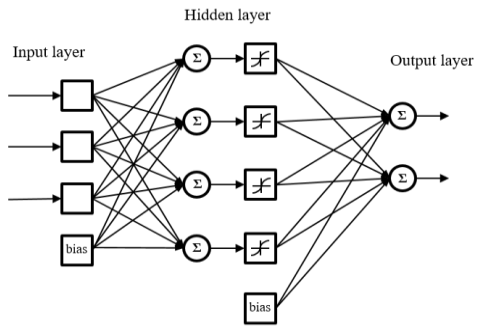


*Fig. 2. Feed-forward neural network model*

An MLP transforms the inputs into the outputs through the non-linear function; called the transfer function or activation function, expressed by:

$$x_h = f_1([x_i],[w_{i,h}]) = f_1\left(\sum_{i=1}^{d}(x_i * w_{i,h})\right) \quad (1)$$

$$x_o = f_2([x_h],[w_{h,o}]) = f_2\left(\sum_{h=1}^{nh}(x_h * w_{h,o})\right) \quad (2)$$

where $f_1, f_2$ are the activation functions of the hidden nodes and the output nodes, respectively. $x_h$ and $x_o$ are the output of each hidden node $h$ and output node $o$. $w_{i,h}$ is a connecting weight between the input $i$ and the hidden node $h$ while $w_{h,o}$ connects between the hidden node $h$ and the output $o$. In general, the activation function applied to the hidden node is the sigmoid function and that for the output is usually a linear function. The functions are expressed as:

Sigmoid function

$$\text{sigmoid}(x) = \frac{1}{1+e^{-x}} \quad (3)$$

Linear function

$$\text{linear}(x) = x \quad (4)$$

where $x$ is a value or a vector.

Since the ANN learns the mathematical model by training the network, the training rule is essential for a learning algorithm. The updating rules determine how connection weights are changed. The learning algorithm finds the optimal weights by minimizing the objective function defined by the distance error between the target value and the output from the network. Let the weights vector be $W = [W_1, W_2]$, where $W_1 = [w_{i,h}]$ and $W_2 = [w_{h,o}]$. The ANN find the optimal solutions by minimizing the sum of error:

$$E(W) = \sum_{d \in D}\left(t_d - F(x_d, W)\right)^2 \quad (5)$$

where $D$ is a set of training data and $d$ is the index of each training data. The target and output values are $t_d$ and $F(x_d, W)$, respectively. The output $F(x_d, W)$ can be calculated by

$$F(x_d, W) = f_2(f_1(x_d, W_1), W_2) \quad (6)$$

### 2.2. Differential evolution algorithm

Differential evolution algorithm is a population-based optimization method derived from the Genetic algorithm (GA). The method consists of three operations, i.e., mutation, crossover, and selection for generating new candidate solutions. Unlike GA, the weight called 'Scaling Factor: $F$' multiplies the difference between the randomized two population vectors to add to the third one and obtain the mutant vector. The DE crossover operator uses a crossover probability; named 'Crossover Rate: $CR$' in the range of [0,1] to combine the mutant vector with the target vector to create a trial vector. In selection, the trial candidate vector replaces the target vector if it gives a superior solution; otherwise, the original candidate remains unchanged. Many variant DE methods are different in the step of mutation and crossover [1, 7, 8]. In this work, we apply the basic mutation scheme called DE/rand/1/bin to avoid the effect of other improvements to the DEAW performance. The following steps describe the DE algorithm.

- Step I: (Initialization) Randomly initial population vectors $x_i$ ; $i = 1, \dots, NP$
- Step II: (Mutation) Generate a mutant vector $v_i$ by adding weighted difference between two population vectors to a third one. The equation can be expressed as:

$$v_i = x_{r1} + F * (x_{r2} - x_{r3}) \quad (7)$$

  where $x_{r1}, x_{r2}, x_{r3}$ are 3 randomized distinct vectors and different from $x_i$, and $F$ is a scaling factor in the range [0.5,1].
- Step III: (Crossover) Create a trial vector $u_i$ from $x_i$ and $v_i$ by

$$IC = rand(1, ndim) \quad (8)$$

$$u_{i,j} = \begin{cases} v_{i,j} & if \quad \text{rand}(0,1) \le CR \ or \ j = IC \\ x_{i,j} & if \quad \text{rand}(0,1) > CR \end{cases} \quad (9)$$

  where $(i,j)$ is an element $j^{th}$ of vector $i$ and $CR$ in [0,1] is a crossover rate.
- Step IV: (Selection) Choose the vector for the next generation by comparing the objective function values of $x_i$ and $u_i$:

$$x_i^{new} = \begin{cases} x_i & if \quad f(x_i) < f(u_i) \\ u_i & if \quad otherwise \end{cases} \quad (10)$$

  Repeat Step II–IV until reaching the termination conditions.

### 2.3. Training neural network by using differential evolution

Applying DE to train the network, the vectors of connecting weights in ANN are used as the individual population vector of the DE algorithm, i.e., a set of population vectors $W = \{W_i\}$, where $i = 1, \dots, NP$ and $NP$ is the number of populations. Let $X = \{x_d\}, T = \{t_d\}$ where $d = 1, \dots, ndata$ are the set of training and target data vectors, respectively. $F(\cdot)$ is the composite of activation functions in the network and $F(x_d, W_i)$ is an output corresponding to $x_d$ and $W_i$. In each iteration, the current weight vectors of ANN are obtained from the DE approach by reducing the error between the target $T$ and the output obtained from $F(X, W_i)$ in the selection process.

As described in section II, the range of the weights affects the approximated result of the activation function. Thus, the performance of the DE algorithm used for ANN training significantly depends on the initialization range and the bounds. The ANN training algorithm should initialize the weights in a small bound and extend it later.

In our study, the DEAW algorithm initializes both ranges and bounds of the weights by small values at the beginning. Then, the algorithm adjusts the bound corresponding to the mutant vectors and the number of the current iterations in the process. If a component value of a mutant vector is greater than the upper bound or less than the lower bound, then the bound is extended. As a result, the search space gradually broads, and the magnitude of the difference vector also slightly increases. In practice, it is difficult to determine where the range is satisfied unless several empirical tests.

The DEAW algorithm applies an adaptive process to the mutation step for automatic bound adjustment. The amount of extending rate depends on the current iteration. This strategy increases the rapid exploration ability of the algorithm at the beginning stage and decreases it at the later stage. The equation for adjustment is expressed as:

$$ext\_rate = \frac{1}{iter} \quad (11)$$

where $iter$ is the number of current iteration. Algorithm in the figure 3 shows our enhanced DE with adaptive weights bound for training ANN. Also, table 1 represents all notations.

(Initialization)
$W \leftarrow W_i, i = 1, \ldots, NP$
*initial* $Fbest, W_{best}$
*Do until reaching termination conditions*:
**while** $i \leq NP$ **do**
    (Mutation)
    $r1, r2, r3 \leftarrow random \in [1, NP]$
    $r1 \neq r2 \neq r3 \neq i$
    $V_i \leftarrow W_{r1} + F \times (W_{r2} + W_{r3})$
    (Bound adjustment)
    *loop1*:
    **if** $j \leq ndim$ **then**
        **if** $V_{i,j} > UB$ **then**
            $UB \leftarrow UB + ext\_rate$
            $V_{i,j} \leftarrow$ random $\in [LB, UB]$
        **end if**
        **if** $V_{i,j} < LB$ **then**
            $LB \leftarrow LB - ext\_rate$
            $V_{i,j} \leftarrow$ random $\in [LB, UB]$
        **end if**
    **end if**
    $j \leftarrow j + 1$
    **goto** *loop1*.
    (Crossover)
    $IC \leftarrow random \in [1, ndim]$
    *loop2*:
    **if** $j \leq ndim$ **then**
        **if** *rand(0,1)*$\leq$ CR || $j = IC$ **then**
            $U_{i,j} \leftarrow V_{i,j}$
        **else**
            $U_{i,j} \leftarrow W_{i,j}$
        **end if**
    **end if**
    $j \leftarrow j + 1$
    **goto** *loop2*.
    (Selection)
    $Err_{U_i} \leftarrow 0$
    *loop3*:
    **if** $d \leq ndata$ **then**
        $Err_{U_i} \leftarrow Err_{U_i} + (t_d - F(x_d, U_i))^2$
    **end if**
    $d \leftarrow d + 1$
    **goto** *loop3*.

    $Err_{U_i} \leftarrow \frac{1}{ndata} \times Err_{U_i}$
    **if** $Err_{U_i} < Err_{W_i}$ **then**
        $W_i \leftarrow U_i$
        $Err_{W_i} \leftarrow Err_{U_i}$
    **end if**
    **if** $Err_{U_i} < Fbest$ **then**
        $Fbest \leftarrow Err_{U_i}$
        $W_{best} \leftarrow U_i$
    **end if**
    $i \leftarrow i + 1$
**end while**

*Fig. 3. DEAW algorithm*

*Table 1. Notation*

| Notation | Detail |
|---|---|
| $NP$ | population size |
| $ndata$ | number of training data |
| $ndim$ | dimension of the weight vector where $ndim = [(indim + nbias) \times nhidden] + [(nhidden + nbias) \times outdim]$ |
| $indim$ | dimension of the inputs |
| $outdim$ | dimension of the outputs |
| $nhidden$ | number of hidden nodes |
| $nbias$ | number of bias nodes |
| $W$ | a set of weights vectors; $W = \{W_i\,; i = 1, \ldots, NP\}$ |
| $X$ | a set of input data; $X = \{x_d\,;\, d = 1, \ldots, ndata\}$ |
| $T$ | a set of targets corresponding to $X$; $T = \{t_d\,;\, d = 1, \ldots, ndata\}$ |
| $UB, LB$ | upper and lower bounds, respectively |
| $F$ | a scaling factor |
| $CR$ | a crossover rate |
| $ext\_rate$ | extending rate |
| $F(x, W)$ | the output of ANN for $(x, W)$ |
| $Fbest$ | minimum error obtained by current best weight vector |
| $W_{best}$ | the current optimal weight vector |

## 3. Experimental results and discussion

To verify the efficiency of our proposed method and control parameter values, we apply the DEAW algorithm to train the feed-forward neural network for solving function approximation problems. The details of the experiments are described in the following subsections.

### 3.1. Experimental setup

In this work, we apply the DE as a learning algorithm to feed-forward neural networks with one hidden layer. The number of nodes in the input layer depends on each problem and includes one bias. The number of hidden nodes is varied appropriately depending on the complexity of the problem and also includes one bias. The algorithm applies the sigmoid function to the hidden nodes while the linear function to the output nodes.

Each experimental study performs 30 runs. We use a trimmed mean method for calculating the average values of the results to eliminate the outliers. In our tests, we trim 15% of the results, i.e., five runs for both best and worst cases. The maximum iteration depends on the training dataset and the complexity of the problem. The configuration of DE is simple. The algorithm uses a basic scheme called DE/rand/1/bin and general control parameters, $F = 0.5$, $CR = 0.9$. The population size is 50 for all experiments. More individual settings for each study are described in the following subsections.

### 3.2. Function approximation problems

To observe the performance of our proposed enhancement, we first apply the DEAW algorithm to the 1D function approximation. Two testing functions are described as:

$$f_1(x) = \sin(2\pi x) \times (4\pi x) \tag{12}$$

$$f_2(x) = \sin(2\pi x) \times \sin(3\pi x) \times \sin(5\pi x) \tag{13}$$

The data of each function is uniformly generated on $x \in [0,1]$, 100 data for training and 199 testing data including the training data. As illustrated in figure 4, both functions are multimodal with 6 and 10 local maxima/minima, respectively.

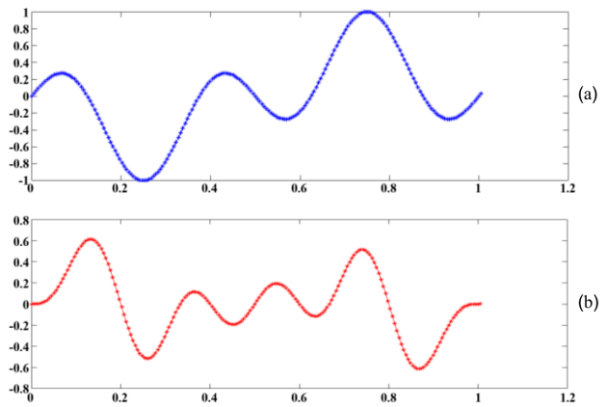


*Fig. 4. Illustrated graphs of the functions: (a) $f_1$ and (b) $f_2$ on [0,1]*

This study concerns the effects on the ANN performance caused by the weight bound and the activation scale. Both the initial and limit of weight bound are essential for the efficiency of the performance of ANN. Thus, we conducted two experiments. First, we observed the effects of different combination of fixed limit bounds with varied activation scales. Fig. 5(a) shows the values of the Sigmoid function generated on the various interval ranges. The graphs generated on the limit bounds have the similar shape but different output ranges. A small bound gives small output ranges, whereas a wide bound gives a larger one. However, as seen in the figure, the outputs are almost not changed where $x < -10$ and $x > 10$. Thus, we only investigated the limit bound settings, $[-1,1], [-10,10], [-20,20]$ and $[-30,30]$ for our experiments.

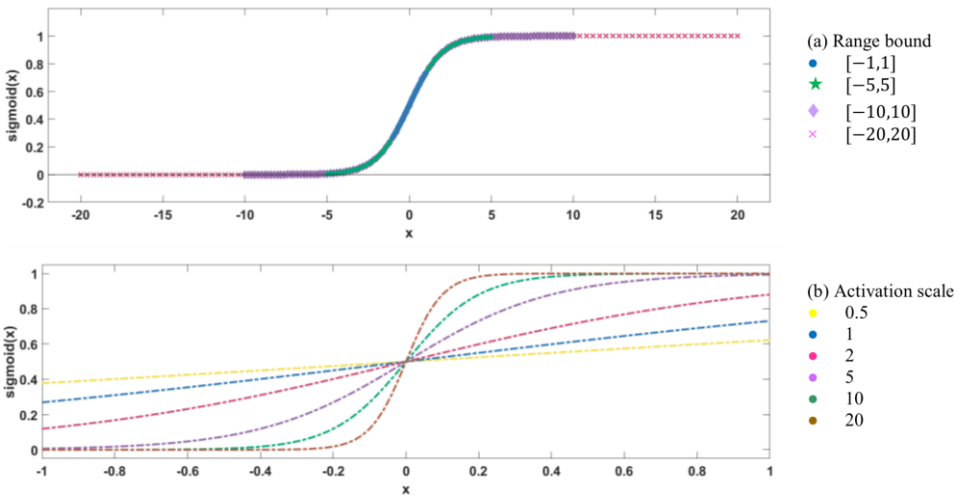


*Fig. 5. (a) The outputs from Sigmoid function as an activation function with scale =1. (b) Each range of bound also gives the same shapes but different output ranges. The outputs obtained by various activation scales express similar shapes but different slopes*

Fig. 5(b) shows the output obtained by varying the scale of activation function. The outputs give similar shapes but different slopes. Large scales show extreme slope while small scales show slight slope. In this study, we then use 1, 10, 20, and 30 as observation scales. Note that a general ANN usually uses [-1,1] for the bound and 1 for the activation scale. Second, we initialized a small range of weight bound, i.e $[-2,2]$ or $[-10,10]$ and then the range is gradually extended during the mutation process. For the ANN structure, we applied a structure 2-10-1 for this experiment. The algorithm runs for 50000 iterations for function $f_1$ and 150000 for $f_2$, or the mean error (VTR) reaches 0.5e-3. Tables 2 and 3 illustrate the results of the training and testing. The best scale for each bound represented in bold.

### 3.2.1. The effects of varying ranges of weight bound and activation scales

As shown in tables 2 and 3, a standard configuration, limit weight bound as $[-1,1]$ and activation scale as 1, gives unsatisfied results, i.e. the errors are greater than the VTR. In table 2, the results of the $f_1$ approximation obtained by limiting the bound to $[-1,1]$ and $[-10,10]$ with scale 1 show unsuccessful converge to the VTR. Nevertheless, increasing of activation scale can improve the accuracy but has to trade-off with high standard deviation values, i.e., unreliable results. For the limit bounds $[-20,20]$ and $[-30,30]$, the results show that scale 1 gives acceptable errors. Then, increasing the activation scale increases a small error rate.

Similarly, the results obtained from the second function, $f_2$, are presented in table 3. The bound limit to $[-1,1]$ with the scale 1 of the activation function also gives an unsatisfied error, but increasing the scale shows better performance. For the ranges $[-10,10]$, $[-20,20]$, and $[-30,30]$, increasing the activation scale to 10 gives the best result, then the efficiency decreases slightly. These experiments express the satisfying results using a suitable fixed limit range of bound with a regular activation scale 1. But, if the bound is improper, increasing the scale to the large one improves the accuracy of the results by trading off a higher standard deviation (SD).

*Table 2. Training and testing result of $f_1$ with different fixed limit bounds and various activation scales*

| | Train | Test | Train | Test | Train | Test | Train | Test |
|---|---|---|---|---|---|---|---|---|
| Bound | [-1,1] | | | | | | | |
| Act. Scale | 1 | | 10 | | 20 | | 30 | |
| Mean | 2.1379E-01 | 2.1509E-01 | 8.7346E-02 | 8.6543E-02 | 3.4065E-02 | 3.4196E-02 | **4.9487E-03** | **4.8475E-03** |
| SD | 1.0520E-04 | 1.0724E-04 | 2.2854E-03 | 2.3133E-03 | 4.4727E-03 | 4.5838E-03 | 3.4863E-03 | 3.6537E-03 |
| %SD | 0.0492 | 0.0499 | 2.6165 | 2.6730 | 13.1299 | 13.4044 | 70.4473 | 75.3722 |
| S/F | 0/30 | | 0/30 | | 0/30 | | 0/30 | |
| Bound | [-10,10] | | | | | | | |
| Act. Scale | 1 | | 10 | | 20 | | 30 | |
| Mean | 4.7658E-02 | 4.7415E-02 | 1.3538E-04 | 1.3512E-04 | 1.3054E-04 | 1.3103E-04 | **1.2804E-04** | **1.2847E-04** |
| SD | 2.6946E-02 | 2.6802E-02 | 8.4570E-05 | 8.2669E-05 | 6.8728E-05 | 6.7929E-05 | 5.8379E-05 | 5.8734E-05 |
| %SD | 56.5402 | 56.5268 | 62.4674 | 61.1826 | 52.6479 | 51.8407 | 45.5928 | 45.7201 |
| S/F | 0/30 | | 25/5 | | 25/5 | | 25/5 | |
| Bound | [-20,20] | | | | | | | |
| Act. Scale | 1 | | 10 | | 20 | | 30 | |
| Mean | **1.2673E-04** | **1.2489E-04** | 1.6685E-04 | 1.6779E-04 | 1.4308E-04 | 1.4447E-04 | 2.3952E-04 | 2.4720E-04 |
| SD | 3.7550E-05 | 3.495E-05 | 5.7644E-05 | 5.8589E-05 | 5.2012E-05 | 5.2410E-05 | 1.7268E-04 | 1.8891E-04 |
| %SD | 29.6301 | 27.988. | 34.5478 | 34.9179 | 36.3523 | 36.2783 | 72.0959 | 76.4200 |
| S/F | 30/0 | | 30/0 | | 26/4 | | 22/8 | |
| Bound | [-30,30] | | | | | | | |
| Act. Scale | 1 | | 10 | | 20 | | 30 | |
| Mean | **1.2911E-04** | **1.2750E-04** | 1.5695E-04 | 1.5805E-04 | 1.4834E-04 | 1.4948E-04 | 1.3211E-04 | 1.2271E-04 |
| SD | 4.2856E-05 | 4.3647E-05 | 6.567E-05 | 6.5685E-05 | 7.2725E-05 | 7.4669E-05 | 5.639E-05 | 4.1808E-05 |
| %SD | 33.1950 | 34.2331 | 41.5588 | 41.5588 | 49.0256 | 49.9537 | 42.4949 | 34.0699 |
| S/F | 27/3 | | 30/0 | | 29/1 | | 27/3 | |

*Table 3. Training and testing results of $f_2$ with different fixed limit bounds and various activation scales*

| | Train | Test | Train | Test | Train | Test | Train | Test |
|---|---|---|---|---|---|---|---|---|
| Bound | [-1,1] | | | | | | | |
| Act. Scale | 1 | | 10 | | 20 | | 30 | |
| Mean | 8.5423E-02 | 8.6.63E-02 | 5.8407E-02 | 5.8800E-02 | 2.4274E-02 | 2.4286E-02 | **9.0211E-03** | **9.0736E-03** |
| SD | 4.1820E-05 | 4.4285E-05 | 3.0044E-04 | 3.3011E-02 | 5.7640E-04 | 6.1962E-04 | 1.3748E-04 | 1.5214E-04 |
| %SD | 0.0490 | 0.0515 | 0.5144 | 0.5614 | 2.3745 | 2.5513 | 1.5239 | 1.6767 |
| S/F | 0/30 | | 0/30 | | 0/30 | | 0/30 | |
| Bound | [-10,10] | | | | | | | |
| Act. Scale | 1 | | 10 | | 20 | | 30 | |
| Mean | 3.0107E-02 | 3.0446E-02 | **1.8191E-04** | **1.7828E-04** | 2.8801E-04 | 2.8779E-04 | 2.4614E-04 | 2.4672E-04 |
| SD | 2.6566E-03 | 2.7404E-03 | 1.0940E-04 | 1.0852E-04 | 2.3135E-04 | 2.3233E-04 | 1.5117E-04 | 1.5087E-04 |
| %SD | 8.617 | 9.0009 | 60.1378 | 60.8799 | 80.3295 | 80.7274 | 61.4153 | 61.1510 |
| S/F | 0/30 | | 27/3 | | 23/7 | | 24/6 | |
| Bound | [-20,20] | | | | | | | |
| Act. Scale | 1 | | 10 | | 20 | | 30 | |
| Mean | 3.9421E-03 | 3.9733E-03 | **3.4243E-04** | **3.4050E-04** | 4.3055E-04 | 4.3112E-04 | 4.0058E-04 | 3.9842E-04 |
| SD | 3.7996E-03 | 3.8353E-03 | 3.3185E-04 | 3.3096E-04 | 4.3222E-04 | 4.3536E-04 | 5.1463E-04 | 5.1377E-04 |
| %SD | 96.3855 | 96.5287 | 96.9113 | 97.2004 | 100.3894 | 100.9824 | 128.4717 | 128.9524 |
| S/F | 11/19 | | 22/8 | | 20/30 | | 22/8 | |
| Bound | [-30,30] | | | | | | | |
| Act. Scale | 1 | | 10 | | 20 | | 30 | |
| Mean | 1.4220E-03 | 1.4105E-03 | **7.9663E-04** | **7.9655E-04** | 1.3334E-03 | 1.3472E-03 | 1.1072E-03 | 1.1647E-03 |
| SD | 9.0660E-04 | 9.2014E-04 | 9.7159E-04 | 9.8190E-04 | 1.7056E-03 | 1.7215E-03 | 1.3743E-03 | 1.4455E-03 |
| %SD | 63.7547 | 65.2372 | 121.9622 | 123.2691 | 127.9126 | 127.7852 | 124.1269 | 124.1072 |
| S/F | 10/20 | | 18/12 | | 16/14 | | 16/14 | |

### 3.2.2. The efficiency of extendable weight bound

*A. The performance on 1D-function approximation*

As shown in experiment 1, proper limit bounds are different for $f_1$ and $f_2$. Our DEAW algorithm with extendable weight bound modification is applied to demonstrate the efficiency of adjustable bound. Since the most appropriate range for both functions is $[-20,20]$, the initial margin of the bound is set to $[-2,2]$ and $[-10,10]$ and also combined with various activation scales. The structure of neural networks and termination conditions are the same as in experiment 1. The results of the method applied to $f_1$ and $f_2$ are shown in tables 4 and 5, respectively. The best scale for each bound represented in bold.

Table 4 shows that by setting the initial bound to [-2,2] with the scale 1, the error cannot reach the VTR while success in the setting [-10,10]. Both initial bounds give the absolute values of weight components in the interval [10,20], which is similar to the observation in experimental result 1. Larger activation scales combined with the DEAW algorithm provide better results for a small initial range while giving a few differences for a broader initialization, but the standard deviation becomes higher if the scale exceeds. The final bound is also the same as obtained by Experiment 1, i.e. $[-20,20]$. In addition, the number of success cases using the DEAW algorithm increases, and the error rates decrease.

From table 5, the results also give similar performance. The narrow initial bound provides better accuracy when the activation scales increase; however, an exceedingly large scale raises the high standard deviation. The final absolute values of the weight components lie in [20,30], the same as experiment 1.

Moreover, the DEAW algorithm also performs better in the number of success cases and the error rates compared to previous experiments. Hence, the results of both experiments show that increasing the scale of activation function can improve the efficiency of unsuitable fixed limit bound; however, it trades off higher standard deviation where the scale exceeds. In addition, gradually and adaptively adjusting the bound of the weights leads to better performance and more efficient results than the fixed limit bound.

*B. The performance on 2D-function approximation*

To verify the performance on 2D-function approximation problem, we applied the DEAW method to approximate a complex sine function expressed as:

$$f_3(x_1, x_2) = 0.5(sin(5x_1) + sin(5x_2)) \tag{14}$$

where the data is uniformly generated on $x_1, x_2 \in [-1,1]$, 100 data for training and 199 testing data including the training data. For the ANN structure, we used a structure 2-10-1 with activation scale 1 for this experiment and set the iterations to 10000.

The tests are divided into 2 steps. First, we applied the range [-2,2] as a fixed bound and adjustable bound with the activation scale 1. Then, we observed the final range of adaptive bound and used it as an appropriated fixed bound. The results of 2D-function approximation are presented in the table 6 and also illustrated in figure 6.

*Table 4. Training and testing results of $f_1$ by using small initial bound with extendable capability and various scales of activation function*

| | Train | Test | Train | Test | Train | Test | Train | Test |
|---|---|---|---|---|---|---|---|---|
| Ini. Bound | [-2,2] | | | | | | | |
| Act. Scale | 1 | | 10 | | 20 | | 30 | |
| Mean | 7.1854E-02 | 7.1033E-02 | 1.0772E-04 | 1.0749E-04 | **9.9939E-05** | **1.0027E-04** | **9.9954E-05** | **1.0008E-04** |
| SD | 7.0817E-03 | 7.0683E-03 | 2.3063E-05 | 2.3675E-05 | 4.7903E-08 | 5.2718E-07 | 2.1096E-08 | 7.9188E-07 |
| %SD | 9.8556 | 9.9508 | 21.4108 | 22..244 | 0.0479 | 0.5257 | 0.0211 | 0.7912 |
| Best range | - | | [0,10] , (10,20] | | **[0,10] , (10,20]** | | **[0,10] , (10,20]** | |
| S/F | 0/30 | | 30/0 | | 30/0 | | 30/0 | |
| Ini. Bound | [-10,10] | | | | | | | |
| Act. Scale | 1 | | 10 | | 20 | | 30 | |
| Mean | **9.9921E-05** | **9.7.36E-05** | 1.3479E-04 | 1.3562E-04 | 1.6926E-04 | 1.7040E-04 | 1.0465E-04 | 1.1441E-04 |
| SD | 9.1541E-08 | 2.6754E-06 | 5.1366E-05 | 5.2019E-05 | 1.3662E-04 | 1.3827E-04 | 1.4954E-05 | 4.2545E-05 |
| %SD | 0.0916 | 2.7572 | 38.1071 | 38.3574 | 80.7149 | 81.1425 | 14.2903 | 37.1848 |
| Best range | **(10,20] , (20,30]** | | (10,20] , (20,30] | | (10,20] , (20,30] | | (10,20] , (20,30] | |
| S/F | 30/0 | | 30/0 | | 24/6 | | 27/3 | |

*Table 5. Training and testing results of $f_2$ by using small initial bound with extendable capability and various scales of activation function*

| | Train | Test | Train | Test | Train | Test | Train | Test |
|---|---|---|---|---|---|---|---|---|
| Ini. Bound | [-2,2] | | | | | | | |
| Act. Scale | 1 | | 10 | | 20 | | 30 | |
| Mean | 2.7737E-02 | 2.7386E-02 | 2.3435E-04 | 2.3510E-04 | **1.0715E-04** | **1.0778E-04** | 1.6960E-04 | 1.7072E-04 |
| SD | 2.8388E-03 | 2.7984E-03 | 1.8049E-04 | 1.8150E-04 | 1.9345E-05 | 1.9620E-05 | 1.8635E-04 | 1.8790E-04 |
| %SD | 10.2349 | 10.2184 | 77.0168 | 77.2002 | 18.0548 | 18.2037 | 109.8780 | 110.0575 |
| Best range | - | | (10,20] , (20,30] | | **(10,20] , (20,30]** | | (10,20] , (20,30] | |
| S/F | 0/30 | | 24/6 | | 27/3 | | 23/7 | |
| Ini. Bound | [-10,10] | | | | | | | |
| Act. Scale | 1 | | 10 | | 20 | | 30 | |
| Mean | 1.7726E-03 | 1.7853E-03 | **3.0116E-04** | **2.9888E-04** | 3.6320E-04 | 3.6522E-04 | 3.3510E-04 | 3.3838E-04 |
| SD | 2.1968E-03 | 2.2189E-03 | 1.0539E-04 | 1.0301E-04 | 4.7594E-04 | 4.7803E-04 | 3.1736E-04 | 3.2125E-04 |
| %SD | 123.9316 | 124.2888 | 34.9953 | 34.4642 | 131.0420 | 130.8873 | 94.7069 | 94.9380 |
| Best range | (20,30] , (30,50] | | **(30,50] , (20,30]** | | (30,50] , (20,30] | | (30,50] , (20,30] | |
| S/F | 12/18 | | 24/6 | | 21/9 | | 19/11 | |

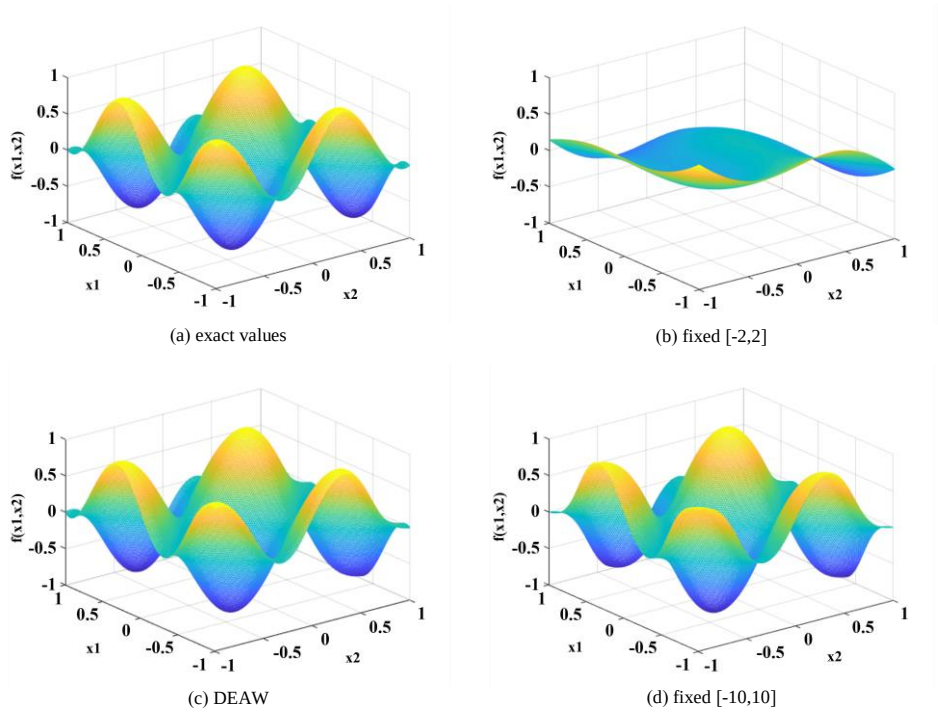


(a) exact values (b) fixed [-2,2]

(c) DEAW (d) fixed [-10,10]

*Fig. 6. Illustrated Graphs of Complex-sine function $f_3$: (a) exact values, (b) approximated values with fixed bound [-2,2], (c) approximated values obtained by the DEAW algorithm and (d) approximated valued with fixed suitable bound [-10,10]*

*Table 6. Training and testing results of Complex sine function using fixed and extendable bound*

| Complex sine function $f_3$ | | | | | | |
|---|---|---|---|---|---|---|
| Ini. Bound | [-2,2] | | [-2,2] | | [-10,10] | |
| capability | extendable | | fixed | | fixed | |
| Act. Scale | 1 | | 1 | | 1 | |
| No. hidden | 10 | | 10 | | 10 | |
| | Train | Test | Train | Test | Train | Test |
| Mean MSE | 5.520 E-04 | 7.870 E-04 | 1.521 E-01 | 1.554 E-01 | 1.706 E-05 | 4.403 E-04 |
| SD | 0.00058 | 0.00053 | 0.00368 | 0.00352 | 0.00001 | 0.00008 |
| Avg. range | UB | LB | - | | - | |
| | 9.12 | -9.53 | | | | |

As shown in table 6, the ANN with fixed bound [-2,2] cannot properly approximate the function, as illustrated in figure 6(b). By using the DEAW method, on the other hands, the error rate reaches to 5.520e-4 which can represent the function as shown in figure 6(c). The average of final bound obtained from the DEAW algorithm is in the range of [-10,10]. Applying this appropriated range gives the best performance.

### 3.2.3. The comparison experiments

*A. Comparison on 1D-function approximation problems*

Hereafter, we utilized the small initial bound, $[-2,2]$, and the activation scale, 10, to demonstrate the efficiency of the DEAW algorithm by applying it to other three 1-D functions used in [15, 18, 29-30]. Figure 7 (a), (b), (c) express the details of each function and table 7, 8, 9 show the comparison results with those work.

The results of the DEAW algorithm compared with the performance of PSO-based algorithms [18, 29] are shown in table 7. The compared methods are tested on $f_4$ using the weight bound [0,1] and varying numbers of hidden nodes. A small number of hidden nodes using PSO-BP gave the worst results. Their works presented the best MSE around 4e-5 using 7 hidden nodes, whereas the DEAW reached the VTR at 1e-5 using only 3 hidden-layer nodes with an adaptive weight-bound strategy.

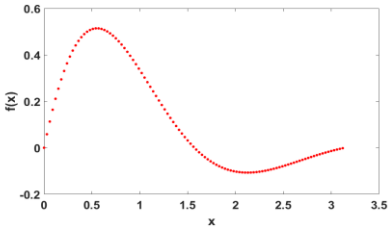


(a) $f_4(x) = \sin(2x) \times e^{-x}$ , $x \in [0, \pi]$
Training: identical sampling interval of 0.03 from $[0, \pi]$
Testing: identical sampling interval of 0.1 from $[0{,}02, \pi]$

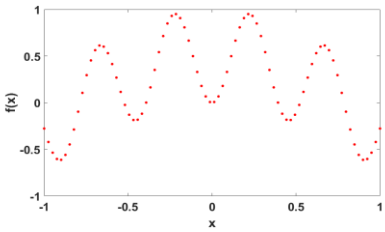


(b) $f_5(x) = \sin(8x) \times \sin(6x)$ , $x \in [-1,1]$
Training: uniformly sampled 80 points
Testing: uniformly sampled 160 points including testing points

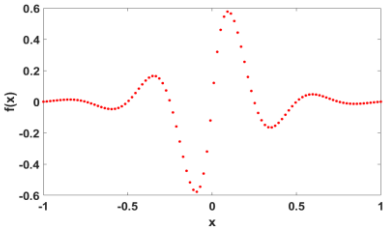


(c) $f_6(x) = \sin(4\pi x) \times e^{-|5x|}$ , $x \in [-1, 1]$
Training: uniformly sampled 100 points
Testing: uniformly sampled 200 points including testing points

*Fig. 7. Illustrated graphs of the 3 functions and details of each dataset*

For PSOGSA comparison, the results show that the DEAW method gives lower MSE. The difference results of both 3 and 7 hidden nodes provides the two-tailed P values less than 0.0001. By conventional criteria, this is considered to be statistically significant with 95% confidence interval.

Next, we applied the DEAW algorithm to compare with the performance in [15] using NN-based on the PSO learning method. The PSO initializes the weights in the fixed range $[-1,1]$. After running to 2000 iterations, see table. 8, RMSE of the PSO method reaches $0.29 \pm 0.02$, while the DEAW method also gives a better result at $0.23 \pm 0.03$. The t-test gives the two-tailed P value less than 0.0001. This difference is considered to be statistically significant with 95% confidence interval. However, both experiments are not satisfied the appropriate approximation, as illustrated in figure 8(a). The DEAW method then continues by running 30000 iterations with ten hidden nodes. As a result, the DEAW can reach the RMSE 1e-2, as illustrated in figure 8(b).

In the last experiment, we compared our method with the work based on the Radial basis function neural network (RBFN) and wavelet neural network (WNN) [30]. In that work, the researcher measured the accuracy by using the normalized square root mean square ($N_e$) calculated by the following equation:

$$N_e = \frac{1}{\sigma_y}\sqrt{\sum_{i=1}^{n}(y_i - f_i)^2} \tag{15}$$

where $y$ and $f$ are the target and output values of the network, respectively. $n$ is the total number of testing samples, and $\sigma_y$ is the standard deviation of the target values. A small $N_e$ indicates high accuracy. This experiment, the VTR setting is 1e-6.

As shown in the figure 9 the results indicate that our proposed method gives better approximated values than RBFN (upper-green) and expresses appreciated results as WNN (upper-magenta).

*Table 7. The comparison of PSO based method and our DEAW method on $f_4$*

| | PSO-BP [30] | | PSOGSA [18] | | DEAW | |
|---|---|---|---|---|---|---|
| Input/Output | 1/1 | | 1/1 | | 1/1 | |
| Bound | BP [-50,50], PSO [0,1] | | [0,1] | | Initial [-2,2] | |
| NP | 200 | | 200 | | 30 | |
| Max iteration | 200+1500 | | 500 | | 2000 | |
| Hidden nodes | 3 | 7 | 3 | 7 | 3 | 7 |
| Avg MSE | 4.8984e-04 | 1.4333e-04 | 9.6113e-03 | 6.7104e-03 | **9.8220e-06** | **9.9500e-06** |
| Med MSE | n/a | n/a | 9.9619e-03 | 5.4945e-03 | **9.8745e-06** | **9.9757e-06** |
| STD | n/a | n/a | 2.7267e-03 | 5.4070e-03 | **1.6755e-07** | **4.2176e-08** |
| Best MSE | 3.2781e-04 | 4.2074e-05 | 5.5411e-.3 | 9.5455e-04 | **9.4330e-06** | **9.8665e-06** |
| Worst MSE | **7.266e-04** | **2.7363e-04** | n/a | n/a | 9.9574e-06 | 9.9957e-06 |

*Table 8. The comparison of PSO based method and our DEAW method on $f_5$*

| | PSO [15] | DEAW | | |
|---|---|---|---|---|
| Input/Output | 1/1 | 1/1 | | |
| Bound | Fixed [-1,1] | Initial [-2,2] | | |
| NP | 30 | 30 | | |
| Hidden nodes | 8 | 8 | 8 | 10 |
| iteration | 2000 | 2000 | 30000 | 30000 |
| RMSE | 0.29±0.02 | 0.23±0.03 | 0.04±0.01 | 0.01±0.0001 |

*Table 9. The comparison of RBFN and WNN methods and DEAW method on $f_6$*

| | ANN [29] | | DEAW |
|---|---|---|---|
| | RBFN | WNN | |
| Input/Output | 1/1 | 1/1 | 1/1 |
| Hidden nodes | n/a | n/a | 7 |
| Bound | Fixed [-1,1] | Fixed [-1,1] | Initial [-2,2] |
| NP | - | - | 30 |
| iteration | n/a | n/a | 30000 |
| $N_e$ | 9.11658 | 0.207205 | 0.19260 |

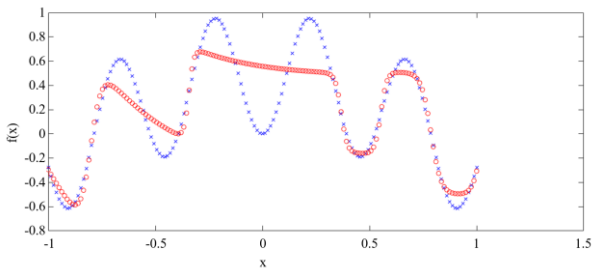


*(a)*

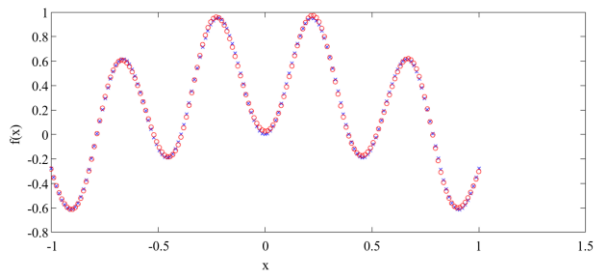


(b)

*Fig. 8. Illustrated graphs of different RMSEs. (a) RMES reaches 2e-1 while (b) reaches 1e-2*

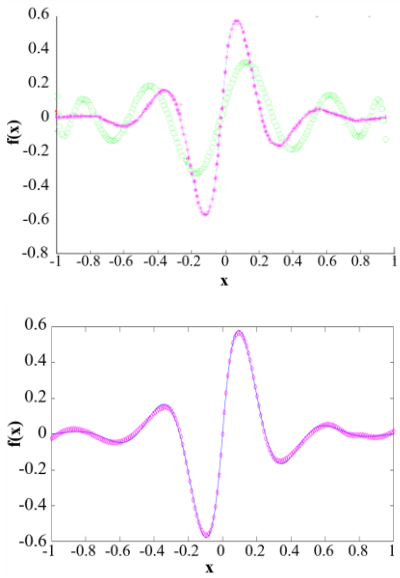


*Fig. 9. Illustrated graphs of RBFN and WNN [29] (upper) and DEAW algorithm (lower). The result of the RBFN method is represented in green while the results of WNN and DEAW methods are in magenta*

### *B. Comparison on 2D-function approximation problems*

For more comparison tests, we applied the DEAW algorithm to approximate the 2D functions which are used in [5]. The functions are represented as follows.

$$f_7(x_1, x_2) = \frac{3.2(1.25+\cos(5.4x_2))}{6+6(3x_1-1)^2} \tag{16}$$

$$f_8(x_1, x_2) = (x_1^2 - x_2^2)\sin(5x_1) \tag{17}$$

where the data is uniformly generated on $x \in [-1,1]$, 100 data for training. For the ANN structure, we used a structure 2-14-1 and 2-9-1 with activation scale 1 for this experiment of $f_7$ and $f_8$, respectively. The iteration is set to 30000.

In these experiments, the DEAW approximates the 2D-function $f_7$, $f_8$ to compare with MMWNN-GA method in [5]. As seen in table 10, the error rate of our proposed method reaches 4.41E-03 which is higher than the MMWNN-GA method. However, an illustration of the approximated values using the DEAW algorithm in figure 10 shows that the DEAW can suitably represent the function of $f_7$.

*Table 10. Comparison results of 2D-function $f_7$ using MMWNN-GA [5] and the DEAW method*

| | **MMWNN-GA** | **DEAW** |
|---|---|---|
| No. of Hidden nodes | 14 | 14 |
| Initial range | - | [-2,2] |
| Bound capability | fixed | extendable |
| MSE | 7.89E-04 | 4.41E-03 |

Next, the DEAW algorithm is demonstrated with the 2D-function $f_8$. The results in table 11 show that our proposed simple method approximates accurately as well as MMWNN-GA method. The approximation function of the DEAW algorithm displays in figure 11.

*Table 11. Comparison results of 2D-function $f_8$ using MMWNN-GA [28] and the DEAW method*

| | **MMWNN-GA** | **DEAW** |
|---|---|---|
| No. of Hidden nodes | 9 | 9 |
| Initial range | - | [-2,2] |
| Bound capability | fixed | extendable |
| MSE | 4.86E-03 | 4.09E-03 |

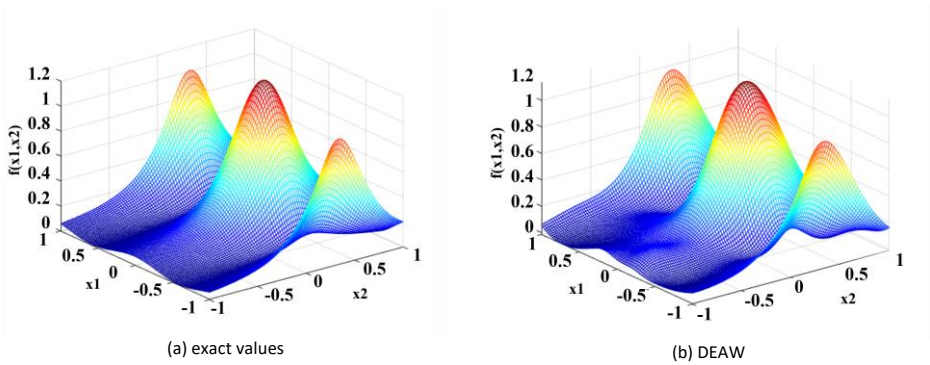


(a) exact values (b) DEAW

*Fig. 10. Graphs of 2D-function $f_7$ (a) exact values, (b) approximated values obtained by the DEAW algorithm*

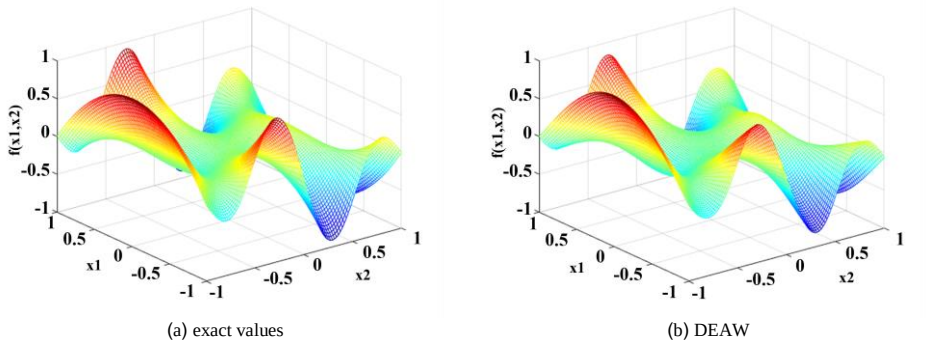


(a) exact values (b) DEAW

*Fig. 11. Graphs of 2D-function $f_8$ (a) exact values, (b) approximated values obtained by the DEAW algorithm*

## 4. Conclusions

This study applies an alternative approach for training the feed-forward neural networks relying on the differential evolution (DE) algorithm for global search abilities and to overcome the limitation of local search methods. Our DEAW algorithm improves the performance of the DE training by using small initial weight bounds and adaptive adjustment strategies in the mutation process. The proposed method gives more efficient results than using the fixed limit bound. Moreover, increasing the scale of the activation function improves the efficiency of unsuitable fixed limit bound. The DEAW can achieve the solution at high accuracy with simple configurations for solving function approximation problems. In addition, testing on 1D-functions, the method performs better than the compared BP and PSO-based training methods in term of accuracy and convergence. For the 2D-function problems, the proposed method gives comparative results to MMWNN-GA. Future work study could investigate applying the proposed weight adjustment strategies to other learning tasks such as classification and system identification problems.

## Acknowledgement

The Development and Promotion of Science and Technology Talents Project and Department of Mathematics, Faculty of Science, Khon Kaen University, Fiscal Year 2022.

## References

[1] Baioletti M., Di Bari G., Milani A., Poggioni V.: Differential Evolution for Neural Networks Optimization. Mathematics 8(1), 2020, 69 [http://doi.org/10.3390/math8010069].
[2] Bartlett P. L.: For Valid Generalization, the Size of the Weights is More Important than the Size of the Network. Proceedings of the 9th International Conference on Neural Information Processing Systems, 1996, 134–140.
[3] Bartlett P. L.: The sample complexity of pattern classification with neural networks: the size of the weights is more important than the size of the network. IEEE Transactions on Information Theory 44, 1998, 525–536 [http://doi.org/10.1109/18.661502].
[4] Chen L.: A global optimization algorithm for neural network training. Proceedings of International Conference on Neural Networks 1993, 443–446 [http://doi.org/10.1109/IJCNN.1993.713950].
[5] Chihaoui M., Bellil W., Amar C. B.: Multi Mother Wavelet Neural Network based on Genetic Algorithm for 1D and 2D Functions Approximation. Proceedings of the International Conference on Fuzzy Computation and International Conference on Neural Computation 2010, 429–434 [http://doi.org/10.5220/0003083704290434].
[6] Cong H., Nguyen N., Huy V. N., Bùi T.: The Influence of Initial Weights on Neural Network Training. Journal of Science and Technology 95, 2013, 18–25.
[7] Das S., Suganthan P. N.: Differential Evolution: A Survey of the State-of-the-Art. IEEE Transactions on Evolutionary Computation 15, 2011, 4–31 [http://doi.org/10.1109/TEVC.2010.2059031].
[8] Das S., Mullick S. S., Suganthan P. N.: Recent advances in differential evolution – An updated survey. Swarm and Evolutionary Computation 17, 2016, 1–30 [http://doi.org/10.1016/j.swevo.2016.01.004].
[9] Dhar V. K., Tickoo A. K., Koul R., Dubey B. P.: Comparative performance of some popular artificial neural network algorithms on benchmark and function approximation problems. Pramana 74, 2010, 307–324 [http://doi.org/10.1007/s12043-010-0029-4].
[10] Gao Y., Liu J.: A modified differential evolution algorithm and its application in the training of BP neural network. IEEE/ASME International Conference on Advanced Intelligent Mechatronics 2008, 1373–1377.
[11] Garro B. A., Sossa H., Vázquez R. A.: Evolving Neural Networks: A Comparison between Differential Evolution and Particle Swarm Optimization. Advances in Swarm Intelligence 2011, 447–454 [http://doi.org/10.1007/978-3-642-21515-5_53].
[12] Hahm N., Hong B. I.: An approximation by neural networkswith a fixed weight. Computers and Mathematics with Applications 47, 2004, 1897–1903 [http://doi.org/10.1016/j.camwa.2003.06.008].
[13] Ismailov V. E.: Approximation by neural networks with weights varying on a finite set of directions. Journal of Mathematical Analysis and Applications 389, 2012, 72–83 [http://doi.org/10.1016/j.jmaa.2011.11.037].
[14] Jesus R. J., Antunes M. L., da Costa R. A., Dorogovtsev S. N., Mendes J. F., Aguiar R. L.: Effect of the initial configuration of weights on the training and function of artificial neural networks. Mathematics 9, 2021, 1–16 [http://doi.org/10.3390/math9182246].
[15] Mendes R., Cortez P., Rocha M., Neves J.: Particle swarms for feedforward neural network training. Proceedings of the International Joint Conference on Neural Networks – IJCNN'02 2002, 1895–1899 [http://doi.org/10.1109/IJCNN.2002.1007808].
[16] Mezura M. E., Velázquez R. J., Coello C.: A comparative study of differential evolution variants for global optimization. GECCO 2006 – Genetic and Evolutionary Computation Conference 1, 2006, 485–492 [http://doi.org/10.1145/1143997.1144086].
[17] Migdady H.: Boundness of a Neural Network Weights Using the Notion of a Limit of a Sequence. International Journal of Data Mining and Knowledge Management Process 4, 2014, 1–8 [http://doi.org/10.5121/ijdkp.2014.4301].
[18] Mirjalili S. A., Hashim S. Z. M., Sardroudi H. M. Training feedforward neural networks using hybrid particle swarm optimization and gravitational search algorithm. Applied Mathematics and Computation 218, 2012, 11125–11137 [http://doi.org/10.1016/j.amc.2012.04.069].
[19] Morse G., Stanley K. O.: Simple Evolutionary Optimization Can Rival Stochastic Gradient Descent in Neural Networks. Proceedings of the Genetic and Evolutionary Computation Conference 2016, 477–484 [http://doi.org/10.1145/2908812.2908916].
[20] Mohamad F. A., Nor A. M. I., Wei H. L., Koon M. A.: Differential evolution: A recent review based on state-of-the-art works. Alexandria Engineering Journal 61(5), 2022, 3831–3872 [http://doi.org/10.1016/j.aej.2021.09.013].
[21] Piotrowski A. P.: Differential Evolution algorithms applied to Neural Network training suffer from stagnation. Applied Soft Computing 21, 2014, 382–406 [http://doi.org/10.1016/j.asoc.2014.03.039].
[22] Prechelt L.: A quantitative study of experimental evaluations of neural network learning algorithms: Current research practice. Neural Networks 9, 1996, 457–462 [http://doi.org/10.1016/0893-6080(95)00123-9].
[23] Prieto A., Prieto B., Ortigosa E. M., Ros E.: Neural networks: An overview of early research, current frameworks and new challenges. Neurocomputing 214, 2016, 242–268 [http://doi.org/10.1016/j.neucom.2016.06.014].
[24] Rumelhart D. E., Hinton G. E., Williams R. J.: Learning representations by back-propagating errors. Nature 323, 1986, 533–536 [http://doi.org/10.1038/323533a0].
[25] Si T., Hazra S., Jana N. D.: Artificial Neural Network Training Using Differential Evolutionary Algorithm for Classification. Advances in Intelligent and Soft Computing 232, 2012, 769–778 [http://doi.org/10.1007/978-3-642-27443-5-88].
[26] Storn R., Price K.: Differential Evolution A Simple and Efficient Heuristic for global Optimization over Continuous Spaces. Journal of Global Optimization 11, 1997, 341–359 [http://doi.org/10.1023/A:1008202821328].
[27] Subudhi B., Jena D.: An improved differential evolution trained neural network scheme for nonlinear system identification. International Journal of Automation and Computing 6, 2009, 137–144 [http://doi.org/10.1007/s11633-009-0137-0].
[28] Yang S., Ting T. O., Man K. L., Guan S. U.: Investigation of Neural Networks for Function Approximation. Procedia Computer Science 17, 2013, 586–594 [http://doi.org/10.1016/j.procs.2013.05.076].
[29] Zainuddin Z., Pauline O.: Function Approximation Using Artificial Neural Networks. International Journal of Systems Applications, Engineering and Development 1, 2007, 173–178 [http://doi.org/10.5555/1466915.1466916].
[30] Zhang J. R., Lok T. M., Lyu M. R.: A hybrid particle swarm optimization–back-propagation algorithm for feedforward neural network training. Applied Mathematics and Computation 185, 2007, 1026–1037 [http://doi.org/10.1016/j.amc.2006.07.025].
[31] UCI machine learning benchmark repository. the UC Irvine Machine Learning Repository, 2019 [http://archive.ics.uci.edu/ml/datasets.php].

**M.Sc. Saithip Limtrakul**
e-mail: saithiplim@kkumail.com

Ph.D. candidate in Applied Mathematics at Department of Mathematics, Faculty of Science, Khon Kaen University, Thailand. The author's research area focuses on artificial intelligence, neural network, optimization, image processing, simulation and visualization.

http://orcid.org/0000-0002-7207-6640

**Ph.D. Jeerayut Wetweerapong**
e-mail: wjeera@kku.ac.th

Assistant Professor in Department of Mathematics at the Faculty of Science, Khon Kaen University, Thailand. The author's research interests include optimization and computational intelligence.

http://orcid.org/0000-0001-5053-3989

http://doi.org/10.35784/iapgos.3396

*received: 30.12.2022 | revised: 12.03.2023 | accepted: 15.03.2023 | available online: 31.03.2023*

# APPLICATION OF EXPLAINABLE ARTIFICIAL INTELLIGENCE IN SOFTWARE BUG CLASSIFICATION

**Lukasz Chmielowski[1,2], Michal Kucharzak[1,2], Robert Burduk[2]**

[1]Nokia Solutions and Networks sp. z o.o., Warsaw, Poland, [2]Wroclaw University of Science and Technology, Faculty of Information and Communication Technology, Wroclaw, Poland

***Abstract.*** *Fault management is an expensive process and analyzing data manually requires a lot of resources. Modern software bug tracking systems may be armed with automated bug report assignment functionality that facilitates bug classification or bug assignment to proper development group. For supporting decision systems, it would be beneficial to introduce information related to explainability. The purpose of this work is to evaluate the use of explainable artificial intelligence (XAI) in processes related to software development and bug classification based on bug reports created by either software testers or software users. The research was conducted on two different datasets. The first one is related to classification of security vs non-security bug reports. It comes from a telecommunication company which develops software and hardware solutions for mobile operators. The second dataset contains a list of software bugs taken from an opensource project. In this dataset the task is to classify issues with one of following labels crash, memory, performance, and security. Studies on XAI-related algorithms show that there are no major differences in the results of the algorithms used when comparing them with others. Therefore, not only the users can obtain results with possible explanations or experts can verify model or its part before introducing into production, but also it does not provide degradation of accuracy. Studies showed that it could be put into practice, but it has not been done so far.*

**Keywords:** software bug assignment, software bug triaging, explainable artificial intelligence, text analysis, vulnerability

# ZASTOSOWANIE WYJAŚNIALNEJ SZTUCZNEJ INTELIGENCJI W KLASYFIKACJI USTEREK OPROGRAMOWANIA

***Streszczenie.*** *Zarządzanie usterkami jest kosztownym procesem, a ręczna analiza danych wymaga znacznych zasobów. Nowoczesne systemy zarządzania usterkami w oprogramowaniu mogą być wyposażone w funkcję automatycznego przypisywania usterek, która ułatwia klasyfikację usterek lub przypisywanie usterek do właściwej grupy programistów. Dla wsparcia systemów decyzyjnych korzystne byłoby wprowadzenie informacji związanych z wytłumaczalnością. Celem tej pracy jest ocena możliwości wykorzystania wyjaśnialnej sztucznej inteligencji (XAI) w procesach związanych z tworzeniem oprogramowania i klasyfikacją usterek na podstawie raportów o usterkach tworzonych przez testerów oprogramowania lub użytkowników oprogramowania. Badania przeprowadzono na dwóch różnych zbiorach danych. Pierwszy z nich związany jest z klasyfikacją raportów o usterkach związanych z bezpieczeństwem i niezwiązanych z bezpieczeństwem. Dane te pochodzą od firmy telekomunikacyjnej, która opracowuje rozwiązania programowe i sprzętowe dla operatorów komórkowych. Drugi zestaw danych zawiera listę usterek oprogramowania pobranych z projektu opensource. W tym zestawie danych zadanie polega na sklasyfikowaniu problemów za pomocą jednej z następujących etykiet: awaria, pamięć, wydajność i bezpieczeństwo. Badania przeprowadzone przy użyciu algorytmów związanych z XAI pokazują, że nie ma większych różnic w wynikach algorytmów stosowanych przy porównywaniu ich z innymi. Dzięki temu nie tylko użytkownicy mogą uzyskać wyniki z ewentualnymi wyjaśnieniami lub eksperci mogą zweryfikować model lub jego część przed wprowadzeniem do produkcji, ale także nie zapewnia to degradacji dokładności. Badania wykazały, że można to zastosować w praktyce, ale do tej pory tego nie zrobiono.*

**Słowa kluczowe:** przypisywanie usterek oprogramowania, klasyfikacja usterek oprogramowania, wyjaśnialna sztuczna inteligencja, analiza tekstu, podatności

## Introduction

For large scale software development many tools related to the environment are usually used including among others code repositories, bug tracking systems or decision support systems. Part of them might use machine learning predictions. They are supporting or providing different decisions like assigning priority, severity, group to investigate or solve problem, or label issue as security related or not. An example of black-box model application for identifying security bugs is described in publication [9]. In contrast to black-box solutions a proposition of application of one based on expert rules is shown in paper [2]. Bug mining tool to identify and analyze security bugs using naive bayes and tf-idf was shown in International Conference on Reliability Optimization and Information Technology [4]. Both methods used allow solution to be explainable, but this circumstance was not used. The main aim was to analyse possibilities of application of the explainable artificial intelligence (XAI) in specific cases related to software development.

There are two major taxonomies related to explainability of Machine Learning (ML) models. The first, related to distinction between transparency (including models that are transparent by design), including post-hoc explainability. The second taxonomy, which concerns XAI methods tailored to explain deep learning models. In this context, XAI uses classification criteria based on ML techniques, e.g., representation vectors, layerwise attention [3]. As the first taxonomy is more general and extensive, it is used as a baseline definition of XAI in this document. General review on XAI and its various applications can be found in material [16].

According to the best knowledge of authors there is no application of explainable artificial intelligence techniques in neither solving the problem of assigning security labels nor group responsible for investigating or solving software bug. Nevertheless, there are articles related to possible applications of XAI techniques and their benefits into a system that suggests patches into source code. According to authors of publication [14] in cases where proposed patches are provided without explanations they are usually ignored. In that paper was a statement that those kinds of systems which support developers in way that it can be explained to them is a future of supporting tools in software development.

Another application of explainable artificial intelligence in software development was found in paper [11]. There is a description of works related to predict whether the software commit is risky. To explain it uses predefined features extracted from commits like among others number of modified lines, files, subsystems, and information if change was related to fixing defect. In article [1] are shown results of application of model agnostic explanation methods like LIME and iBreak on bug prediction models. Paper [10] presents assigning the bug severity level. Even if it is not strictly related to XAI methods, at one of steps it is uses algorithm based on dictionary of critical terms related to appropriate severity level. That information might be useful to support the creation of expert systems to support or provide such decisions when there is lack of trust in black-box models.

Explainable artificial intelligence systems might be applied in cases where there is special need for trust in model predictions especially in safety critical applications [6]. Part of those white-box models make the option to generate rules which might be verified by experts with domain knowledge possible. Those kinds of solutions might be useful especially in systems with high responsibility. One of methods of extracting rules which might be verified by experts is to use univariate tree classifier. Then the tree structure might be inspected. Another use case is to provide expert support by providing decision of model with explainable rule extracted from tree. Example of publication with use of such trees is paper [13]. For extracting rules with a decision tree from black-box model as example may be an article [5]. The research questions which are being answered in the work are presented below:

- What is accuracy when comprising standard and easily explainable algorithms?
- What benefits might that gives?
- Does information provided by explainable models seem to be consistent?

## 1. Methods

The data used for research comes from two different sources:

1. Internal company data:
   The purpose of internal data is to distinguish between security and non-security issues. Due to trade secrets no details about the quantity of samples could be provided, but information about distribution of data is shown in table 1. Another example of article using data comes also from NOKIA is publication [8].

*Table 1. Diagram of tree build on dataset from Mozilla to recognize types of issues*

| Type of issue | Percent of reports |
|---|---|
| Security related issues | 4.1 % |
| Non-security related issues | 95.9 % |

2. Mozilla Defect Dataset:
   Data from Mozilla is widely available. It contains software bugs labeled as performance problem, security related issue or crash, memory. Details with quantity of samples of dataset extracted for this publication are shown in table 2. Samples with multiple labels were removed. Generally, publicly available bug reports from Mozilla projects are accessible, among others, in repository [12] or can be gathered with script [7].

*Table 2. Distribution of type od issue (Mozilla Defect Dataset)*

| Type of issue | Percent of reports |
|---|---|
| Crash related issue | 66.3 % |
| Memory related issue | 11.4 % |
| Security related issue | 11.2 % |
| Performance related issue | 11.1 % |

For chosen selected classification not found any publication which has data to comparison. The selection of those specific datasets is justified by the fact that relatively no such deep domain knowledge is required to interpret those cases. Research has been carried out in both cases according to the same experimental protocol. Firstly, on raw text data extracted from title of cases was performed preprocessing contains among others, removing special characters, stopwords then applying lemmatization. In the next step vectorization was applied with usage of tf-idf with limitation of max features parameter to 1000. Features which were taken into consideration by tf-idf are both unigrams and bigrams. On data prepared that way calculations were performed with usage of different algorithms. Results of selected standard algorithms used for XAI applications were compared against rest which were introduced. The method to explain results was univariate tree to extract the rules. Moreover, most important features according to different models were extracted to be compared in subjective way. That extraction may potentially be used in context of creation expert rules.

## 2. Results and discussion

Comparison of results with usage of both types of algorithms which can be used straightforward to as explainable and not are shown in tables 3–8. Headings used in tables are:

- kNN – k – Nearest Neighbors;
- LR – Logistic Regression;
- NB – Naive Bayes;
- SVC – Support Vector Classifier;
- XGBoost – eXtreme Gradient Boosting;
- tree x-y-z – Decision Tree Classifier where:
  - x – minimum number of samples required to split an internal node leaf,
  - y – minimum number of samples required to split an internal node,
  - z – maximum depth of tree.

*Table 3. Comparison most important features related to label issue as security related or not (internal company data) in condition of selected algorithm*

| tree 5-5-15 | LR | SVC | XGBoost |
|---|---|---|---|
| vulnerability | vulnerability | vulnerability | vulnerability |
| sensitive | security | sensitive | sensitive |
| security | svm | security | security |
| svm | sensitive | svm | svm |
| password | sec | scan | password |

As is shown in table 3 most important features for chosen classifiers related to task to distinguish if case is security related or not are: vulnerability, svm, sensitive, security. For use case related to label issue as performance, security, crash, or memory related problem following terms are most important: crash, leak, memory (table 4). It is noticeable in both of cases that at least some of the same features are common for most important classifiers. This is also confirmed in figure 1 and figure 2. Diagrams (figures 1–3) present decision making process, how the classification is performed with the use of decision trees. Each of them shows a section of the decision tree related to one of the discussed problems. Analyzing the content of diagram in figure 3, the root node is shown at the top. The first text line of that node indicates that the decision depends on frequency of occurrence of keyword *vulnerability*. It is shown that in that case, if value of parameter related to *vulnerability* is above threshold, the condition for node is False. Therefore, following the arrow (branch) marked False, the next node is selected. It has the majority class Yes, what means it is related to security as it was expected. As that one node is not a leaf node, algorithm follows the next conditions. Color of node which is used for presentation depends on the purity of the node. In this example security related issues are in blue and non-security related ones are in orange. There is also presented a measure of impurity which is in that case Gini.

*Table 4. Comparison most important features related to type of issue (Mozilla Defect Dataset) in condition of selected algorithm*

| tree 5-5-15 | LR | SVC | XGBoost |
|---|---|---|---|
| crash | crash | crash | crash |
| regression | application | leak | leak |
| content | intermittent | memory | regression |
| memory | leak | usage | addresssanitizer |
| slow | moz_crash | lazily | build |

Results between decision tree as one which is interpretable by design (transparent model) and support vector classifier which requires external XAI techniques to be explained (post-hoc explainability) were used for explainability comparison.

With significance threshold at $\alpha = 0.05$, performing paired *t* test 5x2cv procedure returned $p - value = 0.19$. As $p - value > \alpha$, the null hypothesis cannot be rejected, and it may be concluded that the performance of the two algorithms is not significantly different. That is expected as we gain explainability, without loss of quality of results. More details about used test procedure is in [15].

*Table 5. Comparison of results related to label issue as security related or not (internal company data)*

| | kNN | | LR | | NB | | SVC | | XGBoost | |
|---|---|---|---|---|---|---|---|---|---|---|
| class | prec | recall | prec | recall | prec | recall | prec | recall | prec | recall |
| Security related | 0.96 | 0.84 | 0.98 | 0.79 | 0.32 | 0.90 | 0.97 | 0.85 | 0.99 | 0.76 |
| Non-security related | 0.99 | 1.00 | 0.99 | 1.00 | 1.00 | 0.92 | 0.99 | 1.00 | 1.00 | 0.92 |

*Table 6. Comparison of results related to label issue as security related or not (internal company data)*

| | tree 5-5-10 | | tree 5-5-15 | | tree 10-10-15 | | tree 3-3-15 | | tree 5-5-5 | |
|---|---|---|---|---|---|---|---|---|---|---|
| class | prec | recall | prec | recall | prec | recall | prec | recall | prec | recall |
| Security related | 0.93 | 0.86 | 0.93 | 0.86 | 0.92 | 0.82 | 0.95 | 0.84 | 0.96 | 0.79 |
| Non-security related | 0.99 | 1.00 | 0.99 | 1.00 | 0.99 | 1.00 | 0.99 | 1.00 | 0.99 | 0.99 |

*Table 7. Comparison of results related to type of issue (Mozilla Defect Dataset)*

| | kNN | | LR | | NB | | SVC | | XGBoost | |
|---|---|---|---|---|---|---|---|---|---|---|
| class | prec | recall | prec | recall | prec | recall | prec | recall | prec | recall |
| Crash | 0.88 | 0.94 | 0.97 | 0.97 | 0.97 | 0.47 | 0.98 | 0.96 | 0.98 | 0.95 |
| Memory | 0.72 | 0.38 | 0.83 | 0.46 | 0.12 | 0.65 | 0.78 | 0.59 | 0.69 | 0.33 |
| Performance | 0.72 | 0.65 | 0.83 | 0.88 | 0.76 | 0.68 | 0.83 | 0.88 | 0.97 | 0.49 |
| Security | 0.52 | 0.47 | 0.70 | 0.74 | 0.25 | 0.69 | 0.69 | 0.74 | 0.38 | 0.85 |

*Table 8. Comparison of results related to type of issue (Mozilla Defect Dataset)*

| | tree 5-5-10 | | tree 5-5-15 | | tree 10-10-15 | | tree 3-3-15 | | tree 5-5-5 | |
|---|---|---|---|---|---|---|---|---|---|---|
| class | prec | recall | prec | recall | prec | recall | prec | recall | prec | recall |
| Crash | 0.98 | 0.95 | 0.98 | 0.95 | 0.98 | 0.95 | 0.98 | 0.95 | 0.98 | 0.92 |
| Memory | 0.77 | 0.33 | 0.77 | 0.33 | 0.69 | 0.30 | 0.80 | 0.31 | 0.78 | 0.17 |
| Performance | 0.99 | 0.59 | 0.99 | 0.59 | 0.99 | 0.59 | 0.99 | 0.59 | 0.98 | 0.43 |
| Security | 0.41 | 0.87 | 0.99 | 0.87 | 0.41 | 0.87 | 0.41 | 0.90 | 0.33 | 0.87 |

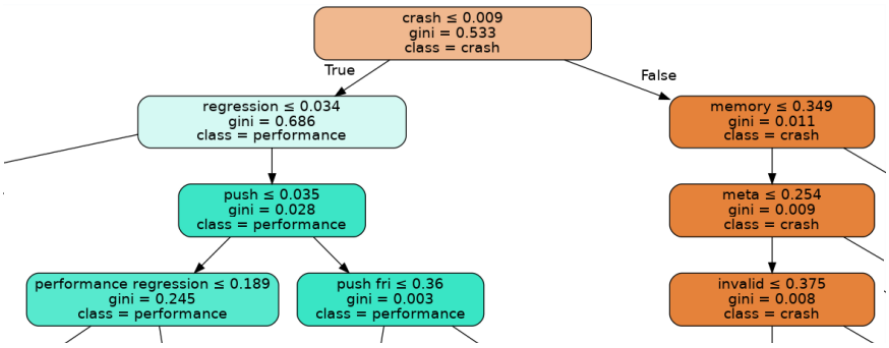


*Fig. 1. Diagram of tree build on dataset from Mozilla to recognize types of issues*

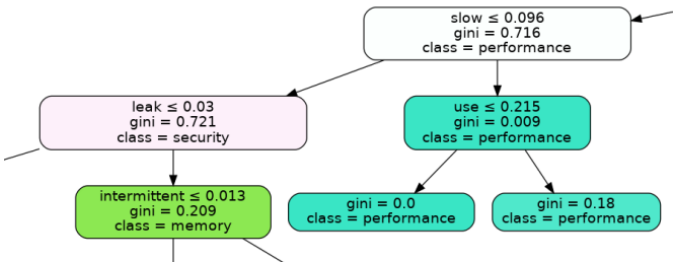


*Fig. 2. Diagram of tree build on dataset from Mozilla to recognize types of issues*

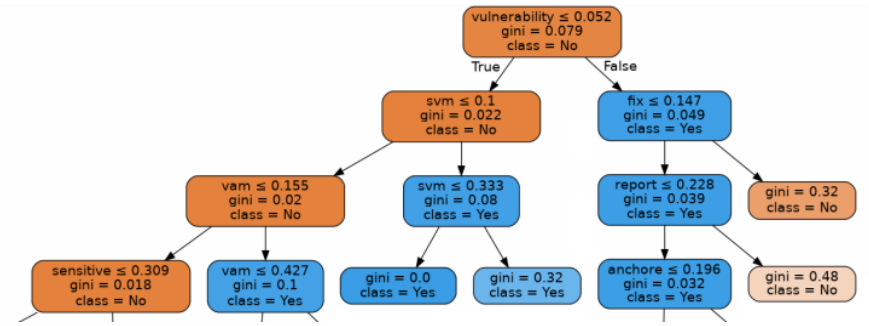


*Fig. 3. Diagram of tree built on internal company dataset to recognize security related issues*

## 3. Conclusion

The paper discusses potential application of the explainable artificial intelligence in software bug report classification. In the article the authors discuss the possibility of using XAI methods in the context of assigning a department, group, or any label for software bug reports created by the user or testers. According to authors there is currently no application of such solution, however there are papers which consider different, but sometimes confused with the mentioned problem. That similar, but significantly different topic is software bug prediction, which aims to indicate whether introducing software change will lead to a defect. The presented results show experimental research with the use of simulations of predictions of type of software bug or classify the issue as security related or not. One of the steps in the research was to apply explainable artificial intelligence methods and compare results between standard black-box methods and XAI ones. The result of comparison on Mozilla data shows that it can be useful. When applying XAI methods on dataset with company internal data it can be clearly noticed that rules generated seem to be legit and might be potentially used for explaining decisions or suggestions. For both cases there have been gathered most important features according to the trained models. In the presented diagrams (figures 1–3) the way how chosen built models make the decisions are shown. For one algorithm shown that has been applied, the decision-making process is shown. For each step (node) a decision condition is presented, what is the main class of samples that meets the specified conditions of the current node. To sum up this paper clearly shows that there is a possibility to apply explainable artificial intelligence methods in the context of problems related to bug assignment and the results are reasonable.

## Author contributions

Author contributions statement L.C. independently conceived the experiments; L.C., M.K., R.B. analyzed results; L.C. wrote original draft; M.K., R.B. provided editorial suggestions; L.C., M.K. conducted editing of work; L.C., M.K., R.B. attempted to disprove the novelty. All authors reviewed the manuscript.

## Acknowledgements

This work has been carried out in cooperation between NOKIA and Wroclaw University of Science and Technology in context of a Ph.D. grant under the fourth edition of the Implementation Doctorate Programme.

## Conflicts of interests

The authors declare no conflicts of interests.

## References

[1] Aleithan R.: Explainable Just-In-Time Bug Prediction: Are We There Yet? 43rd International Conference on Software Engineering: Companion Proceedings (ICSE-Companion), 2021, 129–131 [http://doi.org/10.1109/ICSE-Companion52605.2021.00056].
[2] Anjali, Mohan D., Sardana N.: Visheshagya: Time based expertise model for bug report assignment. Ninth International Conference on Contemporary Computing (IC3), 2016, 1–6 [http://doi.org/10.1109/IC3.2016.7880218].
[3] Barredo Arrieta A. et al.: Explainable Artificial Intelligence (XAI): Concepts, taxonomies, opportunities and challenges toward responsible AI. Information Fusion 58, 2020, 82–115 [http://doi.org/10.1016/j.inffus.2019.12.012].
[4] Behl D., Handa S., Arora A.: A bug Mining tool to identify and analyze security bugs using Naive Bayes and TF-IDF. International Conference on Reliability Optimization and Information Technology (ICROIT), 2014, 294–299 [http://doi.org/10.1109/ICROIT.2014.6798341].
[5] Carlevaro A., Maurizio M.: A New SVDD Approach to Reliable and Explainable AI. IEEE Intelligent Systems 37.2, 2022, 55–68 [http://doi.org/10.1109/ACCESS.2022.3180026].
[6] Carlevaro A. et al.: Counterfactual Building and Evaluation via eXplainable Support Vector Data Description. IEEE Access 10, 2022 [http://doi.org/10.1109/MIS.2021.3123669].
[7] Castelluccio M. et al.: bugbug. Available online: https://github.com/mozilla/bugbug (accessed on 02.11.2022).
[8] Chmielowski L., Kucharzak M.: Impact of Software Bug Report Preprocessing and Vectorization on Bug Assignment Accuracy. Progress in Image Processing, Pattern Recognition and Communication Systems. Edited by Michal Choraś, et al.: Springer International Publishing, Cham 2022, 153–162 [http://doi.org/10.1007/978-3-030-81523-3_15].
[9] Choquette-Choo C. A. et al.: A Multi-label, Dual-Output Deep Neural Network for Automated Bug Triaging. 18th IEEE International Conference On Machine Learning And Applications (ICMLA), 2019, 937–944 [http://doi.org/10.1109/ICMLA.2019.00161].
[10] Gujral S., et al.: Classifying bug severity using dictionary based approach. International Conference on Futuristic Trends on Computational Analysis and Knowledge Management (ABLAZE), 2015, 599–602 [http://doi.org/10.1109/ABLAZE.2015.7154933].
[11] Khanan C. et al.: JITBot: An Explainable Just-In-Time Defect Prediction Bot. 35th IEEE/ACM International Conference on Automated Software Engineering (ASE), 2020, 1336–1339.
[12] Lamkanfi A., Pérez J., Demeyer S.: The Eclipse and Mozilla defect tracking dataset: A genuine dataset for mining bug information. 10th Working Conference on Mining Software Repositories (MSR), 2013, 203–206 [http://doi.org/10.1109/MSR.2013.6624028].
[13] Matzka S.: Explainable Artificial Intelligence for Predictive Maintenance Applications. Third International Conference on Artificial Intelligence for Industries (AI4I), 2020, 69–74 [https://doi.org/10.1109/AI4I49448.2020.00023].
[14] Monperrus M.: Explainable Software Bot Contributions: Case Study of Automated Bug Fixes. IEEE/ACM 1st International Workshop on Bots in Software Engineering (BotSE), 2019, 12–15 [http://doi.org/10.1109/BotSE.2019.00010].
[15] Raschka S.: 5x2cv paired ttest. Available online: https://rasbt.github.io/mlxtend/user_guide/evaluate/paired_ttest_5x2cv (accessed on 04.01.2021).
[16] Vilone G. Longo L.: Explainable Artificial Intelligence: a Systematic Review. 2020 [http://doi.org/10.48550/arXiv.2006.00093].

**M.Sc. Eng. Łukasz Chmielowski**
e-mail: lukasz.chmielowski@nokia.com

Łukasz Chmielowski received a M.Sc. degree with distinction in Computer Science with specialization in Intelligent Information Systems. He is currently working towards Ph.D. in Information and Communication Technology at Wroclaw University of Science and Technology (Poland). He is with the Nokia Solutions and Networks sp. z o.o. (Poland) for five years. He is working with machine learning techniques related to natural language processing and software bug assignment.

http://orcid.org/0000-0001-6970-8144

**Ph.D. Eng. Michał Kucharzak**
e-mail: michal.kucharzak@pwr.edu.pl

Michał Kucharzak received his Ph.D. in computer science in area of network optimization. In recent years, he cooperated with numerous R&D centers and has been a member of reviewer committees for many international journals, program, and technical committees for various conferences as well. His current research interests are primarily in the areas of network modeling and network optimization with special regard to overlays, simulations, design of efficient algorithms and wireless system protocols, including software testing and quality assurance.

http://orcid.org/0000-0001-5068-5229

**D.Sc. Eng. Robert Burduk**
e-mail: robert.burduk@pwr.edu.pl

Robert Burduk is professor of Computer Science in the Department of Systems and Computer Networks, Faculty of Information and Communication Technology, Wroclaw University of Science and Technology, Poland. He received an Ph.D. and D.Sc. degrees in Computer Science in 2003 and 2014 respectively. His research interests cover among the others: machine learning, classifier selection algorithms and multiple classifier systems. He serves on program committees of numerous international conferences, published over 100 papers and edited 5 books.

http://orcid.org/0000-0002-3506-6611

http://doi.org/10.35784/iapgos.3383

*received: 23.12.2022 | revised: 1.02.2023 | accepted: 12.03.2023 | available online: 31.03.2023*

# AUTOMATIC DETECTION OF ALZHEIMER'S DISEASE BASED ON ARTIFICIAL INTELLIGENCE

**Achraf Benba, Kerchaoui Abdelilah**

Mohammed V University in Rabat, Ecole Nationale Supérieure d'Arts et Métiers, Electronic Systems Sensors and Nanobiotechnologies, Rabat, Morocco

***Abstract.*** *Alzheimer's disease is a neurodegenerative disease that progressively destroys neurons through the formation of platelets that prevent communication between neurons. The study carried out in this project aims to find a precise and relevant diagnostic solution based on artificial intelligence and which helps in the early detection of Alzheimer's disease in order to stop its progression. The study went through a process of processing MRI images followed by training of three deep learning algorithms (VGG-19, Xception and DenseNet121) and finally by a step of testing and predicting the results. The results of the accuracy metric obtained for the three algorithms were respectively 98%, 95%, 91%.*

**Keywords**: Alzheimer's disorder, artificial intelligence, deep learning, signal processing

## AUTOMATYCZNE WYKRYWANIE CHOROBY ALZHEIMERA W OPARCIU O SZTUCZNĄ INTELIGENCJĘ

***Streszczenie.*** *Choroba Alzheimera jest chorobą neurodegeneracyjną, która stopniowo niszczy neurony poprzez tworzenie płytek krwi, które uniemożliwiają komunikację między neuronami. Badania prowadzone w ramach tego projektu mają na celu znalezienie precyzyjnego i trafnego rozwiązania diagnostycznego opartego na sztucznej inteligencji, które pomoże we wczesnym wykryciu choroby Alzheimera w celu zatrzymania jej postępu. Badanie przeszło przez proces przetwarzania obrazów MRI, po którym następowało szkolenie trzech algorytmów głębokiego uczenia (VGG-19, Xception i DenseNet121), a na koniec etap testowania i przewidywania wyników. Wyniki metryki dokładności otrzymane dla trzech algorytmów wyniosły odpowiednio 98%, 95%, 91%.*

**Słowa kluczowe**: choroba Alzheimera, sztuczna inteligencja, głębokie uczenie się, przetwarzanie sygnału

## Introduction

Dementia is a condition that is often chronic or progressive in nature and causes cognitive ability to deteriorate beyond what may be anticipated from the typical effects of biological aging [9]. Memory, thought, orientation, understanding, calculation, learning capacity, language, and judgment are all impacted. Currently, dementia is the seventh most common cause of mortality globally among all diseases and one of the main reasons of reliance and impairment among elderly people [9]. The major goal of this project is to develop a diagnostic method based on artificial intelligence algorithms for the early diagnosis of dementia and, more particularly, Alzheimer's disease. Artificial intelligence presents a set of theories and techniques applied to create machines capable of simulating human intelligence. The study was based on an MRI database, exploited in order to automatically detect the different stages of severity of Alzheimer's disease. To successfully find this solution, we must focus on improving the performance of these algorithms and more specifically on the accuracy metric. The more value of this metric increases the more the detection becomes precise. There are several studies in the literature which amin to classify Alzheimer disease.

In [4], the researchers proposed a method of classification of Alzheimer's disease based on the close learning by transfer, they started with the step of preprocessing the MRI images acquired in the database. ADNI data, using the Freesurfer software. The pretreatment techniques that were used are the skull stripping technique, which is used to extract the brain from the skull, a technique for normalizing intensities and correcting movement. To extract the features from the processed images, they opted to use the VGG 16 algorithm through which they performed two types of classification, a binary classification in particular between two different classes of the three proposed classes (AD, CN MCI) and a normal classification that is made between all ADNI classes. The final test accuracy result was 95.73%. In [7], the researchers proposed a classification study of Alzheimer's disease by three different CNN algorithms including GoogleNet, AlexNet and ResNet-18 based on the Transfer Learning approach. Was carried out on an age margin of 55 years to 100 years with a sample of 7800 MRI ADNI images, the database was divided into 5 classes presenting the degrees of the disease AD, CN, EMCI, LMCI MCI. The test accuracy values obtained by the study were 96.39%, 94.08% and 97.51% respectively. In [6], the researchers proposed a classification study based on the characteristics of the hippocampus (volume and morphology), they adopted the methodology of combining a multi-model based on the CNN algorithm to ensure at the same time the segmentation of the hippocampus and the classification of the disease, this method was evaluated on the T1 weighting of a database to constitute the following classes 97 AD, 233 MCI and 119 NC. of 88.9% for the binary classification of AD versus NC and the accuracy of 76.2% for the classification of MCI versus NC.

## 1. Database aquisition

The database used for this study was used in [5]. It has a total of 6,400 MRI images resized to 128 × 128 and divided into 4 classes, Mild_Demented (896 images), Moderate_Demented (64 images), Non_Demented (3,200 images) and Very_Mild_Demented (2,240 images). In addition, this database contains images that have been taken in two sections: a longitudinal section and a cross section. These images were taken using T1 weighting, this sequence is obtained by setting IRM to shorts TE defined as the time between delivery of the RF pulse and reception of the echo signal, and a longer TR which presents the duration between successive pulse sequences applied to the same slice.

## 2. Methodology

The pre-processing of the data presents the second stage of the study through which the processing of the acquired data is carried out. In our case, we have radiological images (MRI) whose pre-processing is done by applying digital algorithms to them. The choice of its processing algorithms may depend on the properties and type of the chosen radiological image.

The determination of the relative intensity (brightness) of the tissues in an MRI image is made by the following factors:

- Gradient waveforms and radio frequency pulse to use.
- The intrinsic characteristics T1 and T2 of the different tissues that means the duration of TR and RF set.
- The proton density of different tissues.

To prepare our MRI database for the training step of the chosen CNNs algorithms we used a nonlinear enhancement algorithm known as histogram equalization which allows contrast enhancement of samples with low luminosity. Its principle is that it makes it possible to separate the pixels into distinct groups

if there are few output values over a wide range. It is only effective when the original image has low contrast to begin with; otherwise, histogram equalization can degrade image quality. In this case, the adaptive histogram equalization is improved. This procedure facilitates the detection of image features by CNN algorithms.

Then, we proceeded to the normalization of the intensities of the MRI images acquired, because these images are not comparable from one MRI, from one subject and from one visit to another, even if the same protocol is used. Which can influence the performance and prediction of the CNN algorithms to be trained. This approach brings the intensities to a common scale [0, 1] of all people diagnosed.

Then we proceeded to convert the IRM image, from a single-channel image (grayscale) to a three-channel image (RGB) to train the CNN transfer learning algorithms implemented in this study.

After performing the pre-processing of the acquired MRI images, we proceeded to the training stage of the applied CNN algorithms [1] based on the transfer learning technique. This study targeted three large deep learning algorithms (VGG19, DenseNet and Xception) already pre-trained on an ImageNet-type database. ImageNet is an image database organized according to the hierarchy of WordNet [10]. It is designed for use in visual object recognition software research.

Before the start of the training step of the three algorithms mentioned on the paragraph above, we ensured the division of the database into two sets with a parameter of test_size equal to 0.3, in other words, 70% of the images in the database were used to train these algorithms and 30% to test them.

To avoid performance degradation issues, a database class balancing method has been applied known as SMOTE. It is an oversampling technique that seeks to increase the size of minority classes. In our case, this technique was set to a value of random state equal to 0.

The VGG-19 algorithm is a CNN algorithm consisting of 16 layers of Conv2D and 5 layers of MaxPooling. The layers of Conv2D make it possible to extract the characteristics of an image by applying filters to its various pixels, on the other hand, the operation of the MaxPooling makes it possible to reduce the information generated by the convolutional layers to store it efficiently.

Xception is the second CNN algorithm applied. It takes the form of a linear stack of depth-separable convolution layers with a very complex architecture [3]. It includes 36 convolution layers forming the basis for network feature extraction, these 36 layers are structured into 14 modules, all of which have residual linear connections around them except for the first and last module.

The role of the residual connections added in this algorithm is to reduce the use of resources during the matrix calculation without modifying the number of parameters and to improve the performance of the algorithm [8].

In this study, this algorithm was applied with a neural network consisting of two fully connected layers identical to those of VGG-19 with the same techniques for reducing the overfitting phenomenon already used. DenseNet presents the last algorithm applied in this study, it consists of a single 7×7 Conv2D layer, 58 3×3 Conv2D, 61 1×1 Conv2D and 4 Average Pooling layers. In our case we added 3 fully connected layers with the use of three Regularizer of 0.0001, three dropout layers respectively set to 0.7, 0.5, 0.2 and two layers of BatchNormalization to minimize the overfitting problem.

As long as the number of layers of the CNN network increases, the algorithm becomes very deep, which generates the problem of the evanescence of the gradient (a very rapid decrease in the values of the gradients during the back propagation causing the cancellation of the gradient and the stop learning) which degrades the training process of the CNN algorithm. This is where this algorithm comes in to solve this problem through the simplification of the connectivity scheme between the layers. We have exceptionally resized the dimensions of the image for this algorithm because it requires 224×224×3 to have good performance.

The three algorithms (VGG-19, Xception and DenseNet121) were trained on tensor flow which is an open-source library for training machine learning algorithms. The training process was carried out based on the parameters as follow: Learning-rate of 0.00001, Adam optimizer, Epochs number of 500, Batch-size of 32 and Categorical cross entropy as function cost.

*Table 1. Confusion matrix corresponding to VGG-19 Algorithm, Xception Algorithm and DenseNet121 Algorithm*

| | | Mild_Demented | Moderate_Demented | Non_Demented | Very_Mild_Demented |
|---|---|---|---|---|---|
| **VGG-19** | **TP** | 980 | 980 | 970 | 960 |
| | **TN** | 2959 | 2972 | 2954 | 2937 |
| | **FP** | 13 | 0 | 24 | 39 |
| | **FN** | 14 | 14 | 18 | 30 |
| **Xception** | **TP** | 920 | 940 | 960 | 950 |
| | **TN** | 2962 | 2969 | 2897 | 2858 |
| | **FP** | 4 | 0 | 74 | 110 |
| | **FN** | 72 | 49 | 27 | 40 |
| **DenseNet121** | **TP** | 880 | 870 | 910 | 860 |
| | **TN** | 2844 | 2915 | 2789 | 2750 |
| | **FP** | 76 | 0 | 132 | 161 |
| | **FN** | 89 | 104 | 58 | 118 |

*Table 2. Performance of VGG-19 Algorithm, Xception Algorithm and DenseNet121 Algorithm*

| | | Mild_Demented | Moderate_Demented | Non_Demented | Very_Mild_Demented |
|---|---|---|---|---|---|
| **VGG-19** | **Exactness** | **0.99** | **1** | 0.99 | **0.98** |
| | **Precision** | 0.99 | **1** | **0.98** | 0.96 |
| | **Recall** | **0.99** | 0.99 | **0.98** | **0.97** |
| | **F1_mesure** | **0.99** | 0.99 | **0.98** | **0.97** |
| **Xception** | **Exactness** | 0.98 | 0.98 | 0.98 | 0.98 |
| | **Precision** | **1** | **1** | **1** | **1** |
| | **Recall** | 0.93 | 0.93 | 0.93 | 0.93 |
| | **F1_mesure** | 0.96 | 0.96 | 0.96 | 0.96 |
| **DenseNet121** | **Exactness** | 0.96 | 0.96 | 0.96 | 0.96 |
| | **Precision** | 0.92 | 0.92 | 0.92 | 0.92 |
| | **Recall** | 0.91 | 0.91 | 0.91 | 0.91 |
| | **F1_mesure** | 0.91 | 0.91 | 0.91 | 0.91 |

## 3. Results and discission

After finishing the training step of the algorithms (VGG-19, Xception, DenseNet121) on the parameters noted in table 1. They gave the accuracy results mentioned in the figures 1–3.

To ensure this training step of the three algorithms, we applied a categorical cross entropy type cost function which measures the classification performance of the CNN algorithms. It gives results between 0 and 1, the more its value tends towards 0, the more error between the prediction and the test image is minimal (figure 4–6).

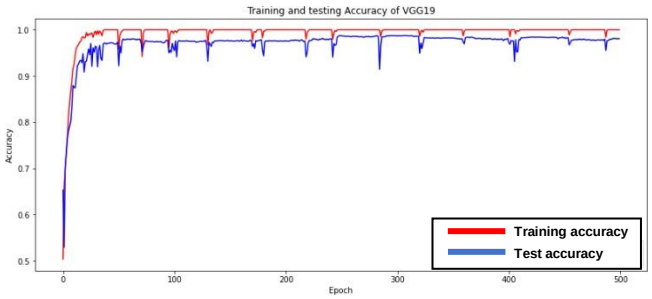


*Fig. 1. Accuracy results corresponding to VGG-19*

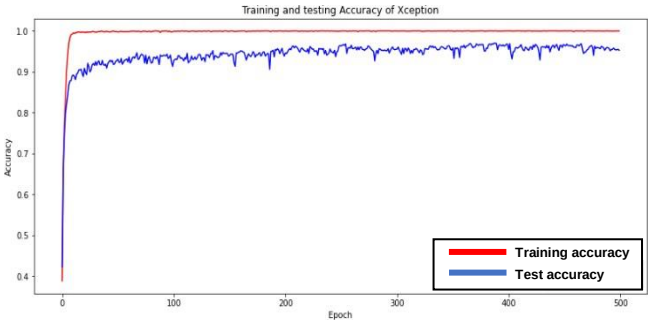


*Fig. 2. Accuracy results corresponding to Xception*

We need a number of epochs of 500 because a minimum value of this parameter can generate an underfitting problem that arises from the inability of the algorithms to scale their performance during the training phase. And a batch size of 32 to avoid the problem of resource consumption and acceleration of the training speed, because a very large value of this second parameter can accelerate the training speed which sometimes influences the phase learning of the CNN algorithms. However, a very small value of this parameter can slow down the training speed of the CNN algorithms for each epoch which can require more calculation and therefore more memory resources.

A large number of epochs can also cause an overfitting problem. In other words, it can influence the training process of the algorithms by diverging the training accuracy from that of the test. To avoid the appearance of this problem, we applied an optimization algorithm called Adam's algorithm, which updates the variables (Weights) of the neural network, with a value of learning rate equal to 0.00001 which allows to ensure a good adjustment of the rate of changes of these variables (Weights) in order to fix them on values where the errors between the cost function of training and test are greatly minimized.

The values of the overall accuracy of the three applied CNN algorithms were respectively 98%, 95%, 91%. To evaluate the performance of a CNN algorithm, it must first go through the confusion matrix which gives the values of the parameters TP, TN, FP, FN. In our case, we had the following confusion matrix results.

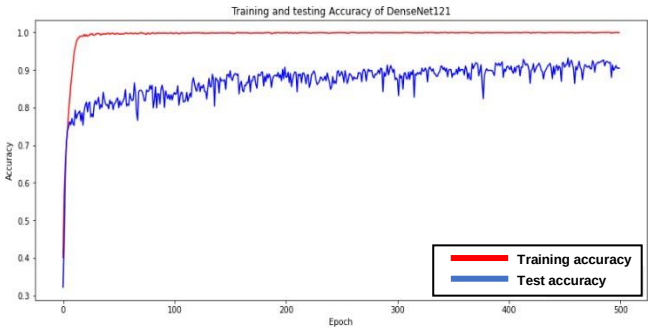


*Fig. 3. Accuracy results corresponding to DenseNet121*

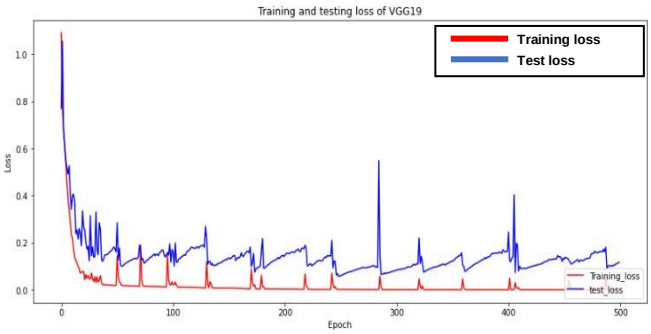


*Fig. 4. Results of the cost function corresponding to VGG-19*

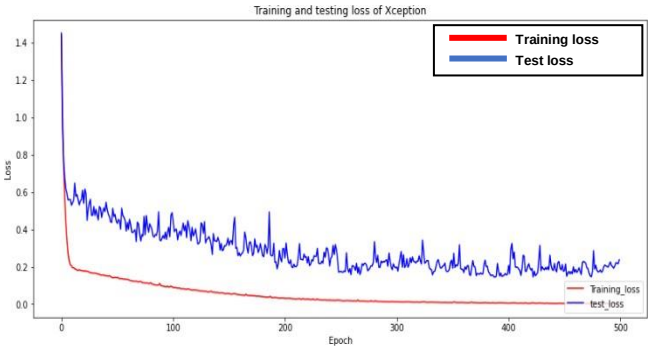


*Fig. 5. Results of the cost function corresponding to Xception*

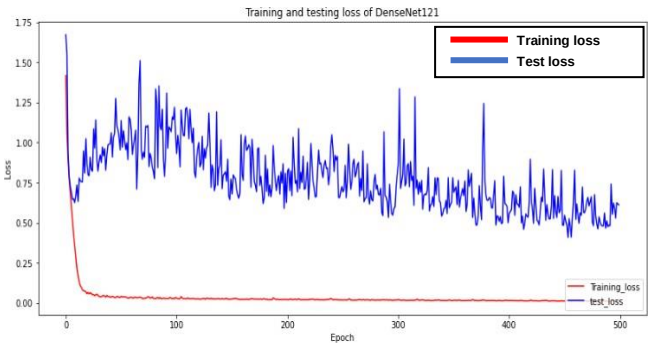


*Fig. 6. Results of the cost function corresponding to DenseNet121*

After calculating the values of the parameters TP, TN, FP, FN mentioned in the table 1, an evaluation of the performance of the three algorithms (VGG-19, Xception, DenseNet121) was made based respectively on the values of the four metrics accuracy, precision, recall and F1-measurements. Table 2 presents the final results of the performance analysis of the three algorithms used.

If we compare the results of the values of accuracy and precision (table 2) of the VGG-19 algorithm, we will notice that these values for the 4 classes are very close to each other with error values noted respectively 0.01, 0, 0.01, 0.02, and a maximum accuracy of 100% at the class level (Moderate_Demented) which means that this algorithm is very efficient at the level of this class compared to other classes which have completed 99% for Mild_Demented and Non_Demented and 98 respectively % for the Very_Mild_Demented class. For the results of the Xception algorithm, note that the accuracy and precision values for the 4 classes are slightly different from each other with error values noted respectively 0.02, 0.02, 0.03, 0.04, and a maximum accuracy of 98% at the level of the two classes Mild_Demented and Moderate_Demented which means that this algorithm is very efficient at the level of these two classes compared to the two other classes which have respectively achieved accuracy of 97% for Non_Demented and 96% for Very_Mild_Demented. For the results of the last DenseNet121 algorithm, note that the accuracy and precision values for the 4 classes are also different from each other with error values noted respectively 0.04, 0.03, 0.05, 0.07, and a maximum accuracy of 97% at the level of the Moderate_Demented class which means that this algorithm is efficient at the level of this class compared to the other classes which have respectively achieved accuracy of 96% for Mild_Demented, 95% for Non_Demented and 93% for Very_Mild_Demented. So from these comparison results we can conclude that the most efficient algorithm in this study is the VGG-19.

## 4. Conclusion

Dementia is a chronic or progressive illness that causes cognitive capacity to degrade beyond what may be expected from the normal consequences of biological aging. Memory, cognition, orientation, understanding, computation, learning capacity, language, and judgment are all influenced. Dementia is currently the sixth leading cause of mortality globally and one of the leading causes of reliance and impairment among the elderly. The primary purpose of this research is to create a diagnostic tool based on artificial intelligence algorithms for the early detection of dementia, especially Alzheimer's disease. This was accomplished by utilizing a database including numerous MRI brain scans from various classes of patients. Also we performed an evaluation of three pre-trained CNN algorithms named VGG-19, Xception and DenseNet121. This study used the transfer learning technique through which the three CNN algorithms gave the accuracy values 98%, 95% and 91% respectively.

## References


[1] Albawi S. et al.: Understanding of a convolutional neural network. International conference on engineering and technology (ICET), IEEE, 2017, 1–6.

[2] Brownlee J.: Gentle introduction to the Adam optimization algorithm for deep learning. Machine Learning Mastery 3, 2017.

[3] Chollet F.: Xception: Deep learning with depthwise separable convolutions. Proceedings of the IEEE conference on computer vision and pattern recognition, 2017, 1251–1258.

[4] Jain R. et al.: Convolutional neural network based Alzheimer's disease classification from magnetic resonance brain images. Cognitive Systems Research 57, 2019, 147–159.

[5] Kaplan E. et al.: Feed-forward LPQNet based automatic alzheimer's disease detection model. Computers in Biology and Medicine 137, 2021, 104828.

[6] Liu M. et al.: A multi-model deep convolutional neural network for automatic hippocampus segmentation and classification in Alzheimer's disease. Neuroimage 208, 2020, 116459.

[7] Shanmugam J. V. et al.: Alzheimer's disease classification using pre-trained deep networks. Biomedical Signal Processing and Control 71, 2022, 103217.

[8] Szegedy C. et al.: Inception-v4, inception-resnet and the impact of residual connections on learning. Thirty-first AAAI conference on artificial intelligence, 2017.

[9] World Health Organization, 2012. Dementia: a public health priority. World Health Organization.

[10] Yang K. et al.: Towards fairer datasets: Filtering and balancing the distribution of the people subtree in the imagenet hierarchy. Proceedings of the 2020 conference on fairness, accountability, and transparency, 547–558.



**Prof. Achraf Benba**
e-mail: achraf.benba@ensam.um5.ac.ma


Was born in El Jadida, Morocco, on 1990. He received the Ph.D. degree in electrical engineering from ENSAM, Mohammed V University, Rabat, Morocco, in 2017. He is a member of E2SN teams at ENSAM, Mohammed V University. His interests are in speech processing for detecting people with neurological disorders and Cardiac abnormalities.


http://orcid.org/0000-0001-7939-0790

**Eng. Abdelilah Kerchaoui**
e-mail: kerchaoui.abdelilah1999@gmail.com


Engineer Kerchaoui Abdelilah graduated from the National School of Arts and Crafts of Rabat, spatialized in the biomedical field and more precisely in hospital instrumentation. He began his higher education with a DUT in electrical engineering for a period of 2 years from 2017 to 2019 followed by an engineering course in biomedical field for a period of 3 years from 2019 to 2022. He realized development & research projects in medical signal processing and artificial intelligence.


http://orcid.org/0009-0004-9561-5960

http://doi.org/10.35784/iapgos.3387

*received: 23.12.2022 | revised: 14.03.2023 | accepted: 23.03.2023 | available online: 31.03.2023*

# IMPLEMENTATION OF AN ARTIFICIAL INTELLIGENCE-BASED ECG ACQUISITION SYSTEM FOR THE DETECTION OF CARDIAC ABNORMALITIES

**Achraf Benba[1], Fatima Zahra El Attaoui[1], Sara Sandabad[2]**

[1]Mohammed V University in Rabat, Ecole Nationale Supérieure d'Arts et Métiers, Electronic Systems Sensors and Nanobiotechnologies, Rabat, Morocco, [2]Ecole Normale Supérieure de l'Enseignement Technique de Mohammadia, Electrical Engineering and Intelligent Systems, Hassan II University of Casablanca, Casablanca, Morocco

***Abstract.*** *The electrocardiogram (ECG) is a common test that measures the electrical activity of the heart. On the ECG, several cardiac abnormalities can be seen, including arrhythmias, which are one of the major causes of cardiac mortality worldwide. The objective for the research community is accurate and automated cardiovascular analysis, especially given the maturity of artificial intelligence technology and its contribution to the health area. The goal of this effort is to create an acquisition system and use artificial intelligence to classify ECG readings. This system is designed in two parts: the first is the signal acquisition using the ECG Module AD8232; the obtained signal is a single derivation that has been amplified and filtered. The second section is the classification for heart illness identification; the suggested model is a deep convolutional neural network with 12 layers that was able to categorize five types of heartbeats from the MIT-BIH arrhythmia database. The results were encouraging, and the embedded system was built.*

**Keywords**: electrocardiogram, arrhythmias, artificial intelligence, convolution neural network

## WDROŻENIE SYSTEMU POZYSKIWANIA EKG OPARTEGO NA SZTUCZNEJ INTELIGENCJI W CELU WYKRYWANIA NIEPRAWIDŁOWOŚCI SERCA

***Streszczenie.*** *Elektrokardiogram (EKG) to powszechny test, który mierzy aktywność elektryczną serca. W zapisie EKG można zauważyć kilka nieprawidłowości serca, w tym arytmie, które są jedną z głównych przyczyn śmiertelności sercowej na całym świecie. Celem społeczności naukowej jest dokładna i zautomatyzowana analiza układu sercowo-naczyniowego, zwłaszcza biorąc pod uwagę dojrzałość technologii sztucznej inteligencji i jej wkład w obszar zdrowia. Celem tych wysiłków jest stworzenie systemu akwizycji i wykorzystanie sztucznej inteligencji do klasyfikacji odczytów EKG. System ten składa się z dwóch części: pierwsza to akwizycja sygnału za pomocą modułu EKG AD8232; uzyskany sygnał jest pojedynczą pochodną, która została wzmocniona i przefiltrowana. Druga sekcja to klasyfikacja identyfikacji chorób serca; sugerowany model to głęboka konwolucyjna sieć neuronowa z 12 warstwami, która była w stanie sklasyfikować pięć typów uderzeń serca z bazy danych arytmii MIT-BIH. Wyniki były zachęcające i zbudowano system wbudowany.*

**Słowa kluczowe**: elektrokardiogram, arytmie, sztuczna inteligencja, konwolucyjna sieć neuronowa

## Introduction

Cardiovascular illnesses are the leading cause of death worldwide, and their prevalence rises with age. The electrocardiogram (ECG) is one of the earliest exams used for diagnosis; it is a recording of the heart's electrical activity acquired by attaching tiny electrodes to the body. It is normally made up of three important waves: the P wave, the QRS complex, and the T wave [7]. ECG interpretation is a critical skill for clinicians to acquire; reading errors are common and can lead to misdiagnosis. Using artificial intelligence for decision-making is the goal of numerous studies in the literature [6, 11, 16]. The goal of this work is to create a system for acquiring and classifying ECG signals that is based on an ECG module for acquisition and deep learning to be used afterwards to simplify and facilitate cardiologists' tasks. This technique enables for the capture and categorization of data in five categories: normal, left bundle branch block [19, 20], right bundle branch block [5], atrial prematurity [9, 14], and ventricular premature contraction [14].

Many publications, such as [14, 15, 18], and [10], deal with the acquisition and categorization of cardiac anomalies utilizing ECG signals. They created and deployed a smart health care monitoring equipment that visualizes the ECG signal and counts the number of heartbeats at a reasonable cost. The AD8232 module is used to display the ECG signal in real time. Many additional studies employed ECG signal classifications based on artificial intelligence algorithms to detect cardiac problems early and treat them appropriately [2, 4, 17]. The feature extraction stage is critical in classification, and several techniques for identifying and categorizing ECG heartbeats have been widely employed, including wavelet transform, filter banks, hidden Markov models, support vector machines, and others. The convolutional neural network (CNN) is a neural network used for anticipating and deep learning because of its amazing performance in the fields of image and voice and has a high potential to find significant patterns in data. Convolutional neural networks are similar to artificial neural networks in that they have a convolution layer, a subsampling layer, and a fully connected layer that is the same as the multilayer perceptron (MLP). In [8], they introduced an automated feature extraction method that eliminates the need for human feature extraction and preprocessing. It focuses on identifying five major macro-classes: Non-ectopic, Supraventricular ectopic (S), Ventricular ectopic (V), Fu-sion (F), and Unknown (Q). Their suggested method for ECG beat categorization consists of three major phases. Detection of ECG beats, sample extraction, and categorization Their method had a 92.7% accuracy. Another heartbeat classification technique based on artificial networks and fuzzy relations with an accuracy rating of 80-85% was utilized in [3]. An efficient system based on the MLP-NN classifier is shown using two alternative feature extraction approaches. Our task entails acquiring the ECG signal and classifying heart disorders, more specifically arrhythmias. As a result, we must acquire the signal while filtering and amplifying it in order to classify it into one of five categories based on a 12-layer convolutional neural network: Normal, Left Bundle Branch Block, Right Bundle Branch Block, Atrial Prematurity, and Premature Ventricular Contraction. The accuracy of this approach was 99.56%. However, before reaching this stage, the signal must first go through a series of data preparation and segmentation stages. Figure 1 depicts an overview of the system. In this work, we will present the materials utilized for acquisition and categorization, as well as the study's methodology, experimental findings, and conclusion.

## 1. Methodology

The initial stage in this process is the acquisition of ECG signals, which was accomplished with the help of AD8232, a signal conditioning block that may be utilized for ECG and other biopotentiometric measurements. It is intended to extract, amplify, and filter tiny bio potential signals in the presence of distracting

factors such as mobility or distant electrode location. This enables the output signal to be easily acquired by an ultra-low power analog-to-digital converter (ADC) or an integrated microcontroller. Disposable electrodes were employed in this experiment because they are faster, easier, and more sanitary than reusable electrodes or wet electrodes. They are placed on various bodily regions to get an ECG signal [1].

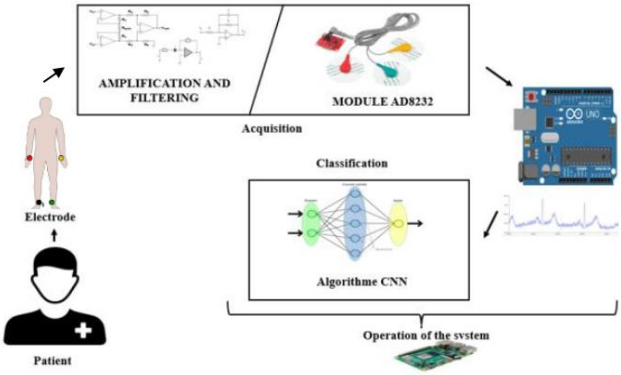


*Fig. 1. Overview of the used system*

The sensor's output signal is received by the analog pins on the Arduino Uno board. Ar-duino UNO is an open-source microcontroller based on the Microchip ATmega328. There are six analog pins on this board. The Arduino programming software is used to program this microcontroller. This board operates on both 5 V and 12 V. It has a maximum clock rate of 16 MHz and is a 10 bit microcontroller with 32 KB of flash program memory. C is the programming language used.

The disposable electrodes included with the AD8232 kit are put on the test subject's bare skin on his right and left chest and right and left thigh while he is laying on his back. Figure 2 depicts the recovered signal utilizing our acquisition technology.

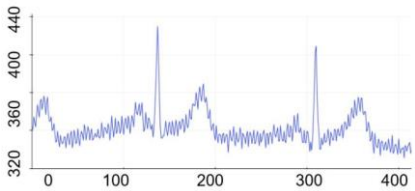


*Fig. 2. Extracted signal using our acquisition system*

The categorization is the second phase in this project. To handle the signal, which is a one-dimensional time series with uniform interval sampling, we propose a one-dimensional CNN with 12 layers. The hardware configuration utilized in the implementation is an HP 2000 laptop with an Intel(R) (TM) i3-3110M CPU at 2.40GHz, 4 GB of RAM, and the Windows 10 "64-bit" operating system. The programming language is Python, and the environment is Kaggle with Keras and skit learn libraries. The ECG signals were taken from PhysioBank's MIT-BIH arrhythmia database [13]. It is made up of 47 ECG recordings taken by the BIH Arrhythmia Laboratory over the course of 48 half hours. Each ECG recording is made up of two leads. Each signal is captured at 360 Hz, and these recordings have been evaluated and confirmed by at least two cardiologists, and they have been split as follows for our model.

*Table. 1. Database description*

| Type of signal | Number of annotations |
|---|---|
| Normal | 75011 |
| Left Bundle Branch Block | 8071 |
| Right branch block | 7255 |
| Atrial prematurity | 7129 |
| Premature ventricular contraction | 2546 |

To improve classification accuracy, the signal must be denoised (figure 3). In this example, the wavelet transform approach is used to preprocess the ECG data. The non-stationary data is split into discrete frequency band scale signals. The filter employs an adaptive threshold filtering method, and the Sym4 wavelet function from the Symlet family of wavelet functions is chosen since it is the most similar to the ECG signal. The convolutional neural network can automatically extract features from data; we just applied simple filtering to the signal to increase the generalization of the network and eliminate signal distortion.

For this model, we have normal, left bundle branch block, right bundle branch block, premature atrial beats, and premature ventricular beats, all of which are illnesses noted for each pulse in the MIT-BIH data. The process starts with R-peak detection (R-wave position detection is triggered when the adaptive threshold is exceeded), the dataset is then divided into 360 samples and centered around the detected R-peaks, and each segment is then normalized using Z-score normalization to address the issue of amplitude scaling and eliminate the offset effect before being fed to the CNN network for training and testing (figure 4).

The database is unbalanced, which might influence convolutional neural network feature learning and lower recognition accuracy. To decrease the data unbalance utilized for training, we oversample the under-represented classes, randomly duplicate the under-represented classes, and reject the over-represented classes after pre-processing and segmentation (table 2 and 3).

In this study, we present a 12-layer one-dimensional CNN to process a one-dimensional time series with uniform interval sampling. To preserve the general characteristics of the input data, we use the average pooling layer rather than the maximum pooling layer. With a total of eight alternate convolution and pooling layers, the proposed CNN network features one more alternate convolution and pooling layer than the current CNN network. They are followed by two completely connected layers and a dropout layer, as indicated in the flowchart (figure 5).

The first layer is convolved with a core size of 13 and a filter count of 16. Applying a medium-pooling layer of size 3 reduces Layer 2's output to 179*16. Then, the Layer 2 feature map is convolved with a core size of 15, and Layer 3 has 32 filters. Once more, a mean-pooling layer of size 3 is utilized, bringing the number of neurons down from 176*16 to 89*32. (layer 4). There are 64 filters in layer 5, with an average pooling size of 17. The output is decreased to 44*64 after layer 5, which is followed by an average-pooling layer with a size of 3. (layer 6). The output of layer 6 is convolved with layer 7, which has a core size of 19 and 128 filters. The next layer is a pooling layer with a size of 3. (layer 8). In Layer 9, the exclusion layer is set at 50%. Linking layer 10 to layer 11 are 35 neurons. Layer 11 connects five neurons to the SoftMax layer, which gives each problem type a probability. A linear recovery unit serves as the activation function prior to each mean clustering layer (ReLU). In order to prevent overfitting, the L2 factor of 5 is applied to all completely linked layers.

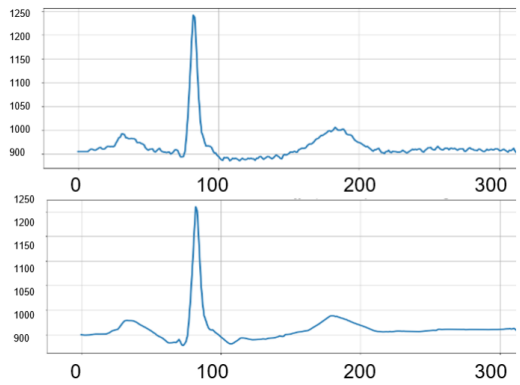


*Fig. 3. ECG signal before and after denoising from MIT-BIH data*

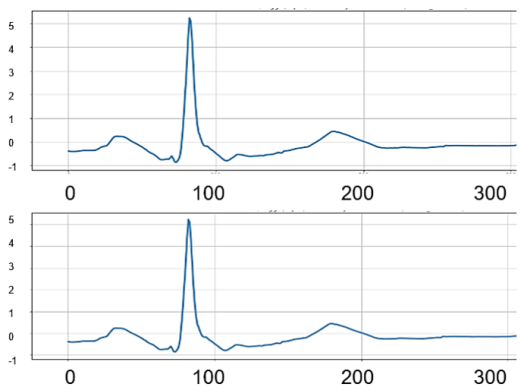


*Fig. 4. Signal after normalization with Z-score and detection of the R peak*

*Table. 2. Unbalanced database*

| *N* | *V* | *A* | *R* | *L* |
|---|---|---|---|---|
| 75% | 2.5% | 7.1% | 7.3% | 8.1% |

*Table. 3. Rebalanced database*

| *N* | *V* | *A* | *R* | *L* |
|---|---|---|---|---|
| 20% | 20% | 20% | 20% | 20% |

## 2. Results

Using stratified sampling, we dispersed 80% of the data in the training set and 20% in the test set. Kaggle's GPU was used to train the model. To develop our network, we utilized the TensorFlow framework, with the maximum number of epochs set to 40. Training took around 30 minutes, and the network parameters were saved in a local file to be used later.

As indicated in figures 6 and 7, the test had an accuracy of 99.56% and a loss of 4%. The confusion matrix (figure 8) was then used to assess the algorithm's sensitivity (Sen), which is the percentage of properly predicted positive people. Its specificity (Spe), which is the percentage of accurately predicted negative persons, and its positive prediction rate (Ppr), are calculated as follows:

- Sen=TP/(TP+FN)
- Spe=TN/(TN+FP)
- Ppr=TP/(TP+FP)

where (TP) is the number of true positives, (FP) is the number of false positives, (TN) is the number of true negatives, and (FN) is the number of false negatives (FN).

The sensitivity, specificity, and positive prediction rate of the model in the classification range between 98 and 100%, indicating that it is a model that clinicians may use to help them with their diagnosis.

## 3. Discussions

This CNN network outperformed other models in terms of overall classification accuracy (99.56%) for the classification of micro classes in the arrhythmia dataset, as well as 40-fold cross-validation to demonstrate the robustness of the algorithm compared to is [12], where they used a random forest classifier to recognize five main classes (N, Q, S, V, F), achieving 94.61% accuracy. Other studies employed a deep genetic collection of classifiers to categorize the extended duration ECG signal, achieving on 17 arrhythmia classifications on the same database.

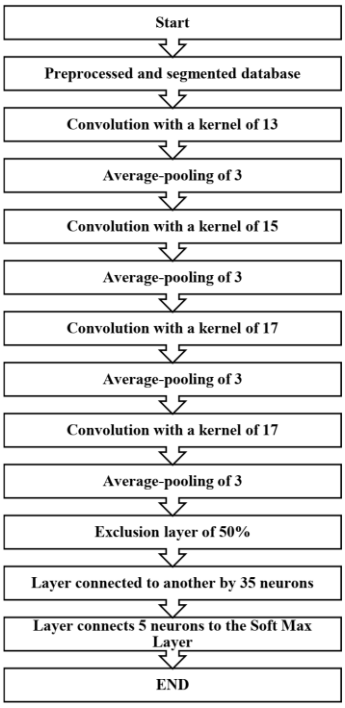


*Fig. 5. Flowchart of the model CNN*

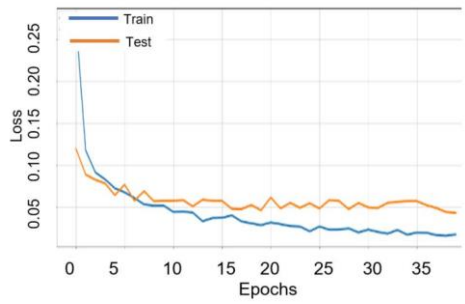


*Fig. 6. Loss curve*

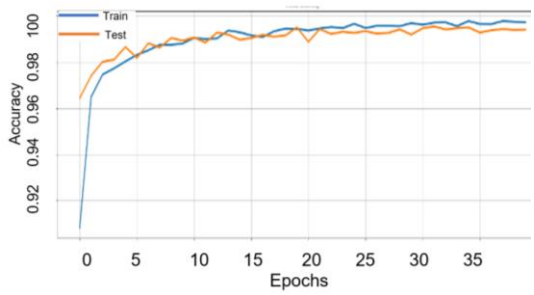


*Fig. 7. Accuracy curve*

Following the classification that yielded substantial results, a model was developed in order to test it with our recovered signal on actual individuals. This model was built on a Raspberry Pi board, and then tests were run to ensure that our system worked properly. Because the signal was retrieved from a normal patient, the first findings revealed a decent categorization. Figure 9 shows how it might be used on different people with anomalies to view the results on a screen.

| | | | | |
|---|---|---|---|---|
| 1502 | 1 | 1 | 19 | 3 |
| 0 | 1669 | 0 | 0 | 0 |
| 0 | 0 | 1602 | 3 | 0 |
| 4 | 0 | 0 | 1567 | 1 |
| 2 | 0 | 0 | 1 | 1615 |

True label

Predicted label

*Fig. 8. Confusion matrix whith normalization*

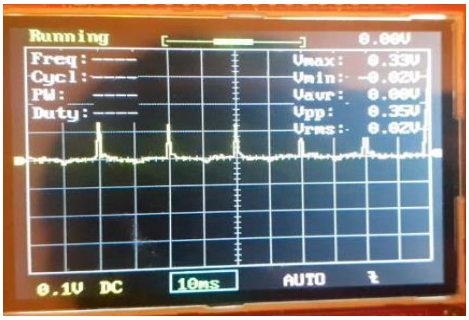


*Fig. 9. Real visualization of extracted ECG Signal*

## 4. Conclusion

In this work, we were able to acquire the ECG signal using a card that integrates the entire acquisition chain, including amplification and filtering, and we were able to select a powerful algorithm for the data, thanks to the network's advantages in terms of automatic signal processing without the need for signal extraction, which is very useful and beneficial when compared to other algorithms. In this context, we recommend that the quality of the obtained signal be improved. Aside from the proposed solution, which is the Raspberry Pi, the cloud can be a good option to visualize the signal, process it through the model, and present the findings.

## References

[1] AD8232 DS. Single-Lead, Heart Rate Monitor Front End. Analog Device, 2013.
[2] Ahsan M. M., Siddique Z.: Machine learning-based heart disease diagnosis: A systematic literature review. Artificial Intelligence in Medicine 29, 2022, 102289 [http://doi.org/10.1016/j.artmed.2022.102289].
[3] Atal D. K., Singh M.: Arrhythmia classification with ECG signals based on the optimization-enabled deep convolutional neural network. Computer Methods and Programs in Biomedicine, 196, 2020, 105607 [http://doi.org/10.1016/j.cmpb.2020.105607].
[4] Day T. G. et al.: Artificial intelligence, fetal echocardiography, and congenital heart disease. Prenatal Diagnosis 41(6), 2021, 733–742 [http://doi.org/10.1002/pd.5892].
[5] Farinha J. M. et al.: Frequent premature atrial contractions as a signalling marker of atrial cardiomyopathy, incident atrial fibrillation and stroke. Cardiovascular research, 2022, cvac054 [http://doi.org/10.1093/cvr/cvac054].
[6] Giudicessi J. R. et al.: Artificial intelligence–enabled assessment of the heart rate corrected QT interval using a mobile electrocardiogram device. Circulation 143(13), 2021, 1274–1286 [http://doi.org/10.1161/circulationaha.120.050231].
[7] Han C. et al.: QRS complexes and T waves localization in multi-lead ECG signals based on deep learning and electrophysiology knowledge. Expert Systems with Applications 199, 2022, 117187 [http://doi.org/10.1016/j.eswa.2022.117187].
[8] Hassan S. U. et al.: Classification of cardiac arrhythmia using a convolutional neural network and bi-directional long short-term memory. Digital Health 8, 2022 [http://doi.org/10.1177/20552076221102766].
[9] Higuchi K. et al.: How to use bipolar and unipolar electrograms for selecting successful ablation sites of ventricular premature contractions. Heart Rhythm 19(7), 2022, 1067–1073 [http://doi.org/10.1016/j.hrthm.2021.12.035].
[10] Karri M., Annavarapu C. S.: A real-time embedded system to detect QRS-complex and arrhythmia classification using LSTM through hybridized features. Expert Systems with Applications 214, 2023, 119221 [http://doi.org/10.1016/j.eswa.2022.119221].
[11] Kwon J. M. et al.: Artificial intelligence assessment for early detection of heart failure with preserved ejection fraction based on electrocardiographic features. European Heart Journal-Digital Health 2(1), 2021, 106–116 [http://doi.org/10.1093/ehjdh/ztaa015].
[12] Li T., Zhou M.: ECG classification using wavelet packet entropy and random forests. Entropy 18(8), 2016, 285 [http://doi.org/10.3390/e18080285].
[13] Moody G. B., Mark R. G.: The impact of the MIT-BIH arrhythmia database. IEEE engineering in medicine and biology magazine 20(3), 2001, 45–50 [http://doi.org/10.1109/51.932724].
[14] Rahman M. A. et al.: Remote monitoring of heart rate and ECG signal using ESP32. 4th International Conference on Advanced Electronic Materials, Computers and Software Engineering (AEMCSE), 2021, 604–610 [http://doi.org/10.1109/AEMCSE51986.2021.00127].
[15] Reis C. Q., Robar J. L.: Evaluation of the feasibility of cardiac gating for SBRT of ventricular tachycardia based on real-time ECG signal acquisition. Journal of Applied Clinical Medical Physics, 2022, e13814 [http://doi.org/10.1002/acm2.13814].
[16] Ribeiro J. M. et al.: Artificial intelligence and transcatheter interventions for structural heart disease: a glance at the (near) future. Trends in cardiovascular medicine 32(3), 2022, 153–159 [http://doi.org/10.1016/j.tcm.2021.02.002].
[17] Vamseekrishna A. et al.: Low-Cost ECG-Based Heart Monitoring System with Ubidots Platform. Embracing Machines and Humanity Through Cognitive Computing and IoT, 2023 [http://doi.org/10.1007/978-981-19-4522-9_6].
[18] Vinther M. et al.: A randomized trial of His pacing versus biventricular pacing in symptomatic HF patients with left bundle branch block (His-alternative). Clinical Electrophysiology 7(11), 2021, 1422–1432 [http://doi.org/10.1016/j.jacep.2021.04.003].
[19] Zhu K. et al.: The physiologic mechanisms of paced QRS narrowing during left bundle branch pacing in right bundle branch block patients. Frontiers in Cardiovascular Medicine 9, 2022 [http://doi.org/10.3389/fcvm.2022.835493].

**Prof. Achraf Benba**
e-mail: achraf.benba@ensam.um5.ac.ma

Received the Ph.D. degree in electrical engineering from ENSAM, Mohammed V University, Rabat, Morocco, in 2017. He is a member of E2SN teams at ENSAM, Mohammed V University. His interests are in speech processing for detecting people with neurological disorders and Cardiac abnormalities.

http://orcid.org/0000-0001-7939-0790

**Eng. Fatima Zahra El Attaoui**
e-mail: fatimazahra.elattaoui98@gmail.com

Received the engineering degree in biomedical engineering from ENSAM, Mohammed V University, Rabat, Morocco, in 2022. she is interested in the detection of heart disease using artificial intelligence. Specialist before sale in a Moroccan company of distribution and importation of biomedical equipment.

http://orcid.org/0009-0001-0196-0500

**Prof. Sara Sandabad**
e-mail: s.sandabad@isem.ac.ma

Received the B.Sc. and the M.Sc. degrees in Electrical Engineering from ENSET, Mohamed V University of Rabat (Morocco) and the Ph.D. degree from ENSIAS from the Mohamed V University of Rabat, all in Electrical Engineering, in 2010, 2012, and 2016, respectively. Currently, she is a Professor of Electrical Engineering at ISEM, Hassan II University of Casablanca. She is also an academic member of Laboratory of Control and Mechanical Characterization of Materials and Structures, ENSEM, Hassan II University of Casablanca, Morocco.

http://orcid.org/0000-0002-0813-6178

http://doi.org/10.35784/iapgos.3239

*received: 4.11.2022 | revised: 6.12.2022 | accepted: 12.03.2023 | available online: 31.03.2023*

# DEVELOPMENT AND MODELING OF THE ANTENNA SYSTEM THE DIRECTION FINDER UNMANNED AERIAL VEHICLE

**Juliy Boiko[1], Oleksiy Polikarovskykh[2], Vitalii Tkachuk[3]**

[1]Khmelnytskyi National University, Department of Telecommunications, Media and Intelligent Technologies, Khmelnytskyi, Ukraine, [2]Odessa National Maritime University, Department of Technical Cybernetics and Information Technologies, Odessa, Ukraine, [3]Khmelnytskyi National University, Department of Mechanical Engineering Technology, Khmelnytskyi, Ukraine

***Abstract.*** *The article is devoted to the design the proposed construction of the antenna system for the direction-finding complex of the unmanned aerial vehicle (UAV). The experimental part is represented by the results of mathematical modeling the behavior of the antenna in different parts the operating frequency range. The effectiveness of the adopted design solutions was evaluated in comparison with analogues of leading companies in the world. Based on the results of the research, the areas of application the antenna as part of the built-in functional mobile UAV direction finding systems were determined.*

**Keywords**: antennas, radiation pattern, modeling, voltage control

# OPRACOWANIE I MODELOWANIE SYSTEMU ANTENOWEGO CELOWNIKA BEZZAŁOGOWEGO STATKU POWIETRZNEGO

***Streszczenie.*** *Artykuł poświęcony jest zaprojektowaniu proponowanej konstrukcji systemu antenowego dla zespołu radionawigacyjnego bezzałogowego statku powietrznego (BSP). Część eksperymentalna jest reprezentowana przez wyniki matematycznego modelowania zachowania anteny w różnych częściach zakresu częstotliwości pracy. Skuteczność przyjętych rozwiązań konstrukcyjnych została oceniona w porównaniu z odpowiednikami wiodących firm na świecie. Na podstawie wyników przeprowadzonych badań określono obszary zastosowania anteny w ramach wbudowanych funkcjonalnych mobilnych systemów radionamierzania bezzałogowych statków powietrznych.*

**Słowa kluczowe**: anteny, charakterystyka promieniowania, modelowanie, sterowanie napięciem

## Introduction

Direction finding and positioning the location of the source of radio emission (RES) is an important task in the implementation of the introduction of measures for radio monitoring, solved in the interests of civil and special services, including during antiterrorist and military operations.

For a direction finder, the efficiency of solving the problem of radio monitoring depends on characteristics such as the accuracy of the measurement of the angle of arrival radio waves, the type of polarization of the direction-finding signals, the spatial resolution breaking capacity, sensitivity and operating frequency range. Specified the characteristics of the radio direction finder are largely determined by the parameters of the antenna system used. Therefore, research and development radio direction finders for small UAVs [4, 9, 13] is a very relevant scientific practical task for: increasing the accuracy of measuring the angular coordinates of RES; increasing resolution in angular coordinates; increasing the sensitivity of the receiving antenna system; reducing the weight and size parameters of the equipment.

When designing radio direction finders [3, 5], satisfy-meeting the above requirements, an important task is the development of antenna systems and methods for processing received signals that take into account the diffraction distortions of the measured electromagnetic field, which are a consequence of the scattering of incident waves on the elements max design of the antenna system of its fairing, under conditions of a priori unknown polarization of the received radio waves and an indefinite number of sources of radio radiation.

Achieving this goal required solving the following tasks: – analysis of the current state and prospective development trends theories, techniques and technologies for the production of direction-finding antenna systems topics; – research and development of signal processing methods, minimizing which influence the influence of diffraction distortions of the measured field on the accuracy of positioning, and antenna systems for their implementation in radio direction finders; – studies of promising ways to build ultra-wideband linear direction-finding antenna arrays with a beam-forming circuit based on a printed Rotman lens, which increase the sensitivity of direction finding.

At the current moment in the development of antenna systems for the design of direction-finding complexes of UAVs, it is possible to single out the design of the TCI antenna, in particular models 641, 643. In general, the design of such an antenna is based on the general provisions described above regarding the parameters of the Vivaldi antenna. However, the key feature of such antennas is the use of ultra-broadband directional antenna elements that do not have a phase centre. The antenna contains systems of the TEM horn type (built on two identical mirror-curved relative to each other conductive plates) with strips that expand, and each of the strips is divided into two parts by a gap (analogous to the Vivaldi antenna discussed [12]). In fig. 1 a and b, respectively, present the designs of TCI antennas.

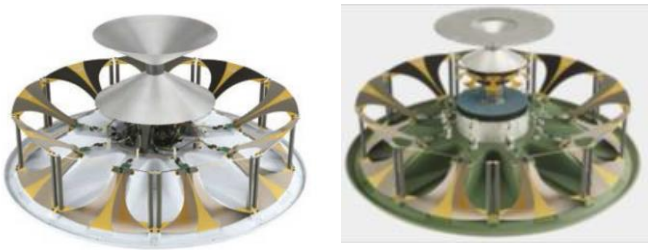

a b

*Fig. 1. Design of TCI antennas: a) TCI 643, b) TCI 647D*

Analysis of the design features of antenna systems without a phase center allows us to state that the basis of the design of such ultra-broadband antennas includes a set of TEM horns and Vivaldi antennas. Among similar solutions, in the subject area of the article, it is possible to single out the Rohde&Schwarz antenna systems based on phased antenna arrays [8], symmetrical antenna vibrators and frame-type antennas [2, 11].

As stated in the statement of the research task, the proposed article examines the results of simulation of a relatively new design of the antenna [7], which is being developed for UAV direction finding and contains the TSA (Tapered Slot Antenna) concept. It should be noted that specifying a specific task for designing an antenna system gives a variety of shapes and proportions between its structural elements. The analysis of existing information on this issue revealed the following patterns for TSA: the width of the slit determines the lower frequency of the working range; the length determines the gain in the middle and at the upper edge of the frequency band; the shape of the open slit determines the frequency characteristics of the antenna element [6]. It is believed that TSA with an exponentially increasing gap width have the most acceptable frequency characteristics.

The article will present the results of modeling the characteristics of antenna elements of antenna systems using software modeling tools. ANSYS 2022 FHSS software was used as software for modeling elements of antenna systems. HFSS is an industry-standardized 3D electromagnetic simulation tool fields HFSS technology allows calculation of electric and magnetic fields, currents, *S*-parameters, radiation fields in the near and far zone. The calculation process is fully automated, the user only needs to determine the geometric parameters, material properties and the desired result.

## 1. Element of an antenna system made of slotted elements of a traveling wave with printed lenses for full azimuth direction finding sources of radio emission with arbitrary polarization

The possibility of receiving and direction-finding UAV signals with arbitrary polarization is an essential technical parameter of a DF antenna system designed for compact placement on a mobile carrier. However, the analysis of modern DF antenna systems manufactured by such large manufacturers as Rohde & Schwarz, TCI, Alaris Antennas, CRFS showed that only a few of them produce DF antenna systems for receiving signals from arbitrary polarization. Therefore, the development of antenna systems of this type, taking into account the development of UAVs, is an urgent task.

In this section, an antenna system for full-azimuth direction finding of radio emission sources with arbitrary polarization in the frequency range from 1 GHz to 5 GHz, which consists of slotted elements, has been developed and studied. As a single antenna element of the developed antenna system, it is proposed to use a pair of orthogonal elements of the Vivaldi type with metamaterial polarization-selective lenses in their openings (Fig. 2).

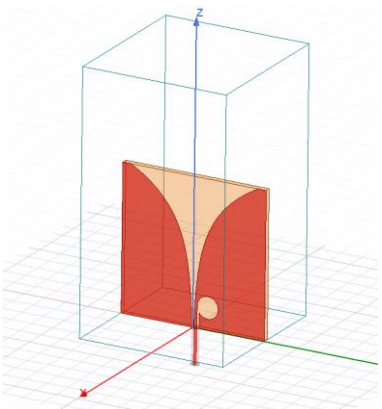


*Fig. 2. Basic single antenna element of the system*

The antenna elements are made according to the technology for the production of printed circuit boards on a dielectric microwave material RO4003 with double-sided metallization by Rogers. The thickness of the dielectric is 0.508 mm, overall dimensions of elements – 340 mm × 340 mm. In accordance with Fig. 1, the Vivaldi antenna is an ultra-broadband printed emitter built on the basis of an expanding slit line. In this case, a consistent transition between the non-radiating slit line and free space can be made using an exponential slit line in the form of a Vivaldi slit [6, 12]. As a result, such a design transforms traveling surface waves into radiating leakage waves. The relationship between geometric parameters and characteristics of the antenna was established experimentally [9].

A distinctive feature of the proposed embodiment of the Vivaldi antenna is the use of a printed lens in its aperture, which increases the cross-polarization isolation and improves the radiation pattern and input characteristics of the antenna elements.

## 2. Mathematical description of the antenna element

In accordance with Fig. 2, the Vivaldi antenna is an ultra-wideband printed radiator, which is built on the basis of an expanding slot line. In this case, a coordinated transition between the non-radiating slot line and free space can be implemented using an exponential slot line in the form of a Vivaldi slot [6, 12]. This design results in the transformation of traveling surface waves into radiant leakage waves. The relationship between the geometric characteristics and features of the antenna was established experimentally [8]. The exponential taper of a thin metal Vivaldi antenna located in the *XY* plane (Fig. 3) can be described by points *P*1 and *P*2 at points with coordinates (*X*l, *Y*l) and (*X*2, *Y*2), respectively, as well as by the opening coefficient *R*.

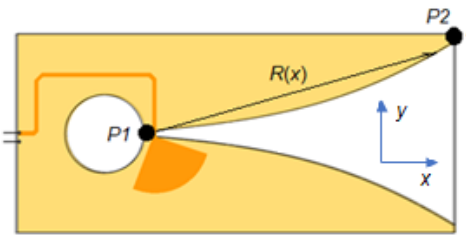


*Fig. 3. Design of a Vivaldi antenna element with parameters for an analytical description*

Between points *P*1 and *P*2, the exponential cone is described by the following differential equations:

$$\frac{dy}{dx} = Ry + C, \tag{1}$$

where *R* is the antenna opening curvature factor and *C* will represent the offset from y chosen so that *P*1 and *P*2 are points on the line *y*(*x*), Fig. 3.

Then the general solution of equation (1) will look like:

$$y = C_1 e^{Rx} + C_2 \tag{2}$$

$$C_1 = \frac{y_2 - y_1}{e^{Rx_2} - e^{Rx_1}} \tag{3}$$

$$C_2 = \frac{y_1 e^{Rx_2} - y_2 e^{Rx_1}}{e^{Rx_2} - e^{Rx_1}}. \tag{4}$$

Thus, the mathematical model of the upper curved edge of the antenna element can be represented as:

$$\underline{R}(x) = x\underline{e}_x + |C_1 e^{Rx} + C_2|\, \underline{e}_y, \quad x_1 \le x \le x_2. \tag{5}$$

The length of the section curvature the antenna element will be described mathematically as follows:

$$l(x) = \int_{\xi=x_1}^{x} \left|\dot{\underline{R}}(\xi)\right| d\xi =$$

$$= \frac{1}{R}\left[\sqrt{1 + (C_1 R)^2 e^{2Rx}} - arctanh\left(\sqrt{1 + (C_1 R)^2 e^{2Rx}}\right)\right]. \tag{6}$$

Thus, to represent the curves describing the petals of the Vivaldi antenna, you can use a couple of equations [6]:

$$x = x_1 + K(x_2 - x_1), \tag{7}$$

$$y = \frac{(y_2 - y_1)e^{R(x_2 + K(x_2 - x_1))} + y_2 e^{Rx_2} - y_2 e^{Rx_1}}{e^{Rx_2} - e^{Rx_1}} \tag{8}$$

The following notations are used in formulas 1–8: $\dot{\underline{R}}(\xi)$ is the derivative of *R*(*x*) where *R* is the radius of curvature of the antenna lobe; $y_1$ is the antenna lobe overlap coordinate relative to the abscissa axis (Fig. 3); $y_2$ is the distance from the middle of the upper part of the antenna to the lobe – opened the antenna; *x* is a variable belonging to the interval 0… $x_2$ and defining the function y, which determines the change in the lobe curve from overlapping to opening the antenna; $x_1$ is a variable that determines the lower point of the beginning of the antenna lobe; $x_2$ is the lobe height and the height of the entire antenna (Fig. 2); *K* is the value of the coefficient.

## 2.1. Antenna modeling

The conducted studies have shown that without changing the design of the antenna radiator, completely different radiation patterns can be obtained by changing the phase relationships at the inputs of the antenna vibrators. This feature will be used in the construction of a UAV amplitude direction finder with high resolution. Consider the features of the development of a broadband radiator of the antenna system.

To analyse the basic element of the direction finder antenna, we performed the following stages of solution proposed research, see Fig. 4.

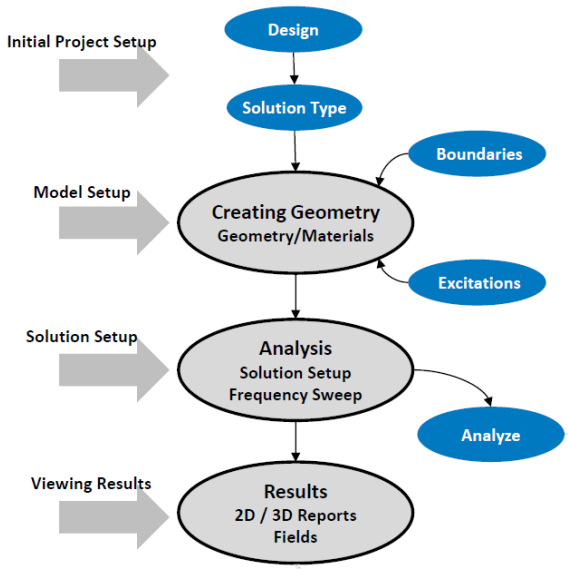


*Fig. 4. Overview of solution process in ANSYS 2022 FHSS environment*

During the calculations, the following was found: it is impossible to cover the required frequency range of 100–3000 MHz with a simple TSA antenna element; it is impossible to obtain an acceptable standing wave ratio (SWR) of the antenna element in a wide frequency range; the shape of the DC antenna element retains acceptable characteristics of the frequency range within an octave [10].

To eliminate these shortcomings, it is proposed to divide the design of the antenna element into three components, which must be connected according to the scheme shown in Fig. 5.

In the absence of control voltage U1 and U2, the working area of the radiating element is L1 of both radiating vibrators and the radiating element provides the necessary characteristics in the upper part of the operating frequency range.

When the control voltage U1 is applied, the working area of the radiating element is L1 together with L2. In this case, the radiating element has good characteristics in the middle part of the operating range (while they are much worse in the upper and lower parts of the operating range). And finally, when the control voltage U2 is applied, the working area of the radiating element is its entire surface, which provides good performance characteristics of the lower part of the operating frequency range.

The following characteristics of the antenna element were modeled: distribution of the E-component of the field, Fig. 6.

Simulation tools made it possible to obtain the structure of the current density distribution on the antenna surface, see Fig. 7, and the corresponding picture of the distribution of charges on the surface of the antenna, see Fig. 8.

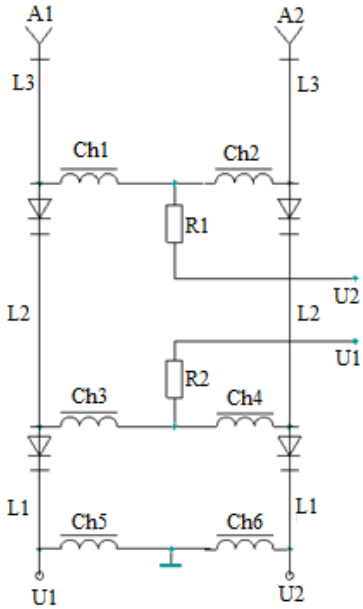


*Fig. 5. Schematic diagram of the antenna element*

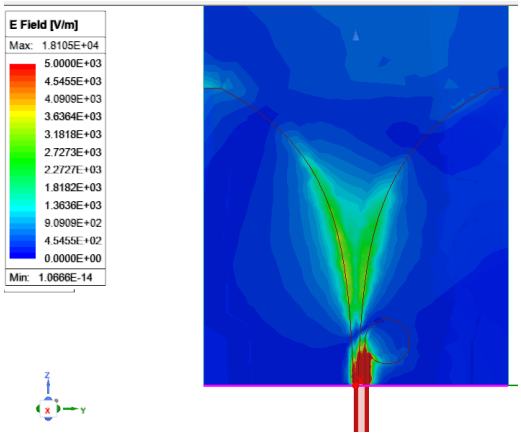


*Fig. 6. Electrical component distribution, simulation in ANSYS 2022 FHSS*

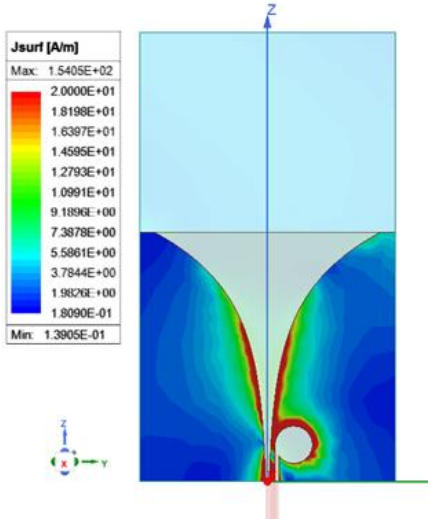


*Fig. 7. Structure of the current density distribution on the antenna surface in the ANSYS 2022 FHSS environment*

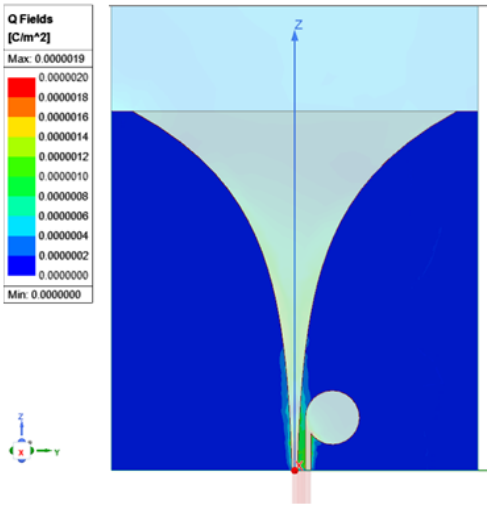


*Fig. 8. Charge distributions on the surface of an antenna system element in the ANSYS 2022 FHSS environment*

The directions of the Umov-Poynting vector for the antenna element were found (Fig. 9) and the pattern of losses in the space of the opening of the antenna element was determined (Fig. 10).

The input characteristics of a single element are shown in figures 11–15.

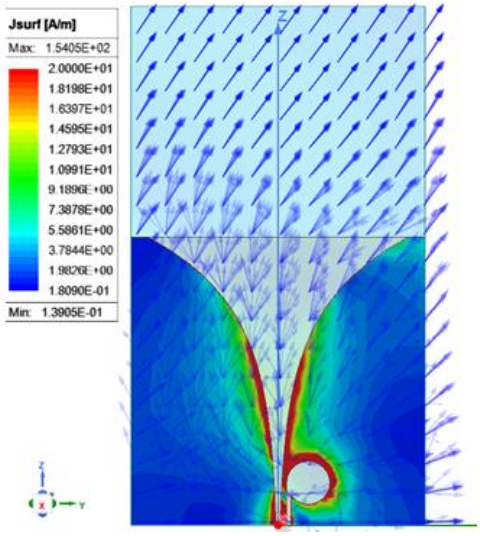


*Fig. 9. Directions of the Umov-Poynting vector for an antenna element in the ANSYS 2022 FHSS environment*

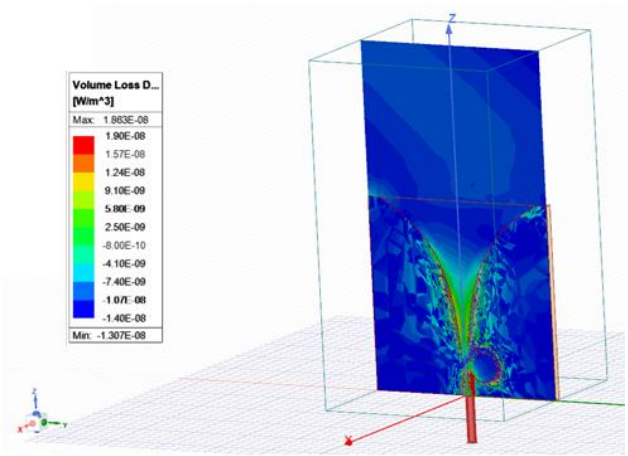


*Fig. 10. The pattern of volumetric losses in the space of the opening of the antenna element*

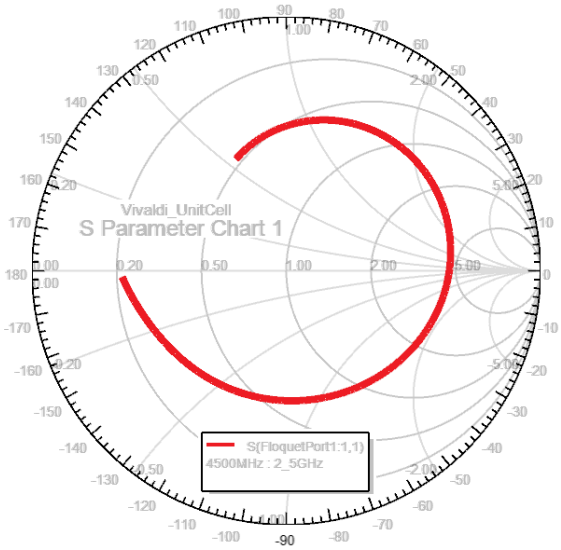


*Fig. 11. Smith's nomogram of the Vivaldi antenna element (2 GHz–5 GHz)*

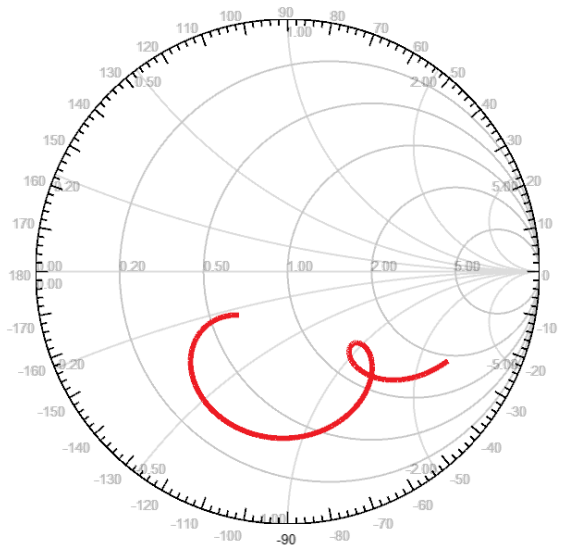

*Fig. 12. Smith's nomogram of the Vivaldi antenna element (0.1 GHz–5 GHz)*

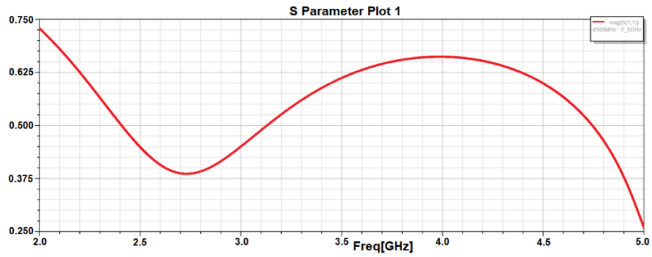


*Fig. 13. S-Parameter antenna element of the antenna system (2 GHz –5 GHz)*

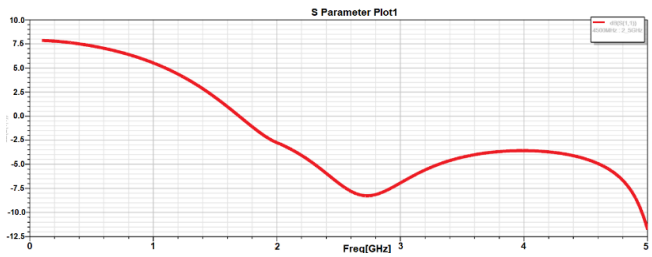


*Fig. 14. S-Parameter antenna element of the antenna system (100 MHz –5 GHz)*

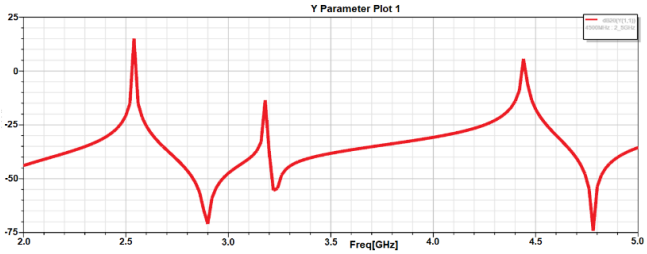


*Fig. 15. Y-Parameter antenna element of the antenna system*

To use the element under study as part of the radio direction finder antenna system, a two-stage amplitude-phase direction finding method is proposed, which involves the introduction of tables of mutual phases between adjacent antenna elements, for which the amplitudes of the signals received at the current time are maximum. The initial bearing estimate is determined by the amplitude method. The corrected bearing is determined by the phase distribution of the signal on the elements with the maximum amplitude. The correlation-interferometric method can also be applied.

The correlation-interferometric method can also be applied direction finding [1]. However, in this case, the antenna system will have to be supplemented with an antenna element with a circular radiation pattern, as implemented but in TCI direction-finding antenna systems [3], and tabulate the amplitude-phase radiation patterns of the elements. Thus, in this section, an antenna system for full-azimuth direction finding of radio emission sources with arbitrary polarization has been developed and studied. The advantages of the proposed design include the following:

- simplicity of design and manufacturability;
- metamaterial lenses in the apertures of antenna elements allow;
- correct phase distortions and improve their radiation pattern, input characteristics and cross-polarization isolation;
- simultaneous reception of signals on two orthogonal polarizations.

An analysis of works [2–12] shows that for direction finding antenna systems, classical vibrator antennas, less often slot antennas and TEM horns, have found the greatest application, and the most common direction-finding method is correlation-interferometric. The antenna systems themselves often have a ring geometry, while the receiving and processing equipment is located in the geometric center of the system. In the frequency range below 1 GHz, this the constructive solution does not have a noticeable effect on the parameters of the antenna system and the radio direction finder as a whole, since the radius of the antennas in the ring arrays is significantly larger than the dimensions of the receiving and processing equipment.

For the frequency range above 1 GHz, the size ratio changes significantly, and the structural elements of the receiving and processing equipment are scatterers, the dimensions of which are commensurate with the dimensions of the antenna elements of the system and their distance. As a rule, in this case, the design of the central part of the antenna is deliberately used as a reflector, which is clearly seen in the design of the ADD075 antenna system from Rohde & Schwarz [11]. This solution has some disadvantages, among which we pay attention to the linear vertical size of the central metal post. In some cases, for example, when placed on a mast, when connecting antenna systems of other frequency ranges or lightning protection elements [7], the height of the central vertical scattering structure is significantly greater than the length of the antenna elements of the system. Such a ratio of linear dimensions can lead to a significant irregularity of the antenna element radiation pattern in the vertical plane, and, as a result, to a significant decrease in sensitivity from the corresponding elevation directions, which is unacceptable for radio monitoring systems, especially UAVs.

To solve this problem, two variants of ring antenna arrays from modified dipoles [7] were developed and studied for the frequency range from 1 GHz to 5 GHz. into construction vibrators located in the immediate vicinity of the central rack, additional resistive loads are introduced to ensure the stability of the shape of the radiation pattern of each element in the array in the frequency band with an overlap factor of more than 3.

## 2.2. Calculation of the radiating element

The calculation of the radiating element was carried out in three stages: first, the optimal structure was calculated in the high-frequency part of the operating range, then in the mid-frequency part, and finally in the low-frequency part. On Fig. 16 shows the characteristics of the antenna element in the case of common-mode excitation in the absence of a control voltage.

On Fig. 17 shows the characteristics of the antenna element in the case of antiphase excitation in the absence of control voltages (HF part).

The simulation results allow us to study the process of changing the directional characteristic of the radiator in the operating frequency range. In particular, in Fig. 15 and Fig. 16 shows the spatial radiation patterns of the emitter and the gains in the operating frequency range.

From Fig. 16 and Fig. 17, we establish that in the frequency range of 1100–2500 MHz (HF part of the operating function) the antenna element has good characteristics in terms of antenna diagram, amplification factor and standing wave ratio (SWR) Fig. 18.

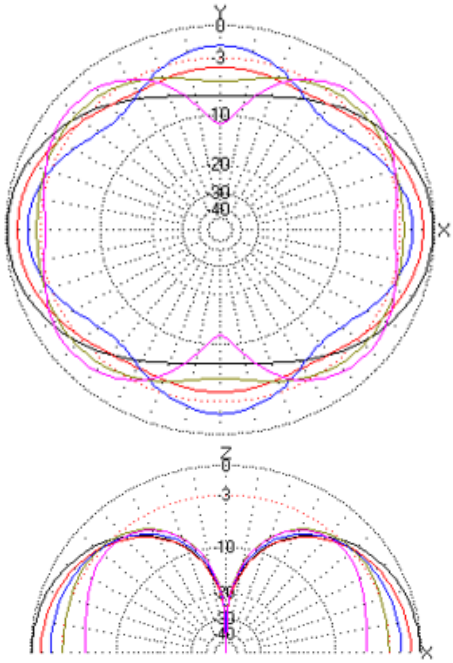


7.3(dBi) = 0dB

| Freq | R | jX | Ga | F/B | ON |
|---|---|---|---|---|---|
| 1100.0 | 37.6 | -666.6 | 7.3 | -0.0 | On |
| 1450.0 | 8.2 | -201.6 | 6.4 | -0.0 | On |
| 1800.0 | 4.2 | -118.2 | 5.5 | -0.0 | On |
| 2150.0 | 3.6 | -77.9 | 5.1 | -0.4 | On |
| 2500.0 | 4.9 | -49.6 | 5.8 | -2.0 | On |

*Fig. 16. Characteristics of the antenna element with common-mode excitation in the absence of control voltages (HF part)*

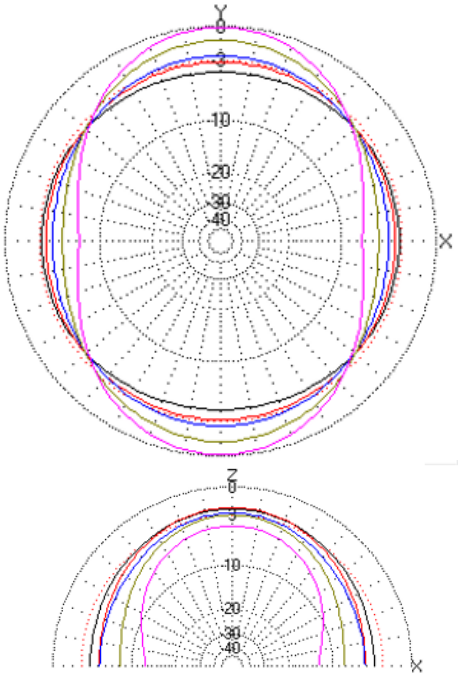


7.4(dBi) = 0dB

| Freq | R | jX | Ga | F/B | ON |
|---|---|---|---|---|---|
| 1100.0 | 76.4 | -348.5 | 5.2 | -0.4 | On |
| 1450.0 | 23.9 | -132.0 | 5.4 | -0.8 | On |
| 1800.0 | 19.1 | -77.4 | 4.9 | -1.3 | On |
| 2150.0 | 20.2 | -50.0 | 6.3 | -3.2 | On |
| 2500.0 | 22.7 | -32.8 | 7.4 | -5.7 | On |

*Fig. 17. Characteristics of the antenna element in the case of anti-phase excitation in the absence of control voltages (HF part)*

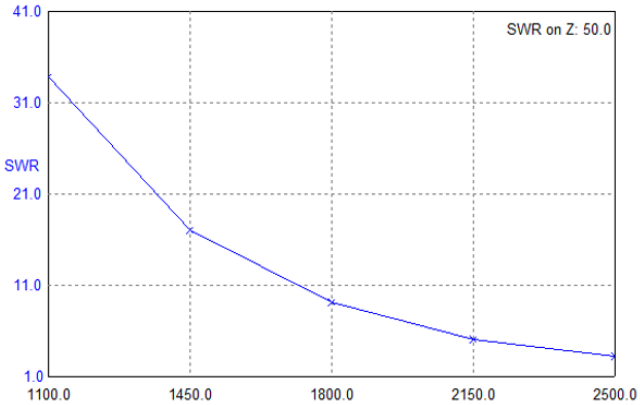


*Fig. 18. SWR characteristics of the antenna element under anti-phase excitation in the absence of control voltages (HF Part)*

When the control voltage U1 is applied to the main antenna element, the second segment is connected to two vibrators, which practically translates the antennas into the middle part of the frequency range. At the same time, in the HF part of the range, its characteristics deteriorate, and in the LF part of the operating range, poor matching and a low gain are observed. The working properties of the antenna element are shown in Fig. 19. The middle part of the operating range occupies the band from 400 to 1200 MHz. By applying the control voltage U2, the entire antenna structure is put into operation, providing good performance
in the lower part of the operating range. At the same time, the characteristics of the antenna element in HF become even worse (antenna diagrams are distorted and side lobes appear, the presence of which is highly undesirable when building direction finding devices), and in the middle part of the range antenna diagrams deteriorate.

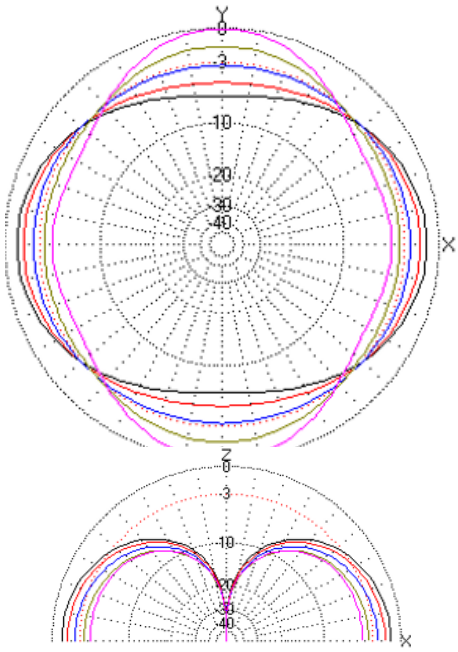


7.8(dBi) = 0dB

| Freq | R | jX | Ga | F/B | ON |
|---|---|---|---|---|---|
| 300.0 | 0.0 | 63.4 | 6.9 | -0.0 | On |
| 500.0 | 0.3 | 129.7 | 6.3 | 0.0 | On |
| 700.0 | 7.6 | 276.6 | 5.4 | 0.0 | On |
| 900.0 | 147.5 | 1133.9 | 6.3 | -1.1 | On |
| 1100.0 | 52.9 | -715.7 | 7.8 | -2.3 | On |

*Fig. 19. Characteristics of the antenna diagram of the antenna element with common-mode excitation in the presence of a control voltage U1 (middle part of the frequency range)*

The characteristics (antenna diagrams) of the antenna element with anti-phase excitation in the presence of the control voltage U2 (LF part) are presented in Fig. 20.

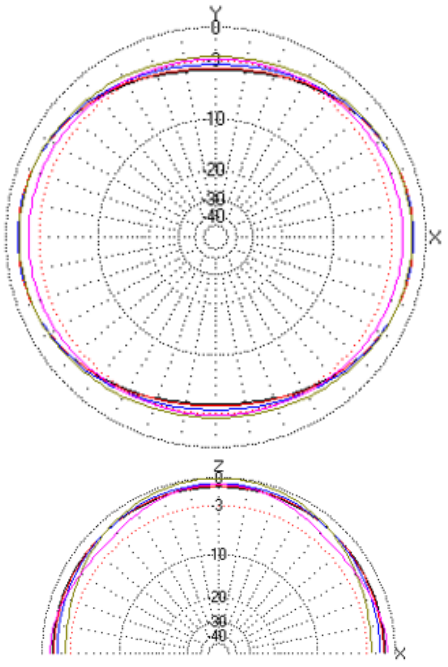


5.7(dBi) = 0dB

| Freq | R | jX | Ga | F/B | ON |
|---|---|---|---|---|---|
| 100.0 | 0.0 | 17.1 | 4.8 | -0.0 | On |
| 200.0 | 0.0 | 35.5 | 4.9 | -0.1 | On |
| 300.0 | 0.2 | 56.8 | 5.2 | -0.2 | On |
| 400.0 | 0.7 | 83.5 | 5.7 | -0.6 | On |
| 500.0 | 2.7 | 120.1 | 5.1 | -1.2 | On |

*Fig. 20. The characteristics (antenna diagrams) of the antenna element with anti-phase excitation in the presence of the control voltage U2 (LF part)*

Thus, by dividing the operating frequency range into three sections, it is possible to cover the frequency range of 100–2500 MHz with good performance.

Based on the simulation results, a prototype antenna was developed, Fig. 21.

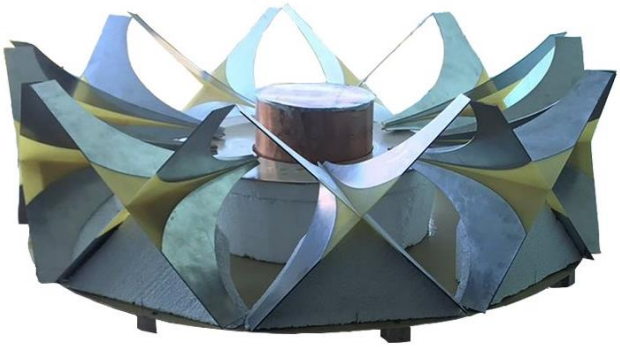

*Fig. 21. Prototype of the manufactured antenna*

The antenna was manufactured in the context of the implementation of a grant from the Ministry of Education and Science of Ukraine on the scientific topic "Development of a broadband direction-finding system for determining the location of military and non-military UAVs" state registration number 0122U001211.

## 3. Conclusion

The paper presents the results of the development and modeling of a broadband antenna system for UAV direction finding. The research covered the issues of analytical description of the antenna system based on the prototype – the Vivaldi antenna. The article presents a mathematical description of the Vivaldi antenna element model. An experimental relationship between the geometrical parameters and characteristics of the antenna has been established. A review of the current state of the issue of designing antenna systems based on the concept of constructing ultra-wideband directional antenna elements in the absence of a phase centre. The main trends in the modern design of broadband antenna systems are determined. The main parameters of the proposed broadband antenna are determined by the method of mathematical modeling. The parameters of the proposed antenna in the frequency range under various excitation conditions are investigated, and the specifics of the application of such a system under the conditions of its possible operation as part of UAV direction-finding complexes are given.

## References

[1] Boiko J., Karpova L., Eromenko O., Havrylko Y.: Evaluation of phase-frequency instability when processing complex radar signals. International Journal of Electrical and Computer Engineering 10(4), 2020, 4226–4236 [http://doi.org/10.11591/ijece.v10i4.pp4226-4236].

[2] Ershadi S. E. et al.: Rotman lens design and optimization for 5G applications. International Journal of Microwave and Wireless Technologies 10(9), 2018, 1048–1057 [http://doi.org/10.5604/20830157.1121333].

[3] Ghaemi K., Ma R., Behdad N.: A Small-Aperture, Ultrawideband HF/VHF Direction-Finding System for Unmanned Aerial Vehicles. IEEE Transactions on Antennas and Propagation 66(10), 2018, 5109–5120 [http://doi.org/10.1109/TAP.2018.2858210].

[4] Ghamari M. et al.: Unmanned Aerial Vehicle Communications for Civil Applications: A Review. IEEE Access 10, 2022, 102492–102531 [http://doi.org/10.1109/ACCESS.2022.3208571].

[5] Jensen M. A., Mahmood A., Mehmood R.: A compact low-cost direction-finding system for unmanned aerial vehicles. Proceedings of 12th European Conference on Antennas and Propagation EuCAP 2018, London 2018, 1–4 [http://doi.org/10.1049/cp.2018.0983].

[6] Kazici S., Loutridis A., Caratelli D.: A Novel Class of Super-Elliptical Vivaldi Antennas with Enhanced Radiation Properties. IEEE International Symposium on Antennas and Propagation and USNC-URSI Radio Science Meeting, Atlanta 2019, 259–260 [http://doi.org/10.1109/APUSNCURSINRSM.2019.8888948].

[7] Keshavarzian P., Okoniewski M., Nielsen J.: Active Phase-Conjugating Rotman Lens with Reflection Amplifiers for Backscattering Enhancement. IEEE Trans. on Microwave Theory and Techniques 68(1), 2020, 405–413 [http://doi.org/10.1017/S1759078718000934].

[8] Parkhomey I. et al.: Assessment of quality indicators of the automatic control system influence of accident interference. Telkomnika (Telecommunication Computing Electronics and Control) 18(4), 2020, 2070–2079 [http://doi.org/10.12928/TELKOMNIKA.v18i4.15601].

[9] Parkhomey I., Boiko J., Eromenko O.: Methodology for the Development of Radar Control Systems for Flying Targets with an Artificially Reduced RCS. Journal of Robotics and Control (JRC) 3(4), 2022, 402–408 [http://doi.org/10.18196/jrc.v3i4.15440].

[10] Pfeiffer C.: Fundamental Efficiency Limits for Small Metallic Antennas. IEEE Transactions on Antennas and Propagation 65(4), 2017, 1642–1650 [http://doi.org/10.1109/TAP.2017.2670532].

[11] R&S®ADDx Single-Channel DF Antennas Product overview [http://www.sekorm.com/doc/1094983.html] (available: 03.11.2022).

[12] Stockbroeckx B., Vander Vorst A.: Copolar and cross-polar radiation of Vivaldi antenna on dielectric substrate. IEEE Transactions on Antennas and Propagation 48(1), 2000, 19–25 [http://doi.org/10.1109/8.827381].

[13] Valavanis K. P., Vachtsevanos G. J.: Handbook of Unmanned Aerial Vehicles – Dordrecht, Springer 2015 [http://doi.org/10.1007/978-90-481-9707-1].

**D.Sc. Eng. Juliy Boiko**
e-mail: boykoym@khmnu.edu.ua

In 2002 he received a Candidate of Science degree (Ph.D.) at the Institute of Electrodynamics of the National Academy of Sciences of Ukraine in the field of device design and development of methods for measuring electrical and magnetic quantities. In 2015, he received a Doctor of Science degree (D.Sc. in Engineering) at the State University of Telecommunications (Kyiv, Ukraine) in the field of signal reception, synchronization, signal processing in telecommunication systems. Currently, Full Professor of the Department of Telecommunications, Media and Intelligent Technologies, Khmelnytskyi National University (Khmelnytskyi, Ukraine). Research includes issues related to the development of devices for the automation of devices and systems, the theory of coding, synchronization systems, diagnostics and signal processing.

http://orcid.org/0000-0003-0603-7827

**D.Sc. Eng. Oleksiy Polikarovskykh**
e-mail: polalexey@gmail.com

In 2006 he received a Candidate of Science degree (Ph.D.) at the Vinnitsa National Technical University in the field of radio measuring instruments. In 2015, he received a Doctor of Science degree (D.Sc. in Engineering) at the State University of Intellectual Technologies and Communication (Odessa, Ukraine) in the field of signal synthesis in telecommunication systems. In 2019 Full Professor of the Department of Telecommunications, Media and Intelligent Technologies, Khmelnitsky National University (Khmelnitsky, Ukraine). Currently, Full Professor of the Department of Technical Cybernetics and Information Technologies, Odessa National Maritime University (Odessa, Ukraine). Research includes issues related to the development of devices for signal synthesis, the theory of cybersecurity and Software Defined Radio.

http://orcid.org/0000-0002-1893-7390

**Ph.D. Eng. Vitalii Tkachuk**
e-mail: tkachukvi@khmnu.edu.ua

In 2011 he received a Candidate of Science degree (Ph.D.) at the Khmelnytskyi National University of Sciences in the field machine science. Currently the head of the Department of Mechanical Engineering Technology, Khmelnytskyi National University (Khmelnytskyi, Ukraine). Scientific research includes issues related to the design and manufacture of mechanical devices and structures. Engineering analysis of the performance of mechanisms, as well as issues related to the development of means of automating devices and systems.

http://orcid.org/0000-0003-0640-2740

http://doi.org/10.35784/iapgos.3371

*received: 15.12.2022 | revised: 13.03.2023 | accepted: 13.03.2023 | available online: 31.03.2023*

# SENSOR PLATFORM OF INDUSTRIAL TOMOGRAPHY FOR DIAGNOSTICS AND CONTROL OF TECHNOLOGICAL PROCESSES

**Krzysztof Król[1,2], Tomasz Rymarczyk[1,2], Konrad Niderla[1,2], Edward Kozłowski[3]**

[1]Research and Development Center, Netrix S.A., Lublin, Poland, [2]WSEI University, Lublin, Poland, [3]Lublin University of Technology, Faculty of Management, Lublin, Poland

***Abstract:*** *This article presents an industrial tomography platform for diagnosing and controlling technological processes. The system has been prepared in such a way that it is possible to add individual sensors that cooperate with the system of an intelligent cyber-physical platform with an open architecture. In addition, it is possible to configure and cooperate with external systems freely. As part of the experimental work, a platform has been developed that allows individual subsystems and external customer systems to work together. The cyber-physical system, a new generation of digital systems, focuses mainly on the complex interaction and integration between cyberspace and the physical world. A cyber-physical system consists of highly integrated computing, communication, control and physical elements. It focuses mainly on the complex interaction and integration between cyberspace and the physical world.*

**Keywords**: electrical capacitance tomography, cyber-physical systems, sensors, electrical impedance tomography

## PLATFORMA SENSOROWA TOMOGRAFII PRZEMYSŁOWEJ DO DIAGNOSTYKI I STEROWANIA PROCESAMI TECHNOLOGICZNYMI

***Streszczenie.*** *W artykule przedstawiono przemysłową platformę tomograficzną wykorzystywaną do diagnostyki i sterowania procesami technologicznymi. Aplikacja pozwala na dodawanie poszczególnych czujników współpracujących z systemem inteligentnej platformy cyber-fizycznej o otwartej architekturze, a dodatkowo możliwa była dowolna konfiguracja i współpraca z systemami zewnętrznymi. W ramach prac eksperymentalnych opracowano platformę, która umożliwia współpracę poszczególnych podsystemów i zewnętrznych systemów klienta. System cyberfizyczny, koncentruje się głównie na złożonej interakcji i integracji między cyberprzestrzenią a światem fizycznym. System cyberfizyczny składa się z wysoce zintegrowanych elementów obliczeniowych, komunikacyjnych, kontrolnych i fizycznych. Rozwiązanie koncentruje się głównie na złożonej interakcji i integracji między cyberprzestrzenią a światem fizycznym.*

**Słowa kluczowe**: tomografia pojemnościowa, systemy cyber-fizyczne, sensory, tomografia impedancyjna

## 1. General principles of the system

The portal allows the user to manage the data collected on the server by reading current or historical data. Sensor data is sent to the database and can be viewed and read anytime. Individual sensors can be added to the system and communicate using MQTT, OPC, and Kafka. The system continuously displays data from sensors measuring various physical quantities.

It is a system that allows building a platform for Industry 4.0 by combining the system with smart sensors [1, 2, 7, 12, 17]. Furthermore, a unique solution is using industrial tomography with appropriate algorithms to analyse and diagnose technological processes.

The networking of intelligent sensors, many advantages can bring many benefits to industrial environments, such as the combination of information and operational technologies. Although operational technologies include hardware and software systems that control processes on the shop floor, they have generally not been integrated into a network or wider information system. This connection allows computer components to communicate directly with other machines and central servers, exchanging information via the computer network.

It will also reduce the number of operations required; improve performance and resource utilisation; minimise the life cycle cost of the asset; speed up decision-making; buy and sell products as services, expand business opportunities and enable new business models to emerge for manufacturing. Therefore, the requirements for emerging factories that form global networks of assets, storage systems and manufacturing processes in cyber-physical systems are key issues.

Cyber-physical systems make it possible to increase the level of effectiveness and efficiency in industrial value creation through the amount of real-time information on technical processes [5, 13, 18]. To fully exploit cyber-physical systems, the information gathered should include the knowledge of the personnel. Often this knowledge is only available informally, and the problem is formalising it. However, due to the high value of this knowledge, systematic collection, categorisation, and mapping methods should be introduced. Furthermore, the availability of this knowledge can be used to develop operational guidelines, which are an essential part of decision support systems.

An example might be the repair of a faulty machine. The first time a fault occurs, the troubleshooting process should be documented so that if it occurs again, there are guidelines for action, and each troubleshooter can benefit from the effect of the learning curve. However, the system-based capturing, categorising and mapping of hidden knowledge requires additional employee effort. Therefore, it is necessary to explain the overall added value based on the availability of action guidelines after the development and implementation of a decision support system [19, 20, 21].

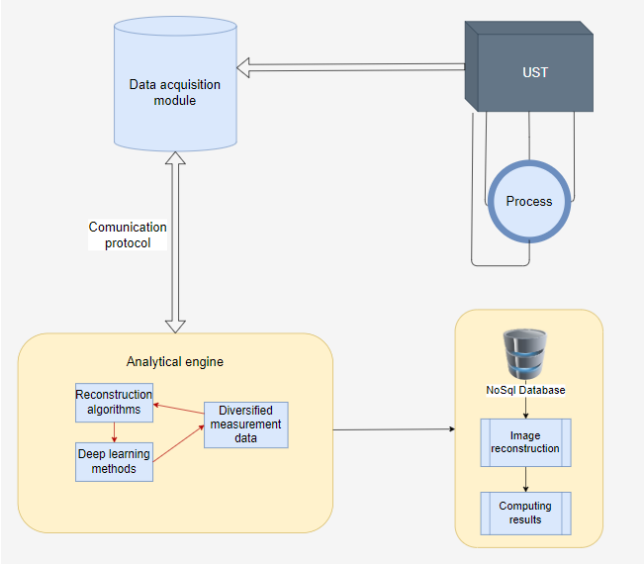


*Fig. 1. Model of a sensor platform with an analytical system*

In industrial research, it is often necessary to carry out measurements that cannot be carried out using non-destructive methods without interfering with the inside of the tested object. The presented system consists of a network of intelligent sensors using wired and wireless communication, which allows the acquisition of data from various sources, directly or indirectly, related to the production process (figure 1).

Sensors and measuring devices are connected to the communication interface whose task is to read the signal from the selected sensor, process it into a consistent form and then send the read and processed data to the acquisition module (figures 2, 3 and 4). The algorithm was trained using learning data obtained by computer simulation from real models to solve the inverse problem. In addition, the conductivity values of individual pixels of the output vector made it possible to obtain images of the interior of the tested objects.

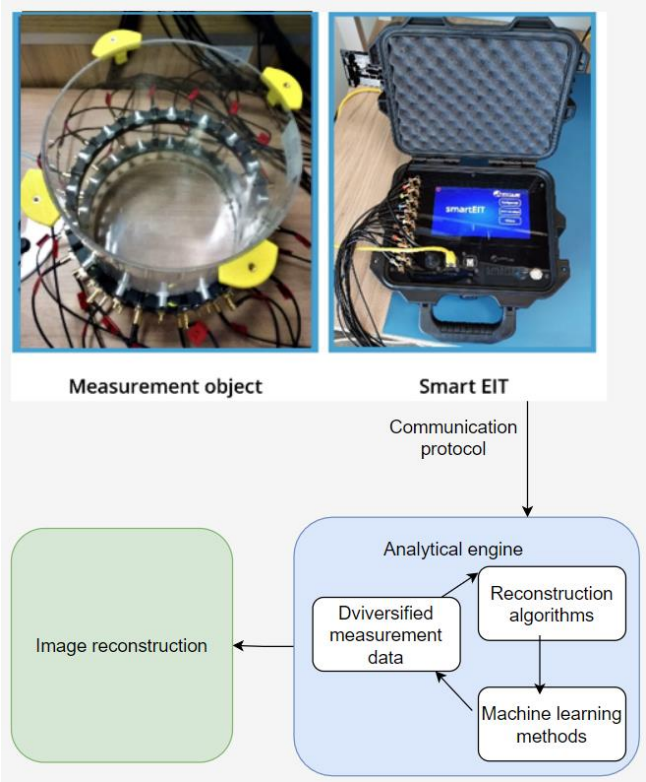


*Fig. 2. Measurement system with a model of data transmission, collection and analysis*

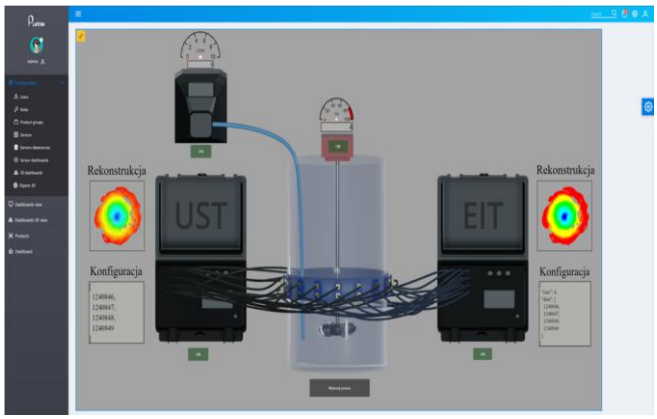


*Fig. 3. Digital twin – simulation*

The research presented focuses on electrical impedance tomography (EIT), a non-invasive imaging technique that visualises the dynamic distribution of electrical conductivity within the test object. In this method, the sensitivity of EIT solutions to measurement, numerical and model errors requires adapting model parameters to specific cases. In the traditional approach, studies performed with EIT tomography are computationally resource-intensive, resulting in complexity. Therefore, the best solutions are sought to reduce the computational effort by finding suitable algorithms to improve the quality of the measurements. The authors used the logistic regression method to reconstruct tomographic images.

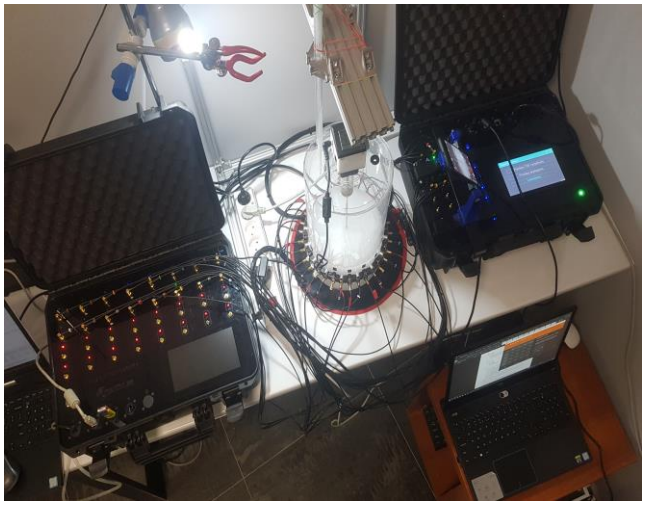

*Fig. 4. Digital twin – real model*

A cloud computing model (PLATOM Cloud) has been developed. The system design is based on containers with the possibility of deploying them in the cloud. Using containers makes it possible to use the public and private clouds at the location specified by the customer. The model is based on virtualisation and resource aggregation. The starting point for the developed concept of communication protocols of the PLATOM platform is a general architecture model that considers the data flow between five basic types of components, i.e. measurement, control and service components, including central, computational, timestamp, GUI and data. The control architecture and data communication platform technology has been developed. Measurement and control, and service components have been incorporated into the PLATOM platform. Measurement and control components are devices with dedicated software designed to collect data from measurement devices used to monitor the state of the process (tomograph, camera, flow meter, etc.) and to set values of settings on active devices of the process (inverters, control valves, etc.).

On the other hand, service components are responsible for implementing individual PLATOM platform services and are not directly connected to the process measurement and control devices. Instead, they operate as elements of the PLATOM Cloud in the form of software modules on dedicated server computers. The following functionalities/modules are implemented within these components: repository, computing module, database module for storage and distribution, central module and GUI modules. The diagram in the figure (figure 5) illustrates the platform concept with the division into measurement and control components and service components with the indication of the data transmission direction.

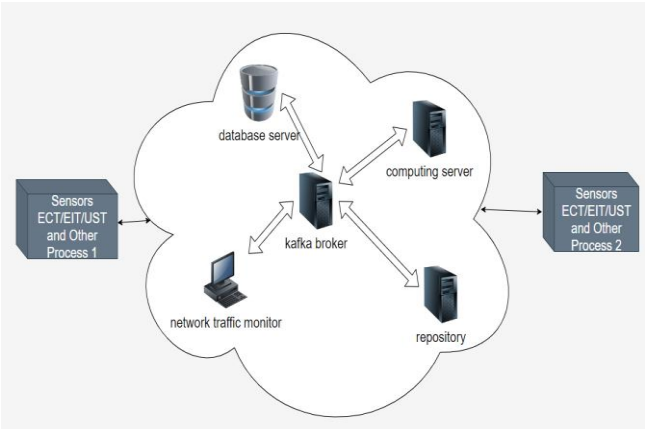


*Fig. 5. Schematic diagram of the built computational cloud*

## 2. System development

The preparation of the system was divided into several tasks. The main challenge of this phase was to develop 3D and 4D (time-resolved) imaging models and techniques for industrial crystallisation and fermentation processes using process tomography techniques.

In the first task, mathematical investigations were carried out using existing software tools for modelling the crystallisation process, enabling the selection of a technologically optimal algorithm for visualising the process in terms of ultrasonic, electrical and capacitive tomography measurements. In the next task, the research focused on developing mathematical models of the fermentation process and selecting an optimal technological algorithm for the visualisation of the process in ultrasonic, electrical and capacitive tomography measurements. In the third task, several analyses were conducted by applying mathematical models describing time-resolved tomographic measurements and visualising the results obtained in industrial batch crystallisation and fermentation processes. The next task allowed the development of new technology for tomographic measurements using ultrasonic tomography (UST) to control and seriation batch crystallisation processes [8–11]. This task required the development of hardware solutions and appropriate algorithmic tools. As part of the task, several works were carried out to develop tools for modelling the crystallisation process taking into account reaction kinetics and crystal particle growth through a population equilibrium model. The hardware solutions developed made it possible to increase the efficiency of ultrasonic wave penetration into crystal suspensions in terms of reflection and transmission tomography methods. Measurement cards were also developed for cooperation with probes of different ultrasonic wave frequencies. A method of effectively placing active elements (ultrasonic transmitters) on the rim of the vessel (reactor) where the crystallisation process occurred was also developed. At the same time, a model for spatially resolved and time-resolved (3D and 4D) measurement of crystal size and density using tomographic data reconstruction has been developed. The work carried out as part of the task also included the development of a new concept for adaptive control of homogeneous crystal growth by ultrasonic activation. A number of crystallisation measurements were carried out to test the concept of continuous and time-resolved measurements. The crystallisation measurements were carried out at different reactant dosing rates and at different substrate mixing rates. The collected results of the task directly contributed to creating a demonstration set for the measurement of batch crystallisation processes using process tomography techniques.

The implementation of the next task focused on developing new technology for tomographic measurements using capacitive (ECT) and resistive (ERT) tomography techniques to control and manage the biogas fermentation process. The work carried out in this task included the development of tools for modelling the fermentation process, considering mixing methods, including pneumatic mixing. Work also involved increasing the efficiency of tomographic imaging by simultaneously applying capacitive and resistive tomography techniques. Similar to ultrasound tomography, models have been developed for the efficient placement of measurement electrodes and their mutual positioning. It is particularly important for 3D and 4D measurements. In addition, time-resolved measurements were carried out to investigate the possibility of improving the efficiency of the fermentation process using process tomography techniques. All the research, tests and simulations carried out, combined with the hardware components developed, led to the development a demonstration measurement setup. In the next task, process measurements were performed with the developed demonstration workstations to verify the results of numerical simulations with the developed solution elements in the context of application in industrial installations. In the last task, assumptions were developed for algorithms of reconstruction and visualisation of process tomography images were developed [3, 23-26, 28].

The platform consists of special tanks for carrying out the crystallisation. The tanks are equipped with special holders that allow the mutual arrangement of the transducers to be changed and the measurement system to be adapted to the crystallisation process to be analysed. The platform allows ultrasonic tomography measurements in both transmission and reflection modes of ultrasonic waves. Furthermore, the hardware platform can work with transducers of different frequencies.

Measurements are made in 32 channels. 3D and 4D measurements are possible for both techniques. The results obtained can be directly visualised on the measuring device. Due to the high speed of measurement data acquisition and the development of new image reconstruction techniques, it is possible to obtain images in less than 250 ms. During the crystallisation process, the crystals formed to change the physical properties of the medium. As the number of crystals increases, the density of the medium changes. Density changes increase the speed of propagation of ultrasonic waves. Based on these changes and the known size of the container, the crystal density can be spatially measured throughout the process. The developed models were used to design the crystallisation process. Within the fermentation process, using a novel method of simultaneous measurement of resistive and capacitive tomography for analysis and control allowed the detection of heterogeneities. As the measurements were made at high speed, it was possible to control the stirrer by implementing FPGAs. The measurements carried out showed that the delay or reaction time between the detection of inhomogeneities and the operation of the agitator is less than 1 ms, which fully meets the parameters specified in the milestone. As with ultrasound tomography, a demonstration platform was developed to analyse fermentation processes. The demonstration platform also required the development of reliable software to control the measurements and reconstruct the huge amount of tomographic data (as the acquisition speed increases, so do the amount of data).

## 3. Measurement

### 3.1. EIT measurement system

The designed tomograph uses EIT technology to study the cross-sections of closed spaces. The spatial distribution of the impedance can be determined, and the internal structure of the medium can be visualised by measuring the voltages on electrodes directly adjacent to the medium. Thanks to the built-in microcomputer, it is possible to carry out EIT measurements and view the reconstructions based on them. It also has a network interface for data transfer to an external server. The tomograph measures voltages by switching channels according to the polar method. First, multiplexers connect the EXC and GND outputs to two opposite electrodes. A current flows, the intensity of which is programmed to a set value. Then the signal input is successively connected to the remaining electrodes on which the voltage to GND is measured. After 14 measurements, the measurement information is disconnected, the forcing electrodes are switched to the next pair, and the cycle is repeated. The 224 (16x14) results were converted into 192 (16x12) values of the voltages between the measuring electrodes. The image reconstruction algorithm then transforms the results.

### 3.2. Logistic regression

When creating a reconstruction in EIT, we need to answer the question of which finite elements belong to inclusion in the field of view. We define a logistic regression model to create the reconstruction for each finite element. Let $(\Omega, F, P)$ be a probability space, and for the finite element, we define a random variable $Y$ with discrete distribution, where $Y:\Omega \rightarrow \{0,1\}$. In the presented approach, if the finite element belongs to inclusion, we put on the realisation of random variable $Y$ is equal to 1 (i.e. y = 1); otherwise, 0. The main objective is to determine whether the finite element belongs to inclusion based on signal $x \in \boldsymbol{R}^m$ obtained from sensors. For this purpose, we must define a classifier $f:\boldsymbol{R}^m \rightarrow \{0,1\}$). In this paper, logistic regression has been used to create a classifier. The logistic regression model is used to estimate the binomial (or multinomial) distribution of the response variable $Y$ based on the realisation of the input variables $X: \in \boldsymbol{R}^m$ (in other words, we determine $P(Y = y|X)$, where y∈ {0,1}).In the literature $P(Y = 1|X)$ value denotes the success probability, but $P(Y = 0|X)$ – defeat probability [14, 16-17, 27].

### 3.3. Results

A measurement system consisting of a SmartEIT tomograph and a measurement object with 16 sensors was used (Fig. 6). The image reconstructions are shown in figure 7, where three variants of the algorithms were compared, comparing the images obtained by the methods Logistic with Elasticnet [6], Logistic with Db12 wavelet [4], Logistic with Sym9 wavelet [21] were compared. Table 1 corresponds to figure 5 and presents a comparative analysis of the reconstructions obtained. Based on the indicators: Accuracy, Sensitivity, Specificity, PPV, NPV, Detection Rate, and Level. Basic properties of the first model describing the view area. Number of electrodes: 16, type of electrodes: linear, number of nodes: 1338, number of finite elements: 2502. In this case, the decomposition level j = 2 was used for wavelet analysis.

*Table 1. Summary of reconstruction of pattern presented in figure 7*

| Methods | Elastic net | Db12 | Sym9 |
|---|---|---|---|
| Accuracy | 0.957 | 0.950 | 0.946 |
| Sensitivity | 0.609 | 0.646 | 0.589 |
| Specificity | 0.995 | 0.982 | 0.985 |
| PPV | 0.925 | 0.797 | 0.803 |
| NPV | 0.959 | 0.963 | 0.957 |
| Detection Rate | 0.059 | 0.063 | 0.057 |
| Level | 0.50 | 0.30 | 0.27 |

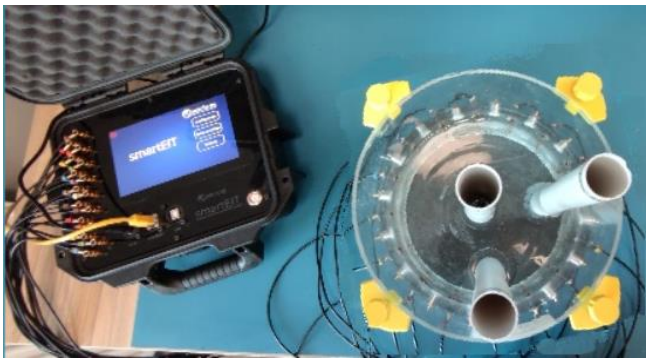


*Fig. 6. Measuring system using the SmartEIT electric impedance tomograph*

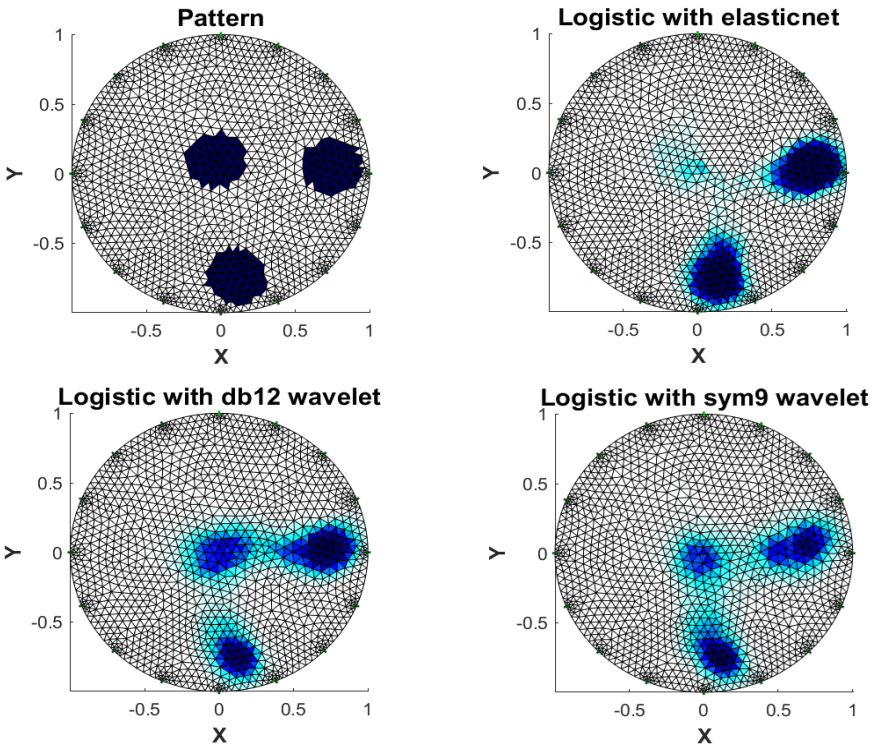


*Fig. 7. Image reconstruction – 16 sensors, three objects: Pattern, Logistic with Elasticnet, Logistic with Db12 wavelet, Logistic with Sym9 wavelet*

## 4. Conclusions

An industrial tomography platform used for process diagnostics and control has been developed. Adding additional sensors to the platform, which work together, is possible. It allows individual subsystems and external customer systems to work together and focus on developing algorithms and models for image analysis and reconstruction. All the presented algorithms were found suitable for practical applications in industrial tomography. Furthermore, the proposed research results contain essential information that may contribute to accelerating machine learning methods in industrial tomography.

## References


[1] Akhtari S. et al.: Intelligent embedded load detection at the edge on industry 4.0 powertrains applications. 5th international forum on research and technology for society and industry – RTSD2019, 2019, 427–430.

[2] Assawaarayakul C. et al.: Integrate digital twin to exist production system for industry 4.0. 4th technology innovation management and engineering science international conference (TIMES-iCON) 2019, 1–5.

[3] Banasiak R. et al.: Study on two-phase flow regime visualisation and identification using 3D electrical capacitance tomography and fuzzy-logic classification. International Journal of Multiphase Flow 58, 2014, 1–14 [http://doi.org/10.1016/J.IJMULTIPHASEFLOW.2013.07.003].

[4] Daubechies I.: Orthonormal Bases of Compactly Supported Wavelets. Communications on Pure and Applied Mathematics 41(7), 1988, 909–96.

[5] He J. et al.: Locality-aware replacement algorithm in flash memory to optimise cloud computing for smart factory of industry 4.0. IEEE Access 5, 2017, 16252–16262.

[6] Hui Z., Hastie T.: Regularisation and Variable Selection via the Elastic Net. Journal of the Royal Statistical Society: Series B (Statistical Methodology) 67(2), 2005, 301–20.

[7] Król K. et al.: Intelligent Sensor Platform with Open Architecture for Monitoring and Control of Industry 4.0 Systems. European Research Studies Journal 24(2), 2021, 597–606.

[8] Kania K. et al.: Image reconstruction in ultrasound transmission tomography using the Fermat's Principle. Przegląd Elektrotechniczny 96(1), 2020, 186–189.

[9] Kłosowski G. et al.: Maintenance of industrial reactors supported by deep learning driven ultrasound tomography. Eksploatacja i Niezawodność – Maintenance and Reliability 22(1), 2020, 138–147 [http://doi.org/10.17531/ein.2020.1.16].

[10] Kłosowski G. et al.: Neural hybrid tomograph for monitoring industrial reactors. Przegląd Elektrotechniczny 97(12), 2020, 190–193.

[11] Kłosowski G. et al.: Quality Assessment of the Neural Algorithms on the Example of EIT-UST Hybrid Tomography. Sensors 20, 2020 [http://doi.org/10.3390/s20113324].

[12] Kłosowski G. et al.: Using an LSTM network to monitor industrial reactors using electrical capacitance and impedance tomography – a hybrid approach. Eksploatacja i Niezawodność – Maintenance and Reliability 25(1), 2023, 11 [http://doi.org/10.17531/ein.2023.1.11].

[13] Kong X. T. et al.: Cyber physical ecommerce logistics system: an implementation case in Hong Kong. Comput Ind Eng 139, 2020, 106170.

[14] Kozłowski E. et al.: Logistic regression in image reconstruction in electrical impedance tomography. Przegląd Elektrotechniczny 97(5), 2020, 95–98.

[15] Kozłowski E. et al.: The use of principal component analysis and logistic regression for cutter state identification. Innovations in Industrial Engineering, Springer International Publishing 2021, 396–405.

[16] Kozłowski E. et al.: Application of the logistic regression for determining transition probability matrix of operating states in the transport systems. Eksploatacja i Niezawodność – Maintenance and Reliability, 22(2), 2020, 192–200 [http://doi.org/10.17531/ein.2020.2.2].

[17] Kozłowski E. et al.: Assessment model of cutting tool condition for real-time supervision system. Eksploatacja i Niezawodność – Maintenance and Reliability, 21(4), 2019, 679–685 [http://doi.org/10.17531/ein.2019.4.18].

[18] Lins T. et al.: Cyber-physical production systems retrofitting in context of industry 4.0. Comput Ind Eng 139, 2020, 106193, 59.

[19] Manavalan E., Jayakrishna K.: A review of internet of things (iot) embedded sustainable supply chain for industry 4.0 requirements. Comput Ind Eng 127, 2019, 925–953.

[20] Occhiuzzi C. et al.: Rfid technology for industry 4.0: architectures and challenges. IEEE international conference on RFID technology and applications (RFID-TA) 2019, 181–186.

[21] Percival D. B, Walden A.: Wavelet Methods for Time Series Analysis 4. Cambridge University Press, 2000.

[22] Poór P. et al.: Predictive maintenance 4.0 as next evolution step in industrial maintenance development. International Research Conference on Smart Computing and Systems Engineering – SCSE, 2019, 245–253.

[23] Rymarczyk T., Sikora J.: Optimisation Method and PCA noise suppression application for Ultrasound Transmission Tomography. Przegląd Elektrotechniczny 96(2), 2020, 90–93.

[24] Rymarczyk T.: New methods to determine moisture areas by electrical impedance tomography. International Journal of Applied Electromagnetics and Mechanics 52(1–2), 2016, 79–87 [http://doi.org/10.3233/JAE-162071].

[25] Rymarczyk T. et al.: Ultrasonic tomography for reflection and transmission wave analysis. Przegląd Elektrotechniczny 96(3), 2020, 170–173.

[26] Rymarczyk T. et al.: The use of the autoencoder to improve images in ultrasound tomography. Przegląd Elektrotechniczny 96(8), 2020, 160–163.

[27] Rymarczyk T. et al.: Logistic Regression for Machine Learning in Process Tomography. Sensors 19(15), 2020 [http://doi.org/10.3390/s19153400].

[28] Rymarczyk T. et al.: Analysis of vertical and horizontal flows of liquids and gases through a wire-mesh sensor. Przegląd Elektrotechniczny 96(3), 2020.



**M.Sc. Eng. Krzysztof Król**
e-mail: krzysztof.krol@netrix.com.pl

He is an employee of the Research and Development Department at the Research and Development Centre of Netrix S.A. and an assistant at the Higher School of Economics and Innovation in Lublin. Associated with computer science for over 14 years. He conducts scientific research in the field of process tomography, IoT and sensor networks. He conducts scientific research in the field of process tomography, IoT and sensor networks.

http://orcid.org/0000-0002-0114-2794



**D.Sc. Tomasz Rymarczyk**
e-mail: tomasz.rymarczyk@netrix.com.pl

Director in Research and Development Center Netrix S.A. His research area focuses on applying non-invasive imaging techniques, electrical tomography, image reconstruction, numerical modelling, image processing and analysis, process tomography, software engineering, knowledge engineering, artificial intelligence and computer measurement systems.

http://orcid.org/0000-0002-3524-9151



**M.Sc. Konrad Niderla**
e-mail: konrad.niderla@netrix.com.pl

He manages at Netrix S.A. the programming and research department. In his work he deals with the development of new methods of control and measurement in the field of automation and tomography as well as artificial intelligence.

http://orcid.org/0000-0003-1280-0622



**D.Sc. Edward Kozłowski**
e-mail: e.kozlovski@pollub.pl

Professor in the Department of Quantitative Methods in Management at the Faculty of Management, Lublin University of Technology. His scientific interests include optimal control of stochastic systems, modelling of decision support systems under conditions of incomplete information about the system, time series analysis, valuation of information.

http://orcid.org/0000-0002-7147-4903


http://doi.org/10.35784/iapgos.3434

*received: 13.01.2023 | revised: 5.03.2023 | accepted: 12.03.2023 | available online: 31.03.2023*

# FEATURES OF THE IMPLEMENTATION OF COMPUTER VISION IN THE PROBLEMS OF AUTOMATED PRODUCT QUALITY CONTROL

**Nataliia Stelmakh[1], Ihor Mastenko[1], Olga Sulima[2], Tetiana Rudyk[2]**

[1]National Technical University of Ukraine "Igor Sikorsky Kyiv Polytechnic Institute", Department of Instrument Production and Engineering, Kyiv, Ukraine,
[2]National Technical University of Ukraine "Igor Sikorsky Kyiv Polytechnic Institute", Department of Mathematical Physics and Differential Equations, Kyiv, Ukraine

***Abstract.*** *The article analyzes the fields of application of machine vision. Special attention is focused on the application of Machine Vision in intelligent technological systems for product quality control. An important aspect is a quick and effective analysis of product quality directly at the stage of the technological process with high accuracy in determining product defects. The appropriateness and perspective of using the mathematical apparatus of artificial neural networks for the development of an intelligent technological system for monitoring the geometric state of products have been demonstrated. The purpose of this study is focused on the identification and classification of reed tuber quality parameters. For this purpose, new methods of identification and classification of quality control of various types of defects using computer vision and machine learning algorithms were proposed.*

**Keywords**: machine vision, intelligent technological system, quality control, neural networks

## CECHY IMPLEMENTACJI WIZJI KOMPUTEROWEJ W PROBLEMACH AUTOMATYCZNEJ KONTROLI JAKOŚCI PRODUKTÓW

***Streszczenie.*** *W artykule dokonano analizy obszarów zastosowań widzenia maszynowego. Szczególną uwagę zwrócono na zastosowanie widzenia maszynowego w inteligentnych systemach technologicznych kontroli jakości wyrobów. Ważnym aspektem jest szybka i skuteczna analiza jakości produktu bezpośrednio na etapie procesu technologicznego z dużą dokładnością w określaniu wad produktu. Pokazano celowość i perspektywę wykorzystania aparatu matematycznego sztucznych sieci neuronowych do budowy inteligentnego systemu technologicznego do monitorowania stanu geometrycznego wyrobów. Celem badań jest identyfikacja i klasyfikacja parametrów jakościowych rurek trzcinowych. W tym celu zaproponowano nowe metody identyfikacji i klasyfikacji kontroli jakości różnego rodzaju defektów z wykorzystaniem wizji komputerowej i algorytmów uczenia maszynowego.*

**Słowa kluczowe**: wizja maszynowa, inteligentne systemy technologiczne, kontrola jakości, sieci neuronowe

## Introduction

Modern technological equipment of various functional purposes must fully meet the requirements of digital production and have the ability to quickly integrate into the structure of intelligent smart enterprises, which turn into intelligent cyber-physical technological systems. Machine Vision (MV) is a necessary component of such intelligent cyber-physical technological systems and a promising method of automation, which allows you to maintain operations of capture, movement of various objects, in particular parts [2], maintain quality control [13, 14], contribute to the improvement of technology. security [5], etc. In addition, machine vision is increasingly used in modular machine tools.

Machine vision is one of the fastest-growing fields in the field of intelligent technologies. According to forecasts in the USA, the total machine vision market in the industry will reach 12.29 billion US dollars by 2023 [4].

The given data indicate a high need for large companies to implement maximum automation of technological processes, in particular operations of product quality control [6]. The growing demand for machine vision systems is due to the fourth industrial revolution, Industry 4.0, and the development of such technologies as artificial intelligence and the Internet of Things.

The rapid growth of demand for Machine Vision technologies is closely related to the development of information technologies. Machine Vision technology is distinguished by the recognition of images of objects with the help of images, followed by their presentation in the form of two-dimensional projections, which in turn are processed with the help of mathematical transformations into text information.

Whenever it comes to mass production, issues of ensuring quality, efficiency, and minimizing time costs arise. To solve these issues, the industry is increasingly resorting to modern means of automation, namely the continuous operation of automated production lines with intermediate quality control. Recently, thanks to the effective combination of information technology and modern digital cameras, image processing have become more accessible. The quality and capabilities of image processing software have become higher, and more reliable while providing better initial product quality control [3]. Therefore, the application of Machine Vision technologies in intelligent technological systems for product quality control is appropriate and relevant.

Currently, machine vision is widely used in medicine, the automotive industry, robotics, the military, biotechnology, and industrial production. This is due to the fact that these industries have clearly formulated tasks that can be successfully solved using Machine Vision technology [12].

The use of classical methods of product quality control is associated with additional costs of human labour and largely depends on the nervous and physiological state of workers-controllers. An important aspect is also the fastest and most effective analysis of the quality of products at the stage of the technological process with high accuracy in determining the defects of the manufactured products. Therefore, the application of modern computer-based technologies is becoming more and more relevant in intelligent technological systems to control the quality of products and the state of technological processes and production facilities (machine tools, tools, technological equipment, etc.).

## 1. Materials and methods

At present, the development of methods and algorithms for image processing and machine vision has been allocated enough domestic and foreign publications in various fields of mechanical engineering. For example, in [7], the authors consider in detail the methods of solving computer vision tasks, and cite their advantages and disadvantages. The prerogative of using Gaussian transformations to simplify algorithm calculations, based on the interpretation of objects, is noted. The authors consider alternative applications of machine vision in solving tasks in systems with limited resources, namely unmanned aerial vehicles, mobile devices, robotics and satellite systems.

Wide possibilities of application of neural networks, due to their flexibility, and the ability to adapt in almost any field, in particular in machine vision, are shown in [11]. The possibilities of computer vision to learn for programmed goals are considered. The advantage mentioned in this work is that the created systems are flexible and can adapt to such tasks, taking into account the variability of conditions and variable factors.

Kazemian et al. developed a computer vision system for real-time adaptive manufacturing extrusion output quality control [1]. The neural network in this work is used to create feedback control systems that ensure the speed of extrusion and, if necessary, control the feed. In this system, the cameras are located perpendicular to the object of control, and the system perceives the layer of material as a straight line and interprets it as a dynamic width through mathematical transformations, which is used to analyze the extrusion process [1].

Researchers Moru and Borro in their work [8] used high-precision equipment for the development of computer vision systems aimed at sub-pixel quality inspection of gears. Cameras with a telecentric lens, with a calibration error of only 0.06 pixels at the time, made it possible to ensure a measurement accuracy of up to ±0.02 mm. To carry out control, they developed three simultaneously working algorithms for checking the internal and external diameter and the number of teeth.

In [10], the authors of Sahoo S. K., Sharma M. M., Choudhury B. B. propose a system for dynamic control of glass bottles. The first image was viewed by a high-resolution intelligent camera. Then, some techniques were depicted to reduce noise and improve the quality of the images produced. Segmentation techniques were used to separate the background from the original image and render the image in vector form for outlier detection. An artificial neural network trained using the error backpropagation algorithm was used to analyze the obtained graphics for the extraction of defective features. The authors of this work compared different classification algorithms using three feature extraction methods with and without sensor implementation in the machine view verification system.

The analysis of the latest research and publications showed virtually unlimited use of Machine Vision technologies. An important element of Machine Vision technologies in intelligent technological systems should be the possibility of prompt and as accurate recognition of specified types of defects with their subsequent separation and utilization, which significantly increases the productivity of product quality control processes.

Machine Vision is a three-level system consisting of a video information collection system, analysis, description and recognition system, and artificial intelligence.

In the video information collection system, information about the image, with the help of optical-electronic converters and video sensors, is provided as part of electrical signals. Information obtained in this way is processed hierarchically. First, the image is processed by video processors. Here, the key parameter is the contour of the image, which is specified by the coordinates of many of its points. The optical system projects the image on the sensitive elements, while the previously larger size of the working area is covered by the sensor.

The system of analysis, description and recognition includes a high-performance computing node and complex software and algorithmic support for processing the received image.

Artificial intelligence, as a rule, includes a specialized computing unit and a software neural network.

The main components of the machine vision system are:

- lighting elements;
- optics;
- optical data capture sensor (machine vision camera);
- optical data processing system and computer node;
- data transmission system and means of communication.

The components of the machine vision system provide automation of industrial processes in intelligent technological systems as follows (Fig. 1). The working area, where the parts are placed, is illuminated by lamps. A video camera is located above the working area, information about which is sent to the main unit of the Machine Vision system via cable or wireless communication. From the main block of information (in a processed form) the controlled automation system device is presented. The automation system in the form of work or actuators for processing sorting or quality control of parts, their orderly placement in containers with a clear correspondence of information coming from the software of the Machine Vision system.

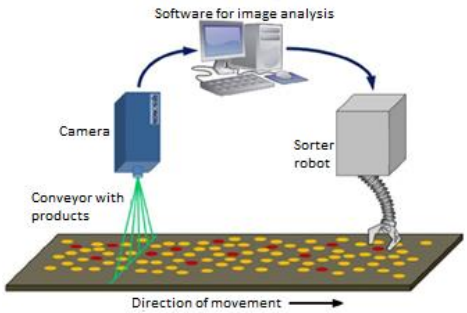


*Fig. 1. Scheme of operation of the machine vision system*

The intensive implementation and development of Industry 4.0 put robotics, artificial intelligence, machine vision, big data cloud computing and machine learning at the forefront. This created large-scale opportunities for improving the quality of products, reducing pollution, automating processes, increasing the stability of production cycles, and reducing operational costs for the involvement of the human factor in the operations of the manufacturing process. Industry 4.0 makes it possible to create intelligent cyber-physical technological systems, so-called "smart factories", which are based on the use of various sensors to control automated processes. One of the main effective technologies contributing to this is Machine Vision, which is an integral component of automated production. This technology is most widely used for automated product quality control. Machine Vision technology allows you to exclude such human factors as fatigue, unimportance, limited ability to quickly process a large amount of information, and others. The preferred machine type is continuous 24/7 control of set parameters, with the ability to process information at a speed of 20,000 k/s, while human capabilities are limited to 24 k/s.

As it was determined, the methods of higher computer vision for their operation involve the use of sensors, cameras and computing power, often cloud-based, which in due time makes production lines more optimized, saves the area of production premises, provides increases industrial safety due to the exclusion of many components. Also, this technology is effective in reducing labor costs. thanks to this, it also ensures the overall level of product quality, more precisely screening out low-quality or defective products.

The technology works on the basis of algorithms with programmed defects, which are detected by a computer program during the analysis of the received images from the production line. The obtained two-dimensional values are analyzed by software based on the mathematical apparatus of Gaussian transformations. Unnecessary noise and structural elements of production lines are filtered out. The final result of digital processing is obtained and compared with the programmed database of existing defects to identify the state of the controlled object. If deviations are found, the product is sent to one of two streams, reprocessing or recycling into waste.

As an example of the importance of using Machine Vision technologies, we will cite a study by the World Security Fund. According to their data, almost 75% of single aircraft approaches and landings occur at airports where precision approach instruments are unavailable or absent, in poor visibility conditions. In this regard, one of the important directions of improvement of on-board avionics is the development of hardware and software complexes of enhanced vision (Enhanced Vision Systems, EVS). As sources of information in such systems, television video sensors, infrared (IR) sensors of various sections, millimeters radars (MR), laser locators (LL), databases of terrain relief along flight routes, databases of airports and runway objects can be used. (RWP), navigation parameters and a number of others.

Analysis of systems and capabilities of computer vision methodology. The described advantages of using Machine Vision will be considered in more detail in the example of solving typical tasks [8]:

1. Recognition is a classic task that arises in image processing and detection of some characteristics of an object. This task is easily solved, but machine vision is still not able to withstand human qualities, in a situation with objects that go beyond the programmed limits.
2. Identification – an indication of a special instance of the object. For example, identification of a person, fingerprints or license plate. In intelligent technological systems – reading of QR codes, which mark or technological documentation.
3. Detection – the obtained results are checked if a certain condition is present. For example, in medicine, the presence of possible damaged cells or tissues in images is under a microscope. Sometimes it is used to compare areas on the analyzed images, to detect minor deviations.
4. Evaluation – determination of the position or orientation of a certain object relative to the camera. An example of the application of this technique can be assisting the work hand in removing objects from the conveyor belt on the product assembly line.
5. Locomotion is a multitasking survey motion in which an image sequence is processed to find a velocity estimate for each point in the image or 3D scene. Examples of such tasks are observation, that is, following the movement of an object.
6. Image restoration – the error of image restoration is noise removal (sensor noise, blurriness of a moving object, etc.). The simplest approach to solving this problem is different types of filters, such as low- or medium-pass filters. More complex methods require the detection of how certain areas of the image should look, and based on this, create their changes.

Machine Vision is not limited to basic methods for solving problems. It is multifaceted. Each of the tasks can be considered differently by the so-called genetic algorithms, but all the main approaches are:

- contour analysis is a curve (a set of curves) that is the end point of the object in the image, therefore, with the help of this method, not a complete image of the object is analyzed, but only the obtained contour, which provides the speed algorithm, due to the initial limitation;
- pattern search – the most advanced method in computer vision, designed to detect certain, programmed, features of an object on the generated image;
- search outside templates – occurs in the recognition of deviations from the standard, namely, the finding of defects, chips, cracks, pigmentation, and deviations from the given geometric parameters;
- data fusion – designed to obtain effective results by processing different types of signals received from cameras and sensors.

Complex performance of tasks requires multi-chamber systems that will be used in arrays. Cameras are used to track the movement of individuals indoors or in places with limited visibility (warehouses in seaports, factory areas, etc.). They are also used for traffic management in intelligent transport systems. The main areas of use of this technology are: production automation; video surveillance from a UAV; 3D movies; interactive AR/VR games; recognition of persons, movement, identification, etc.

Today, when solving tasks in intelligent cyber-physical technological systems, one cannot do without the use of specialized software. The main ones are listed below [1].

OpenCV (Open-Source Computer Vision Library) is a library of computer vision algorithms, image processing and general-purpose numerical algorithms. Implemented in C/C++, also developed for Python, Java, Ruby, Matlab, Lua and other languages.

PCL (Point Cloud Library) is a large-scale open-source project for processing 2D/3D images and cloud points. The PCL platform contains many algorithms, including filtering, feature estimation, surface reconstruction, registration, model selection, and segmentation.

ROS (Robot Operating System) is a software development platform for robots. It is a set of tools, libraries and applications that simplify the development of complex and efficient programs for managing many types of work [9].

MATLAB is a high-level language and interactive environment for programming, numerical calculations and visualization of results. With MATLAB you can analyze data, develop algorithms, and create models and programs.

CUDA (Compute Unified Device Architecture) is a hardware and software architecture for parallel computing that allows you to significantly increase computing performance through the use of Nvidia graphics processors.

SimpleCV is a system for creating applied computer vision. Provides access to a large number of computer vision tools similar to OpenCV, Rygame, etc. Does not require deep loading into the theme. It is suitable for rapid prototyping.

## 2. Experiment and results

Reed tubers, from a few places of their cultivation and with differences, were chosen as the research object of the sample, and several reference products were also chosen. The main learning criteria were selected, such as pigmentation, color, geometric dimensions, inner film, cracks, chips and defects during cutting (Fig. 2). The samples are not raw data, which are digitized for each type of deviation using a digital camera to generate training and test training sets.

According to the peculiarity of the products, namely the various natural factors of shape, pigmentation and colour. The technological process involves the application of a continuous control method. It includes the distribution of products according to eleven quality characteristics, which include various defects: cracks, damage by pests, pigmentation, length deviations, diameter distribution and deviations from the shape. We proposed using optical cameras that work by analogy with the human eye to determine these characteristics. The use of ultrasonic or infrared sensors does not provide a complete picture due to the local concentration of the investigated area. The use of mechanical contact methods is limited by the variety of product shapes.

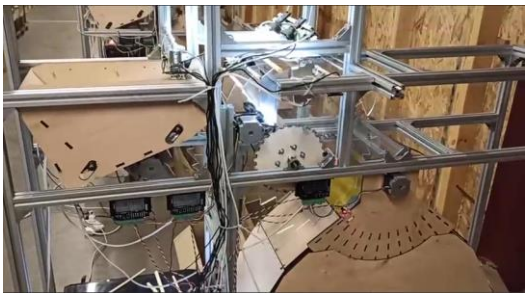

*Fig. 2. Collection of data from samples of reed tubes and their quality control*

11 classifiers were created, both for training and for test sets, each of them was assigned a single defect, but machine vision recognizes combinations as well (Fig. 3). After entering the data, they are analyzed for the presence of the main deviation criteria, each product carries its fate in the initial process, after analyzing the data, the study offers three options for the final classification: finishing, waste and finished product.

Image preprocessing is very necessary to optimize the model and reduce the computation time. The resulting images are not guaranteed to contain all information related to the task. For example, the background content may contain a large part of the image, which will lead to unnecessary calculations in the next stage of identification. Thus, filtering techniques can improve the quality of captured images and remove unnecessary content. The final step is to compress the image to reduce data redundancy in the image so that it can be quickly uploaded to the cloud and stored without taking up a lot of space.

Noise removal is the main procedure for signal amplification, for this preliminary control the area is highlighted in white, for better detail and additional illumination of the control area is added (Fig. 4)

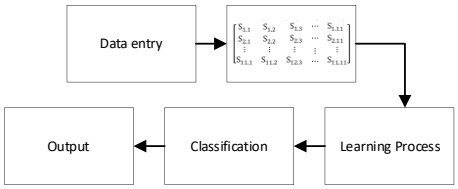


*Fig. 3. Setting up machine learning*

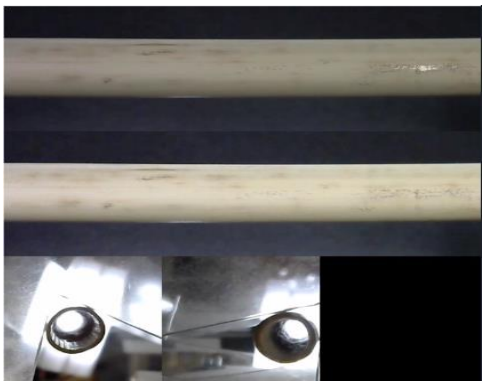

*Fig. 4. Defective reed tube, in the control area*

The database used by the image identification algorithm contains collected product image samples labelled according to classifiers, separated in an indicative way on the training and evaluation images. In the training phase, training images are performed for continuous parameter correction with a supervised learning approach to minimize prediction errors. However, model evaluation is essential to find a good network structure and an appropriate learning strategy, thus obtaining a practical model for identification and retention. Finally, the built classification model analyzes the processed image in real-time and provides feedback to the next controller ("defective product", "refinish defect" or "defect-free product").

## 3. Conclusions

The rapid spread of machine vision technology covers almost the entire field of industrial production. The implementation of Machine Vision technology in intelligent technical systems of the smart-enterprise type gives high results where this technology is implemented. This, in turn, contributes to the implementation of the ideas of the fourth industrial revolution Industry 4.0 and reduces the participation of people in the same type of routine tasks in production.

In the perspective of further research, there is the development of a computer vision system that provides monitoring of the actual geometric state of the product (workpiece) and its comparison with the (learned) using mathematical neural network devices. By applying machine vision technology in comparison to other methods, observing and optimal methods, we obtained a high level of repeatability and robustness at a significantly lower cost. The high advantage is that every manufactured product is inspected for all kinds of defects and compensation from the human eye, the deployed system can work continuously without loss of productivity.

## References

[1] Desmond K. et al.: A machine vision algorithm for quality control inspection of gears. The International Journal of Advanced Manufacturing Technology 106(1-2), 2020, 105–120.
[2] Domel A. et al.: Autonomous pick and place operations in industrial production. 12th Intern. Conf. on Ubiquitous Robots and Ambient Intelligence (URAI 2015), Kintex, Goyang, Korea, 356.
[3] Dyatlov E. I.: Machine vision (analytical review). Mathematical machines and systems 2, 2013, 32–40.
[4] Guo Y. et al.: Rotational projection statistics for 3D local surface description and object recognition. International journal of computer vision 105(1), 2013, 63–86.
[5] Industrial Machine Vision Market by Component (Hardware (Camera, Frame Grabber, Optics, Processor), and Software (Deep Learning, and Application Specific)), Product (PC-based, and Smart Camerabased), Application, End-User. Global Forecast to 2023 [https://www.researchandmarkets.com/research/k6lrbk/global_industrial?w=5].
[6] Johnson A. E.: Spin-images: a representation for 3-D surface matching: Diss. Andrew Edie Johnson – Pittsburgh, Pennsylvania, 1997.
[7] Lisovsky A. L.: Application of neural network technologies for management development of systems. Strategic decisions and risk management 11(4), 2020, 378–389.
[8] Mastenko I. et al.: Vision yak nevidyemna chastyna intelektual'nykh tekhnolohichnykh system. Tekhnichni Nauky Ta Tekhnolohiyi 4(26), 2021, 58–65 [http://doi.org/10.25140/2411-5363-2021-4(26)-58-66].
[9] Mastenko I. V., Stelmakh N. V.: Generative design of a frame type construction. KPI Science News 2, 2021, 81–89.
[10] Sahoo S. K. et al.: A Dynamic Bottle Inspection Structure. Computational Intelligence in Data Mining 711, 2019, 873–884.
[11] Stelmakh N.: Software module for accelerated technological preparation of assembly small-scale production of devices. Visn. NTUU "KPI". Eng. 54, 2009, 12–17.
[12] Tymchyshyn R. M. et al.: Modern approaches to solving computer vision problems. Control systems and machines 6, 2018, 46–73.
[13] Zhong Y., Fengyu X., Yue W.: Analysis and experiment of workpiece quality detection based on industrial robot. 23rd Intern. Conf. on Mechatronics and Machine Vision in Practice (M2VIP), 2016, 1–6.
[14] Zuxiang W., Lei Z., Junpeng F.: Design of safety capacitors quality inspection robot based on machine vision. 1st Intern. Conf. on Electronics Instrumentation Information Systems (EIIS), 2017, 1–4.

**Ph.D. Nataliia Stelmakh**
e-mail: n.stelmakh@kpi.ua

Associate professor in Department of Instrument Production and Engineering at the Faculty of Instrumentation Engineering, National Technical University of Ukraine "Igor Sikorsky Kyiv Polytechnic Institute". Author and co-author of more than 50 scientific papers, 10 patents for utility models. Research interests: automation and computer-integrated technologies, assembly of devices and preparation of production, computer vision.

http://orcid.org/0000-0003-1876-2794

**M.Sc. Ihor Mastenko**
e-mail: ihormas@gmail.com

Ihor Mastenko received a master's degree in automation and computer-integrated technologies from the National Technical University of Ukraine "Igor Sikorsky Kyiv Polytechnic Institute", Faculty of Instrumentation Engineering 2020. Since 2021, he is a graduate student of the Department of Instrument Production and Engineering. His research interests are in the study of computer vision for production processes, machine learning, and the technology of manufacturing optoelectronic devices.

http://orcid.org/0000-0002-2953-4589

**Ph.D. Olga Sulima**
e-mail: olgasulimakpi@gmail.com

Associate professor in Department of Mathematical Physics and Differential Equations, National Technical University of Ukraine "Igor Sikorsky Kyiv Polytechnic Institute". She received Ph.D. degree in 1989. Main scientific interests: Differential equations, quasilinear systems of differential equations, method of teaching higher mathematics in universities, analytical and ecological instrumentation, formation of mathematical competence students of the technical university.

http://orcid.org/0000-0002-5811-7717

**Ph.D. Tetiana Rudyk**
e-mail: ru58@ukr.net

Associate professor in Department of Mathematical Physics and Differential Equations, National Technical University of Ukraine "Igor Sikorsky Kyiv Polytechnic Institute". She received Ph.D. degree in 1986. Research interests: theory of optimal control, applied mathematics, analytical and environmental instrumentation, magnetic therapy devices, formation of mathematical competence of students of the technical university.

http://orcid.org/0000-0003-1121-4963

http://doi.org/10.35784/iapgos.3476

*received: 2.02.2023 | revised: 12.03.2023 | accepted: 13.03.2023 | available online: 31.03.2023*

# SELF-OSCILLATING PARAMETRIC HUMIDITY SENSOR WITH FREQUENCY OUTPUT SIGNAL

**Iaroslav O. Osadchuk, Oleksandr V. Osadchuk, Vladimir S. Osadchuk, Lyudmila V. Krylik**
Vinnytsia National Technical University, Vinnytsia, Ukraine

***Abstract.*** *A self-oscillating parametric humidity sensor has been developed that implements the principle of "humidity-frequency" conversion into hybrid integrated circuit based on a microelectronic transistor structure with a negative differential resistance, in which the humidity-sensitive element is a resistor of the HR202 type. For the purposes of determining parameters self-oscillating parametric humidity sensor with frequency output a mathematical model has been developed that takes into account the effect of humidity on a sensitive resistive element, which is an integral element of the device. Based on the mathematical model, analytical expressions for the transformation function and the sensitivity equation are obtained. It is shown that the main contribution to the conversion function is made by relative humidity. The computer simulation and experimental studies of a self-oscillating parametric humidity sensor with a frequency output signal contributed to obtaining the main parameters and characteristics, such as the dependence of the generation frequency on changes in relative humidity in the range from 30% to 99%, the change in sensitivity on relative humidity, the dependence of the active and reactive components of the impedance in the frequency range from 50 kHz to 2 GHz; standing wave ratio, change in logarithmic magnitude and spectra of the output signal of a parametric humidity sensor with a frequency output signal in the LTE-800 Downlink frequency range. The obtained electrical characteristics confirm the operability of the developed device. The sensitivity of the developed self-oscillating parametric humidity sensor in the range of relative humidity change from 30% to 99% has a value from 332.8 kHz/% to 130.2 kHz/%.*

**Keywords: s**elf-oscillating parametric humidity sensor with frequency output, negative differential resistance, humidity-sensitive resistor

# SAMOOSCYLACYJNY PARAMETRYCZNY CZUJNIK WILGOTNOŚCI Z CZĘSTOTLIWOŚCIOWYM SYGNAŁEM WYJŚCIOWYM

***Abstrakcyjny.*** *Opracowano samooscylujący parametryczny czujnik wilgotności realizujący zasadę konwersji „wilgotność-częstotliwość" do hybrydowego układu scalonego opartego na mikroelektronicznej strukturze tranzystorowej o ujemnej rezystancji różnicowej, w której elementem czułym na wilgotność jest rezystor typu HR202 typ. Na potrzeby wyznaczania parametrów samooscylującego parametrycznego czujnika wilgotności z wyjściem częstotliwościowym opracowano model matematyczny uwzględniający wpływ wilgoci na czuły element rezystancyjny, będący integralną częścią urządzenia. Na podstawie modelu matematycznego uzyskuje się wyrażenia analityczne dla funkcji transformacji i równania wrażliwości. Pokazano, że główny udział w funkcji konwersji ma wilgotność względna. Symulacja komputerowa i badania eksperymentalne samooscylującego parametrycznego czujnika wilgotności z wyjściowym sygnałem częstotliwościowym przyczyniły się do uzyskania głównych parametrów i charakterystyk, takich jak zależność częstotliwości generacji od zmian wilgotności względnej w zakresie od 30% do 99%, zmiana czułości na wilgotność względną, zależność składowej czynnej i reaktywnej impedancji w zakresie częstotliwości od 50 kHz do 2 GHz; współczynnika fali stojącej, zmiany wielkości logarytmicznej i widma sygnału wyjściowego parametrycznego czujnika wilgotności przy częstotliwościowym sygnale wyjściowym w zakresie częstotliwości LTE-800 Downlink. Uzyskane charakterystyki elektryczne potwierdzają sprawność opracowanego urządzenia. Czułość opracowanego samooscylującego parametrycznego czujnika wilgotności w zakresie zmian wilgotności względnej od 30% do 99% przyjmuje wartość od 332,8 kHz/% do 130,2 kHz/%.*

**Słowa kluczowe:** samooscylacyjny parametryczny czujnik wilgotności z wyjściem częstotliwościowym, ujemna rezystancja różnicowa, rezystor wrażliwy na wilgoć

## Introduction

The creation and maintenance of optimal microclimate parameters in industrial premises is primarily determined by the sanitary, hygienic and technological requirements of production, since the deviation of microclimate parameters from the norms leads to disruptions in the flow of technological processes in the national economy and affects the well-being of producers (people). The effectiveness of technical diagnostic tools and devices for monitoring environmental parameters depends on the quality of primary transducers, which are the main sensitive organs of measuring equipment. Humidity sensors are an important type of sensors for physical quantities [3–5, 10, 11, 14].

Currently, there is a rapid development of semiconductor humidity sensors, the creation of which became possible only at a certain stage in the development of science, as well as microelectronics technology. The use of modern microelectronic technologies contributes to the development and manufacture of microelectronic humidity sensors with high accuracy and sensitivity to the measuring parameter and insensitive to other external factors, small weight and size, and low power consumption [1, 8, 12, 13]. It should be noted that the existing analog measuring transducers have a number of disadvantages, which include a small output signal, significant measurement errors, as well as low sensor output signal powers, which leads to low noise immunity and low speed [15–19].

## 1. Analysis of recent research and publications

A promising direction in the development and creation of microelectronic humidity sensors is research in the field of humidity frequency transducers based on transistor structures with negative differential resistance. Studies in this area have shown that reactive properties and negative differential resistance are inextricably linked, and the versatility and simplicity of radio electronic devices based on transistor structures with negative resistance is the prospect of their practical use. Self-oscillating parametric humidity sensors that implement the "humidity-frequency" conversion principle are characterized by simplicity and versatility, as well as accuracy and noise immunity [6, 7, 22].

## 2. Formulation of the problem

The aim of the work is to create and study a self-oscillating parametric humidity sensor based on a microelectronic transistor structure, in which the bipolar and field-effect transistors act as active elements of the self-oscillator. In this oscillator, energy losses in the oscillatory system are compensated by the energy of negative differential resistance, and a humidity-sensitive resistive element is included in the feedback circuit.

To achieve the goals in the article, you need to solve the following tasks:

1. analyze the existing scientific sources, as well as justify the use of a semiconductor transistor structure with a negative differential resistance to build self-oscillating parametric humidity sensors;

2. to develop a mathematical model of a parametric humidity sensor, which takes into account the dependence of the parameters of bipolar and field-effect transistors on power supply modes and changes in humidity acting on a humidity-sensitive resistive element and its effect on the output frequency of a self-oscillating parametric sensor;
3. to obtain the parametric dependence of the transformation functions and the sensitivity of the self-oscillating sensor on changes in humidity;
4. to carry out experimental studies of a self-oscillating parametric humidity sensor;
5. draw conclusions on the conducted research.

## 3. Mathematical model of self-generating humidity sensor

The self-oscillating humidity sensor with a frequency output signal is built on the basis of a microelectronic transistor structure with a negative differential resistance, in which the humidity-sensitive element is a resistor of the HR202 type (Fig. 1) [23].

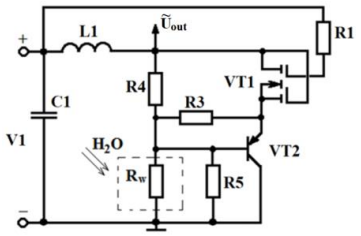


*Fig. 1. Electric circuit of self-oscillating humidity sensor with frequency output signal*

The self-oscillating humidity sensor with a frequency output signal consists of a field effect transistor VT1 and the bipolar transistor VT2, a humidity-sensitive resistor $R_W$, resistances R1, R3, R4, R5, capacitance C1 and inductance L1. The oscillatory circuit of the self-oscillating sensor is formed by the equivalent impedance capacitance at the drain electrodes of the field-effect transistor VT1 and the collector of the bipolar transistor VT2, as well as the passive inductance L1.

The humidity-sensitive element is included in a resistive divider R4-R5 with parallel connection to the resistor R5, which operates on direct current and provides a choice of operating point for the bipolar transistor VT2. A change in the resistance of the humidity-sensitive resistive element with a change in moisture causes a shift in the operating point of the bipolar transistor VT2, which in turn causes a change in the operating point on the volt-ampere characteristics of the self-oscillating parametric transducer, which is preselected in the falling section. Due to the fact that through a humidity-sensitive resistor at a supply voltage of 5 V and maximum humidity, when its resistance drops to several kilo Ohms, it is necessary to limit the flowing current to about 1.5 mA, resistor R5 was connected in parallel. With such a circuit solution, the direct current flowing through the humidity-sensitive element does not exceed 1.2 mA and the maximum voltage drop is 1.45 V, which does not allow it to fail.

The humidity-sensitive resistor $R_W$ is affected by a change in humidity, which leads to a change in both the equivalent capacitance of the oscillatory circuit and the negative differential resistance at the output of the humidity sensor, which causes a change in the resonant frequency of the self-oscillating parametric sensor. Energy losses in the oscillatory circuit are compensated by the energy of the negative differential resistance [18]. Resistors R1, R3, R4, R5 supply power to the self-oscillating parametric sensor through a constant voltage source V1. Capacitance C1 prevents the passage of high-frequency alternating current through the DC voltage source. The current-voltage characteristic of the self-oscillating parametric humidity sensor has a descending section, confirming the existence of a negative differential resistance in this section. The circuit of a self-oscillating parametric humidity sensor with a humidity-sensitive resistive element HR202 (Fig. 1) was assembled on a BFT93 bipolar transistor and a BF998 field-effect transistor to ensure operation in the microwave range. The mode of transistors VT1 and VT2 for direct current was as follows: the current in the drain circuit of the field-effect transistor VT1 is 2.25 mA, and the drain voltage is 5 V. The circuit resistances have the following values R1 = 1.0 kOhm; R3 = 5.0 kOhm; R4 = 5.2 kOhm; R5 = 20.0 kOhm. The oscillator inductance has a value of 1.7 nH. Based on the experimental studies, the above operation mode, at a humidity of 30%, corresponded to the generation frequency of 822.0 MHz, and at 99% humidity – 806.8 MHz. The proposed generator circuit makes it possible to obtain an output voltage of up to 4.7 V in a wide frequency range. The frequency instability of the self-oscillating parametric humidity sensor corresponded to the level of $1.35 \cdot 10^{-5}$ Hz.

To determine the conversion function and the sensitivity equation, an equivalent high-frequency nonlinear circuit of a self-oscillating humidity sensor with a frequency output signal with a humidity-sensitive resistive element was developed (Fig. 2).

Due to the fact that the humidity-sensitive resistor operates on direct current in the non-linear equivalent circuit of the self-oscillating transducer, its inductive properties are not taken into account, since they are not distributed. Due to the comb structure of the humidity-sensitive resistor, in the equivalent circuit, its capacitive properties can be taken into account by connecting the capacitance in parallel, but the change in this capacitance due to changes in humidity in this sensor design is a fraction of a picofarad.

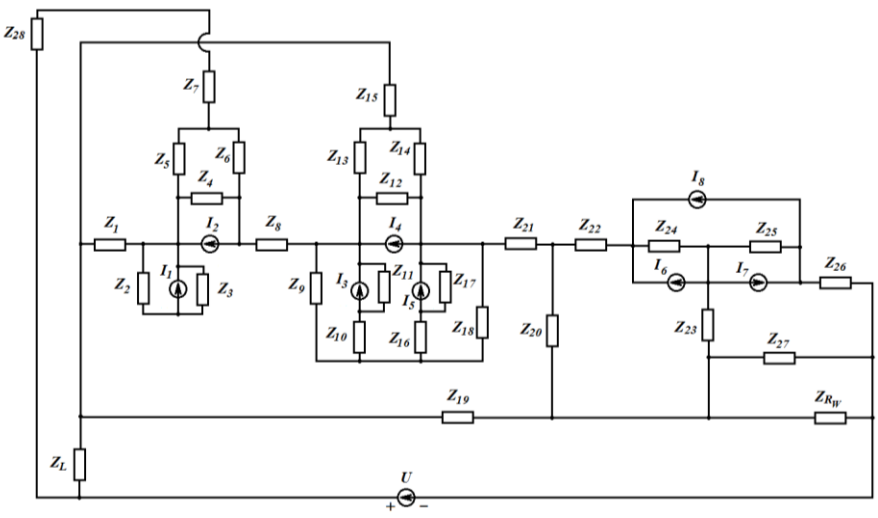

*Fig. 2. Transformed equivalent high-frequency nonlinear circuit self-oscillating humidity sensor*

The elements of the equivalent high-frequency nonlinear circuit (Fig. 2) are described by the following quantities:

$$Z_L = j\omega L,\ Z_{R_W} = \frac{R_W(W)}{1+\omega^2 R_W^2(W)C_W^2} - j\frac{R_W^2(W)\omega C_W}{1+\omega^2 R_W^2(W)C_W^2},$$

$$Z_1 = R_{d1} + R'_{d1} + j\omega L_{d1},\ Z_2 = R_{bd1} - j\frac{1}{\omega C_{bd1}},\ Z_3 = \frac{1}{j\omega C_d},$$

$$Z_4 = R_{ds1},\ Z_5 = \frac{1}{j\omega C_{gd1}},\ Z_6 = \frac{1}{j\omega C_{gs1}},$$

$$Z_7 = R_{g1} + R'_{g1} + j\omega L_{g1},\ Z_8 = R_{ds1},\ Z_9 = \frac{1}{j\omega C_{bd2}},$$

$$Z_{10} = R_{bd2},\ Z_{11} = \frac{1}{j\omega C'_d},\ Z_{12} = R_{ds2},\ Z_{13} = \frac{1}{j\omega C_{gd2}},$$

$$Z_{14} = \frac{1}{j\omega C_{gs2}},\ Z_{15} = R_{g2} + R'_{g2} + j\omega L_{g2},\ Z_{16} = R_{bs3},$$

$$Z_{17} = \frac{1}{j\omega C_s},\ Z_{18} = \frac{R_{b2}}{1+\omega^2 R_{b2}^2 C_{bs2}^2} - j\frac{R_{b2}^2\omega C_{bs2}}{1+\omega^2 R_{b2}^2 C_{bs2}^2},$$

$$Z_{19} = R_4,\ Z_{20} = R_3,\ Z_{21} = R_{s2} + R'_{s2} + j\omega L_{s2},$$

$$Z_{22} = R_e + R'_e + j\omega L_e,\ Z_{23} = R_B + R'_B + j\omega L_B,\ Z_{24} = \frac{1}{j\omega C_e},$$

$$Z_{25} = \frac{1}{j\omega C_c},\ Z_{26} = R_c + R'_c + j\omega L_c,\ Z_{27} = R_5,\ Z_{28} = R_1$$

where $W$ – humidity; $L$ – inductance of the oscillatory circuit; $R_W(W)$ – resistance of the humidity-sensitive resistive element; $R_1$ – resistance serves to prevent breakdown of the gate dielectric; $R_3, R_4$ – divider resistance; $R_5$ – resistance is used to linearize the characteristics of the humidity sensitive resistive element; $R_d$ – drain resistance; $R'_d$ – ohmic drain resistance; $L_d$ – drain electrode inductance; $C_{bd}$ – substrate-drain capacity; $R_b$ – resistance of the substrate; $C_{bs}$ – substrate-source capacitance; $R_{bd1}, R_{bd2}$ – volume resistance p-n substrate-drain junction; $R_{bs3}$ – volume resistance p-n substrate-source junction; $C_d, C'_d$ – drain junction capacitance p-n; $C_s$ – capacitance p-n source junction; $R_{ds}$ – drain-source resistance; $C_{gs}$ – gate-source capacitance; $C_{gd}$ – gate-drain capacity; $R_g$ – resistance of the gate electrode; $R'_g$ – ohmic resistance of the gate electrode; $L_g$ – inductance of the gate electrode; $I_1$ – substrate-drain junction current; $I_2$, $I_4$ – source-drain currents; $I_3$ – substrate-drain-source junction current; $I_5$ – substrate-source transition current; $R_{ds1}$ – total resistance of the drain-source of the first gate of the double-gate transistor VT1; $R_s$ – source resistance; $R'_s$ – ohmic source resistance; $L_s$ – source electrode inductance; $R_B$ – base resistance; $R'_B$ – ohmic resistance of the base electrode; $L_B$ – base electrode inductance; $C_e$ – capacitance of the emitter junction; $C_c$ – capacitance of the collector junction; $R_e$ – resistance of the emitter junction; $R'_e$ – ohmic resistance of the emitter electrode; $L_e$ – emitter electrode inductance; $R_c$ – resistance to the collector junction; $R'_c$ – ohmic resistance of the collector electrode; $L_c$ – collector electrode inductance; $I_6$ – emitter-base current of the transistor VT2; $I_7$ – collector-base current of the transistor VT2; $I_8$ – emitter-collector current of the transistor VT2 [9, 21, 25].

Without knowing the parameters of humidity transducers, it is impossible to create them, so the task was to develop a mathematical model, based on the solution of which the conversion function and sensitivity equations, the main metrological parameters of measuring transducers will be determined. For this, a high-frequency nonlinear circuit of a self-oscillating humidity sensor with a frequency output signal with a humidity-sensitive resistive element HR202 was developed (Fig. 2).

According to the positive feedback loop of this circuit, an equation is defined, on the basis of which an analytical expression of the conversion function is obtained, that is, the dependence of the output frequency on the change in humidity ($F_0$):

$$F_0 = \frac{\pi \cdot R_W(W)\cdot C_{eb}\cdot C_{ds}\cdot C_{cb}}{4\cdot\pi^2\cdot L\cdot R_W(W)\cdot C_{eb}\cdot C_{ds}\cdot C_{cb}} \pm \pm\frac{\sqrt{\pi^2\cdot R_W^2(W)\cdot C_{eb}^2\cdot C_{ds}^2\cdot C_{cb}^2 + A_6}}{4\cdot\pi^2\cdot L\cdot R_W(W)\cdot C_{eb}\cdot C_{ds}\cdot C_{cb}} \quad (1)$$

where

$$A_1 = 4\cdot\pi^2\cdot L\cdot R_W^2(W)\cdot C_{eb}\cdot C_{ds}^2\cdot C_{cb}^2,$$
$$A_2 = 4\cdot\pi^2\cdot L^2\cdot C_{eb}^2\cdot C_{ds}^2,$$
$$A_3 = 4\cdot\pi^2\cdot L\cdot R_W^2(W)\cdot C_{eb}^2\cdot C_{ds}\cdot C_{cb}^2,$$
$$A_4 = L\cdot C_{eb}\cdot C_{ds}^2 + L\cdot C_{eb}^2\cdot C_{ds},$$
$$A_5 = 4\cdot\pi^2\cdot L\cdot R_W^2(W)\cdot C_{eb}^2\cdot C_{ds}^2\cdot C_{cb},$$
$$A_6 = A_1 - A_2 + A_3 + A_4 + A_5.$$

Due to the fact that the humidity-sensitive resistor is included in the lower arm of the resistive divider, therefore, in the analytical equation of the conversion function, it is necessary to use the «-» sign and the output frequency of the transducer decreases with increasing humidity. If a humidity-sensing resistor is included in the upper arm of the resistive divider, the «+» sign must be used in the conversion function, and the output frequency of the transducer will increase with increasing humidity.

Based on equation (1), the analytical expression for the sensitivity (2) of the developed self-oscillating parametric humidity sensor is determined:

$$S_W^{F_0} = \frac{\pi\cdot C_{eb}\cdot C_{ds}\cdot C_{cb}\left(\frac{\partial R_W(W)}{\partial W}\right)}{4\cdot\pi^2\cdot L\cdot R_W(W)\cdot C_{eb}\cdot C_{ds}\cdot C_{cb}} \pm \frac{(B_1+B_2+B_3+B_4)\cdot\left(\frac{\partial R_W(W)}{\partial W}\right)}{\pm\frac{\sqrt{\pi^2\cdot R_W^2(W)\cdot C_{eb}^2\cdot C_{ds}^2\cdot C_{cb}^2 + A_6}}{4\cdot\pi^2\cdot L\cdot R_W(W)\cdot C_{eb}\cdot C_{ds}\cdot C_{cb}}} - \left(\frac{\pi\cdot R_W(W)\cdot C_{eb}\cdot C_{ds}\cdot C_{cb}}{4\cdot\pi^2\cdot L\cdot R_W^2(W)\cdot C_{eb}\cdot C_{ds}\cdot C_{cb}} \pm \pm\frac{\sqrt{\pi^2\cdot R_W^2(W)\cdot C_{eb}^2\cdot C_{ds}^2\cdot C_{cb}^2 + A_6}\left(\frac{\partial R_W(W)}{\partial W}\right)}{4\cdot\pi^2\cdot L\cdot R_W^2(W)\cdot C_{eb}\cdot C_{ds}\cdot C_{cb}}\right) \quad (2)$$

where

$$B_1 = \pi^2\cdot R_W(W)\cdot C_{eb}^2\cdot C_{ds}^2\cdot C_{cb}^2,$$
$$B_2 = 4\cdot\pi^2\cdot L\cdot R_W(W)\cdot C_{eb}\cdot C_{ds}^2\cdot C_{cb}^2,$$
$$B_3 = 4\cdot\pi^2\cdot L\cdot R_W(W)\cdot C_{eb}^2\cdot C_{ds}\cdot C_{cb}^2,$$
$$B_4 = 4\cdot\pi^2\cdot L\cdot R_W(W)\cdot C_{eb}^2\cdot C_{ds}^2\cdot C_{cb}.$$

The analytical dependence of the resistance $R_W(W)$ of the humidity-sensitive resistor on changes in humidity and temperature was obtained by approximating and interpolating this parameter provided by the manufacturer in the datasheet and described by expression (3). The error of the 3D mathematical description of the resistance $R_W(W)$ is 0.2%.

$$R_W(W,T) = a + b\ln(R_W) + c/T + d(\ln(R_W))^2 + e/T^2 + \\ + f(\ln(R_W))/T + g(\ln(R_W))^3 + h/T^3 + i(R_W)/T^3 + \\ + j(\ln(R_W))^2/T, \quad (3)$$

where $T$ – ambient temperature; $a,b,c,d,e,f,g,h,i,j$ – approximation coefficients:

$a$=160.6061051; $b$=–18.6534062; $c$=3789.316024; $d$=–1.04223052; $e$=–135316.566; $f$=531.6381046; $g$=0.103813382; $h$=733991.7173; $i$=2636.940718; $j$=–36.4837064.

On Fig. 3 shows a 3D model of the dependence of the resistance $R_W(W)$ of a humidity-sensitive resistor on changes in humidity and temperature. To reduce the error in the description of this parameter, it is necessary to calibrate and introduce a correction factor for each instance of the humidity-sensitive resistor, thus it is possible to increase the accuracy of measuring the informative parameter.

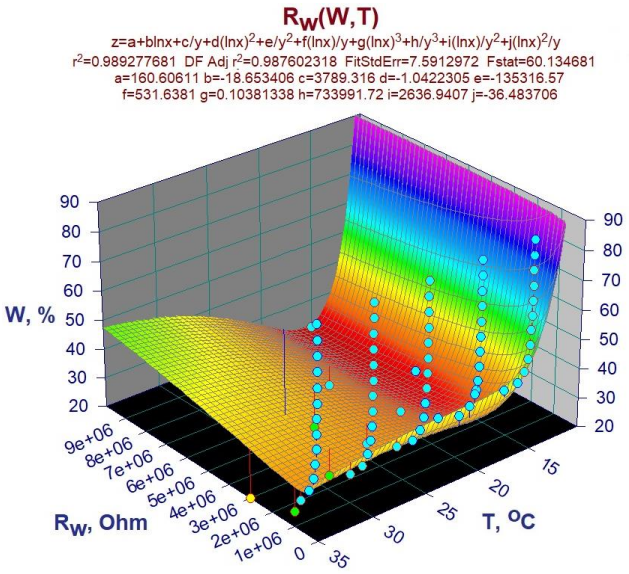


*Fig. 3.3D model of the dependence of the resistance* $R_W(W)$

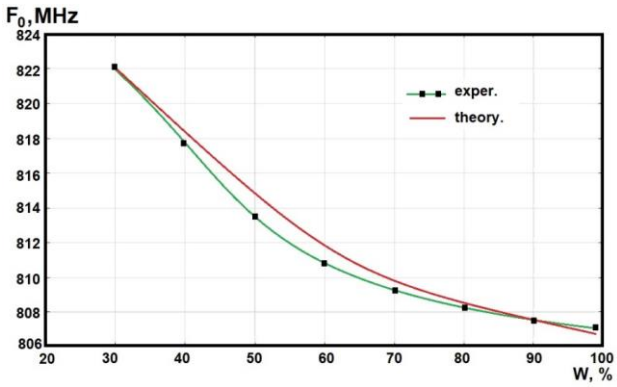


*Fig. 4. Theoretical and experimental dependences generation frequency from changes in relative humidity and 25°C temperature*

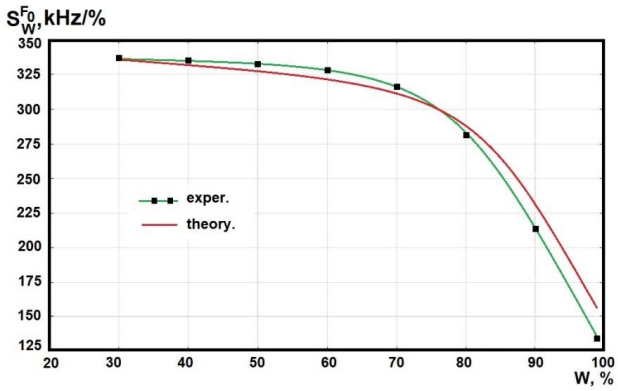


*Fig. 5. Experimental and theoretical dependencies sensitivity to changes in relative humidity and 25°C temperature*

On the basis of expression (1), the transformation function of a self-oscillating parametric humidity sensor was theoretically calculated and experimentally studied (Fig. 4).

Based on expressions (1) and (2) in the Scilab 6.11 environment, the conversion function and sensitivity of the self-oscillating parametric humidity sensor were calculated with parallel processing of experimental data, which are presented in Fig. 4 and Fig. 5.

The sensitivity of the developed self-oscillating parametric humidity sensor in the relative humidity range from 30% to 99% takes values from 332.8 kHz/% to 130.2 kHz/%. With the minimum sensitivity (130 kHz/%) and the standard method of measuring frequency, i.e. using a time gate of 1 sec., the frequency can be measured with an accuracy of 1 Hz, so 130000 readings fall on 1% humidity, and the entire range from 30% up to 99% - 10350000 counts, which corresponds to a 23-bit ADC. The measurement error of the developed self-oscillating parametric humidity sensor, according to this method, is 0.01%, despite the fact that a standard sensitive resistive element is used.

Since almost all semiconductor devices are subject, to a greater or lesser extent, to the influence of temperature changes, in the proposed self-oscillating parametric humidity sensor, it is necessary to take into account the effect of temperature on the output parameters of the device. One of the methods to compensate for the influence of temperature on the measuring transducer is the use of a microcontroller with an additional temperature sensor. Using the analytical expression (3) and subsequent mathematical processing of the informative signal, it is possible to compensate for the effects of temperature.

## 4. Computer modelling and experimental studies

To confirm the theoretical results and conduct experimental studies, the electrical circuit of a self-oscillating parametric humidity sensor with a humidity-sensitive resistive element (Fig. 1) was studied in the LTSpice XVII circuit simulation environment [24] (Fig. 6). The studies were carried out in the range of change in the resistance of the humidity-sensitive resistive element R2 from 1300 kOhm to 1.3 kOhm, which corresponds to an increase in the value of relative air humidity from 30% to 99% at a temperature of 25°C.

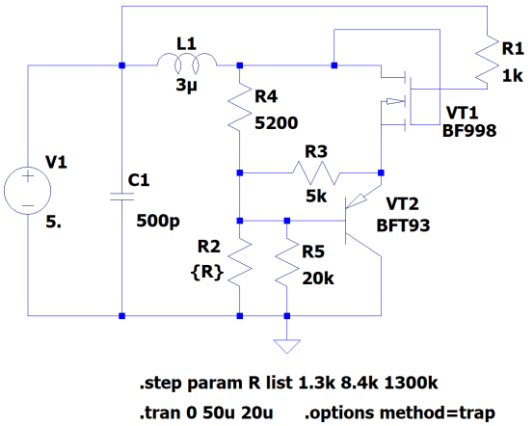


*Fig. 6. Electric circuit of self-oscillating humidity sensor in a circuit environment LTSpice XVII simulation*

On Fig. 7 shows the experimental dependence of the alternating voltage at the output of the self-oscillating sensor on time at a temperature of 25°C and a relative humidity of 30%, 75%, 99%.

Since the self-oscillating parametric humidity sensor is built on the basis of a transistor structure with a negative differential resistance and can operate in a wide frequency range, experimental studies were carried out from low frequencies to microwave frequencies to determine the optimal operating frequencies for various tasks of using the developed device. In the range from 50 kHz to 6 MHz to work directly with 8-bit microcontrollers, with some loss in measurement accuracy. From 50 kHz to 80 MHz for direct operation with 32-bit Teency-type microcontrollers with medium humidity measurement accuracy. From 50 kHz to 250 MHz for FPGA operation with high measurement accuracy and parallel data streams from multiple transducers. And finally, as the case considered in this paper, in the radio frequency range from hundreds of megahertz to 2 GHz, in the form of a radio frequency measuring transducer, with a high accuracy of measuring an informative parameter. Based on the above described applications of the self-oscillating parametric humidity sensor, experimental studies of the main parameters in the frequency range from 50 kHz to 2 GHz were carried out.

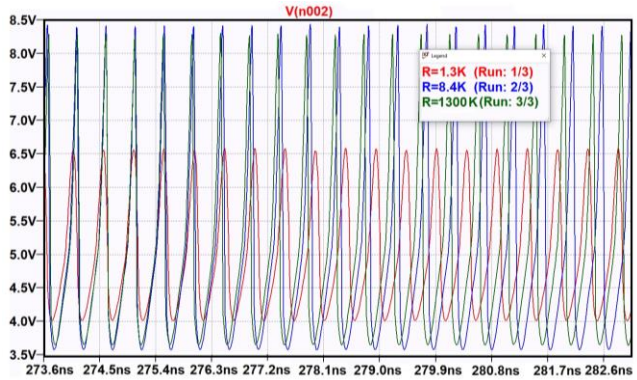


*Fig. 7. Computer-simulated dependence of the alternating voltage at the output of a self-oscillating sensor in the LTSpice XVII circuit simulation environment*

To conduct experimental studies of a self-oscillating sensor, an experimental setup has been developed, the block diagram of which is shown in Fig. 8.

The LiteVNA vector analyzer is an improvement over the popular NanoVNA and SAA2. It is currently one of the best vector handheld network analyzers (VNAs) and comprehensive indicators of semiconductor microwave devices, it is as small as the NanoVNA and is able to satisfy the ultra-wide measurement range from 50 kHz to 6.3 GHz [20]. To minimize power consumption and size, LiteVNA uses only one mixer with multiple internal RF switches for S11 and S21 measurements and IFFT calculations for TDR and DTF measurements. The LiteVNA vector analyzer provides faster scan speeds and more scan points, as well as a wider measurement range. Combined with an easy-to-use NanoVNA-compliant interface, LiteVNA can be easily used as a laboratory and field testing tool [20].

With a measurement range of up to 6.3 GHz, LiteVNA can handle common ham radio and IoT applications, as well as new 5 GHz tests to enable the latest 5.8 GHz Wi-Fi and 5.8 GHz imaging systems. Below are experimental data on the study of a self-oscillating humidity sensor with an output frequency signal. An experimental sample of a self-oscillating humidity sensor was developed on the basis of a double-gate MOSFET BF998 transistor and a bipolar transistor BFT93, forming a semiconductor structure with a negative differential resistance. In the Scilab 6.11 environment, on the basis of experimental data, the current-voltage characteristics of a transistor structure based on a BFT93 bipolar transistor and a BF998 MOSFET are constructed, which are shown in Fig. 9. The family of current-voltage characteristics of a transistor structure with a negative differential resistance was obtained by replacing the voltage divider R4, RW, R5 with an additional control voltage source V2. Experimental studies were carried out with control voltages in the range from 0.5 V to 3.0 V with a step of 0.5 V.

On Fig. 10 shows the Smith chart of the impedance S11, that is, the impedance of the structure under study in the frequency range from 50 kHz to 2 GHz. On Fig. 11 shows the impedance of the structure under study in polar coordinates. On Fig. 12 shows the standing wave ratio (SWR) in the same frequency range, and in Fig. 13 change in the active and reactive components of the self-oscillating humidity sensor impedance in the frequency range from 50 kHz to 2 GHz.

As noted above, the self-oscillating parametric humidity sensor is built on the basis of a transistor structure with a negative differential resistance, and a change in the impedance of the transistor structure makes a contribution to the frequency tuning from a change in humidity. Therefore, the study of the impedance (both active and reactive impedance components in a wide frequency range) of this structure is an integral part of the device development. This structure is a two-terminal, therefore, experimental studies of S11 parameters are carried out in the active mode with power supply through the RF + DC power module. It consists of high frequency inductors and capacitors with ultra-wide band, near ideal and no resonant point. An insulating capacitance is used to isolate DC current and prevent leakage of DC voltage into downstream circuits or instrumentation. The high frequency inductance isolates the AC information flow to prevent high frequency signals from leaking into the power system.

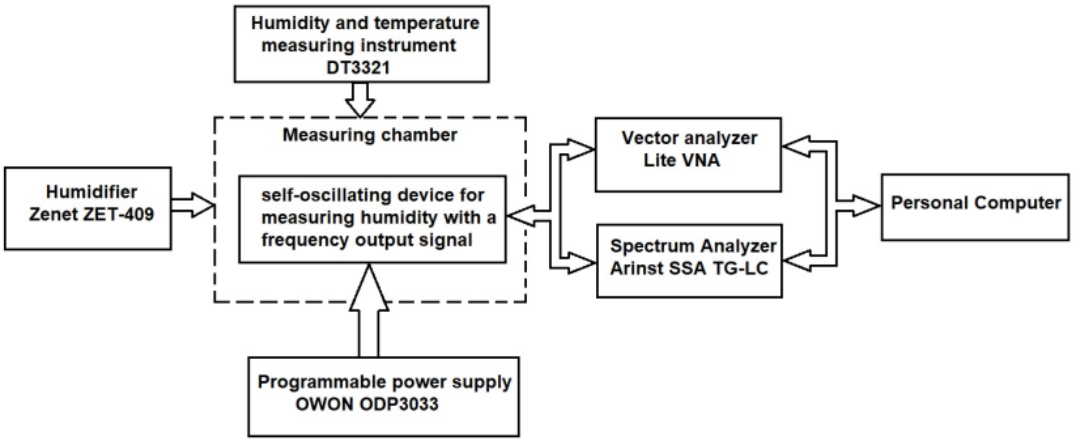


*Fig. 8. Block diagram of the experimental setup*

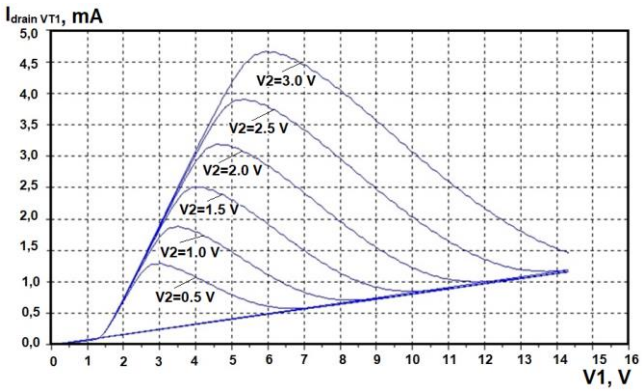


*Fig. 9. Volt-ampere characteristics of the transistor structure based on bipolar BFT93 and MOSFET BF998 transistors*

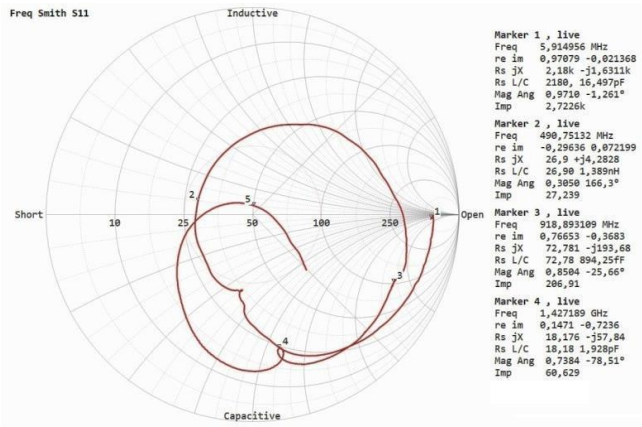


*Fig. 10. Smith chart of the S11 self-oscillating impedance humidity sensor in the frequency range from 50 kHz to 2 GHz*

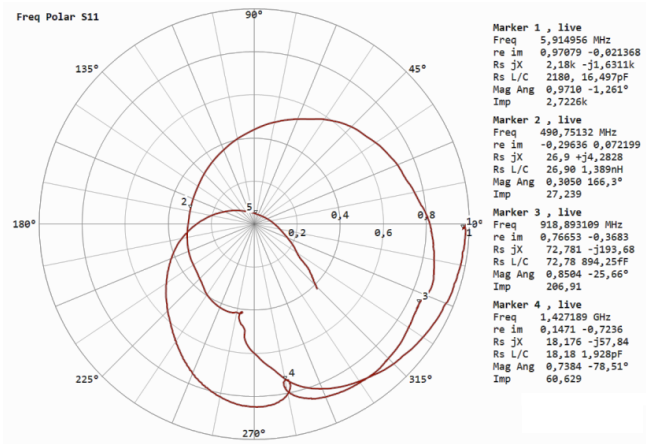


*Fig. 11. Impedance S11 in polar coordinates of a self-oscillating humidity sensor in the frequency range from 50 kHz to 2 GHz*

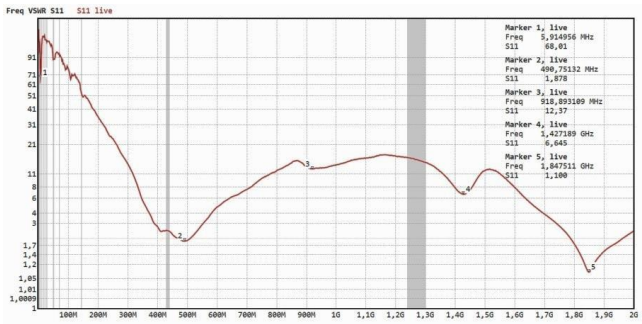


*Fig. 12. SWR of self-oscillating humidity sensor in the frequency range from 50 kHz to 2 GHz*

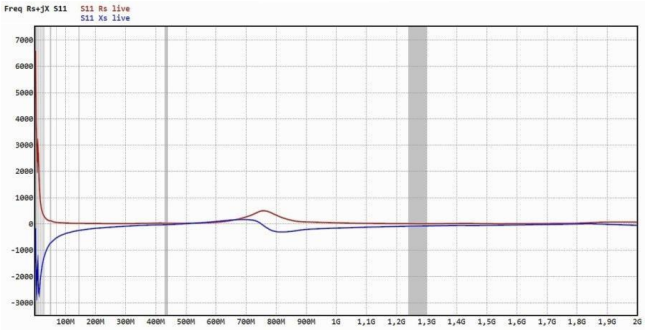


*Fig. 13. Changing the active and reactive components of the impedance self-oscillating humidity sensor in the range frequencies from 50 kHz to 2 GHz*

The experimental dependences of the real and imaginary parts of the parameter S11 are shown in Figs. 14, and in Fig. 15 shows the logarithmic magnitude of the self-oscillating sensor in the frequency range from 50 kHz to 2 GHz. The capacitance of the self-oscillating humidity sensor in the frequency range from 50 kHz to 150 MHz is shown in Fig. 16.

Experimental studies of the output signal spectra of the developed self-oscillating humidity sensor were carried out using an Arinst SSA TG-LC spectrum analyzer.

The LTE range for different countries and application systems is designed for frequencies from 450 MHz to 5925 MHz and is divided into 103 frequency bands. According to the customer's conditions, the frequency range of the humidity sensor is selected in the LTE-800 Downlink range. The 3GPP B20 (800 MHz) LTE band is the second most popular band used by public mobile operators to deploy LTE networks and is also well suited for wide regional coverage for in-building IoT coverage: NB-IoT (LTE Cat -NB1).The use of 800MHz spectrum helps operators to launch LTE services faster and meet market demands [2, 20].

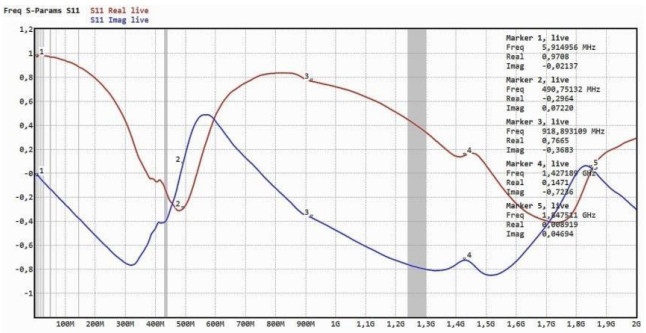


*Fig. 14. Real and imaginary parts of the S11 self-oscillating sensor humidity in the frequency range from 50 kHz to 2 GHz*

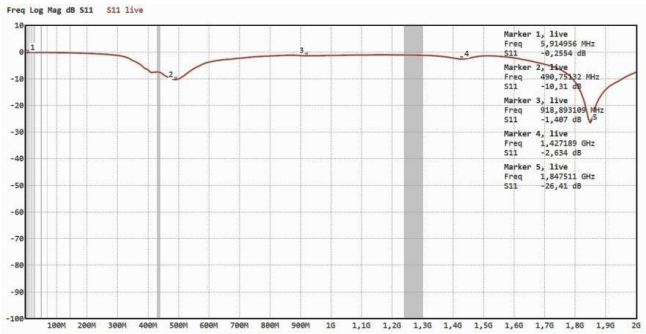


*Fig. 15. Logarithmic magnitude of self-oscillating humidity sensor in the frequency range from 50 kHz to 2 GHz*

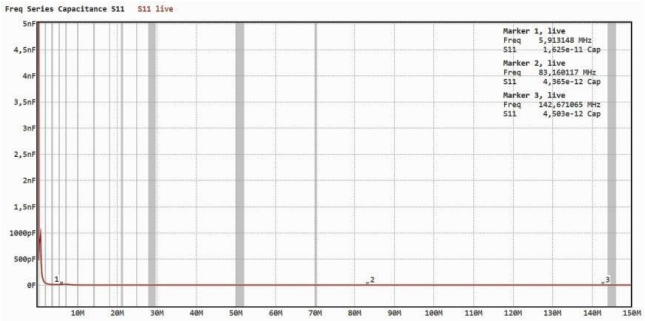


*Fig. 16. Passing capacitance of self-oscillating humidity sensor in the frequency range from 50 kHz to 150 MHz*

Self-oscillating parametric humidity sensor is designed in two versions. The first, as a radio transducer with its own data exchange protocol for a specialized measurement system, but in the LTE band, for deep protection of transmitted data. So is the second option, as a GFSK or MFSK modulation modulator, which is part of standard equipment with a generally accepted data transfer protocol.

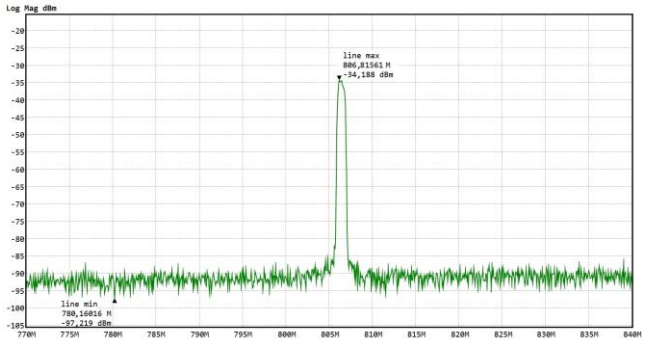


*Fig. 17. Spectrum of a self-oscillating parametric humidity sensor with frequency output signal and humidity sensitive resistive element at 99% humidity and 25°C temperature*

On Fig. 17 shows the spectrum of a self-oscillating parametric humidity sensor with a frequency output signal, designed based on a microelectronic transistor structure with a negative differential resistance, in which the moisture sensing element is a resistor, the transmission frequency is 806.8 MHz at a humidity of 99% and a temperature of 25°C.

Fig. 18 shows the spectrum of a self-oscillating parametric humidity sensor with frequency output at 30% humidity and 25°C, the transmission frequency has value 822.0 MHz.

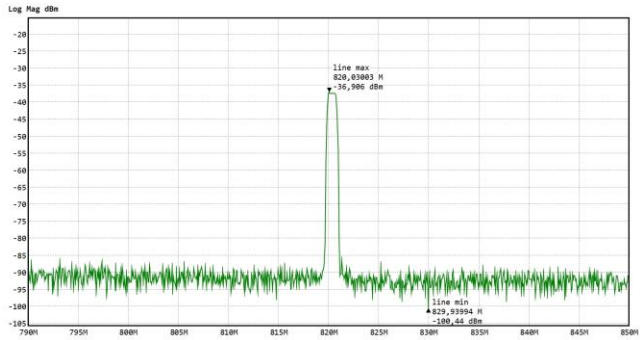


*Fig. 18. Spectrum of self-oscillating parametric humidity sensor with frequency output signal at 30% humidity and 25°C temperature*

## 5. Conclusions

1. A mathematical model has been developed for a self-oscillating parametric humidity sensor with a frequency output signal, which takes into account the influence of relative humidity on a sensitive resistive element, which is an integral element of a parametric transducer, which made it possible to obtain a conversion function, as well as a sensitivity function.
2. In the course of mathematical modeling, analytical expressions for the transformation function and the sensitivity equation of a self-oscillating parametric humidity sensor with an output frequency signal are obtained.
3. Computer modeling and experimental studies of a self-oscillating parametric humidity sensor were carried out, during which the main parameters and characteristics were obtained: the dependence of the generation frequency on changes in relative humidity in the range from 30% to 99%, the change in sensitivity on relative humidity, the dependence of the active and reactive components of the impedance in the frequency range from 50 kHz to 2 GHz, the Smith chart of the S11 parameter in the frequency range from 50 kHz to 2 GHz, the standing wave ratio, the change in the logarithmic magnitude and the spectra of the output signal of the self-oscillating parametric humidity sensor in the LTE-800 Downlink frequency range.
4. The sensitivity of the developed self-oscillating parametric humidity sensor in the range of humidity change from 30% to 99% has a value from 332.8 kHz/% to 130.2 kHz/%.

## References


[1] Assaf T.: A Frequency Modulation-Based Taxel Array: A Bio-Inspired Architecture for Large-Scale Artificial Skin. Sensors 21, 2021, 1−17.
[2] di Benedetto M.-G. et al.: Analysis of NB-IoT technology towards massive Machine Type Communication. University Sapienza di Roma, Roma 2018.
[3] Brown P.: Sensors and actuators: technology and applications. Library Press, New York 2017.
[4] Bury O. A. et al.: Gas sensors on nanostructures: current state and research prospects. Bulletin of the National University "Lviv Polytechnic", Series: Radioelectronics and telecommunications 885, 2017, 113–131.
[5] Czubenko M. et al.: Simple Neural Network for Collision Detection of Collaborative Robots. Sensors 21, 2021, 4235.
[6] Feng Y. et al.: Enhanced Frequency Stability of SAW Yarn Tension Sensor by Using the Dual Differential Channel Surface Acoustic Wave Oscillator. Sensors 23(1), 2023, 464.
[7] Galka A. G. et al.: Microwave Cavity Sensor for Measurements of Air Humidity under Reduced Pressure. Sensors 23(3), 2023, 1498.
[8] Grieshaber D. et al.: Electrochemical Biosensors − Sensor Principles and Architectures. Sensors 8, 2008, 1400−1458.
[9] Grundmann M.: The Physics of Semiconductors. Springer-Verlag, Berlin Heidelberg 2006.
[10] Hang L. et al.: Design and Implementation of Sensor-Cloud Platform for Physical Sensor Management on CoT Environments. Electronics 7, 2018, 1−25.
[11] Lepikh Ya. I. et al.: Intelligent measuring systems based on new generation microelectronic sensors. Astroprint, Odessa 2011.
[12] Manea G. et al.: Integration of sensor networks in cloud computing. UPB Sci. Bull., Series C 78, 2016.
[13] Nagarai A.: Introduction to Sensors in IoT and Cloud Computing Applications. Bentham Science Publishers, Bangalore 2021.
[14] Nelyudov I. Sh. et al.: Automatic control of technological objects. NAU, Kyiv 2018.
[15] Osadchuk A. V. et al.: Mathematical Model Radio-Measuring Frequency Transducer of Optical Radiation Based on MOS Transistor Structures with Negative Differential Resistance. Journal of Nano- and Electronic Physics 13(4), 2021, 04001.
[16] Osadchuk A. V. et al.: Microelectronic Transducer Gas Concentration based on MOSFET with Active Inductive Element. Przegląd Elektrotechniczny 4, 2019, 237−241.
[17] Osadchuk A. V., Osadchuk V. S.: Frequency Transducers of Gas Concentration Based on Transistor Structures with Negative Differential Resistance. Sidorenko A., Hahn H. (eds): Functional Nanostructures and Sensors for CBRN Defence and Environmental Safety and Security. NATO Science for Peace and Security Series C: Environmental Security. Springer, Dordrecht 2020.
[18] Osadchuk V. S. et al.: Reactive properties of transistors and transistor circuits. Universum-Vinnytsia, Vinnytsia 1999.
[19] Osadchuk V. S. et al.: Temperature transducer based on a metal-pyroelectric-semiconductor structure with negative differential resistance. Proc. SPIE 10808, 2018, 108085D.
[20] Sainju P. M.: LTE Performance analysis on 800 and 1800 MHz Bands. Tampere University of Technology. Tampere 2012.
[21] Sze S. M. et al.: Physics of Semiconductor Devices. Wiley-Interscience, Hoboken 2007.
[22] Yang H. et al.: A Study on the Gas/Humidity Sensitivity of the High-Frequency SAW CO Gas Sensor Based on Noble-Metal-Modified Metal Oxide Film. Sensors 23(5), 2023, 2487.
[23] https://datasheetspdf.com/datasheet/HR202.html
[24] LTspice XVII. Analog Devices Corporation, 2018.
[25] SPICE Device Models and Simulation Examples. Oxford University Press, 2020.



**Ph.D. Iaroslav Osadchuk**
e-mail: osadchuk.j93@gmail.com

Candidate of Technical Sciences, associate professor of Information Radioelectronic Technologies and Systems of Vinnytsia National Technical University. Author of more than 180 publications, including 6 monographs, 60 patents for inventions and more than 100 scientific articles in professional journals, of which 27 are in scientometric databases Scopus and Web of Science.

http://orcid.org/0000-0002-5472-0797



**Prof. Vladimir Osadchuk**
e-mail: osadchuk.vs38@gmail.com

Doctor of Technical Sciences, Professor of Information Radioelectronic Technologies and Systems of Vinnitsa National Technical University, Honored Worker of Science and Technology of Ukraine, Academician of the Academy of Engineering Sciences of Ukraine. Author of more than 900 publications, including 22 monographs, 14 textbooks, more than 350 copyright certificates and patents for inventions and more than 550 scientific articles in professional journals, of which 40 are in scientometric databases Scopus and Web of Science.

http://orcid.org/0000-0002-3142-3642



**Prof. Oleksandr Osadchuk**
e-mail: osadchuk.av69@gmail.com

Doctor of Technical Sciences, Professor, Head of the Department of Information Radioelectronic Technologies and Systems of Vinnitsia National Technical University, Academician of the Academy Metrology Ukraine. Author of over 900 publications, including 34 monographs, 17 textbooks, 300 patents for inventions, more than 500 scientific articles in professional journals, of which 69 are in the scientometric databases Scopus and Web of Science.

http://orcid.org/0000-0001-6662-9141



**Ph.D. Lyudmila Krylik**
e-mail: lyudmila.krylik@gmail.com

Candidate of Technical Sciences, associate professor of the Department for Computer Science of Vinnytsia National Technical University. Author of more than 150 publications, including 2 monographs, 12 textbooks, 60 patents for inventions of Ukraine and more than 80 scientific articles in professional journals, of which 6 are in scientometric database Scopus.

http://orcid.org/0000-0001-6642-754X


http://doi.org/10.35784/iapgos.3452

*received: 19.01.2023 | revised: 12.03.2023 | accepted: 12.03.2023 | available online: 31.03.2023*

# DEVELOPMENT OF A MODIFIED METHOD OF NETWORK TRAFFIC FORMING

**Valeriy Kozlovskiy[1], Natalia Yakymchuk[2], Yosyp Selepyna[2], Sergiy Moroz[2], Anatolii Tkachuk[2]**

[1]National Aviation University, Faculty of Cybernetics, Computer and Software Engineering, Department of Information Security, Kyiv, Ukraine, [2]Lutsk National Technical University, Faculty of Computer and Information Technologies, Department of Electronics and Telecommunications, Lutsk, Ukraine

***Abstract.*** *Based on the analysis of the statistical characteristics of heterogeneous network traffic of "Quadruple Play" mobile subscribers, it is shown that it cannot be represented by Poisson or Erlang distributions. It is shown that for such similar traffic, the rate of growth of the required buffer volume increases as the Hurst parameter increases. A method of adaptive traffic formation using the control of the length of intervals of the intensity of the arrival of data packets has been developed. Congestion management is carried out by changing the frequency of the marker generator (GM) on the basis of the results of forecasting the required bandwidth of the system and the required buffer size. The shaper adapts to changes in the length and instantaneous intensity of packet input in real-time.*

**Keywords**: communication channels, mass service theory, self-similarity traffic

## OPRACOWANIE ZMODYFIKOWANEJ METODY FORMOWANIA RUCHU SIECIOWEGO

***Streszczenie.*** *Na podstawie analizy charakterystyk statystycznych heterogenicznego ruchu sieciowego abonentów telefonii komórkowej "Quadruple Play" wykazano, że nie może on być reprezentowany przez rozkłady Poissona lub Erlanga. Pokazano, że dla takiego podobnego ruchu tempo wzrostu wymaganej objętości bufora wzrasta wraz ze wzrostem parametru Hursta. Opracowano metodę adaptacyjnego kształtowania ruchu wykorzystującą sterowanie długością interwałów natężenia napływu pakietów danych. Zarządzanie ograniczeniami odbywa się poprzez zmianę częstotliwości generatora znaczników (GM) na podstawie wyników prognozowania wymaganej przepustowości systemu oraz wymaganej wielkości bufora. Shaper dostosowuje się do zmian długości i chwilowej intensywności wprowadzanych pakietów w czasie rzeczywistym.*

**Słowa kluczowe**: kanał komunikacyjny, teoria usług masowych, ruch samopodobieństwa

## Introduction

Maintenance of heterogeneous traffic flows. Traffic may include voice, video, data, and traffic of mobile subscribers "Quadruple Play". The statistical characteristics of such heterogeneous network traffic can no longer be represented by Poisson or Erlang distributions. Such traffic is self-similar (fractal) and is described with satisfactory accuracy by models of statistical distributions with heavy tails [13].

A characteristic feature of random processes, which are described by distributions with heavy tails, is the combination of the sufficiently low average intensity of the process with sporadic bursts of instantaneous intensity. In addition, in the presence of a heavy tail of the distribution, the convergence of the sample mean to the mathematical expectation deteriorates.

The self-similarity of real-time traffic is considered in the examples of different components of heterogeneous traffic. One of the most important traffic components of modern telecommunications networks is language traffic. The characteristics of the traffic generated by a single voice source are highly dependent on the language coder (codec) used. Most commonly, voice traffic can be viewed as a superposition of a large number of individual independent ON/OFF sources transmitting at the same intensity but with durations distributed according to a heavy-tailed distribution [2, 8].

Initially, the Poisson model was used to analyze traffic in data networks. In the case of high loading, the Poisson model does not agree with the simulation results, and the combined process is highly correlated and exhibits properties of long-term dependence. The self-similarity assessment conducted using various tests showed that the self-similarity property of the total traffic should be taken into account when modeling in the case of high call volume. Both fractal Gaussian noise and more complex multi-component models can be used to model aggregated VoIP traffic [7].

## 1. Literature review

When transmitting video traffic, the method of video encoding is important for determining self-similarity. Typically, interframe coding is used. Since adjacent frames are not very different from each other (because the motion is continuous), this results in a significant correlation between adjacent frames. You can protect yourself from transmission errors by periodically transmitting a full frame. It is also known that video traffic is highly correlated and exhibits long-term dependence, which leads to serious estimation drift and difficulties in assessing convergence. Estimating the self-similar properties of video traffic over large intervals using the R/S analysis method has advantages over other methods of estimating self-similarity. The R/S analysis functions themselves exhibit a scaling property and therefore constitute an optimal reference point system on which to track large-scale phenomena [18, 19].

When studying Variable Bit Rate (VBR) traffic, it was established that long-term dependence looks like artificial non-stationarity. And such a process is called a process with a Level Shift (SL). At the same time, the periodicity of the traffic corresponds to taking into account only the contour correlation function of the video. Thus, when describing network traffic using fractal models, care must be taken not to confuse real non-stationarities with stationary fractal behavior with sporadic bursts of traffic intensity [12]. These effects can produce the same results in many statistical tests. Classical methods of mathematical statistics and fractal theory can distinguish non-stationarity and long-term dependence or estimate the Hurst index in the presence of some types of non-stationarity [15].

As for WWW connections, the self-similarity of network traffic depends on user activity. With lower user activity, which results in a lower average speed, behavior is observed that is typically modeled by Poisson processes. Aggregate WWW traffic at low network load (without losses in buffers) is also well modeled by Poisson processes [14].

Self-similar traffic requires more memory resources of buffer devices than the classic M/M/1 model, which is considered the least favorable compared to others (for example, with a constant or Gaussian service time distribution). The rate of growth of the required amount of memory increases with the increase of the Hurst parameter, which is mainly due to the degree of the grouping of homogeneous packets and bursts of network load [10, 11].

It can also be argued that simply increasing buffer memory (hardware or software) is inefficient. In addition, with the expected increase in the share of data traffic in the total volume, the degree of self-similarity will increase, and the dependence $\rho(q_{buff})$ will grow more and more sharply [9].

To eliminate or at least reduce the harmful effect of traffic similarity, methods of regulation or shaping of the incoming flow (policing-shaping) are usually used [1, 17].

## 2. Researches methodology

As it has been noted, to increase the productivity of information and telecommunication networks, the mass service theory (MST) is used. First, the analytical study of queues concerns the quantification of the phenomenon of waiting for queues using key performance parameters, such as the average length of the queue (average number of customers in the queue; in the analysis of the passage of packets through the switching node – the average number of packets in the buffer memory), the average queue time and average network utilization [5]. Secondly, using simulation modeling methods, the results of the analysis are obtained to solve the following tasks [16]:

a) comparison of waiting time and average number of messages in queues;
b) comparison of parameters of queues M/M/1, M/D/1, and Qd/D/1 and study of the impact of the quality of traffic formation on the probability of blocking and dropping packets for different waiting models.

Therefore, the mathematical model of the switching network node is considered a single-line mass service system (MSS). The statistical characteristics of heterogeneous network traffic at the entrance of such an MSS are determined by the fact that the traffic includes speech, video, data, and traffic of mobile subscribers (Quadruple Play traffic). Such traffic is self-similar by definition (fractal). It is described with satisfactory accuracy by the models G|G|1, G|M|1 or G|G|1|k, G|M|1|k.

When serving requests in a device with a buffer memory of infinite capacity, arbitrary service disciplines can, in principle, give the same results [4, 14]. However, with a limited lifetime of packets $T_{live}$, a necessary condition for their preservation should be compliance with the inequality $T_{serv} \leq T_{live}$, where $T_{serv}$ is the service time (or the average time in the case of a service model with a random length of time) [6].

Also very important is the question of the acceptability of service disciplines (FIFO, LIFO, etc.) in a discrete-time system in terms of service delay and service failure rates. However, regardless of the specific service discipline, the following statement is valid: the better the degree of smoothing of network traffic dispersion, the slower the queue in the buffer memory of the serving device will grow [3].

## 3. Results

Let's consider the functionality of packet transmission efficiency with traffic shaping and smoothing. The effectiveness of packet transmission depends not only on the quality of adaptation but also on key network parameters. Fig. 1 shows the scheme of sequential processing of packet flow parameters.


*Fig. 1. Sequential flow processing*

Classification is carried out according to the hierarchy of priorities; regulation and shaping are intended to transform into a periodic or at least quasi-periodic flow. For systems without feedback, solving the alignment problem data transfer rate can be carried out using "leaky bucket" and "marker bucket" algorithms. The "leaky bucket" algorithm is a traffic control mechanism when a portion of the packet flow that exceeds network bandwidth is simply discarded or marked as redundant or low priority.

When passing through the shapers of the "leaky bucket" or "marker bucket" type, the MSS model and, accordingly, the traffic statistics undergo transformations. In particular, at the output of the "marker bucket" shaper, the traffic acquires a quasi-deterministic (Qd) character with a packet tracking period $T_{arr}$. It is described by the Qd|G|1|k or Qd|M|1|k models. The packet tracking period takes the form $T_{arr} = T_0 + \xi(n)$, where $\xi(n)$ is a normally distributed random variable with zero mathematical expectation. Root square deviation (RMS) is $\sigma_\xi < T_0/6$.

With ideal regulation and shaping of the input flow, the latter becomes deterministic or close to it quasi-deterministic. With a deterministic order of incoming applications and a deterministic processing time, the graph of queue growth is a linear-broken line (Fig. 2). There, for comparison, the dependence of the length of the queue of applications for the M/D/1 model – Poisson flow of applications and deterministic service time is given. Note that in practice both the traffic at the output of the shaper and the packet processing time is quasi-deterministic (Qd).

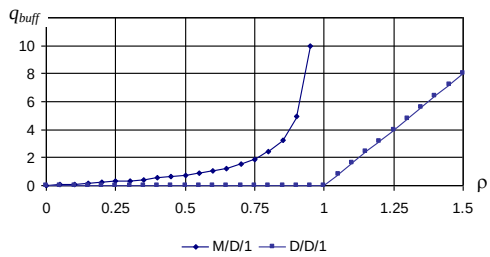


*Fig. 2. Dependences of the length of the request queue (required buffer memory) on the utilization factor for incoming traffic models*

The formation mechanism follows the rule of placing packets in a queue. Each egress port has a set of queues assigned different priorities or weights. The highest (first) priority is given to packets whose arrival intensity does not exceed $C_{IR}$. The second priority is assigned to packets whose arrival intensity is higher than $C_{IR}$, but not higher than $E_{IR}$. Finally, the lowest (third) priority is assigned to packets whose arrival intensity is higher than $E_{IR}$. Conditional determination of the priority of packages is carried out by different colors: green (first priority), yellow (second priority), and red (third priority).

In the process of traffic formation, packets are placed in queues with different priorities. Since all queues have a finite length, packets cannot be placed in them indefinitely. If the switching node's buffer is full, new packets are discarded.

Discard rules are different for packages of different colors. Green packets obey the most lenient rules, and it can be expected that most of these packets will be forwarded to the output queue. The rules for yellow packets are stricter, so their number in the output queue is smaller. The strictest rules are for red packets, which are detected when the buffer overflows.

The general concept of building a shaper and assigning priorities is based on key performance parameters. Network elements and sensors used as service resource analyzers are placed in certain nodes of the network infrastructure to collect performance-related data. For example, these can be cumulative counters of protocol events. At regular intervals, in near real-time, this performance information is transmitted to higher-level service and performance management systems.

Now let's develop a modified method of traffic formation using an adaptive multi-speed marker bucket.

Let the flow shaper have variable parameters: the average intensity of the flow – $C_{IR}$ and the limit intensity of the flow – $E_{IR}$ (Fig. 3). They are determined both by the speed and acceleration of the growth of flow intensity and, accordingly, by changes in the speed and acceleration of buffer filling.

Determining the priority of packets and, accordingly, their conditional coloring is as follows:

- if the short-term intensity of the flow does not exceed the $C_{IR}$ value, the packets are assigned a higher priority (colored in green). Certain package delivery guarantees are provided;
- if the short-term flow intensity is higher than the $C_{IR}$, but not higher than the $E_{IR}$, the packets are assigned a medium priority (coloring in yellow). Delivery of packages is carried out with the greatest efforts, but without providing guarantees (Best Effort delivery mode);
- if the short-term intensity of the flow exceeds the value of the $E_{IR}$, the packets are assigned a lower priority (colored in red). Delivery is not guaranteed, some packets are rejected until the value of the short-term intensity drops below $E_{IR}$. The remaining packets go back into the yellow area.

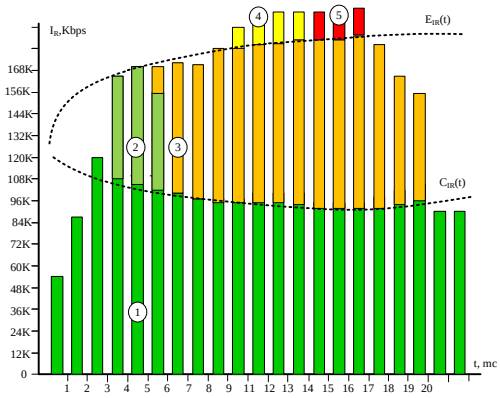


*Fig. 3. Load measurement and packet specification management with an adaptively changing "yellow area" window size: 1 – green packets; 2 – packets that remain conditionally green in case of a short-term exceedance of $C_{IR}$ no more than m seconds; 3 – yellow packets whose flow intensity is higher than $C_{IR}$, but lower than $E_{IR}$; 4 – packets that remain conditionally yellow in case of a short-term exceedance of $E_{IR}$ no more than n seconds, n > m; 5 – red packets that are discarded first*

In contrast to the classic method of traffic formation, the length of the $C_{IR}$ and $E_{IR}$ exceeding intervals is monitored at the same time. Based on the control results, the acceptable values of the number m of conditionally green packets and the number n of conditionally yellow packets are calculated.

Thus, with additional consideration of flow parameters and queue growth rate in the buffer memory, the set of parameters to be optimized expands to two elements, which are described by an additional color: conditionally green and conditionally yellow packets. It is natural to expect a corresponding acceleration of updates of information about loading parameters and a reduction in the reaction time of the marker bucket. These considerations are verified by calculations and computer simulations.

Short-term intensities $E_{IR}$ and $C_{IR}$ will vary within limits that depend on the maximum bandwidth of the switch. Therefore, it is advisable to adapt to the average intensity of packets by changing the intensities of $E_{IR}$ and $C_{IR}$ managing the size of the "yellow range".

The M-th order integrator with variable weighting coefficients $k_1 = k_1(t)$, $k_2 = k_2(t), \dots k_m = k_m(t)$ can estimate speed, acceleration and higher derivatives of the degree of buffer filling. Controlling signals $y_{db}(t-\tau), y_{tb}(t-\tau), y_{dg}(t-\tau)$, regulate the total size of data and markers in the buffers, as well as the frequency of arrival of markers. The parameters of these signals are determined by traffic parameters, primarily by the degree of its self-similarity. In practice, it does not make sense to calculate derivatives of a higher order than the second (velocity and acceleration), since the accuracy of the statistical estimation deteriorates rapidly.

Figure 4 shows the scheme of the M-th order adaptive shaper. According to the above considerations, you should choose $M \le 2$.

Management of the size of the "yellow area" is carried out by changing the frequency of the marker generator (GM) on the basis of the results of forecasting the required bandwidth of the system and the required buffer size. The scheme of the additional forecasting module developed in is based on the Smith predictor, The modification of the Smith predictor consists in replacing the exponential smoothing function with a power-law smoothing function, which is optimal for smoothing self-similar processes with heavy tails of probability distributions.

The main differences between the multi-speed adaptive shaper and the traditional "marker bucket" shaper are as follows.

1. When the counter counts the number $n(t)$ of packets arriving at the input of the generator, the evaluation period $T_{est}$ changes in accordance with the current frequency $f_{mg}(t_{curr})$, assigned to the token generator:

$$T_{ets}(t_{curr}) = \frac{1}{f_{mg}(t_{curr})}$$

2. The accumulator is a digital adder with saturation. This scheme of the adder was chosen in order to avoid overflow fluctuations that may occur when numbers are represented in the additional code.

3. The problem of fractal traffic is sporadic significant bursts of intensity at a rather insignificant average level of intensity over a relatively long observation interval. Therefore, we offer a new approach - an algorithm for ensuring the quality of service, in the presence of the effect of self-similarity. The idea of this algorithm is to modify the mechanisms of traffic formation to ensure the required QoS classes by introducing an additional module for predicting the required buffer size $B_{size}$ for some time ahead according to changes in the intensity of incoming packets. At the same time, the traffic does not conform to a preset profile, but on the contrary, the system bandwidth adapts to the traffic profile. At the same time, losses are reduced and the use of allocated resources is improved.

4. The formation algorithm to prevent traffic congestion works as follows:

- the receiver measures the loss coefficient and returns it to the sender;
- the sender uses these feedback messages to calculate the Round-Trip Time (RTT)
- sender uses RTT and loss ratio to calculate transmission speed;
- the sender adjusts the sending speed.

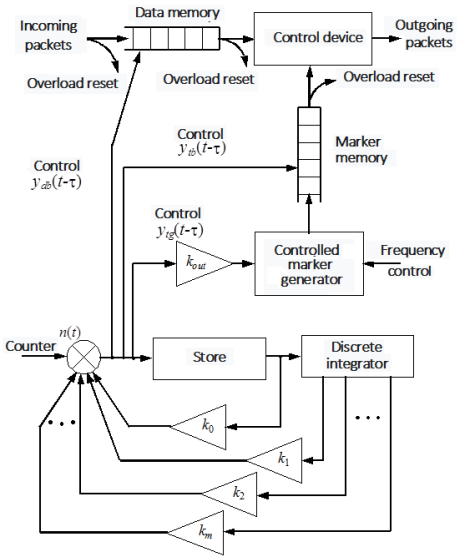


*Fig. 4. Scheme of a multi-speed adaptive marker former (the device for controlling the size of the "yellow area" is not shown)*

A multi-channel system with a divided buffer memory has been developed, which can be interpreted as a parallel structure with single-channel service systems and the same service disciplines.

Assume that each traffic stream has the form Triple Play or Quadruple Play. Before entering the network, it is formed by a multi-channel former. The guaranteed speed $r_i$ of the i-th flow is determined by the expressions:

$$r_i = \frac{B_{S\max}}{\delta\tau_i + \frac{B_{S\max}}{r_p}} \tag{1}$$

where $\delta\tau_i$ is the limit closure of the i-th flow; $B_S$ and $B_{S\max}$ – the current and maximum size of the buffer memory, respectively; $r_p$ is the peak intensity of the i-th flow. Accordingly, the time to fill bucket with $E$ markers will be equal to

$$t_{fE} = \frac{E_{BS}}{E_{IR}} \tag{2}$$

Markers are accumulated over the total time

$$\tau_e = E(\tau_{te} + \tau_{ge}) \tag{3}$$

where $\tau_{te}$ is the length of the marker entering bucket $E$; $\tau_{ge}$ – protective interval.

Adaptation to changing the length and instantaneous intensity of packet input can be done as follows:

- by changing the length of the protective interval to a constant length of the marker;
- by changing the length of the marker at a constant length of the security interval;
- by changing the size of the "yellow area";
- by changing the buffer memory of markers.

## 4. Conclusions

The proposed procedure for forming self-similar network traffic using an adaptive multi-rate marker bucket is quite simple and effective. Simulation results show that it is possible to limit the frequency of the token generator to such a value that all incoming traffic is received and then transmitted without loss or retransmissions. With this method of overload management, elimination of overloads is achieved in a short time, so load fluctuations are also relatively small. Although both congestion and loss of traffic controllability can occur if the duration of bursts exceeds the buffer of dynamic stability of the shaper. For example, if the primary and secondary buffers are full for a period exceeding the allowable timeout, that route or network segment becomes unavailable altogether. Such situations have to be handled with higher-level services.

Asymptotic comparative quality estimates based on the queue length indicator were obtained for classical Poisson and self-similar flows entering a single-channel mass service system (MSS) with class GI/G/1 waiting.

## References


[1] Barreiros M., Lundqvist P.: Policing and Shaping. QOS-Enabled Networks: Tools and Foundations. Wiley, 2015 [http://doi.org/10.1002/9781119109136.ch6].

[2] Chakraborty T. et al.: Searching for Heavy-Tailed Probability Distributions for Modeling Real-World Complex Networks. IEEE Access 10, 2022, 115092-115107 [http://doi.org/10.1109/ACCESS.2022.3218631].

[3] Chang C. S. et al.: SDL Constructions of FIFO, LIFO and Absolute Contractors. IEEE INFOCOM 2009, 738–746 [http://doi.org/10.1109/INFCOM.2009.5061982].

[4] Farhadi V. et al.: Service Placement and Request Scheduling for Data-intensive Applications in Edge Clouds. IEEE Conference on Computer Communications – INFOCOM 2019, 1279–1287 [http://doi.org/10.1109/INFOCOM.2019.8737368].

[5] Han C. et al.: Analytical Study of the IEEE 802.11p MAC Sublayer in Vehicular Networks. IEEE Transactions on Intelligent Transportation Systems 13(2), 2012, 873–886 [http://doi.org/10.1109/TITS.2012.2183366].

[6] He J. et al.: Buffer-Aided Relaying for Two-Hop Secure Communication with Limited Packet Lifetime. IEEE 20th International Conference on High Performance Switching and Routing (HPSR), 2019, 1–7 [http://doi.org/10.1109/HPSR.2019.8807995].

[7] Kirichenko L. et al.: Classification of Fractal Time Series Using Recurrence Plots. International Scientific-Practical Conference Problems of Infocommunications, Science and Technology (PIC S&T), Kharkiv, 2018, 719–724 [http://doi.org/10.1109/INFOCOMMST.2018.8632010].

[8] Kotenko I. et al.: A technique for early detection of cyberattacks using the traffic self-similarity property and a statistical approach. 29th Euromicro International Conference on Parallel, Distributed and Network-Based Processing (PDP), Valladolid, 2021, 281–284 [http://doi.org/10.1109/PDP52278.2021.00052].

[9] Li Z. et al.: Detecting Saturation Attacks Based on Self-Similarity of OpenFlow Traffic. IEEE Transactions on Network and Service Management 17(1), 2020, 607–621 [http://doi.org/10.1109/TNSM.2019.2959268].

[10] Millán G.: Proposal of an Estimator of the Hurst Parameter for a Self-similar Process Representative of the Degree of Randomness of the Recorded Traffic in IEEE 802.3-2005 Networks. OSF Preprints. 2021 [http://doi.org/10.31219/osf.io/pgbvm].

[11] Moltafet M. et al.: Average Age of Information for a Multi-Source M/M/1 Queueing Model With Packet Management. IEEE International Symposium on Information Theory (ISIT), Los Angeles, 2020, 1765–1769 [http://doi.org/10.1109/ISIT44484.2020.9174099].

[12] Patilkulkarni S. et al.: Programmable Delay and Variable Bit Rate Enabled Video Streaming using C++. Third International Conference on Advances in Electronics, Computers and Communications (ICAECC), Bengaluru, 2020, 1–7 [http://doi.org/10.1109/ICAECC50550.2020.9339499].

[13] Plevyak T., Sahin V.: Management of Triple/Quadruple Play Services from a Telecom Perspective. Next Generation Telecommunications Networks, Services, and Management, 2010, 15–52 [http://doi.org/10.1002/9780470594025.ch2].

[14] Ren D. et al.: Adaptive Request Scheduling and Service Caching for MEC-Assisted IoT Networks: An Online Learning Approach. IEEE Internet of Things Journal 9(18), 2022, 17372–17386 [http://doi.org/10.1109/JIOT.2022.3157677].

[15] Serinaldi F.: Use and misuse of some Hurst parameter estimators applied to stationary and non-stationary financial time series. Physica A: Statistical Mechanics and its Applications 389(14), 2010, 2770–2781 [http://doi.org/10.1016/j.physa.2010.02.044].

[16] Wang W. et al.: Software architecture based on message queue. 6th International Conference on Information Science, Computer Technology and Transportation – ISCTT, Xishuangbanna, 2021, 1–5.

[17] Yakymchuk N. et al.: Monitoring of Link-Level Congestion in Telecommunication Systems Using Information Criteria. Informatyka, Automatyka, Pomiary w Gospodarce i Ochronie Środowiska – IAPGOS 12(4), 2022, 26–30 [http://doi.org/10.35784/iapgos.3076].

[18] Zablotskyi V. et al.: Method for Evaluation Quality Parameters of Telecommunications Services. Informatyka, Automatyka, Pomiary w Gospodarce i Ochronie Środowiska – IAPGOS 12(2), 2022, 30–33 [http://doi.org/10.35784/iapgos.2918].

[19] Zhang Y. et al.: Recent Advances on HEVC Inter-Frame Coding: From Optimization to Implementation and Beyond. IEEE Transactions on Circuits and Systems for Video Technology 30(11), 2020, 4321–4339 [http://doi.org/10.1109/TCSVT.2019.2954474].



**Ph.D. Valeriy Kozlovskiy**
e-mail: kzzi@nau.edu.ua

Research interests: Communications, Programmable logic controllers. Research network security. Features of the communication lines organization and operation.

http://orcid.org/0000-0002-8301-5501



**M.Sc. Natalia Yakymchuk**
e-mail: n.yakymchuk@lntu.edu.ua

Research interests: diagnostics and control of the telecommunication networks state, end-to-end diagnostics, congestion management.

http://orcid.org/0000-0002-8173-449X



**Ph.D. Yosyp Selepyna**
e-mail: y.selepyna@lntu.edu.ua

Research interests: Modeling of electronic devices and systems. Digital signal processing and coding in telecommunication systems and networks.

http://orcid.org/0000-0002-2421-1844



**Ph.D. Serhii Moroz**
e-mail: s.moroz@lntu.edu.ua

Author of more than 100 scientific papers, 7 patents for utility models. Research interests: Methodological bases of construction of sensors of physical quantities and measuring modules, Research of info-communication systems in the context of the development of the concept of the Internet of Things.

http://orcid.org/0000-0003-4677-5170



**Ph.D. Anatolii Tkachuk**
e-mail: a.tkachuk@lntu.edu.ua

Vice-dean for R&D Faculty of Computer and Information Technologies, Lutsk National Technical University.
Member of European Alliance for Innovation (EAI), International Association for Technological Development & Innovations (IATDI).

http://orcid.org/0000-0001-9085-7777


http://doi.org/10.35784/iapgos.3295

*received: 15.11.2022 | revised: 13.01.2023 | accepted: 12.03.2023 | available online: 31.03.2023*

# DIGITALIZATION OF ENTERPRISE WITH ENSURING STABILITY AND RELIABILITY

**Gulnar Balakayeva[1], Paul Ezhichelvan[2], Yerlan Makashev[1], Chris Phillips[2], Dauren Darkenbayev[1], Kalamkas Nurlybayeva[1]**

[1]Al-Farabi Kazakh National University, Almaty, Kazakhstan, [2]Newcastle University, Newcastle, United Kingdom

***Abstract.*** *The article is devoted to the development of an information system for automating business processes of a modern enterprise with ensuring stability and reliability, which are implemented by the applications developed by the authors. Goal is to develop improvements to the core digitalization processes of enterprises for sustainable functioning. The authors carried out a deep analysis and described the main stages of the enterprise digitalization process: the process of document approval, business processes of personnel management, etc. The architecture of the information system, a description of business processes and the principles of reliability and fault tolerance of the system being developed have been developed. The developed desktop-client application provides connection to the information system with the help of working computers of the enterprise through a local network with access to the application server. This allows you to reduce damage from accidental or deliberate incorrect actions of users and administrators; separation of protection; a variety of means of protection; simplicity and manageability of the information system and its security system.*

**Keywords**: digitalization, business processes, system architecture, reliability, data security

## CYFRYZACJA PRZEDSIĘBIORSTWA Z ZAPEWNIENIEM STABILNOŚCI I NIEZAWODNOŚCI

***Streszczenie***. *Artykuł poświęcony jest opracowaniu systemu informatycznego do automatyzacji procesów biznesowych nowoczesnego przedsiębiorstwa z zapewnieniem stabilności i niezawodności, które są realizowane przez opracowane przez autorów aplikacje. Celem jest rozwijanie usprawnień podstawowych procesów cyfryzacji przedsiębiorstw dla zrównoważonego funkcjonowania. Autorzy przeprowadzili dogłębną analizę i opisali główne etapy procesu cyfryzacji przedsiębiorstwa: proces akceptacji dokumentów, procesy biznesowe zarządzania personelem itp. Zostały opracowane architektura systemu informatycznego, opis procesów biznesowych oraz zasady niezawodności i odporności na błędy tworzonego systemu. Opracowana aplikacja typu desktop-client zapewnia połączenie z systemem informacyjnym za pomocą pracujących komputerów przedsiębiorstwa poprzez sieć lokalną z dostępem do serwera aplikacji. Pozwala to na ograniczenie szkód wynikających z przypadkowych lub celowych nieprawidłowych działań użytkowników i administratorów; rozdzielenie ochrony; różnorodność środków ochrony; prostotę i łatwość zarządzania systemem informatycznym i jego systemu zabezpieczeń.*

**Słowa kluczowe**: digitalizacja, procesy biznesowe, architektura systemu, niezawodność, bezpieczeństwo danych

## Introduction

The system architecture supports a transactional model that guarantees the integrity of system data throughout all stages of their life cycle. Automation system of the enterprise information system provides automation of formation and accounting (registration) of administrative documents, memos, meetings, and incoming and outgoing correspondence. Clients working outside the enterprise can access the information system through a web browser, as a web client, via a web server. The client application has two possible types of connection to the enterprise information system: a desktop client and a web client [2].

The proposed information system is designed for an efficient operation of the administration (user, client) of the enterprise [3]. The client application has two possible types of connection to the enterprise information system: a desktop client and a web client [19]. The desktop-client application enables connection to the information system using the working computers of the enterprise through the local network, with an appeal to an application server. Clients working outside the enterprise can access the information system through a web browser, as a web client, via a web server [16].

The proposed information system has a layered architecture using a domain-specific tool. The architecture incorporates provisions that seek to guarantee scalability, reliability and security of the system as we explain later [4]. By scalability we mean that the system should be able to handle a potentially large number of users without serious impact on system throughput and response times; reliability provisions would include mechanisms for tolerating crashes of system components with which the users would directly interact; finally, security considerations will be an integral part of the architecture, cutting across all levels of the system from the frontline clients tier to the database backend tier [13].

## 1. Multilevel architecture of the enterprise information system

The proposed information system has a layered architecture using a domain-specific tool. The architecture is the guarantor of the availability, reliability and security of the system [14].

Client applications – applications for end-users, development tools, system administration utilities. The client can be either a Windows application (inside the enterprise) or a web browser (client outside the enterprise).

Server components (service management agent) – application servers host a variety of services that allow clients to perform document processing services such as storing new documents in a Database Management System (DBMS) (backend or data tier), fetching relevant documents from the DBMS and modifying them as per application needs and storing the modified versions back in the DBMS. Supporting these services form the core functionality of the information system. These services fall under two broad categories: general administration and human-resource related [11].

This architecture proposes that these core services be instantiated on more than one host for reasons of scalability and reliability. Thus, a client can connect to any one of these hosts to conduct their document processing activities. Typically, an incoming client is exposed to a list of available hosts from which it randomly selects one host to connect to. Thus, if there are N clients simultaneously accessing the system and if there are H (>1), server hosts, then each host is expected to be servicing, on average, only N/H clients at any given time. Thus, by increasing H as N increases (e.g., during peak usage hours) the average load handled by each server is kept constant, and thereby the overall system performance as seen by clients is maintained [12].

DBMS – storage of data and metadata of documents related to the enterprise. It may also be referred to as the backend or data tier.

File storages (data warehouse) – archives of large or rarely used documents, which are more efficient to keep outside the DBMS; these are managed by their own services.

As indicated above, being part of an organisation's information infrastructure, the system architecture needs to demonstrate certain characteristics that are important for any corporate system:

Reliability. The system architecture supports a transactional model that guarantees the integrity of system data throughout all stages of their life cycle. File document storages allow one to organize reliable storage of documents.

Security. For each object within the system, it can be specified which users or groups have the right to perform certain actions with it. Confidential electronic documents and tasks can be encrypted directly in the system by any Microsoft CryptoAPI-compatible encryption provider, which guarantees protection even from users with unrestricted access to data. Logging of all user actions will allow restoring the history of work with system objects in the event of a security violation. This provides high protection against unauthorized access to document storages of all types.

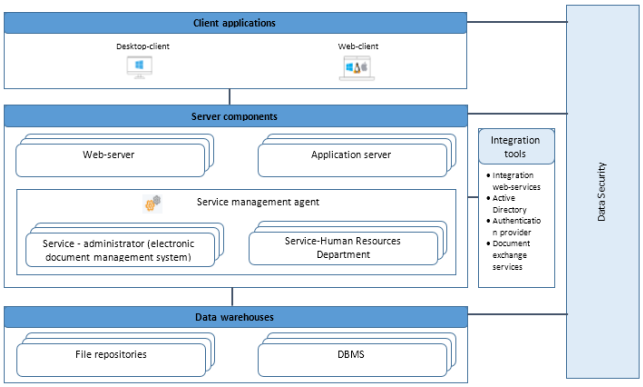


*Fig. 1. Enterprise information system architecture*

## 2. Enterprise digitalization system. Document processing

This supports the storage, processing and management of electronic documents and is designed to simplify the task of document processing by clients in a secure, scalable and reliable manner [17].

For a comprehensive solution to the problems of managing electronic document processes, the system must address the following requirements:

- The digitalization system of the enterprise (Fig. 2) makes it possible comprehensively to automate any work associated with contracts and related documents, including electronic approval. This provides the formation of documents by templates, the formation of registration numbers, registration of storage locations, registration of the availability of original documents, etc.
- Automation system of the enterprise information system provides automation of formation and accounting (registration) of administrative documents, memos, meetings, and incoming and outgoing correspondence.
- Electronic document management system supports the automatic approval of documents, the formation of mailings of documents for review, provides routing of documents, etc.
- System of control over execution of documents and orders allows the automatic formation of orders for the execution of documents, and provides automated control over deadlines.
- Electronic archive of documents solves the problem of archival storage of electronic documents. It allows you to create an archive structure from simple and moderated folders, and supports a search for documents in the information storage database
- System of notifications and reminders provides automatic and timely notification of process participants about current and upcoming events, and allows employees to exchange messages.
- Business process automation system is the core of the system. It is intended for the formation of graphic models of automated processes and ensures the movement of documents along routes. It manages a dynamic role-based process access model. Interacts with all subsystems.

When creating complex information systems, designing their architecture, infrastructure, choosing components and connections between them, a number of specific conceptual requirements aimed at ensuring the security of functioning are taken into account, in addition to the general ones (openness, scalability, portability, mobility, investment protection, etc.) [15]:

- The system architecture is flexible enough i.e. it allows relatively simple development of the infrastructure without fundamental structural changes, and changes in the configuration of the used means, and an increase in the functions and resources of the Information System (IS) in accordance with the expansion of the spheres and tasks of its application;
- The security of the system will be ensured under various types of threats and reliable data protection from design errors, destruction or loss of information, as well as user authorization, workload management, backup of data and computing resources, the fast restoration of IS functioning;
- Will provide comfortable, maximally simplified user access to the services and results of the functioning of the IS based on modern graphical tools, mnemonic diagrams and visual user interfaces;
- The system will be accompanied by updated, complete documentation, providing qualified maintenance and the possibility of developing the IS.

It is proposed to do processing documents according to the following schemes.

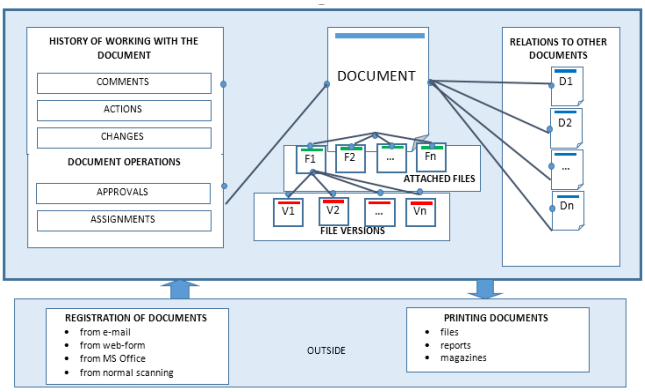


*Fig. 2. Enterprise digitalization system*

## 3. Document approval process

Document approval is the most often demanded business process in any organization. The main purpose of the business process for the organization is to control and monitor the terms (dates) of approvals.

Most companies face the task of approving a document [18].

The steps in the document approval process are suggested as follows:

1. Start of the process. Approval of the document with the indication of the document type -> The initiator fills in the main form for approval
2. Preparation of the document -> form is filled with data according to the template for the document type (for references -> number, executor, text of the reference, from (who), to (whom), date of the execution, for contracts -> contract number, contract date, text of the contract, the electronic version of the document, etc.). According to the type of document, the period for which the participants

in the process must agree on the document is determined automatically: agreement – 5 working days, order – 3 working days, order – 1 working day, memo – 6 working days, etc.
3. Identification of direct supervisors of the initiator for approval. The document is assigned "On approval by the head" status. The head of the initiator either rejects the contract by adding comments or agrees. In the first case, the contract is sent to the initiator for revision, in the second case it goes to the next stage and receives the status "Under agreement with the executers".
4. Approval of the document by the head of the executor's department. The performer is selected. In parallel for all performers the execution sub process is started.
5. After the execution of all participants, the result is collected.
6. Notification of managers about the execution.
7. Document registration. Assigning a number according to the classifier and the nomenclature of the organization's affairs.
8. Completion of the process.

At each stage, it is possible to download, print and return the document for revision.

## 4. Data security architecture development

Only a proven architecture is able to manage effective merging of services, ensure the manageability of the information system, and is able to evolve and resist new threats while maintaining properties such as high performance, simplicity and usability [1].

From a practical point of view, to ensure security, the following principles of building an IS architecture (Fig. 1) are most important:

1. Designing the IS based on the principles of open systems, adhering to recognized standards, using proven solutions, hierarchical organization of IS with a small number of entities at each level – all these contribute to transparency and good manageability of the IS;
2. Continuity of protection in space and time, inability to overcome protection tools, exclusion of a spontaneous or induced transition to an unsafe state – under any circumstances, including abnormal, the protection tool either fully fulfills its functions, or completely blocks access to the system or part of it;
3. Strengthening of the weakest link, minimization of access privileges, separation of functions of maintenance services and responsibilities of personnel [9]. It is assumed that roles and responsibilities are distributed in such a way that one person cannot disrupt a critical process for the organization or create a security breach through ignorance or the order of cybercriminals. With regard to the software and hardware levels, the principle of minimizing privileges implies that users and administrators are only assigned those access rights necessary for them to perform their official duties [10]. This allows one to reduce damage from accidental or deliberate incorrect actions of users and administrators;
4. Separation of defense, a variety of protective equipment, simplicity and controllability of the information system and its security system. The principle of separation of defense requires that we not rely on a single defense line, no matter how reliable it may seem. Physical protection should be followed by software and hardware, identification and authentication by access control, logging and auditing. Layered defense is able not only not to let the intruder through, but also in some cases to identify them by logging and auditing their details [6]. The principle of a variety of protective equipment implies the creation of defensive lines of different nature, so that a potential attacker is required to master various and, if possible, incompatible skills.

A thoughtful and ordered structure of software tools and databases, the topology of internal and external networks directly affects the achieved quality and security of the IS, as well as the complexity of their development. With strict adherence to the rules of structural design, it is much easier to achieve high quality and safety indicators, since the number of possible errors in implementing programs, equipment failures and other failures is reduced, their diagnostics and localization are simplified. In a well-structured system with clearly identified components (client, application server, resource server), the checkpoints are clearly distinguished, which solves the problem of proving the sufficiency of the applied protection means and ensuring the impossibility of circumventing these means by a potential intruder [5].

The following are considered as objects of vulnerability:

- Dynamic computational process of data processing, automated preparation of decisions and development of control actions;
- Object code of programs executed by computational means in the course of IS functioning;
- Data and information accumulated in databases;
- Information provided to consumers and to actuators.

The task is to identify the factors on which the listed threats depend, in the creation of methods and means to reduce their impact on IS security, as well as in the effective allocation of resources to ensure protection of equal strength to all negative influences.

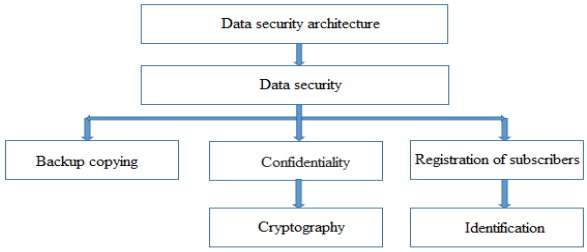


*Fig. 3. Data security architecture development*

## 5. Crash tolerance analytics

It should be emphasized that no matter how powerful security systems are, they cannot guarantee complete reliability of the software and hardware level tolerance to malfunctioning. In this section, we focus on the latter: the host crashes due to hardware related causes. We assume that the application server software is reliable and that the DBMS and archival systems are also reliable and do not crash. We focus on how to cope with crashes of front-end application servers that carry out the tasks of clients – both inside and outside the enterprise, by connecting to the DBMS [8].

The rationale for our starting set of reliability assumptions are two-fold: the DBMS is generally procured from high-quality vendors who offer their own reliability and maintenance guarantees and application server programs are typically developed using well-known design methodologies and are tested prior to deployment. What we cannot control are application server hardware faults that can develop as a result of deterioration over time and, when they lead to a host crash, any clients' work in progress is interrupted requiring those clients to repeat the document processing activities [7].

Recall that we already addressed scalability or load balancing concerns by having $H$ (> 1) servers in the front end and thereby limiting the average number of customers per application server host to a small value of $N/H$. This use of multiple application server hosts will also provide a level of crash tolerance as the customers connected to a crashed host can reconnect to one of the operative hosts and resume their work. However, these reconnecting customers will have to re-execute their entire work using the new hosts, as all the work they did in the crashed server will have been lost. This extra work can be substantial for $N/H$ customers. To see this extent of work loss, let us first model the operational behavior of application servers:

- A client connects to a host and instantiates an application server;
- The server fetches the required documents from the data tier and caches them locally at the host; this involves data transfer from the DBMS to the host;
- The client works on the cached documents for some time;
- The modified document versions are then uploaded to the data tier; this involves data transfer from the host to the DBMS.

Purely to motivate the challenges posed by host crashes, assume that a client's work time is constant and $W$ (>0) time units. Note that if the client works only in read-only mode, no document needs to be uploaded; we ignore these as edge cases for now.

If a host crashes just before a client caches the documents from the DBMS, no work is lost as no work has started; on the other hand, if the host crashes just before a client uploads the modified documents to the DBMS, all the work carried out so far is lost and that client will have to re-start from scratch on the reconnected host. We assume that when a host crashes, the wasted work per client connected to the crashed host is uniformly distributed on $(0,W)$; the expected amount of wasted work will therefore be $W/2$ per client. Since the average number of clients connected to a crashed host is $N/H$, the average total amount of wasted work will be $(N/H)(W/2)$. For example, if we let $N = 20$, $H = 2$, and $W = 10$ minutes, then the average total amount of wasted work that needs to be re-done amounts to 50 minutes. We make the following observations regarding service interruptions when host crashes are allowed:

1. Use of multiple hosts for scalability does not completely address the challenges posed by host crashes;
2. When a host crashes, the load on operational hosts increases: $N/H$ increases to $N/(H-1)$; and,
3. When $W$ is large, the amount of lost work to be repeated can be substantially large.

While 1 and 2 are inevitable, the challenge we will next address therefore will be to explore ways of minimizing the amount of lost work due to a host crash.

## 6. Conclusion

The developed information system is designed for the efficient operation of the administration (user, client) of the enterprise. The client application has the two possible types of connection to the enterprise information system: desktop client and web client. The desktop-client application enables connection to the information system on the working computers of the enterprise through the local network, with an appeal to the application server. Outside the enterprise, the user can work with the information system through web browser, as a web client, with an access to a web server. The developed multilevel architecture, Enterprise digitalization system. Document processing schemes, Document approval process, Data Security Architecture are the guarantor of the availability, reliability and security of the system.

## Acknowledgments

This research was funded by the Science Committee of the Ministry of Education and Science of the Republic of Kazakhstan (Grant #AP09259208)

## References

[1] Andersson J.: Enterprise Information Systems Management. Kungl Tekniska Högskolan, Stockholm, 2002 [https://www.diva-portal.org/smash/get/diva2:9165/FULLTEXT01.pdf].
[2] Balakayeva G. T. et al.: Using NoSQL for processing unstructured Big Data. News of the National Academy of sciences of the Republic of Kazakhstan 6(438), 2019, 12–21.
[3] Balakayeva G., Darkenbayev D.: The solution to the problem of processing Big Data using the example of assessing the solvency of borrowers. Journal of Theoretical and Applied Information Technology 98(13), 2020, 2659–2670.
[4] Duffy D.: Domain Architectures. Models and Architectures for UML Applications. Datasim Education BV, Amsterdam, Netherlands, 2004.
[5] Gill M.: Issues for consideration in mergers and takeovers from a regulatory perspective. BIS Review 60, 2000 [https://www.bis.org/review/r000721b.pdf].
[6] https://downloads.cloudsecurityalliance.org/assets/research/security-guidance/security-guidance-v4-FINAL.pdf
[7] https://essay.utwente.nl/59810/1/MA_thesis_J-W_van_Houwelingen.pdf
[8] https://resources.sei.cmu.edu/asset_files/WhitePaper/2006_019_001_52113.pdf
[9] https://www.imageapi.com/blog/digital-document-management/
[10] https://www.kreyonsystems.com/Blog/digitization-with-document-management/
[11] ISO 15704:2000. Industrial automation systems. Requirements for enterprise-reference architectures and methodologies.
[12] ISO 35.100. Open systems interconnection.
[13] ISO/IEC 2382:2015 Information technology, Vocabulary.
[14] ISO/IEC 42010:2011. System and software engineering – Architecture description, 2011.
[15] Katsaros G. et al.: A Multi-level Architecture for Collecting and Managing Monitoring Information in Cloud Environments. 1st International Conference on Cloud Computing and Services Science, Noordwijkerhout, 2011.
[16] Keith Stouffer K. et al.: Guide to Industrial Control Systems (ICS) Security. NIST Special Publication 800-82, 2015 [http://doi.org/10.6028/NIST.SP.800-82r2].
[17] Panarello A. et al.: Blockchain and IoT Integration: A Systematic Survey. Sensors 18, 2018, 2575 [http://doi.org/10.3390/s18082575].
[18] Panetto H. et al.: New Perspectives for the Future Interoperable Enterprise Systems. Computers in Industry 79, 2016, 47–63 [http://doi.org/10.1016/j.compind.2015.08.001].
[19] Sen J.: Security Privacy Issues in Cloud Computing Computing. [https://arxiv.org/ftp/arxiv/papers/1303/1303.4814.pdf].

**Prof. Gulnar Balakayeva**
e-mail: gulnardtsa@gmail.com

Doctor of Physical and Mathematical Sciences, Professor of the Department of Computer Science, Faculty of Information Technologies, Al-Farabi Kazakh National University, Almaty, Kazakhstan.
Research Interests: Development of big data processing systems, modeling of physical and chemical processes.

http://orcid.org/0000-0001-9440-2171

**Prof. Christofer Phillips**
e-mail: chris.phillips@newcastle.ac.uk

Ph.D., Professor: University of Newcastle upon Tyne, Newcastle, United Kingdom.

http://orcid.org/0000-0002-2470-1659

**Prof. Paul Ezhilchelvan**
e-mail: paul.ezhilchelvan@ncl.ac.uk

Ph.D., Professor: University of Newcastle upon Tyne, Newcastle, United Kingdom.

http://orcid.org/0000-0002-6190-5685

**Ph.D. Dauren Darkenbayev**
e-mail: dauren.kadyrovich@gmail.com

Ph.D., Associate Professor of the Department of Computer Science, Faculty of Information Technologies, Al-Farabi Kazakh National University, Almaty, Kazakhstan. Research Interests: Big data processing. Development of computer systems for the educational process.

http://orcid.org/0000-0002-6491-8043

**Ph.D. Yerlan Makashev**
e-mail: makashev.yerlan70@gmail.com

Candidate of Physical and Mathematical Sciences, Associate Professor of the Department of Computer Science, Faculty of Information Technologies, Al-Farabi Kazakh National University, Almaty, Kazakhstan. Research Interests:Modeling of physical and chemical processes, Development of computing systems.

http://orcid.org/0000-0003-1698-3614

**Ph.D. Kalamkas Nurlybayeva**
e-mail: kalamkas.nurlybayeva@gmail.com

Faculty of Information Technologies, Al-Farabi Kazakh National University, Almaty, Kazakhstan.

http://orcid.org/0000-0002-2069-2564

http://doi.org/10.35784/iapgos.3507

*received: 18.02.2023 | revised: 15.03.2023 | accepted: 25.03.2023 | available online: 31.03.2023*

# MODIFICATIONS OF EVANS PRICE EQUILIBRIUM MODEL

**Serhii Zabolotnii[1], Sergii Mogilei[2]**

[1]Cherkasy State Business-College, Cherkasy, Ukraine, [2]Rauf Ablyazov East European University, Cherkasy, Ukraine

***Abstract.*** *The paper regards the classical Evans price equilibrium model in the free product market in the aspect of regarding the opportunities for expanding (modifying) the model given that is aimed at perfecting the accuracy of its mathematical formulating. As an accuracy criterion, we have chosen a summary quadratic deviation of the calculated indices from the given ones. One of the approaches of modifying the basic Evans model is suggesting there is a linear dependence between price function and time as well as its first and second derivatives. In this case, the model will be described through differential equation of second order with constant coefficients, revealing some oscillatory process. Besides, it is worth regarding a non-linear (polynomial) dependence between demand, supply and price. The paper proposes mathematical formulating for the modified Evans models that have been approbated for real indices of exchange rates fluctuations. It also proves that increase of the differential and/or polynomial order of the given model allows its essential accuracy perfection. Besides, the influence of arbitrary restricting circumstances of the model on its accuracy is regarded. Each expanded Evans model is accompanied by mathematically formulated price and time dependence.*

**Keywords**: Evans model, market equilibrium, equilibrium price, differential equations, market modelling

## MODYFIKACJE MODELU RÓWNOWAGI CENOWEJ EVANSA

***Streszczenie.*** *W artykule rozpatrzono klasyczny model równowagi cenowej Evansa na wolnym rynku produktów w aspekcie możliwości rozbudowy (modyfikacji) danego modelu, zmierzającej do udoskonalenia dokładności jego matematycznego sformułowania. Jako kryterium dokładności wybraliśmy sumaryczne, kwadratowe odchylenie obliczonych indeksów od zadanych. Jednym z podejść do modyfikacji podstawowego modelu Evansa jest sugerowanie istnienia liniowej zależności między funkcją ceny a czasem oraz jej pierwszą i drugą pochodną. W takim przypadku model będzie opisany równaniem różnicowym drugiego rzędu o stałych współczynnikach, ujawniającym pewien proces oscylacyjny. Ponadto warto zwrócić uwagę na nieliniową (wielomianową) zależność pomiędzy popytem, podażą i ceną. W artykule zaproponowano matematyczne sformułowania dla zmodyfikowanych modeli Evansa, które zostały zaaprobowane dla rzeczywistych indeksów wahań kursów walutowych. Udowodniono, że zwiększenie rzędu różniczkowego i/lub wielomianowego danego modelu pozwala na jego zasadniczą poprawę dokładności. Ponadto rozważany jest wpływ dowolnych okoliczności ograniczających model na jego dokładność. Każdemu rozszerzonemu modelowi Evansa towarzyszy matematycznie sformułowana zależność cenowa i czasowa.*

**Słowa kluczowe**: model Evansa, równowaga rynkowa, cena równowagi, równania różnicowe, modelowanie rynku

## Introduction

Investigating market balance is quite important both for economy and other modern science and technology studies, mathematics, modeling etc. The sense of market balance is in establishing certain market conjuncture, that is, certain steady demand and supply interrelation, or market "scissors". Perceiving ways of establishing market balance enables realizing economy planning and forecasting tasks. These determine actuality of the investigation.

As there exists certain functional dependence of supply (descending function) and demand (ascending function) on the produce price, the cross point of curves for demand and supply corresponds to the balance point, the produce price in this point balancing supply and demand. The process of modeling market balance, or establishing equilibrium price, formulates the object of the investigation.

The Evans model [2] is one of the models for establishing equilibrium price. The model is described through differential equation of the first order with constant coefficients. The model admits that primary price for a product is known, and price function proper is related to time. Therefore, the solution of the problem in its present shape results in price change related to time.

Besides, the classical Evans model presumes linear relation of supply and demand to product price. Evidently, the presumption is quite simplified and the model itself requires additional investigation. For that reason, the Evans model for establishing equilibrium price is the subject of investigation. Eventually, the objective is to regard possibilities of expanding the Evans model for improving its accuracy.

The Evans model introduced nearly 100 years ago is now being scientifically criticized [5] for reason of staying efficient in a long perspective though it is not exact enough to describe the process of establishing equilibrium price for a short one. That is another ground to claim it should be additionally investigated and expanded (modified).

The market equilibrium problem stays quite a debate arising issue, numerous scientific approaches and methods being applied to its solution in as numerous works. For instance, the problem is regarded in [10] in which the equilibrium is investigated through labor market.

The issue of differentiating the produce in accordance with equilibrium prices in the manufacture (the model for the simultaneous search with partial depth) is given in [9]. In [4] the stock exchange activity and equilibrium price in the shares market are introduced. Functioning and unique features of the equilibrium price described for transportation networks with perfect competition are regarded in [7], and, under oligopoly, in [1]. Thus, the problem of finding the solution being as well unique promotes another aspect for investigating market balance models.

In [6] market balance model is given as a quasi-variation inequality that is solved through iteration method. The model regards convergence of the model only in a certain point of the neighborhood for the current market state, that is, not solving the whole of the supposed set. Here authors once again deal with a really sophisticated issue of convergence for balance models, and eventually, of presenting the equilibrium price.

Investigating market balance issues, methods of game theory are applied, one of those approaches described in [8]. The latter is employed for complex games, and implies working out an enlarged market abstraction as well as search for the balance in this abstraction, all that resulting in return to the initial market. However, in this investigation framework, to regard the Evans equilibrium price model, the game methods are not to be employed.

The market equilibrium-based approach is also applied to investigate Internet of things: therefore, in [3] paradigm of peripheral calculations is further evolved. Besides, this paper, together with many above mentioned, deals with important restrictions made for the necessary solutions. Indeed, it is worth regarding the related model in connection with corresponding ready-made restrictions for those real processes and phenomena described by the model.

Market balance is also regarded through methods of mathematic programing and operation exploring. Therefore, the analogue for market balance could be considered the balance of optimization criteria that is mathematically described as superposition of objective functions. The example of that

approach is given in [11] exploring economic activity for the subject of transportations market.

All above mentioned approaches seem quite promising for further exploration of market balance. However, they would hardly be employed to modify the Evans model for establishing equilibrium price and improving the model in its accuracy and relation to the real data of a certain market conjuncture. Therefore, this paper, to explore the model given, most frequently applies methods of differential equations and those of optimization. To make calculations and draw diagrams of the given functional correlations, appropriate program instruments will be applied.

## 1. Problem statement

The classical Evans model admits that demand $d = d(p) = d[p(t)]$ and supply $s = s(p) = s[p(t)]$ are linear functions for price $p = p(t)$. The main supposition of the given model implies that rate of price change that is its first derivative in time, is equal to the product of the difference between supply and demand multiplied by a coefficient $\gamma \in R$:

$$\frac{dp}{dt} = \gamma \cdot [d(p) - s(p)], p(0) = p_0 \tag{1}$$

where $p_0$ – is the initial price value for the moment of time $t = 0$.

Obviously, from the application point of view, supply and demand are more dependent on price. Although, whatever functions could be, describing similar dependencies, they can be presented as polynomial and of arbitrary order through polynomial approximation, for instance, through the Taylor series expansion.

Therefore, the following suggestion could be made:

$$d = D_m(p), s = S_n(p) \tag{2}$$

where $D_m(p)$, $S_n(p)$ are polynomials of $m$ and $n$ order correspondingly, $m, n \in N$.

Thus, the modified Evans model is obtained for establishing equilibrium price (1)-(2), which will be called polynomial.

Besides, it is easily demonstrated that classical Evans model is presented as a differential equation of the first order of the form:

$$b \cdot \frac{dp}{dt} + c \cdot p = d \tag{3}$$

where $b, c, d \in R$.

That is, according to (3), the left part of the equation is a linear combination of price function $p = p(t)$ and its first derivative.

Another approach to this model modification as (3) is a suggestion that there exists linear dependence between price function $p = p(t)$, and both its first and second derivatives in time:

$$a \cdot \frac{d^2p}{dt^2} + b \cdot \frac{dp}{dt} + c \cdot p = d \tag{4}$$

where $a \in R$.

The Evans model as (4) is further called the Evans differential model.

Basically, the right part of the equation (4) is a polynomial of *0* order. Supposing, the right part (4) contains a polynomial of derivative *t* with a degree higher than 0 obtain the Evans polynomial differential model, its mathematical formula given below.

Explore the above described models in more detail.

## 2. The Evans classical and differential models

The Evans classical model for establishing equilibrium price is quite much explored. Its solution as (3) is obtained as follows:

$$p(t) = U(t) \cdot V(T)$$

$$b \cdot U \cdot \frac{dV}{dt} + b \cdot V \cdot \frac{dU}{dt} + cUV = d$$

$$U \cdot \left(b \cdot \frac{dV}{dt} + c \cdot V\right) + b \cdot V \cdot \frac{dU}{dt} = d$$

$$b \cdot \frac{dV}{dt} + c \cdot V = 0$$

$$\frac{dV}{V} = -\frac{c \cdot dt}{b}$$

$$V = \exp\left(-\frac{c \cdot t}{b}\right)$$

$$\frac{dU}{dt} = \frac{d}{b} \cdot \exp\left(\frac{c \cdot t}{b}\right)$$

$$dU = \frac{d}{c} \cdot \exp\left(\frac{c \cdot t}{b}\right) d\left(\frac{c \cdot t}{b}\right)$$

$$U = \frac{d}{c} \cdot \exp\left(\frac{c \cdot t}{b}\right) + c_0, c_0 = const$$

$$p(t) = \left(\frac{d}{c} \cdot \exp\left(\frac{c \cdot t}{b}\right) + c_0\right) \cdot \exp\left(-\frac{c \cdot t}{b}\right) =$$

$$= \frac{d}{c} + c_0 \cdot \exp\left(-\frac{c \cdot t}{b}\right)$$

As $p(0) = p_0$, then:

$$\frac{d}{c} + c_0 = p_0$$

$$c_0 = p_0 - \frac{d}{c}$$

Eventually:

$$p(t) = \frac{d}{c} + \left(p_0 - \frac{d}{c}\right) \cdot \exp\left(-\frac{c \cdot t}{b}\right) \tag{5}$$

The Evans differential model as (4) is a non-homogeneous differential equation of second order, with constant factors. In such a statement and with the model's economic interpretation, the model given is analogous to the model of damped oscillations, therefore the discriminant of the characteristic equation (6) in the related homogenous differential equation should be negative:

$$a \cdot k^2 + b \cdot k + c \cdot p = 0 \tag{6}$$

$$D = b^2 - 4ac < 0$$

$$b \in (-2\sqrt{ac}; 2\sqrt{ac})$$

In this case, the roots of the characteristic equation:

$$k_{1,2} = \frac{-b \pm i\sqrt{-D}}{2a}, i = \sqrt{-1}$$

Correspondingly, real *Re*(*k*) and imaginary *Im*(*k*) parts of these roots:

$$Re(k) = \frac{-b}{2a}$$

$$Im(k) = \frac{\sqrt{-D}}{2a}$$

Then the solution of equation (4) will be:

$$p(t) = (c_1 \cdot cos(Im(k) \cdot t) + c_2 \cdot sin(Im(k) \cdot t)) \times$$
$$\times \exp(Re(k) \cdot t) - d/c \tag{7}$$

where $c_1, c_2 = const$.

Evidently, (7) proves, initial assumption $p(0) = p_0$ will not be sufficient for determining constants $c_1, c_2$. Therefore, additional initial statement is needed. The latter, for instance, could be the rate of price change (first derivative of $p(t)$ function for time $t$), or it could be price function proper in a certain moment of time $t$.

Further presume that factual values, both initial and final, of observations of price values are known:

$$p(0) = p_0; p(t_n) = p_n \tag{7a}$$

where $n$ is quantity of observations, $t_n \neq 0$ is an $n$ moment of time $t$.

Put (7a) in expression (7):

$$\begin{cases} p(0) = (c_1 \cdot cos0 + c_2 \cdot sin0) \cdot 1 - \frac{d}{c} = p_0, \\ p(t_n) = (c_1 \cdot cos(Im(k) \cdot t_n) + c_2 \cdot sin(Im(k) \cdot t_n)) \times \\ \times \exp(Re(k) \cdot t_n) - \frac{d}{c} = p_n. \end{cases}$$

$$\begin{cases} c_1 = p_0 + d/c, \\ (c_1 \cdot cos(Im(k) \cdot t_n) + c_2 \cdot sin(Im(k) \cdot t_n)) \cdot \exp(Re(k) \cdot t_n) = \\ = p_n + d/c. \end{cases}$$

$$\begin{cases} c_1 = p_0 + d/c, \\ c_2 \cdot sin(Im(k) \cdot t_n) = \frac{p_n + d/c}{\exp(Re(k) \cdot t_n)} - c_1 \cdot cos(Im(k) \cdot t_n). \end{cases}$$

$$\begin{cases} c_1 = p_0 + d/c, \\ c_2 = \frac{(p_n + d/c) \cdot \exp(-Re(k) \cdot t_n) - (p_0 + d/c) \cdot cos(Im(k) \cdot t_n)}{sin(Im(k) \cdot t_n)}. \end{cases}$$

Substituting $c_1, c_2$ into (7), obtain ultimate Evans differential model.

## 3. The Evans polynomial classical model

Similarly, to the main statement (1) of the Evans classical model, put it as follows:

$$\frac{dp}{dt} = \gamma \cdot [D_m(p) - S_n(p)], p(0) = p_0 \quad (8)$$

The right part of expression (8) is a polynomial of order $m$. For the expression, admit that $m = n$ and put it as:

$$T_n(p) = D_n(p) - S_n(p) \quad (9)$$

where $T_n(p)$ is a polynomial of order $n$.

It means that the Evans model put as (8)-(9) is the Evans polynomial classical model of order $n$.

Considering (8) and (9), put:

$$\frac{dp}{dt} = \gamma \cdot T_n(p)$$

or

$$\frac{dp}{T_n(p)} = \gamma \cdot dt \quad (10)$$

Suppose, $p_i, i = \overline{1,n}$ are roots (they generally differ) of polynomial $T_n(p)$. Then, the equation is like:

$$T_n(p) = \alpha \cdot \prod_{i=1}^{n}(p - p_i) \quad (11)$$

where $\alpha$ is higher polynomial coefficient $T_n(p)$.

Substitute (11) into expression (10):

$$\frac{dp}{\prod_{i=1}^{n}(p-p_i)} = \alpha\gamma \cdot dt \quad (12)$$

Apply the method of undetermined coefficients $A_i \in R$ to the left part of expression (12)

$$\frac{dp}{\prod_{i=1}^{n}(p-p_i)} = \sum_{i=1}^{n}\frac{A_i \cdot dp}{p-p_i} = \alpha\gamma \cdot dt \quad (13)$$

To better demonstrate the given model as (13), put $n = 2$. Obtain:

$$\frac{1}{(p-p_1)(p-p_2)}dp = \left(\frac{A_1}{p-p_1} + \frac{A_2}{p-p_2}\right)dp = \alpha\gamma \cdot dt \quad (14)$$

In (14) apply necessary transformations:

$$\frac{A_1}{p-p_1} + \frac{A_2}{p-p_2} = \frac{A_1p - A_1p_2 + A_2p - A_2p_1}{(p-p_1)(p-p_2)} =$$
$$= \frac{(A_1+A_2)\cdot p - (A_1p_2 + A_2p_1)}{(p-p_1)(p-p_2)} = \frac{1}{(p-p_1)(p-p_2)}.$$

Whereas:

$$\begin{cases} A_1 + A_2 = 0 \\ A_1p_2 + A_2p_1 = -1 \end{cases}$$

By the Cramer method:

$$\Delta = \begin{vmatrix} 1 & 1 \\ p_2 & p_1 \end{vmatrix} = p_1 - p_2$$

$$\Delta_1 = \begin{vmatrix} 0 & 1 \\ -1 & p_1 \end{vmatrix} = 1$$

$$\Delta_2 = \begin{vmatrix} 1 & 0 \\ p_2 & -1 \end{vmatrix} = -1$$

$$A_1 = \frac{\Delta_1}{\Delta} = \frac{1}{p_1 - p_2}$$

$$A_2 = \frac{\Delta_2}{\Delta} = \frac{-1}{p_1 - p_2}$$

Therefore, (14) is put as:

$$\left(\frac{1}{p-p_1} - \frac{1}{p-p_2}\right)dp = \alpha\gamma \cdot (p_1 - p_2) \cdot dt$$

$$\frac{d(p-p_1)}{p-p_1} - \frac{d(p-p_2)}{p-p_2} = \alpha\gamma \cdot (p_1 - p_2) \cdot dt$$

$$\ln|p-p_1| - \ln|p-p_2| = \alpha\gamma \cdot (p_1 - p_2) \cdot t +$$
$$+ \ln(\bar{c}), \bar{c} > 0$$

$$\left|\frac{p-p_1}{p-p_2}\right| = \bar{c} \cdot e^{\alpha\gamma\cdot(p_1-p_2)\cdot t}$$

As $p(0) = p_0$, then

$$\bar{c} = \left|\frac{p_0 - p_1}{p_0 - p_2}\right|$$

Let be $p_1 < p_2$.

Then with $p \in R\backslash[p_1; p_2]$, it comes to:

$$p - p_1 = \bar{c} \cdot e^{\alpha\gamma\cdot(p_1-p_2)\cdot t} \cdot (p - p_2)$$

$$p \cdot \left(1 - \bar{c} \cdot e^{\alpha\gamma\cdot(p_1-p_2)\cdot t}\right) = p_1 - \bar{c} \cdot e^{\alpha\gamma\cdot(p_1-p_2)\cdot t} \cdot p_2$$

$$p(t) = \frac{p_1 - \bar{c}\cdot e^{\alpha\gamma\cdot(p_1-p_2)\cdot t}\cdot p_2}{1 - \bar{c}\cdot e^{\alpha\gamma\cdot(p_1-p_2)\cdot t}} \quad (15)$$

And with $p \in (p_1; p_2)$:

$$p - p_1 = -\bar{c} \cdot e^{\alpha\gamma\cdot(p_1-p_2)\cdot t} \cdot (p - p_2)$$

$$p \cdot \left(1 + \bar{c} \cdot e^{\alpha\gamma\cdot(p_1-p_2)\cdot t}\right) = p_1 + \bar{c} \cdot e^{\alpha\gamma\cdot(p_1-p_2)\cdot t} \cdot p_2$$

$$p(t) = \frac{p_1 + \bar{c}\cdot e^{\alpha\gamma\cdot(p_1-p_2)\cdot t}\cdot p_2}{1 + \bar{c}\cdot e^{\alpha\gamma\cdot(p_1-p_2)\cdot t}} \quad (16)$$

Thus, the Evans polynomial classical model is obtained as (15)-(16).

The Evans polynomial differential model is generally put as:

$$a \cdot \frac{d^2p}{dt^2} + b \cdot \frac{dp}{dt} + c \cdot p = Q_w(t), \quad (17)$$

where $Q_w(t)$ is polynomial of order $w > 0$.

With characteristic equation (6), equation (17) is solved:

$$p(t) = (c_1 \cdot cos(Im(k) \cdot t) + c_2 \cdot sin(Im(k) \cdot t)) \times$$
$$\times \exp(Re(k) \cdot t) + \bar{Q}_w(t), \quad (18)$$

where $c_1, c_2 = const$; $\bar{Q}_w(t)$ is polynomial of order $w > 0$.

To calculate values of coefficients for polynomial $\bar{Q}_w(p)$, substitute it into expression (17) and apply the method of undetermined coefficients. Thus, obtain the Evans polynomial differential model as (17)-(18).

Compare the accuracy of the obtained Evans models.

## 4. Comparing the accuracy of different Evans models with the condition of known parameters

Reveal the notion of the condition of known parameters in the examples (3) and (4). Suppose, parameters *b*, *c*, *d* of these both models are known, or obtained from the previous calculations, whereas parameter *a* of model (4) is unknown. The latter will be named hyperparameter, and changing its value manage the comparative accuracy of model (4) related to model (3).

For practical demonstration of comparing the accuracy of the Evans model for establishing equilibrium price, apply the indices for currency rate of Ukrainian hryvna (UAH) in relation to the US dollar, according to the National Bank of Ukraine (NBU) (table 1).

*Table 1. Currency exchange rates for the pair UAH-USD (NBU data for the first half of 2021) [12]*

| Days | Months | | | | | |
|---|---|---|---|---|---|---|
| | January | February | March | April | May | June |
| 1 | 28.2746 | 28.1324 | 27.9456 | 27.8226 | 27.733 | 27.4674 |
| 2 | 28.431 | 28.0603 | 28.0007 | 27.8324 | 27.7339 | 27.4381 |
| 3 | 28.4028 | 28.0589 | 27.933 | 27.9555 | 27.7205 | 27.3449 |
| 4 | 28.2847 | 27.995 | 27.8477 | 27.939 | 27.7641 | 27.34 |
| 5 | 28.2038 | 27.8885 | 27.7564 | 27.8384 | 27.6744 | 27.2914 |
| 6 | 28.046 | 27.7711 | 27.7091 | 27.8923 | 27.6318 | 27.1923 |
| 7 | 27.9705 | 27.6651 | 27.7431 | 27.9768 | 27.6273 | 27.1764 |
| 8 | 28.0609 | 27.6426 | 27.7016 | 27.9094 | 27.6142 | 27.0906 |
| 9 | 28.0524 | 27.7665 | 27.7486 | 27.9335 | 27.555 | 27.1068 |
| 10 | 28.0524 | 27.8384 | 27.7305 | 28.0156 | 27.4368 | 27.0404 |
| 11 | 28.1926 | 27.844 | 27.6434 | 27.9765 | 27.4166 | 26.9957 |
| 12 | 28.1544 | 27.9671 | 27.6525 | 27.9592 | 27.4665 | 26.9258 |
| 13 | 28.2035 | 27.8304 | 27.6978 | 27.9783 | 27.4572 | 27.0275 |
| 14 | 28.2561 | 27.9038 | 27.6828 | 28.0087 | 27.4281 | 27.1712 |
| 15 | 28.1648 | 27.8461 | 27.7184 | 28.0096 | 27.4553 | 27.1935 |
| 16 | 28.1665 | 27.8468 | 27.6871 | 28.0576 | 27.5461 | 27.305 |
| 17 | 28.1524 | 27.9304 | 27.7295 | 28.0642 | 27.526 | 27.2737 |
| 18 | 28.1652 | 27.8976 | 27.8706 | 27.9014 | 27.5004 | 27.4589 |
| 19 | 28.1929 | 27.9492 | 27.9698 | 27.8558 | | 27.3964 |
| 20 | | 27.9301 | 27.9698 | 27.7715 | | 27.1763 |
| 21 | | | 27.9679 | 27.7867 | | |
| 22 | | | 27.9694 | 27.75 | | |
| 23 | | | 27.8852 | | | |

First, apply classical Evans model (3). Through least squares method (LSM) calculate values of parameters *b*, *c*, *d* for this model and draw diagrams of factual and calculated values (Fig. 1).

In the given case $b = 1.1296$, $c = 0.0596$, $d = 1.6508$, and model (3) itself looks as:

$$1.1296 \cdot \frac{dp}{dt} + 0.0596 \cdot p = 1.6508.$$

Its aggregate quadratic deviation is 8.4789.

Then model (4) for same data and according to condition of known parameters will be as:

$$a \cdot \frac{d^2p}{dt^2} + 1.1296 \cdot \frac{dp}{dt} + 0.0596 \cdot p = 1.6508,$$

where $a \in R$ is hyperparametre.

To calculate *a*, apply LSM to the appropriate model (4):

$$68119.62351 \cdot \frac{d^2p}{dt^2} + 1.1296 \cdot \frac{dp}{dt} + 0.0596 \cdot p = 1.6508$$

that is, $a = 68119.62351$.

In this case, aggregate quadratic deviation will be 4.0413. The diagrams of factual and calculated values of the given model are given in Fig. 2.

Therefore, the index of aggregate quadratic deviation, with known parameters, for differential Evans model (4) is smaller than the corresponding index for the classical model of establishing equilibrium value (3). That demonstrates better accuracy of model (4) related to model (3).

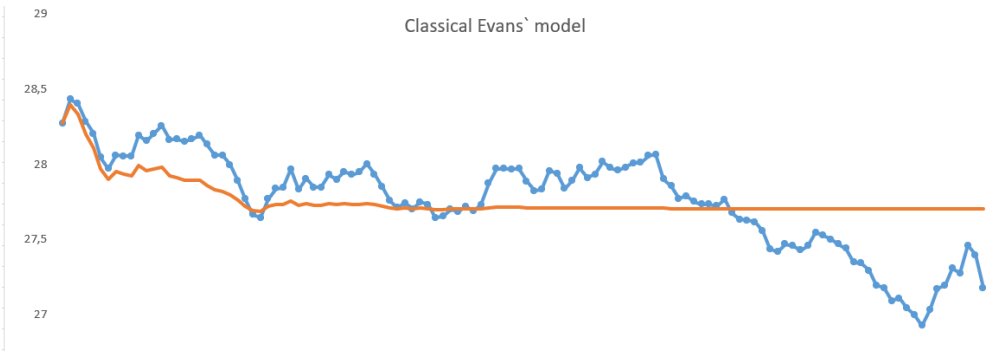


*Fig. 1. Factual and calculated values for classical Evans model*

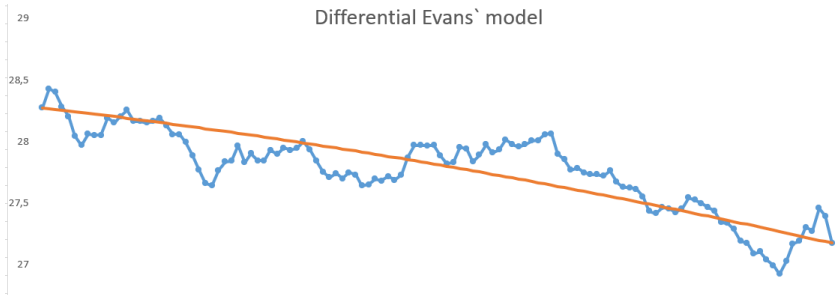


*Fig. 2. Factual and calculated values for differential Evans model with known parameters*

## 5. Comparing the accuracy of different Evans models with unknown parameters

Condition of unknown parameters means that parameters *a*, *b*, *c*, *d* of both models (3) and (4) are unknown and they basically all are hyperparameters. In this case, each of these models is built separately, then to compare their accuracy.

For model (3) in this case nothing matters and previously obtained results stay unchanged. On the contrary, model (4) now is built according to similar principle, that of model (3).

To calculate values *a*, *b*, *c*, *d* apply LSM to the related model. Obtain model (4) as:

$$79.35184 \cdot \frac{d^2p}{dt^2} - 0.7389 \cdot \frac{dp}{dt} + 0.5405 \cdot p = -15.0491$$

Diagrams for factual and calculated values for the given model are in Fig. 3.

However, in this case aggregate quadratic deviation will be 14.3321. That is, the accuracy of model (4) with unknown hyperparameters is lower than the accuracy of both classical and differential Evans models with known parameters. That implies the need for improving the model.

Turn to differential Evans model as (7). Now, assume that all its parameters are hyperparameters, without any numerical restrictions, either limiting, for the initial and final values. Apply LSM to the given model. Obtain:

$$p(t) = (27.2783 \cdot \cos(0.00087 \cdot t) + \\ +0.000001 \cdot \sin(0{,}00087 \cdot t)) \cdot \exp(-0{,}000242 \cdot t) + \\ +26.2753/28.275$$

Diagrams of factual and calculated values of the given model are in Fig. 4.

In the given case, aggregate quadratic deviation will be only 3.8334, that is the best value among all mentioned models. That is the ground to assume that differential Evans model is most accurate among all similar models of establishing equilibrium price, with unknown parameters and without limiting restrictions.

Regard polynomial Evans model as (15)-(16). As roots $p_1$, $p_2$ basically depend on the accuracy of creating supply and demand functions, they are not to be included into hyperparameters of the model. Instead, put $p_1, p_2$ as equal to minimal and maximum values for selected factual price indices. In this case, condition $p \in (p_1; p_2)$ will be realized, so polynomial Evans model will be as (16).

Besides, with $p_0, p_1, p_2$, it is possible to state $\bar{c}$. Therefore, hyperparameters of the model will only be $\alpha, \gamma$. Calculate them applying LSM.

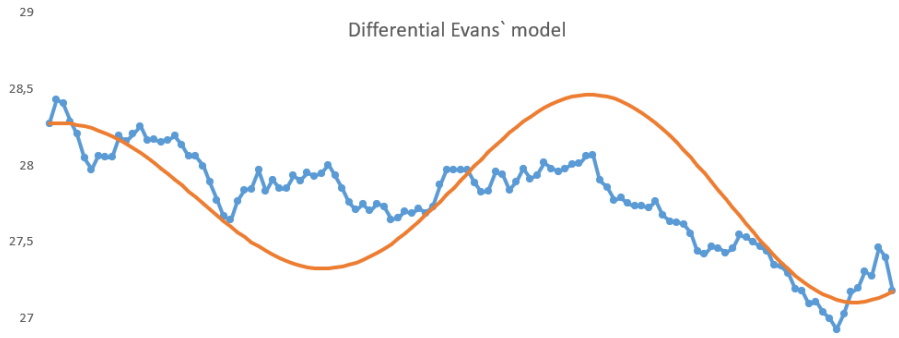


*Fig. 3. Factual and calculated values of differential Evans model with unknown parameters*

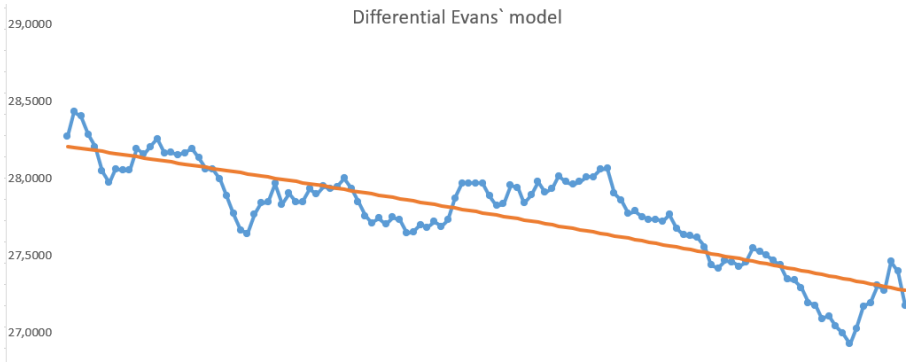


*Fig. 4. Factual and calculated values for differential Evans model with unknown parameters and without limiting restrictions*

Obtain $\alpha = 0.09675, \gamma = 0.19352$. The Evans model will be as follows:

$$p(t) = \frac{26.9258 + 8.624 \cdot e^{0.09675 \cdot 0.19352 \cdot 1.5052 \cdot t} \cdot 28.431}{1 + 8.624 \cdot e^{0.09675 \cdot 0.19352 \cdot 1.5052 \cdot t}}$$

Aggregate quadratic deviation in the given case will be 4.59736. Diagram of the model is given in Fig. 5.

During approbation of polynomial differential Evans model (17)-(18) its parameters will be presented with $a, b, c_1, c_2, Im(k)$, and also the coefficients of polynomial $\bar{Q}_w(t)$ admitting that $w = 1$.

Minimizing aggregated quadratic deviation, obtain hyperparameters:

$a = 0.56;\ b = 1.62;\ c_1 = 0.334, c_2 = 1.583, Im(k) \approx 0$

Besides:

$$\bar{Q}_w(t) = -0.0073 \cdot t + 28.2$$

Also, $Re(k) = -1.441$, aggregated quadratic deviation of the model is 3.99841 – graphically – Fig. 6.

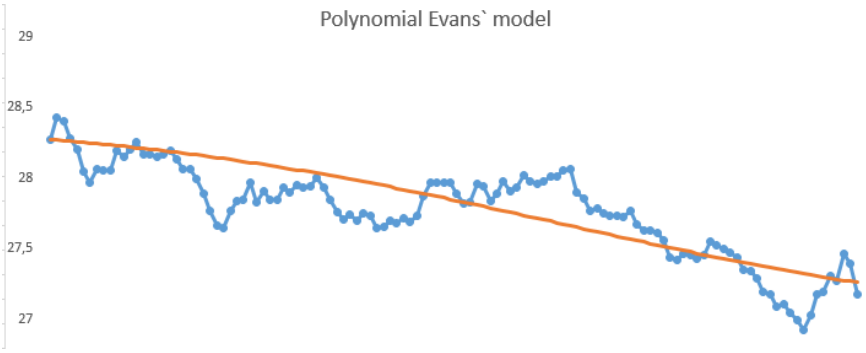


*Fig. 5. Factual and calculated values of polynomial classical Evans model*

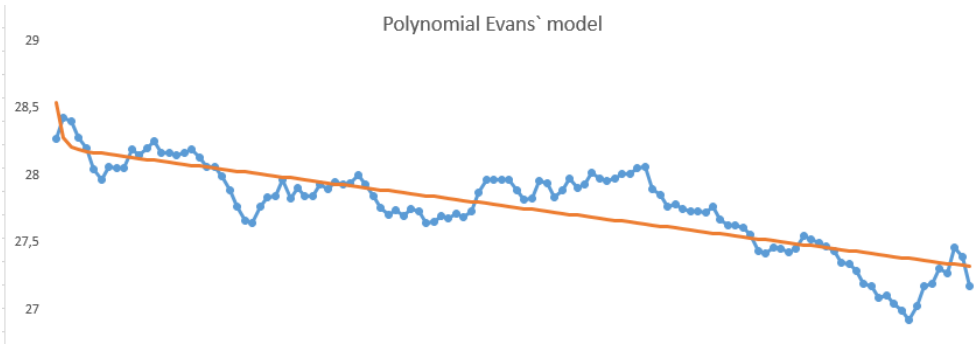


*Fig. 6. Factual and calculated values of polynomial differential Evans model*

## 6. Discussion

Make accuracy gradation, 1 standing for the most accurate model etc., for all models, in table 2.

Obviously, those models which are laid minimum of restrictions, are more accurate as to those that assume restrictions. However, it does not at all mean that, with creating this or that Evans model, the restrictions could be utterly rejected. Analyzing from economic or mathematical view, certain additional conditions related to the model can be either needed or desired. Therefore, while rejecting those conditions, the model can become one that vaguely describes real process or phenomenon it is expected to reproduce. In this case, the accuracy of the model is seen as an arbitrary criterion, as the model itself basically loses its primary purpose.

*Table 2. Accuracy gradation of Evans models*

| Name of the model | Aggregate quadratic deviation | Gradation number |
|---|---|---|
| Classical | 8.4789 | 5 |
| Differential with known parameters | 4.0413 | 3 |
| Differential with unknown parameters and limiting restrictions | 14.3321 | 6 |
| Differential with unknown parameters and without limiting restrictions | 3.8334 | 1 |
| Polynomial classical | 4.59736 | 4 |
| Polynomial differential | 3.99841 | 2 |

Therefore, the conclusion is that constructing Evans models of establishing equilibrium price it is worth looking for a balance between the accuracy of the model and those restrictions laid upon it.

The paper generally applies 2 main approaches, differential and polynomial, to modify classical Evans model. Evidently, other new or combined similar approaches can be proposed, together with criteria of the model's accuracy and perfection.

In addition, obtained solutions for each model are unique. It is evident that though the state of market equilibrium is theoretically unique numerical methods to calculate hyperparameters cannot be applied uniquely. It means each case produces more than one set of hyperparameters of the model. Basically, the fewer parameters the model possesses, the fewer sets of its values can be obtained.

## 7. Conclusions

The problem of market balance and modeling the establishing of equilibrium price at the market of products is a subject of scientific interest for scholar studies and applied specialties in many branches. The problem is regarded by both mathematics and economists, as well as by financial experts, investigators in modeling, computing and informational technology. There are quite many market balance models and also methods and ways of their description. In these studies, both scientists and practical workers besides applying popular approaches most regard essential restrictions of the models, and those are related to their applied character.

This study analyzes possible ways of modifying one of classical market balance models that is the Evans model. That one was essentially expanded and principal models were created to establish equilibrium price, those similar to the Evans model: differential, polynomial and differential polynomial. To this effect, the investigation applied method of increasing order for those differential equations relating to a model. In addition, the paper regards the problem analyzes the restrictions laid upon the model. Therefore, the created models were made mostly accurate according to the criterion of minimized aggregate quadratic deviation.

Obtained results allow admitting the highly promising approaches applied in the paper. New Evans models of increased orders were exposed to demonstrate higher accuracy in establishing market equilibrium price. Further studies are supposed to concentrate on creating more accurate functional relations stated between supply and demand, and product price. That will help in specifying the statement of the related Evans model. Another way to create specified models of equilibrium price is their approbation for real data, hitherto there exists the ability to calculate the related values of hyperparameters of the model.

## References


[1] Almeida Prado F. P., Blavatskyy P.: Existence and uniqueness of price equilibrium in oligopoly model with power demand. Mathematical Social Sciences 111, 2021, 1–10 [http://doi.org/10.1016/j.mathsocsci.2020.12.004].

[2] Dilenko V. O., Tarakanov N. L.: Mathematical Modeling of the Equilibrium Price Formation Taking into Account the Logistic Factor. Business Inform 7, 2020, 125–130 [http://doi.org/10.32983/2222-4459-2020-7-125-130].

[3] Duong Tung Nguyen et al.: Price-Based Resource Allocation for Edge Computing: A Market Equilibrium Approach. IEEE Transactions on Cloud Computing 9(1), 2021, 302–317 [http://doi.org/10.1109/TCC.2018.2844379].

[4] Fujii M., Takahashi A.: Equilibrium Price Formation with a Major Player and its Mean Field Limit. ESAIM: Control, Optimization and Calculus of Variations 28, 2022, 21 [http://doi.org/10.1051/cocv/2022015].

[5] Ji-Huan He et al.: Evans model for dynamic economics revised. AIMS Mathematics 6(9), 2021, 9194–9206 [http://doi.org/10.3934/math.2021534].

[6] Konnov I.: Variational Inequality Type Formulations of General Market Equilibrium Problems with Local Information. Journal of Optimization Theory and Applications 188(2), 2021, 332–355 [http://doi.org/10.1007/s10957-020-01777-9].

[7] Krebsab V., Schmidt M.: Uniqueness of market equilibria on networks with transport costs. Operations Research Perspectives 5, 2018, 169–173 [http://doi.org/10.1016/j.orp.2018.05.002].

[8] Kroer C. et al.: Computing Large Market Equilibria Using Abstractions. Operations Research 70(1), 2022, 329–351 [http://doi.org/10.1287/opre.2021.2163].

[9] Lin Liu, X. Henry Wang: Product differentiation and equilibrium price with partial product search. Economics Letters 205, 2021 [http://doi.org/10.1016/j.econlet.2021.109932].

[10] Llull J.: Immigration, Wages, and Education: A Labour Market Equilibrium Structural Model. The Review of Economic Studies 85(3), 2018, 1852–1896 [http://doi.org/10.1093/restud/rdx053].

[11] Przystupa K. et al.: Constructing Reference Plans of Two-Criteria Multimodal Transport Problem. Transport and Telecommunication 22(2), 2021, 129–140 [http://doi.org/10.2478/ttj-2021-0010].

[12] https://bank.gov.ua/ua/markets/exchangerate-chart?cn%5B%5D=USD (available: 05.01.2023).



**D.Sc. Serhii Zabolotnii**
e-mail: zabolotniua@gmail.com


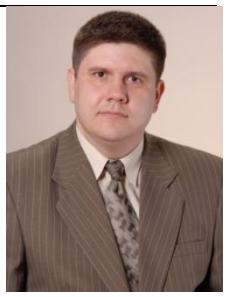

Serhii Zabolotnii was born in 1973 in Cherkasy, Ukraine. In 1995 he graduated the Department of informational technologies of Cherkasy State Technological University. Doctor of Technical Sciences (2015).
Job: professor of the Department of Computer Engineering and Informational Technologies in Cherkasy State Business-College. Scientific interests: statistical data processing, computer modelling.
Author/co-author of more than 150 publications, 1 monography and 7 patents.


http://orcid.org/0000-0003-0242-2234

**Ph.D. Sergii Mogilei**
e-mail: sergiymogiley@gmail.com


Sergii Mogilei was born in 1983 in Cherkasy, Ukraine. He works as a tutor in Rauf Ablyazov East European University (Cherkasy). Philosophy Doctor in Computer Science (2022).
His main scientific interests include mathematical and computer modelling, business analysis, mathematical programming, decision making theory, ML and AI.


http://orcid.org/0000-0002-9296-6827

http://doi.org/10.35784/iapgos.3496

*received: 13.02.2023 | revised: 13.03.2023 | accepted: 15.03.2023 | available online: 31.03.2023*

# A COMPARATIVE STUDY OF VARIOUS MODELS OF EQUIVALENT PLASTIC STRAIN TO FRACTURE

**Volodymyr Mykhalevych[1], Yurii Dobraniuk[1], Victor Matviichuk[2], Volodymyr Kraievskyi[1], Oksana Tiutiunnyk[1], Saule Smailova[3], Ainur Kozbakova[4]**

[1]Vinnytsia National Technical University, Vinnytsia, Ukraine, [2]Vinnytsia National Agrarian University, Vinnytsia, Ukraine, [3]D. Serikbayev East Kazakhstan Technical University, Ust-Kamenogorsk, Kazakhstan, [4] Almaty Technological University, Institute of Information and Computational Technologies CS MHES RK, Almaty, Kazakhstan

***Abstract**. For more then half a centre just the same approach to the simulation of the ductile crack formation was developed independently by the scientific communities of foreign and native researchers. The importance at these studies drastically increased. A set of the characteristics, according to which it is recommendly to perform the detail comparison of the existing fracture models is developed. The examples of the analysis of a number of the most popular models by means of obtaining and study their analytical expressions regarding the conditions of the plane state are given. The generalized relations of the know models and a number of separate relations are obtained.*

**Keywords:** ductile fracture criteria, fracture graph, equivalent plastic strain to fracture, stress triaxiality, plane strain

## BADANIE PORÓWNAWCZE RÓŻNYCH MODELI RÓWNOWAŻNEGO ODKSZTAŁCENIA PLASTYCZNEGO DO PĘKANIA

***Streszczenie**. Od ponad pół wieku to samo podejście do modelowania uszkodzeń podczas odkształceń plastycznych jest opracowywane niezależnie przez zespoły naukowe złożone z naukowców zagranicznych i krajowych. W ostatnich dziesięcioleciach znaczenie tych badań dramatycznie wzrosło. Opracowano zestaw cech, zgodnie z którymi proponuje się przeprowadzenie szczegółowego porównania istniejących modeli zniszczenia. Podano przykłady analizy szeregu najpopularniejszych modeli poprzez uzyskanie i badanie ich wyrażeń analitycznych dla warunków płaskiego stanu naprężenia. Otrzymano uogólnione wskaźniki znanych modeli oraz szereg wskaźników indywidualnych.*

**Słowa kluczowe**: kryteria powstawania pęknięć ciągliwych, wykres pękania, równoważne odkształcenie plastyczne do pękania, trójosiowość naprężeń, naprężenie płaskie

## Introduction

In [1, 6, 8, 11, 12, 20, 23, 27, 28] ductile crack formation theory is constructed. In contrast to the approach [31, 33, 36], devoted to the study of crack growth, the approach considered in this paper is based on the models of summation of continuous material damage. In [20] fracture model, the base of the model being linear damage hypothesis and a notion of the fracture diagram which gives the equivalent plastic strain to fracture as a function of the stress state, is suggested.

In [12, 28] a fracture model, based on nonlinear damage hypothesis , is developed. Approximation of the fracture diagram is proposed. The technique of studying the equivalent plastic strain to fracture on conditions of common torsion and tension of the cylindrical samples, according to various trajectories of the plastic strain dependence on the stress triaxiality, is suggested.

Tensor – linear model of the initially isotropic body is developed in [11]. Generalization of the given theory for the case the initial anisotropy of the equivalent plastic strain to fracture is given in [26], and for the case of non-linear dependence between the increments of the damage and deformation tensors is presented in [27]. In [23] on the base of the tensor–nonlinear model the effects of change of the equivalent plastic strain to fracture are determined analytically and proved experimentally at two-stage deformation, which are not within the frame of the tensor–linear model. The tensor–nonlinear model, which represents the healing of damages, applying for a hot-forming method, is developed and investigation in [27]. On the base of this model in [21], modes were determined, at which the material transforms into the super plasticity state, and the optimization problem is considered. The formulation of a new problem within the framework of this approach and interesting results of its solution were obtained in [24].

One of the key problems of the phenomenological theory of ductile crack formation is the analytical presentation of the dependence of the equivalent plastic strain to fracture on the invariants of the stress and strain states.

The studies of the foreign researchers are devoted to the solution of this problem [3, 4, 5, 9, 10, 29, 32], were published approximately at the same historic period. Judging by the published materials, these directions were developing independently from each other. Therefore, it is advisable to conduct a comparative study of these results. It should be noted, that the popularity of the given foreign researches reached a high level and continues to grow, as it is seen from our studies, presented in table 1 and diagrams in Fig 1. In our opinion, certain numerical data of this popularity could be considered as an indirect index of the relevance of the corresponding studies.

In any of the modern studies [7, 19, 22, 34, 35], an attempt is made to draw at least a fragmentary comparisons of the ductile crack formation theories. The comparison results shows that the scientific community does not completely realize that these research are referred to the same phenomenological approach to the construction of the limit state theory, general statements of which are proposed in [18] and specified in [27].

The lack of mutual references in the above-mentioned publications disorients the scientific community, that uses fracture models. Many researchers have a distorted notion regarding the above-mentioned scientific directions fracture simulation, as those, based on basically different concepts. However, a similar situation is not natural and slows down the intensity of the process of obtaining new results in the limit states theory of the materials.

*Table 1. Number of citations of the papers scientometric bases Google Schoolar, Web of Science and Scopus*

| Reference links to the paper from the list of references | Number of citations Google Schoolar | Number of citations Web of Science | | | Number of citations Scopus | | |
|---|---|---|---|---|---|---|---|
| | | Totally | In 2018 | Percentage of citations in 2018, % | Totally | In 2018 | Percentage of citations in 2018, % |
| [32] | 4288 | 2528 | - | - | 2904 | - | - |
| [10] | 1649 | 793 | - | - | - | - | - |
| [2] | 831 | 497 | 91 | 18 | 584 | 93 | 16 |
| [4] | 1169 | 700 | 108 | 15 | 829 | 118 | 14 |

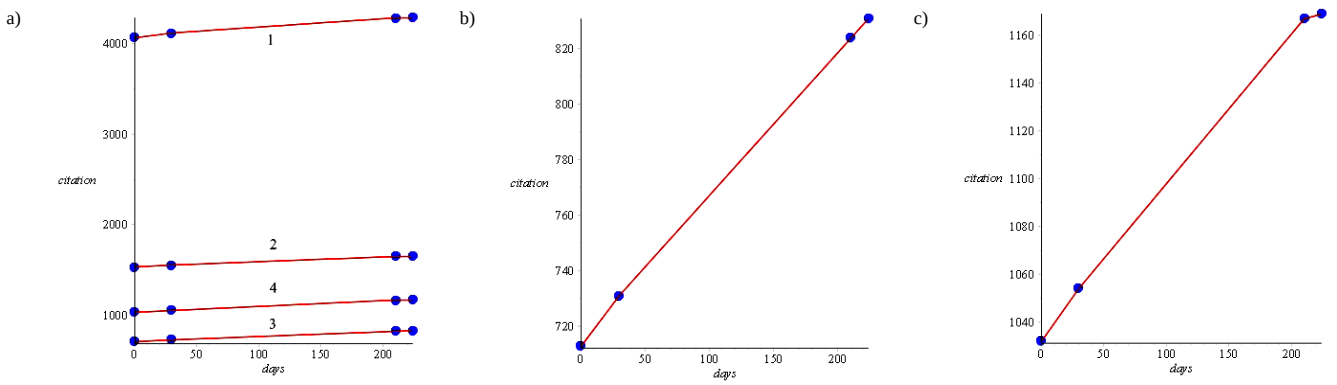


*Fig. 1. Results of the publication citation according to scientometric bases: a) Google schoolar: curves 1 – 4 are constructed on the base of the relations [2, 4, 10, 32]; b), c) Scopus: on the base of the relations [2, 4], correspondingly*

## 1. Aim of the research

The aim of the paper is to develop and substantiate of the classification characteristics, according to which the comparative study of the fracture models can be performed and carry out the corresponding analysis of a number of the most popular models, suggested both by foreign and native scientists.

## 2. Modeling

In foreign studies fracture models are mainly suggested in the form of the integral models, these models fake into consideration the impact on limit values of the equivalent plastic strain to fracture the change of the stress state during the deformation. In such form these models are shown in table 2.

An important characteristic of any model is the number of the parameters, to be determined on the base of the experimental data. Experiments, aimed at the determined on the equivalent plastic strain to fracture in case of different stress states are rather labor intensive and expensive. Thus, the desire to obtain models with an as small number of parameters as possible (one-, two-, three parametric) is quite reasonable.

Depending on the stress-state, when limit equivalent plastic strain to fracture is experimentally determined, the general model obtains the separate form. Corresponding relations are given in table 2.

The approach to the considered fracture simulation is based on the notion of the surface of limit equivalent plastic strain to fracture $\bar{\varepsilon}_{fs}$ depending on the indices, characterizing the no-changeable during the study of one sample stress state of the material. A greater part of the experimental data is obtained on the condition of the plane stress. In this case, the surface of the limit equivalent plastic strain to fracture is converted into the curve

$$\bar{\varepsilon}_{fs} = \bar{\varepsilon}_{fs}(\eta), \ -2 \le \eta \le 2 \tag{1}$$

where the stress triaxiality $\eta$

$$\eta = \frac{3 \cdot \sigma_m}{\bar{\sigma}} \tag{2}$$

$\sigma_m$, $\bar{\sigma}$ – mean stress and equivalent stress (von Mises) respectively.

In different studies the indices of the type (2) are used with different numerical coefficients, it is not essential. All the models, shown in table 2, we converted into (1) and accumulated in table 3. Other known analytical relations are also given in this table.

*Table 2. Limit state models*

| Limit state model's name | | Model | |
|---|---|---|---|
| Cockcroft and Latham–Oh crack formation criterion | Mathematical model in general form [4, 10, 29] | $\int_0^{\bar{\varepsilon}_f} \frac{\langle \sigma_1 \rangle}{\bar{\sigma}} \cdot d\bar{\varepsilon} = C$ | (3) |
| | Determination of the model parameter by the results of the equivalent plastic strain to fracture in shear | $\int_0^{\bar{\varepsilon}_f} \frac{\langle \sigma_1 \rangle}{\bar{\sigma}} \cdot d\bar{\varepsilon} = \varepsilon_k^*$ | (4) |
| | Determination of the model parameter by the results of the equivalent plastic strain to fracture in tension | $\int_0^{\bar{\varepsilon}_f} \frac{\langle \sigma_1 \rangle}{\bar{\sigma}} \cdot d\bar{\varepsilon} = \varepsilon_p^*$ | (5) |
| | Determination of the model parameter by the results of the equivalent plastic strain to fracture in equibiaxial tension | $\int_0^{\bar{\varepsilon}_f} \frac{\langle \sigma_1 \rangle}{\bar{\sigma}} \cdot d\bar{\varepsilon} = \bar{\varepsilon}_{fs}(2)$ | (6) |
| | Determination of the model parameter by the results of the equivalent plastic strain to fracture in nonequibiaxial tension | $\int_0^{\bar{\varepsilon}_f} \frac{\langle \sigma_1 \rangle}{\bar{\sigma}} \cdot d\bar{\varepsilon} = \bar{\varepsilon}_{fs}(1,5)$ | (7) |
| Hydrostatic stress criterion | | $\int_0^{\bar{\varepsilon}_f} \frac{\sigma_m}{\bar{\sigma}} \cdot d\bar{\varepsilon} = C$ | (8) |
| Clift criterion [9] | | $\int_0^{\bar{\varepsilon}_f} \bar{\sigma} \cdot d\bar{\varepsilon} = C$ | (9) |

*Table 2 (continuation). Limit state models*

| | Limit state model's name | Model | |
|---|---|---|---|
| Rice-Tracey (high stress triaxiality approximation) | Mathematical model in general form [32] | $\int_0^{\bar{\varepsilon}_f} \exp\left(\frac{\eta}{2}\right) \cdot d\bar{\varepsilon} = C$ | (10) |
| | Determination of the model parameter by the results of the equivalent plastic strain to fracture in compression | $\int_0^{\bar{\varepsilon}_f} \exp\left(\frac{\eta}{2}\right) \cdot d\bar{\varepsilon} = \varepsilon_c^*$ | (11) |
| | Determination of the model parameter by the results of the equivalent plastic strain to fracture in shear | $\int_0^{\bar{\varepsilon}_f} \exp\left(\frac{\eta}{2}\right) \cdot d\bar{\varepsilon} = \varepsilon_k^*$ | (12) |
| | Determination of the model parameter by the results of the equivalent plastic strain to fracture in tension | $\int_0^{\bar{\varepsilon}_f} \exp\left(\frac{\eta}{2}\right) \cdot d\bar{\varepsilon} = \varepsilon_p^*$ | (13) |
| | Determination of the model parameter by the results of the equivalent plastic strain to fracture in equibiaxial compression | $\int_0^{\bar{\varepsilon}_f} \exp\left(\frac{\eta}{2}\right) \cdot d\bar{\varepsilon} = \bar{\varepsilon}_{fs}(-2)$ | (14) |
| | Determination of the model parameter by the results of the equivalent plastic strain to fracture in nonequibiaxial compression | $\int_0^{\bar{\varepsilon}_f} \exp\left(\frac{\eta}{2}\right) \cdot d\bar{\varepsilon} = \bar{\varepsilon}_{fs}\left(-\frac{3}{2}\right)$ | (15) |
| | Determination of the model parameter by the results of the equivalent plastic strain to fracture in equibiaxial tension | $\int_0^{\bar{\varepsilon}_f} \exp\left(\frac{\eta}{2}\right) \cdot d\bar{\varepsilon} = \bar{\varepsilon}_{fs}(2)$ | (16) |
| | Determination of the model parameter by the results of the equivalent plastic strain to fracture in nonequibiaxial tension | $\int_0^{\bar{\varepsilon}_f} \exp\left(\frac{\eta}{2}\right) \cdot d\bar{\varepsilon} = \bar{\varepsilon}_{fs}\left(\frac{3}{2}\right)$ | (17) |

*Table 3. Limit state models of the material relatively the stress triaxiality index*

| | Models of the equivalent plastic strain to fracture in the plane stress condition | |
|---|---|---|
| (3) | $\bar{\varepsilon}_{fs}(\eta) = \frac{C}{\eta + 2 \cdot \cos\left[\frac{1}{3} \cdot \arccos\left(0,5 \cdot \eta \cdot \left(3 - \eta^2\right)\right)\right]}, \quad -1 < \eta \le 2$ | (18) |
| (4) | $\bar{\varepsilon}_{fs}(\eta) = \frac{\sqrt{3} \cdot \varepsilon_k^*}{\eta + 2 \cdot \cos\left[\frac{1}{3} \cdot \arccos\left(0,5 \cdot \eta \cdot \left(3 - \eta^2\right)\right)\right]}, \quad -1 < \eta \le 2$ | (19) |
| (5) | $\bar{\varepsilon}_{fs}(\eta) = \frac{3 \cdot \varepsilon_p^*}{\eta + 2 \cdot \cos\left[\frac{1}{3} \cdot \arccos\left(0,5 \cdot \eta \cdot \left(3 - \eta^2\right)\right)\right]}, \quad -1 < \eta \le 2$ | (20) |
| (6) | $\bar{\varepsilon}_{fs}(\eta) = \frac{3 \cdot \bar{\varepsilon}_{fs}(2)}{\eta + 2 \cdot \cos\left[\frac{1}{3} \cdot \arccos\left(0,5 \cdot \eta \cdot \left(3 - \eta^2\right)\right)\right]}, \quad -1 < \eta \le 2$ | (21) |
| (7) | $\bar{\varepsilon}_{fs}(\eta) = \frac{2 \cdot \sqrt{3} \cdot \bar{\varepsilon}_{fs}(\sqrt{3})}{\eta + 2 \cdot \cos\left[\frac{1}{3} \cdot \arccos\left(0,5 \cdot \eta \cdot \left(3 - \eta^2\right)\right)\right]}, \quad -1 < \eta \le 2$ | (22) |
| (8) | $\bar{\varepsilon}_{fs}(\eta) = \frac{3 \cdot C}{\eta}, \quad \eta > 0$ | (23) |
| (9) | $\bar{\varepsilon}_{fs}(\eta) = \frac{3 \cdot \sigma_m \cdot C}{\eta}, \quad -2 \le \eta \le 2$ | (24) |
| Dell models [2] | $\bar{\varepsilon}_{fs}(\eta) = \frac{\varepsilon_c \cdot \varepsilon_k^*}{\varepsilon_c + \eta \cdot \left(\varepsilon_c - e \cdot \varepsilon_k^*\right)} \cdot e^{-\eta}, \quad -1 \le \eta \le 1$ | (25) |
| | $\bar{\varepsilon}_{fs}(\eta) = \frac{\varepsilon_k^*}{1 + \eta} \cdot e^{-\eta}$ | (26) |
| (10) | $\bar{\varepsilon}_{fs}(\eta) = C \cdot \exp\left(-\frac{\eta}{2}\right), \quad -2 \le \eta \le 2$ | (27) |
| (11) | $\bar{\varepsilon}_{fs}(\eta) = \frac{\varepsilon_c^*}{\sqrt{e}} \cdot \exp\left(-\frac{\eta}{2}\right), \quad -2 \le \eta \le 2$ | (28) |

*Table 3(continuation). Limit state models of the material relatively the stress triaxiality index*

| | Models of the equivalent plastic strain to fracture in the plane stress condition | |
|---|---|---|
| (12) | $\bar{\varepsilon}_{fs}(\eta)=\varepsilon_k^*\cdot\exp\left(-\frac{\eta}{2}\right),\quad -2\le\eta\le 2$ | (29) |
| (13) | $\bar{\varepsilon}_{fs}(\eta)=\sqrt{e}\cdot\varepsilon_p^*\cdot\exp\left(-\frac{\eta}{2}\right),\quad -2\le\eta\le 2$ | (30) |
| (14) | $\bar{\varepsilon}_{fs}(\eta)=\frac{\bar{\varepsilon}_{fs}(-2)}{e}\cdot\exp\left(-\frac{\eta}{2}\right),\quad -2\le\eta\le 2$ | (31) |
| (15) | $\bar{\varepsilon}_{fs}(\eta)=\frac{\bar{\varepsilon}_{fs}\left(-\frac{3}{2}\right)}{\sqrt[4]{e^3}}\cdot\exp\left(-\frac{\eta}{2}\right),\quad -2\le\eta\le 2$ | (32) |
| (16) | $\bar{\varepsilon}_{fs}(\eta)=e\cdot\bar{\varepsilon}_{fs}(2)\cdot\exp\left(-\frac{\eta}{2}\right),\quad -2\le\eta\le 2$ | (33) |
| (17) | $\bar{\varepsilon}_{fs}(\eta)=\sqrt[4]{e^3}\cdot\bar{\varepsilon}_{fs}\left(\frac{3}{2}\right)\cdot\exp\left(-\frac{\eta}{2}\right),\quad -2\le\eta\le 2$ | (34) |
| [26] | $\bar{\varepsilon}_{fs}(\eta)=\varepsilon_k^*\cdot\exp\left(-\eta\cdot\ln\left(\frac{(1-\eta)\cdot\varepsilon_c^*}{2\cdot\varepsilon_k^*}+\frac{(1+\eta)\cdot\varepsilon_k^*}{2\cdot\varepsilon_p^*}\right)\right),\quad -2\le\eta\le 2$ | (35) |
| | $\bar{\varepsilon}_{fs}(\eta)=\varepsilon_k\cdot\left(\frac{\varepsilon_p}{\varepsilon_c}\right)^{\frac{\eta}{2}}\cdot\left(\frac{\varepsilon_p\cdot\varepsilon_c}{\varepsilon_k^2}\right)^{\frac{\eta^2}{2}},\quad -2\le\eta\le 2$ | (36) |

Designations:
$\sigma_1$ – the maximum principal tensile stress; $\bar{\varepsilon}_f$ – equivalent plastic strain to fracture on conditions an arbitrary process of the deformation ($\eta$= *const* or $\eta\neq$ *const*); *C = const*; $\langle\sigma_1\rangle=\begin{cases}\sigma_1, \sigma_1\ge 0\\ 0, \sigma_1<0\end{cases}$; $\varepsilon_c^*$ – equivalent plastic strain to fracture in compression; $\varepsilon_k^*$ – equivalent plastic strain to fracture in shear; $\varepsilon_p^*$ – equivalent plastic strain to fracture in tension

## 3. Analyses of the obtained relations enables

The analysis of the obtained relations enables to obtain a number of regularities in the variations of the limit equivalent plastic strain to fracture with the increase of the stress triaxiality, represented by the corresponding models. From the relations (18)–(24), (27)–(34) it follows that the form of the given dependence in invariant relatively the value of the parameter for one-parametric Cockcroft and Latham–Oh models, hydrostatic stress, Rice-Tracey and Dell models. All the dependencies are concave and monotone decreasing functions (except Cockcroft and Latham–Oh models) on the domain of definition. Cockcroft and Latham–Oh model reaches the minimal value

$$\left(\bar{\varepsilon}_{fs}\right)_{\min}=\bar{\varepsilon}_{fs}(\eta=\sqrt{3})=\frac{\sqrt{3}}{6}\cdot C \tag{37}$$

We will build the fracture model, based on the relation (25)

$$\int_0^{\bar{\varepsilon}_f}\frac{\varepsilon_c+\eta\cdot(\varepsilon_c-e\cdot\varepsilon_k)}{\varepsilon_c\cdot\varepsilon_k}\cdot e^{\eta}\cdot d\bar{\varepsilon}=1 \tag{38}$$

This model refers to the family of two-parametric models. To make use of the model it is necessary to have the value of the equivalent plastic strain to fracture on conditions of the compression strain $\varepsilon_c^*$ and shear strain $\varepsilon_k^*$. We will generalize this model for the case when limiting values of plastic deformation are known for the arbitrary values of stress triaxiality $\eta$:

$$\bar{\varepsilon}_{fs}=\bar{\varepsilon}_{f1},\ \bar{\varepsilon}_{fs}=\bar{\varepsilon}_{f2}\ \text{correspondingly if}\ \eta=\eta_1,\eta=\eta_2 \tag{39}$$

On conditions of the stationary deformation for two different values of $\eta_1,\eta_2$ on the base of the model (38) we obtain:

$$\bar{\varepsilon}_{f1}=\frac{\varepsilon_c\cdot\varepsilon_k\cdot e^{-\eta_1}}{\varepsilon_c+\eta_1\cdot(\varepsilon_c-e\cdot\varepsilon_k)};\quad \bar{\varepsilon}_{f2}=\frac{\varepsilon_c\cdot\varepsilon_k\cdot e^{-\eta_2}}{\varepsilon_c+\eta_2\cdot(\varepsilon_c-e\cdot\varepsilon_k)} \tag{40}$$

The system of two linear equations (40) relatively $\varepsilon_c^*$ and $\varepsilon_k^*$ will be solved, as a result we obtain

$$\varepsilon_c^*=\frac{\bar{\varepsilon}_{f1}\cdot\bar{\varepsilon}_{f2}\cdot e\cdot(\eta_2-\eta_1)}{\bar{\varepsilon}_{f2}\cdot e^{-\eta_1}\cdot(1+\eta_2)-\bar{\varepsilon}_{f1}\cdot e^{-\eta_2}\cdot(1+\eta_1)};$$
$$\varepsilon_k^*=\frac{\bar{\varepsilon}_{f1}\cdot\bar{\varepsilon}_{f2}\cdot(\eta_2-\eta_1)}{\bar{\varepsilon}_{f2}\cdot\eta_2\cdot e^{-\eta_1}-\bar{\varepsilon}_{f1}\cdot\eta_1\cdot e^{-\eta_2}},\ \eta_1\neq\eta_2 \tag{41}$$

Taking into account the later relations, the model (38) will obtain the form

$$\int_0^{\bar{\varepsilon}_f}\frac{\bar{\varepsilon}_{f2}\cdot e^{-\eta_1}\cdot(\eta_2-\eta)-\bar{\varepsilon}_{f1}\cdot e^{-\eta_2}\cdot(\eta_1-\eta)}{\bar{\varepsilon}_{f1}\cdot\bar{\varepsilon}_{f2}\cdot(\eta_2-\eta_1)}\cdot e^{\eta}\cdot d\bar{\varepsilon} \tag{42}$$

Fracture diagram, that follows from the model (42) has the form

$$\bar{\varepsilon}_{fs}(\eta)=\frac{\bar{\varepsilon}_{f1}\cdot\bar{\varepsilon}_{f2}\cdot(\eta_2-\eta_1)}{\bar{\varepsilon}_{f1}\cdot e^{-\eta_2}\cdot(\eta-\eta_1)-\bar{\varepsilon}_{f2}\cdot e^{-\eta_1}\cdot(\eta-\eta_2)}\cdot e^{-\eta} \tag{43}$$

In separate case if

$$\bar{\varepsilon}_{f1}=\varepsilon_c^*,\ \bar{\varepsilon}_{f2}=\varepsilon_k^*,\ \eta_1=-1,\ \eta_2=0\ \text{or}$$
$$\bar{\varepsilon}_{f2}=\varepsilon_c^*,\ \bar{\varepsilon}_{f1}=\varepsilon_k^*,\ \eta_2=-1,\ \eta_1=0 \tag{44}$$

the relation (43) becomes identical to the model (26).

On the base of the model (43) it is easy to obtain many other relations, which use the values of the equivalent plastic strains at fracture in case of typical tests. In the values of the equivalent plastic strains at fractures are used as such tests according to five various values of stress triaxiality $\eta$={-2, -1, 0, 1, 2}, then we can obtain the number of the separate relations that are equal to the number of combinations of $n$=5 elements taken $r$=2 at a time, i. e.

$$C_5^2=\frac{5!}{2!\cdot(5-2)!}=10 \tag{45}$$

We will give these relations:

$$\bar{\varepsilon}_{fs}(\eta)=\frac{2\cdot\varepsilon_c^*\cdot\varepsilon_p^*\cdot e^{-\eta}}{(1+\eta)\cdot e^{-1}\cdot\varepsilon_c^*+(1-\eta)\cdot e\cdot\varepsilon_p^*};\quad \left(\varepsilon_1=\varepsilon_c^*,\ \varepsilon_2=\varepsilon_p^*,\ \eta_1=-1,\ \eta_2=1\right) \tag{46}$$

$$\bar{\varepsilon}_{fs}(\eta)=\frac{\varepsilon_k^*\cdot\varepsilon_p^*\cdot e^{-\eta}}{\eta\cdot e^{-1}\cdot\varepsilon_k^*+(1-\eta)\cdot e^{0}\cdot\varepsilon_p^*};\quad \left(\varepsilon_1=\varepsilon_k^*,\ \varepsilon_2=\varepsilon_p^*,\ \eta_1=0,\ \eta_2=1\right) \tag{47}$$

$$\bar{\varepsilon}_{fs}(\eta)=\frac{4\cdot\varepsilon_{\eta=-2}\cdot\varepsilon_{\eta=2}\cdot e^{-\eta}}{(2+\eta)\cdot e^{-2}\cdot\varepsilon_{\eta=-2}+(2-\eta)\cdot e^{2}\cdot\varepsilon_{\eta=2}};\quad \left(\varepsilon_1=\varepsilon_{\eta=-2},\ \varepsilon_2=\varepsilon_{\eta=2},\ \eta_1=-2,\ \eta_2=2\right) \tag{48}$$

$$\bar{\varepsilon}_{fs}(\eta)=\frac{\varepsilon_p^*\cdot\varepsilon_{\eta=2}\cdot e^{-\eta}}{(-1+\eta)\cdot e^{-2}\cdot\varepsilon_p^*+(2-\eta)\cdot e^{-1}\cdot\varepsilon_{\eta=2}};\quad \left(\varepsilon_1=\varepsilon_p^*,\ \varepsilon_2=\varepsilon_{\eta=2},\ \eta_1=1,\ \eta_2=2\right) \tag{49}$$

$$\bar{\varepsilon}_{fs}(\eta)=\frac{\varepsilon_{\eta=-2}\cdot\varepsilon_c^*\cdot e^{-\eta}}{(2+\eta)\cdot e\cdot\varepsilon_{\eta=-2}+(-1-\eta)\cdot e^{2}\cdot\varepsilon_c^*};\quad \left(\varepsilon_1=\varepsilon_{\eta=-2},\ \varepsilon_2=\varepsilon_c^*,\ \eta_1=-2,\ \eta_2=-1\right) \tag{50}$$

$$\bar{\varepsilon}_{fs}(\eta)=\frac{2\cdot\varepsilon_k^*\cdot\varepsilon_{\eta=2}\cdot e^{-\eta}}{\eta\cdot e^{-2}\cdot\varepsilon_k^*+(2-\eta)\cdot e^{0}\cdot\varepsilon_{\eta=2}};\quad \left(\varepsilon_1=\varepsilon_k^*,\ \varepsilon_2=\varepsilon_{\eta=2},\ \eta_1=0,\ \eta_2=2\right) \tag{51}$$

$$\bar{\varepsilon}_{fs}(\eta)=\frac{3\cdot\varepsilon_c^*\cdot\varepsilon_{\eta=2}\cdot e^{-\eta}}{(1+\eta)\cdot e^{-2}\cdot\varepsilon_c^*+(2-\eta)\cdot e\cdot\varepsilon_{\eta=2}};\quad \left(\varepsilon_1=\varepsilon_c^*,\ \varepsilon_2=\varepsilon_{\eta=2},\ \eta_1=-1,\ \eta_2=2\right) \tag{52}$$

$$\bar{\varepsilon}_{fs}(\eta)=\frac{3\cdot\varepsilon_{\eta=-2}\cdot\varepsilon_p\cdot e^{-\eta}}{(2+\eta)\cdot e^{-1}\cdot\varepsilon_{\eta=-2}+(1-\eta)\cdot e^{2}\cdot\varepsilon_p};\quad \left(\varepsilon_1=\varepsilon_{\eta=-2},\ \varepsilon_2=\varepsilon_p,\ \eta_1=-2,\ \eta_2=1\right) \tag{53}$$

$$\bar{\varepsilon}_{fs}(\eta)=\frac{2\cdot\varepsilon_{\eta=-2}\cdot\varepsilon_k^*\cdot e^{-\eta}}{(2+\eta)\cdot\varepsilon_{\eta=-2}-\eta\cdot e^{2}\cdot\varepsilon_k^*};\quad \left(\varepsilon_1=\varepsilon_{\eta=-2},\ \varepsilon_2=\varepsilon_k^*,\ \eta_1=-2,\ \eta_2=0\right) \tag{54}$$

The results of the calculations according to the obtained relations as compared with the experimental data are given in Fig. 2. It follows from these results that one-parametric models provide satisfactory quantitative and even qualitative matching only for the narrow range of stress triaxiality, $\eta$.

As it is shown in [12] the equation (26) is used only if $\varepsilon_c^* > e\cdot\varepsilon_k^*$.

For the steel 20A this condition is not fulfilled. Curve 3 in Fig. 2d demonstrates the anomalous behavior at changes of equivalent plastic strain to fracture if $\eta > 0$.

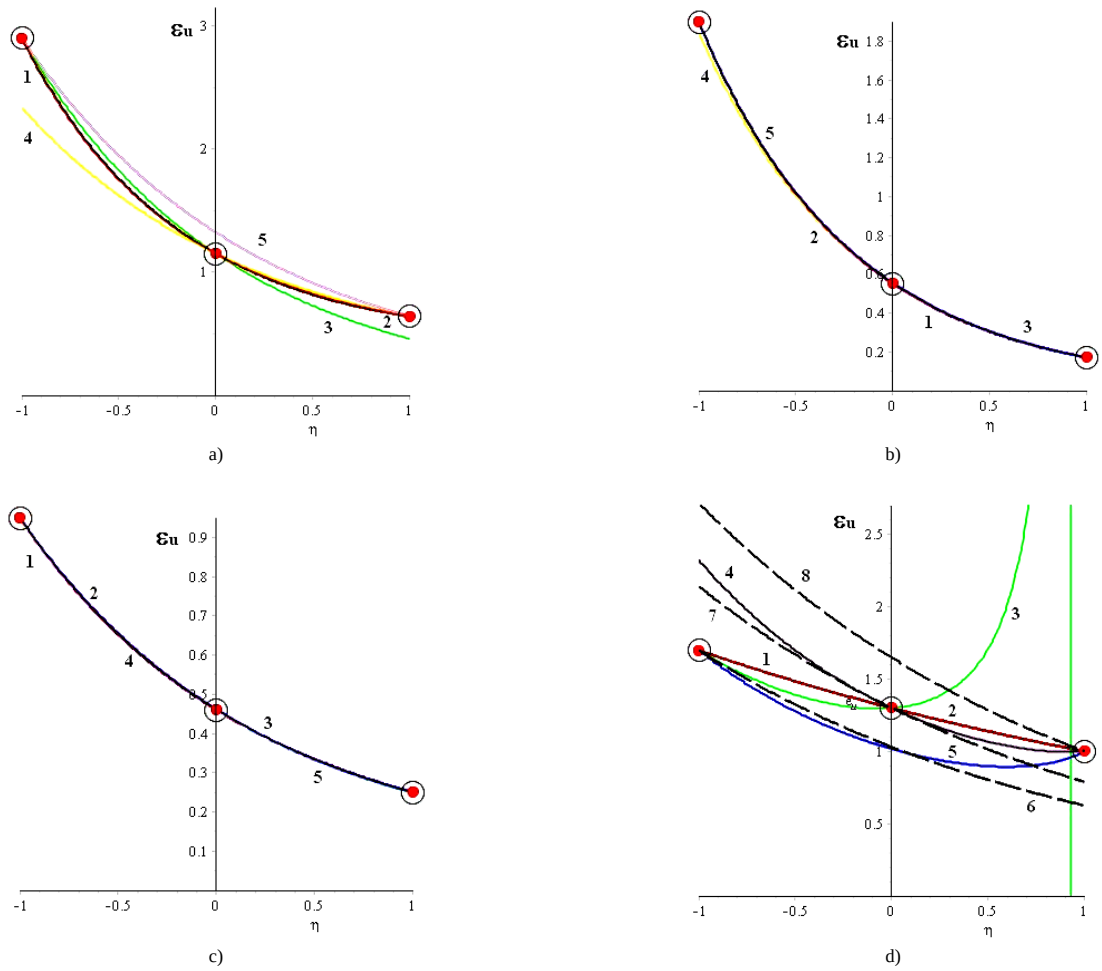


*Fig. 2. Dependences of the equivalent plastic strain to fracture on the stress triaxiality of the alloy VT-1 (a), R12 (b), R6M5 (c), 20-A (d) according to the approximations of the curves of the equivalent plastic strains at fracture: 1 – 8 – according to the relations (35), (36), (25), (47), (46), (28), (29), (30), using the experimental data, presented in [30]*

## 4. Conclusions

1. During the last decades the relevance of the studies, dealing with the equivalent plastic strains at fracture at different schemes of stress states drastically increased.
2. The suggested classification characteristics for the comparison of the fracture models are necessary for the realization of the systematization of the results of the research of these model and development of the substantiated recommendations regarding their usage.
3. Development of the generalized relations for the known fracture models regarding the plane stress enabled to simplify the process of obtaining of the great number of the original separate relations.
4. The obtained analytical dependences provided the possibility to obtain a number of general properties, represented by various models.
5. Models of the equivalent plastic strains at fracture of the sheet materials [2, 3, 4, 13, 14, 15, 16, 17] require separate studies.

## References


[1] Afonin A.: Modelirovanie razrusheniya metallov pri plasticheskoy deformatsii v DEFORM i LS-DYNA, Izvestiya OrelGTU, Mashinostroenie. Priborostroenie 1, 2012, 52–62.
[2] Bai Y., Wierzbicki T.: A new model of metal plasticity and fracture with pressure and Lode dependence. International Journal of Plasticity 24, 1071–1096 [http://doi.org/10.1016/j.ijplas.2007.09.004].
[3] Bao Y., Wierzbicki T.: A comparative study on various ductile crack formation criteria. J Eng Mater Technol 126, 2004, 314–324 [http://doi.org/10.1115/1.1755244].
[4] Bao Y., Wierzbicki T.: On fracture locus in the equivalent strain and stress triaxiality space. International Journal of Mechanical Sciences 1(46), 2004, 81–98 [http://doi.org/10.1016/j.ijmecsci.2004.02.006].
[5] Bao Y., Wierzbicki T.: On the cut-off value of negative triaxiality for fracture. Engineering Fracture Mechanics 72, 2005, 1049–1069 [http://doi.org/10.1016/j.engfracmech.2004.07.011].
[6] Botkin A. et al.: Otsenka povrezhdennosti metalla pri holodnoy plasticheskoy deformatsii c ispolzovaniem modeli razrusheniya Kokrofta-Latama. Deformatsiya i razrushenie materialov 7, 2011, 17–22.
[7] Botkin A. et al.: Prognoziovanie razrusheniya metalla v protsesse intensivnoy plasticheskoy deformatsii dlinnomernoy zagotovki ravnokanalnyim uglovyim pressovaniem konform. Vestnik UGATU 16, 8(53), 2012, 98–103.
[8] Botkin A., Valiev R., Stepin P.: Otsenka povrezhdennosti metalla pri holodnoy plasticheskoy deformatsii s ispolzovaniem modeli razrusheniya Kokroft-Letem i programmnogo kompleksa DEFORM 3D. Innovatsionnyie tehnologii v metallurgii i mashinostroenii, Ekaterinburg 2012, 102–108.
[9] Clift S. et al.: Fracture prediction in plastic deformation processes. International Journal of Mechanical Science 1(32), 1990, 1–17 [http://doi.org/10.1016/0020-7403(90)90148-C].
[10] Cockcroft M., Latham D.: Ductility and the Workability of Metals. Journal of the Institute of Metals 96, 1968, 33–39.
[11] Del G.: Plastichnost deformirovannogo metalla. Fizika i tehnika vyisokih davleniy 11, 1983, 28–32.
[12] Del G.: Tekhnolohycheskaia mekhanyka. Mashynostroenye, Moscow 1978.
[13] Gese H., Oberhofer G., Dell H.: Consistent Modeling of Plasticity and Failure in the Process Chain of Deep Drawing and Crash with User Material Model MF-GenYld + CrachFEM for LS-Dyna, LS-DYNA Anwenderforum 6, Frankenthal 2007.
[14] Hooputra H. et al.: A comprehensive failure model for crashworthiness simulation of aluminium extrusions. International Journal of Crashworthiness 9, 2004, 449–464 [http://doi.org/10.1533/ ijcr.2004.0289].
[15] Hrushko A., OgorodnIkov V.: Predelnoe formoizmenenie v operatsiyah listovoy shtampovki. Udoskonalennya protsesiv i obladnannya obrobki tiskom v metalurgiyi i mashinobuduvanni, Kramatorsk 2004, 186–190.
[16] Hrushko A.: Kartyi materialov v holodnoy obrabotke davleniem. VNTU, Vinnitsa 2015.
[17] Hrushko A.: Parametr napriazhennoho sostoianyia, uchytyvaiushchyi svoistva materyala, y eho vlyianye na plastychnost. Visnyk NTUU "KPI" Mashynobuduvannia 64, 2012, 220–226.
[18] Ilyushin A.: Ob odnoy teorii dlitelnoy prochnosti. Mehanika tverdogo tela 13, 1967, 21–25.
[19] Keller I. et al.: Diagramma predelnyih deformatsiy pri goryachey listovoy shtampovke metallov: obzor modeley materiala, kriteriev vyazkogo razrusheniya i standartnyih ispyitaniy. VSGTU 22(3), 2018, 447–486 [http://doi.org/10.14498/vsgtu1608].
[20] Kolmogorov V. et al.: Plastichnost i razrushenie. Metallurgiya, Moscow 1977.
[21] Kraievskyi V. et al.: Modeling of the materials superplasticity based on damage summation theory. Proc. SPIE 10808, 2018, 108084S [http://doi.org/10.1117/12.2501489].
[22] Matveev M.: Otsenka veroyatnosti razrusheniya metalla pri goryachey plasticheskoy deformatsii spomoschyu kriteriya Kokrofta-Latama. Nauchno-tehnicheskie vedomosti SPbPU. Estestvennyie i inzhenernyie nauki 23(02), 2017, 109–126 [http://doi.org/10.18721/JEST.230211].
[23] Matviychuk V., Aliyev I.: Sovershenstvovaniye protsessov lokal'noy rotatsionnoy obrabotki davleniyem na osnove analiza deformiruyemosti metallov: monografiya. DGMA, Kramatorsk 2009.
[24] Mikhalevich V., Abramchuk I.: Maximum Accumulated Strain for Linear Two-Link Triangle-Like Deformation Trajectories. International Applied Mechanics 57(6), 2021, 720–736 [http://doi.org/10.1007/s10778-022-01121-w].
[25] Mikhalevich V., Lebedev A., Dobranyuk Yu.: Modeling of plastic deformation in a cylindrical specimen under edge compression. Strength of Materials 43(6), 2011, 591–603 [http://doi.org/10.1007/s11223-011-9332-7].
[26] Mikhalevich V.: Models of defects accumulation for solids with original and strain-induced anisotropy. Izvestia Akademii nauk SSSR. Metally 5, 1993, 144–151 [http://doi.org/10.1007/BF02133202].
[27] Mykhalevych V.: Tenzorni modeli nakopychennia poshkodzhen. Universum, Vinnytsia 1998.
[28] Ogorodnikov V.: Otsenka deformiruemosti metallov pri obrabotke davleniem. Vyischa shk., Kyiv 1983.
[29] Oh S., Chen C., Kobayashi S.: Ductile fracture in axisymmetric extrusion and drawing. Part 2. Workability in extrusion and drawing. ASME Journal of Engineering for Industry 101, 1979, 36–44 [http://doi.org/10.1115/1.3439471].
[30] Ohorodnykov V. et al.: Parametry modely, formyruyushchey kartu materyala v protsesakh obrabotky davlenym. Obrabotka materyalov davlenyem 1(26), 2011, 91–97.
[31] Polishchuk L., Bilyy O., Kharchenko Y.: Prediction of the propagation of crack-like defects in profile elements of the boom of stack discharge conveyor. Eastern-European Journal of Enterprise Technologies 6(1), 2016, 44–52 [http://doi.org/10.15587/1729-4061.2016.85502].
[32] Rice J., Tracey D.: On the ductile enlargement of voids in triaxial stress fields. Journal of the Mechanics and Physics of Solids 3, 1969, 201–217 [http://doi.org/10.1016/0022-5096(69)90033-7].
[33] Shatokhin V. et al.: Vibration diagnostic of wear for cylinder-piston couples of pumps of a radial piston hydromachine. Wójcik W., Pavlov S., Kalimoldayev M.: Mechatronic Systems I. Taylor & Francis Group, CRC Press, Balkema book, London, New York 2021, 39–52.
[34] Vlasov A., Gerasimov D.: Realizatsiya modeli Gurso – Tvergarda – Nidelmana dlya raschetov protsessov holodnoy ob'emnoy shtampovki neszhimaemyih materialov. Izvestiya vyisshih uchebnyih zavedeniy. Mashinostroenie 8(689), 2017, 8–17 [http://doi.org/10.18698/0536-1044-2017-8-8-17].
[35] Vlasov A.: O primenenii kriteriya Kokrofta-Letema dlya prognozirovaniya razrusheniya pri holodnoy ob'emnoy shtampovke. Izvestiya TulGU – Tehnicheskie nauki 11(1), 2017, 46–59.
[36] Zinkovskii A. et al.: Finite element model for analysis of characteristics of shrouded rotor blade vibrations. Informatyka, Automatyka, Pomiary w Gospodarce i Ochronie Środowiska – IAPGOS 12(4), 2022, 11–16 [http://doi.org/10.35784/iapgos.3264].



**D.Sc. Eng Volodymyr M. Mykhalevych**
e-mail: mykhalevych@vntu.edu.ua


Professor, Head of the Department of Higher Mathematics, Vinnytsia National Technical University. Research interests include: Mathematical modeling of the limit state of materials and optimization of non-stationary processes of inelastic deformation. The use of computer mathematics systems in scientific research and in the process of teaching higher mathematics to university students. He has published more than 400 scientific papers and created a lot of a number of models of the limit state of materials under conditions of plastic deformation or creep.


http://orcid.org/0000-0003-1557-7331

**Ph.D. Yurii Dobraniuk**
e-mail: dobranukyuriy@gmail.com


Candidate of Science (Engineering), associate professor, Department of Higher Mathematics, Vinnytsia National Technical University. He has published 75 scientific papers. Research interests include optimization problems in damage summation theory; mathematical modeling of the mechanics of forming during plastic deformation processes.


http://orcid.org/0000-0001-6387-6331

**D.Sc. Eng. Victor A. Matviichuk**
e-mail: vamatv50@gmail.com

During more than 35 years of scientific and pedagogical activity, he is the author of more than 220 scientific and educational-methodical works, including 5 monographs, 1 textbook with the seal of the Ministry of Education and Culture of Ukraine, 3 training manuals, 19 copyright certificates and patents for inventions, 9 publications in periodicals, which are included in the Scopus scientometric database.

http://orcid.org/0000-0002-7837-5174

**Ph.D. Volodymyr Kraievsky**
e-mail: volodymyr.kraievskyi@gmail.com

Associate professor of the Computer Engineering Department, Vinnytsia National Technical University. Research interests include optimization problems in damage summation theory; development of phenomenological criteria of destruction; mathematical modeling of the mechanics of forming during plastic deformation processes. He has published 90 scientific works, developed variational models of multi-stage hot deformation. The main areas of his scientific activity are mathematical modeling of the mechanics of forming.

http://orcid.org/0000-0001-6478-253X

**Ph.D. Oksana Tiutiunnyk**
e-mail: tutunnik.oksana@gmail.com

Candidate of Pedagogical Scinces, associate professor, Department of Higher Mathematics, Vinnytsia National Technical University. She has published 60 scientific papers. The main directions of his scientific activity are use of information technologies in the educational process.

http://orcid.org/0000-0002-8544-4246

**Ph.D. Saule Smailova**
e-mail: Saule_Smailova@mail.ru

Saule Smailova is currently a lecturer at the Department of Information Technology, D. Serikbayev East Kazakhstan Technical University, Ust-Kamenogorsk, Kazakhstan.
She is a co-author over 60 papers in journals, book chapters, and confer ence proceedings. Member of Expert Group in the Computer Science specialization of IQAA.

http://orcid.org/0000-0002-8411-3584

**Ph.D. Ainur Kozbakova**
e-mail: ainur79@mail.ru

Ph.D, associate professor of Almaty Technological University, Institute of Information and Computational Technologies CS MHES RK.
Research interests: mathematical modeling of discrete systems, evacuation tasks, operations research, technology design of complex systems.

http://orcid.org/0000-0002-5213-4882